

BERICHTE

aus dem MARUM und dem Fachbereich
Geowissenschaften der Universität Bremen

No. 318

Strasser, M., Kopf, A.

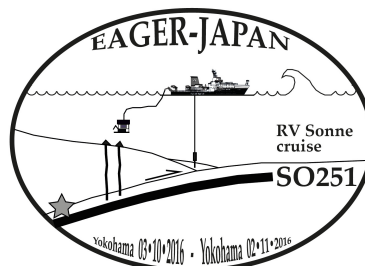
Abegg, F.W.; Asada, M.; Bachmann, A.K.; Cuno, P.; Dos Santos
Ferreira, C.; Fleischmann, T.; Fujiwara, T.; Hatakeyama, E.;
Heesemann, B.R.; Hillman, J.I.T.; Hoehne, M.; Huusmann, H.; Ikari,
M.; Ikehara, K.; Jaeger, F.D.; Kanamatsu, T.; Kang, M.-H.; Kaul, N.E.;
Kioka, A.; Koelling, M.; Lange, K.; Luebben, N.; Matthiessen, T.;
Mchugh, C.M.; Meier, A.; Menapace, W.; Mochizuki, K.; Moernaut, J.;
Molenaar, A.W.; Moore, G.F.; Mu, L.-J.; Nakano, Y.; Pieper, M.; Rex,
M.L.P.A.; Roesner, A.; Schwestermann, T.; Sun, T.; Szczucinski, W.;
Tochterle, P.; Truetner, S.; Usami, K.; Wiemer, G.; Yamaguchi, A.

REPORT AND PRELIMINARY RESULTS OF R/V SONNE CRUISE SO251

EXTREME EVENTS ARCHIVED IN THE GEOLOGICAL RECORD OF JAPAN'S SUBDUCTION MARGINS (EAGER-JAPAN)

LEG A SO251-1, YOKOHAMA - YOKOHAMA, 04.10.2016 – 15.10.2016

LEG B SO251-2, YOKOHAMA - YOKOHAMA, 18.10.2016 – 02.11.2016



Berichte, MARUM – Zentrum für Marine Umweltwissenschaften, Fachbereich
Geowissenschaften, Universität Bremen, No. 318, 217 pages, Bremen 2017

ISSN 2195-9633

Berichte aus dem MARUM und dem Fachbereich Geowissenschaften der Universität Bremen

published by

MARUM – Center for Marine Environmental Sciences

Leobener Strasse, 28359 Bremen, Germany

www.marum.de

and

Fachbereich Geowissenschaften der Universität Bremen

Klagenfurter Strasse, 28359 Bremen, Germany

www.geo.uni-bremen.de

The "Berichte aus dem MARUM und dem Fachbereich Geowissenschaften der Universität Bremen" appear at irregular intervals and serve for the publication of cruise, project and technical reports arising from the scientific work by members of the publishing institutions.

Citation:

Strasser, M., Kopf, A., Abegg, F.W.; Asada, M.; Bachmann, A.K.; Cuno, P.; Dos Santos Ferreira, C.; Fleischmann, T.; Fujiwara, T.; Hatakeyama, E.; Heesemann, B.R.; Hillman, J.I.T.; Hoehne, M.; Huusmann, H.; Ikari, M.; Ikehara, K.; Jaeger, F.D.; Kanamatsu, T.; Kang, M.-H.; Kaul, N.E.; Kioka, A.; Koelling, M.; Lange, K.; Luebben, N.; Matthiessen, T.; Mchugh, C.M.; Meier, A.; Menapace, W.; Mochizuki, K.; Moernaut, J.; Molenaar, A.W.; Moore, G.F.; Mu, L.-J.; Nakano, Y.; Pieper, M.; Rex, M.L.P.A.; Roesner, A.; Schwestermann, T.; Sun, T.; Szczucinski, W.; Toechterle, P.; Truetner, S.; Usami, K.; Wiemer, G.; Yamaguchi, A.: Report and preliminary results of R/V SONNE cruise SO251, Extreme events Archived in the GEological Record of Japan's Subduction margins (EAGER-Japan), Leg A SO251-1, Yokohama - Yokohama, 04.10.2016 – 15.10.2016, Leg B SO251-2, Yokohama - Yokohama, 18.10.2016 – 02.11.2016. Berichte, MARUM – Zentrum für Marine Umweltwissenschaften, Fachbereich Geowissenschaften, Universität Bremen, No. 318, 217 pages. Bremen, 2017. ISSN 2195-9633.

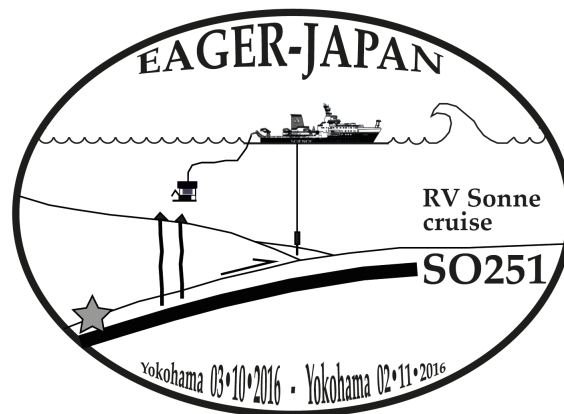
An electronic version of this report can be downloaded from:

<http://nbn-resolving.de/urn:nbn:de:gbv:46-MARUM9>

Please place requests for printed copies as well as editorial concerns with reports@marum.de

Report and preliminary results of
R/V SONNE cruise SO251

**Extreme events Archived in the GEological Record
of Japan's Subduction margins (EAGER-Japan)**



Leg A SO251-1, Yokohama - Yokohama, 04.10.2016 – 15.10.2016

Leg B SO251-2, Yokohama - Yokohama, 18.10.2016 – 02.11.2016

Strasser, M., Kopf, A.,

Abegg, F.W.; Asada, M.; Bachmann, A.K.; Cuno, P.; Dos Santos
Ferreira, C.; Fleischmann, T.; Fujiware, T.; Hatakeyama, E.;
Heesemann, B.R.; Hillman, J.I.T.; Hoehne, M.; Huusmann, H.; Ikari, M.;
Ikehara, K.; Jaeger, F.D.; Kanamatsu, T.; Kang, M.-H.; Kaul, N.E.;
Kioka, A.; Koelling, M.; Lange, K.; Luebben, N.; Matthiessen, T.;
Mchugh, C.M.; Meier, A.; Menapace, W.; Mochizuki, K.; Moernaut, J.;
Molenaar, A.W.; Moore, G.F.; Mu, L.-J.; Nakano, Y.; Pieper, M.;
Rex, M.L.P.A.; Roesner, A.; Schwesternmann, T.; Sun, T.;
Szcucinski, W.; Tochterle, P.; Truetner, S.; Usami, K.; Wiemer, G.;
Yamaguchi, A.

Tabel of content

1. Summary	3
2. Participants	4
3. Research Program / Objectives.....	9
4. Setting of the working area and previous work	11
<i>Japan Trench</i>	11
<i>Nankai Trough</i>	14
5. Narrative of the Cruise.....	17
<i>Leg SONNE251-1, Yokohama - Yokohama, 04.10.2016 – 15.10.2016</i>	17
<i>Leg SO251-2, Yokohama - Yokohama, 18.10.2016 – 02.11.2016</i>	18
6. Methods	21
6.1. Hydroacoustics.....	21
6.1.1. Bathymetric mapping (multibeam EM122, incl. CTD, XSV and XCTD)	21
6.1.2. Sediment echo sounding (With Parasound P70).....	22
6.2. Remotely Operated Vehicle (ROV) Deployments.....	23
6.3. Observatories	24
6.3.1. MeBo CORKs	24
6.3.2. MeBo Plugs (and MTL-sticks).....	25
6.3.3. SmartPlug piezometer	27
6.4. Sediment sampling.....	28
6.4.1. Piston corer (PC)	28
6.4.2. Gravity Coring (GC) on Heat Flow Probe	30
6.4.3. Sediment description	32
6.5. Physical properties.....	34
6.5.1. Magnetic Susceptibility	34
6.5.2. Undrained shear strength and sampling.....	34
6.5.3. Electrical resistance.....	36
6.5.4. Thermal Conductivity	37
6.5.5. Sampling for shore-based analyses	39
6.6. Geochemistry	39
6.7. Heat flow determination	44
6.7.1. MTL temperature measurement	44
6.7.2. Heat flow probe.....	44
7. Initial shipboard results.....	47
7.1. Hydroacoustics.....	47
7.1.1. Bathymetry.....	47
7.1.2. Subbottom Profiles	48
7.2. Remotely Operated Vehicle (ROV) dives	50
7.3. Observatories	55
7.4. Sedimentology.....	58
7.4.1. Japan Trench.....	58
7.4.2. Nankai Trough / Kumano Basin.....	60
7.5. Physical properties.....	63
7.5.1. Magnetic Susceptibility	63
7.5.2. Undrained shear strength	63
7.5.3. Electrical Resistance	68
7.5.4. Thermal Conductivity	71
7.6. Geochemistry	74
7.7. Heat Flow determination	77
8. Data and Sample Storage and Availability	80
9. Acknowledgements	80
10. References	81
11. Appendix.....	84
11.1 Station Lists.....	84
11.2 Core photos,.....	84
11.3 Core Logs,.....	84
11.5 ROV Dive Protocols	84
11.6 Composite core logs	84

1. Summary

At the southeastern edge of the Eurasian Plate, Japan hosts two of the most interesting subduction systems, both prone to devastating megathrust earthquakes: The Japan Trench (JT) east of Honshu with subduction erosion/subsidence in the north, and the Nankai Trough (NT) with a huge accretionary prism in the southwest. In 2011 the JT area was struck by a Magnitude 9 earthquake that caused unusually large slip all the way to the trench, and a series of landslides, which are believed to be partly responsible for amplification of the catastrophic tsunami following the event. At Nankai, frequent M8+ earthquakes are also documented, and landslides and other sediment remobilization processes related to seismicity are attested. Despite the fact that either area has recently been the target of both IODP drilling (Exp343 vs 332/333/338/348) and MARUM cruises (SO219A vs. SO222), remaining gaps in knowledge remain. *R/V Sonne* Research Cruise SO251 was dedicated to collect data and samples to address the EAGER-Japan research project objectives such as (i) characterization and precise dating of extreme event layers, (ii) recovery of long-term instruments monitoring physical triggers to such events, and (iii) study geochemistry and fluid flow and link them to mass wasting in order to determine recurrence time and assess risk in two key scenarios: The mega-earthquake super-cycle in the subsiding, highly segmented Japan Trench, and records of megasplay slip in the Nankai region.

The achievements from SO251-1 to the Japan Trench include:

- Acquisition of a complete high-resolution bathymetric map of the Japan trench axis and nearly 2000 km of subbottom Parasound profiles, covering the entire along-strike extent of the Japan Trench from 36° to 40.3° N,
- Recovery of 5 nearly 10m long piston cores retrieved from the very deep waters (7 to 8 km below sea level).
- Recovery of three double cores on the continental slope, one of which was analyzed onboard while the other is sent to MARUM Bremen for geotechnical tests that simulate deformation behaviour when dynamic loads are applied to the sediment, as is the case during large EQs.

Initial results from SO251-1 are:

- Several smaller submarine landslides (up to several 100's m of lateral extent) are imaged in the new bathymetric data that were either not yet present, or not resolved in the lower-resolution bathymetric dataset acquired before 2011.
- Parasound data image striking, up to several meter thick, acoustically transparent bodies interbedded in the otherwise parallel reflection pattern of the trench fill basins, providing a temporal and spatial inventory of major sediment remobilization events along the Japan Trench with potential quantitative

constraints on volumes and mass fluxes of material mobilized during each event.

- Core from the southern and northern part of the Japan Trench confirm previous findings from the central part near the Tohoku-oki epicenter, that the small deep-sea trench-fill basins, that are associated with very high sedimentation rates, comprise repeated thick turbidite sequences to be further tested for correlation to historic earthquakes.

The main results from SO251-2 at the Nankai Trough encompass:

- Acquisition of a complemented high-resolution, full coverage bathymetric map of the entire Kumano Basin and adjacent slopes, including the associated subbottom Parasound profiles,
- Discovery of more than a dozen flares in the study area, which indicate fluid seepage activity along mud volcano summits, the seafloor trace of the megasplay fault, and other areas yet to be studied in more detail,
- Recovery of gravity cores and piston cores that documented mud breccia at some dome-shaped features, collected slope deposits seaward of the Kumano Basin for geotechnical analysis, and recovered basin deposits to describe background deposition and overlapping sequences throughout the Kumano basin.
- With ROV PHOCA, we successfully retrieved two MeBoPLUG observatories, one MeBoCORK-A observatory, and a GeniusPlug piezometer, where time series data of P and T reveal frequent EQ activity and also excursions owing to meteorological events.
- Cores from selected mud volcanoes reveal seepage of methane-rich fluids given the cemented carbonate conduits embedded in muddy matrix. Shore-based chemical analysis will try to unravel changes in fluid chemistry over time and their link to tectonic processes.
- On MV#2 in the Kumano basin, we discovered a recent (past 4.5 yrs.) mudflow episode towards the NW. Both the moat around the MV and the adjacent seafloor NW of the dome were covered with mud breccia, as evidenced from both HF data and a gravity core. The change is supported when using differential bathymetry methods based on the 2012 (SO222) and 2016 (SO251) data sets.

2. Participants

Leg SONNE251-1, Yokohama - Yokohama, 04.10.2016 – 15.10.2016

NAME	Discipline	Institution
STRASSER, Michael	Chief Scientist	UIBK / MARUM
BACHMANN, Anna Katharina	Hydroacoustics	MARUM
DOS SANTOS FERREIRA, Christian	Hydroacoustics	MARUM
FLEISCHMANN, Timo	Coring / Lab	MARUM
FUJIWARA, Toshiya	Hydroacoustics	JAMSTEC
HILLMAN, Jess Irene Tsahai	PhysProps	GEOMAR
HOEHNE, Mareike	PhysProps	MARUM
IKARI, Matt	PhysProps	MARUM
IKEHARA, Ken	Sedimentology	GSJ / AIST
JAEGER, Fabian Dominik	Coring / Lab	UIBK
KANAMATSU, Toshiya	Sedimentology/Coring	JAMSTEC
KIOKA, Arata	Hydroacoustics	AORI / UIBK
KOELLING, Martin	Geochemistry	MARUM
LANGE, Karl	Hydroacoustics	MARUM
LUEBBEN, Neeske	Geochemistry	MARUM
MCHUGH, Cecilia Maria	Sedimentology	QC/LDEO
MOERNAUT, Jasper	Hydroacoustics	UIBK
MOLENAAR, Ariana	Sedimentology	UIBK
NAKANO, Yukihiko	Coring	MWJ / JAMSTEC
REX, Marie	Lab	MARUM
ROESNER, Alexander	PhysProps / Coring	MARUM
SCHWESTERMANN, Tobias	Hydroacoustics	UIBK
SUN, Tianhaozhe	Hydroacoustics	PGC
SZCZUCINSKI, Witold	Sedimentology	U-Poznan
TOECHTERLE, Paul	Geochemistry	UIBK
TRUETNER, Sebastian	PhysProps	MARUM
USAMI, Kazuko	Sedimentology	GSJ / AIST
WIEMER, Gauvain	PhysProps	MARUM
YAMAGUCHI, Asuka	Sedimentology	AORI

Participating Institutions:

AIST	National Institute of Advanced Industrial Science and Technology, Japan
AORI	Atmosphere and Ocean Research Institute, University of Tokyo, Japan
GEOMAR	Geomar, Kiel, Germany
GSJ	Geological Survey Japan
JAMSTEC	Japan Agency for Marine-Earth Science and Technology, Japan
LDEO	Lamont-Doherty Earth Observatory, Columbia University, USA
MARUM	Center for Environmental Sciences, University of Bremen
MWJ	Marine Works Japan
PGC	Pacific Geoscience Centra, Sidney, B.C., Canada
UIBK	University of Innsbruck, Austria
U-Poznan	University of Poznan, Poland
QC	Queens College, City University of New York, USA

Leg SONNE251-2, Yokohama - Yokohama, 18.10.2016 – 02.11.2016

NAME	Discipline	Institution
KOPF, Achim	Chief Scientist	MARUM
ABEGG, Friedrich Werner	ROV	GEOMAR
ASADA, Miho	Hydroacoustics / Heat Flow	JAMSTEC
BACHMANN, Anna Katharina	Hydroacoustics	MARUM
CUNO, Patrick	ROV	GEOMAR
DOS SANTOS FERREIRA, Christian	Hydroacoustics	MARUM
FLEISCHMANN, Timo	Coring/HF/Observatories	MARUM
HATAKEYAMA, Ei	Coring	MWJ / JAMSTEC
HEESEMAN, Bernd Reinhardt	Heat Flow	MARUM
HOEHNE, Mareike	PhysProps	MARUM
HUUSMANN, Hannes	ROV	GEOMAR
JAEGER, Fabian Dominik	coring/Sedimentology	UIBK
KANG, Min-Hua	ROV trainee	TORI
KAUL, Norbert Emanuel	Heat Flow	MARUM
KIOKA, Arata	Hydroacoustics	AORI / UIBK
LANGE, Karl	Hydroacoustics	MARUM
LUEBBEN, Neeske	Geochemistry	MARUM
MATTHIESSEN, Torge	ROV	GEOMAR
MEIER, Arne	ROV	GEOMAR
MENAPACE, Walter	Sedimentology/Observatories	MARUM
MOCHIZUKI, Kenta	Coring/Sedimentology	Yamaguchi Univ.
MOERNAUT, Jasper	Hydroacoustics	UIBK
MOLENAAR, Ariana Willemina	Sedimentology	UIBK
MOORE, Gregory F.	Hydroacoustics	Hawaii Univ.
MU, Ling-Ji	ROV trainee	TORI
PIEPER, Martin	ROV	GEOMAR
REX, Marie Luise Pia Alina	Heat Flow	MARUM
ROESNER, Alexander	Observatories / PhysProp	MARUM
SCHWESTERMANN, Tobias	Hydroacoustics / Sedi.	UIBK
STRASSER, Michael	Sedimentology	UIBK

Participating Institutions:

AORI	Atmosphere and Ocean Research Institute, University of Tokyo, Japan
GEOMAR	Geomar, Kiel
Hawaii Univ.	University of Hawaii, USA
JAMSTEC	Japan Agency for Marine-Earth Science and Technology, Japan
MARUM	Center for Environmental Sciences, University of Bremen
MWJ	Marine Works Japan
TORI	Taiwan Ocean Research institute, Kaohsiung, Taiwan
UIBK	University of Innsbruck, Austria
Yamaguchi	University of Yamaguchi, Japan

2.2 Participants (crew)

Leg SONNE251-1, Yokohama - Yokohama, 04.10.2016 – 15.10.2016

NAME	Rank
MEYER, Oliver	Master
SOSSNA, Yves Michael	Chief Officer
HOFFSOMMER, Lars	2. Officer
BURZLAFF, Stefan	2. Officer
WALTHER, Anke	Ship's Doctor
LEPPIN, Joerg	Chief Electronic Engineer
PREGLER, Hermann Josef	System Manager
PLOEGER, Miriam	System Manager
HERMESMEYER, Dieter Karl-Heinz	Chief Engineer
STEGMANN, Tim Wolfram	2. Engineer
GENSCHOW, Steffen	2. Engineer
HORSEL, Roman	2. Engineer
ADAM, Patrick	Electrician
DE BUHR, Henning	Electrician
BLOHM, Volker	Fitter
TALPAI, Matyas	MPC / Motorman
MUENCH, Lothar	MPC / Motorman
LUEBKE, Rene	MPC / Motorman
GARNITZ, André	1. Cook
VOGT, Alexander	1. Steward
CAROLINO, Bernardo Orlanda	2. Steward
KROEGER, Sven	2. Steward
ROYO, Luis	2. Steward
SCHRAPEL, Max Karl Andreas	Boatswain
PAPKE, Rene	MPC / A.B.
KRUSZONA, Torsten Frank	MPC / A.B.
BIERSTEDT, Torsten	MPC / A.B.
VOGEL, Dennis	MPC / A. B.
KOCH, Stefan	MPC / A.B.
RIEGER, Willi	MPC / A.B.
SPRENKEL, Sebastian	MPC / A.B.

Leg SONNE251-2, Yokohama - Yokohama, 18.10.2016 – 02.11.2016

NAME	Rank
MEYER, Oliver	Master
GÖBEL, Jens Christian	Chief Officer
HOFFSOMMER, Lars	2. Officer
BURZLAFF, Stefan	2. Officer
WALTHER, Anke	Ship's Doctor
LEPPIN, Jörg	Chief Electronic Engineer
PREGLER, Hermann Josef	System Manager
PLÖGER, Miriam	System Manager
HERMESMEYER, Dieter Karl-Heinz	Chief Engineer
STEGMANN, Tim Wolfram	2. Engineer
GENSCHOW, Steffen	2. Engineer
ADAM, Patrick	Electrician
DE BUHR, Henning	Electrician
BLOHM, Volker	Fitter
HOFFMANN, Georg	MPC / Motorman
MÜNCH, Lothar	MPC / Motorman
BOLIK, Torsten	MPC / Motorman
GARNITZ, André	1. Cook
KOSANKE, Patrick	2. Cook
VOGT, Alexander	1. Steward
CAROLINO, Bernardo Orlanda	2. Steward
KROEGER, Sven	2. Steward
STEEP, Maik Ingo	2. Steward
SCHRAPEL, Max Karl Andreas	Boatswain
PAPKE, Rene	MPC / A.B.
KRUSZONA, Torsten Frank	MPC / A.B.
BIERSTEDT, Torsten	MPC / A.B.
VOGEL, Dennis	MPC / A. B.
KOCH, Stefan	MPC / A.B.
RIEGER, Willi	MPC / A.B.
SPRENKEL, Sebastian	MPC / A.B.

3. Research Program / Objectives

At the southeastern edge of the Eurasian Plate, Japan hosts two of the most interesting subduction systems, both prone to devastating megathrust earthquakes: The Japan Trench (JT) east of Honshu with subduction erosion/subsidence in the north, and the Nankai Trough (NT) with a huge accretionary prism in the southwest (Fig. 3.1). In 2011 the JT area was struck by a M9 earthquake that caused unusually large slip all the way to the trench, and a series of landslides, which are believed to be partly responsible for amplification of the catastrophic tsunami following the event. At Nankai, frequent M8+ earthquakes are also documented, and landslides and other sediment remobilization processes related to seismicity are attested. Despite the fact that either area has recently been the target of both IODP drilling (Exp343 vs 332/333/338/348), and MARUM cruises (SO219A vs. SO222) gaps in knowledge about causes and consequences of submarine earthquake, landslides and tsunamis remain. Advancing science with respect to this research themes is addressed in EAGER-Japan by (i) characterization and precise dating of extreme event layers, (ii) recovery of long-term instruments monitoring physical triggers to such events, and (iii) study geochemistry and fluid flow and link them to mass wasting in order to determine recurrence time and assess risk in two key scenarios: The mega-earthquake super-cycle in the subsiding, highly segmented Japan Trench, and records of megasplay slip in the Nankai region.

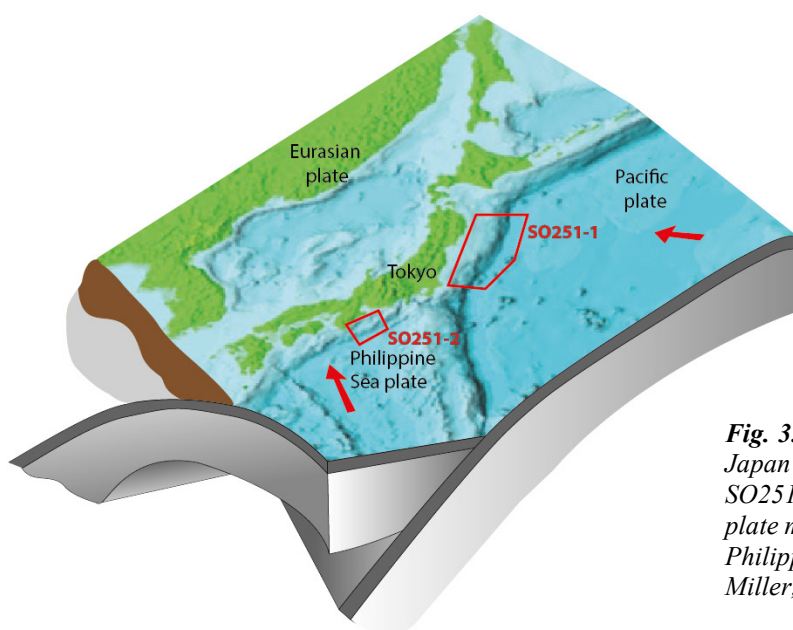


Fig. 3.1: Plate tectonic situation below Japan and outlines of working areas of SO251-1, and -2. Red arrows show plate movement direction of Pacific and Philippine Sea plate (Figure after Miller, 2008).

The overarching goal of R/V Sonne cruise SO251 and subsequent post-cruise research is to investigate fluid- and sediment mobilization processes by mud volcanism, earthquake-triggered seafloor displacement, submarine landslide and related “paleoseismologic event deposits” and to compare inferred earthquake processes and rates along accretionary vs. erosive subduction margins of Japan (Nankai Trough and Japan Trench, respectively).

The goals lie within four research categories, namely:

- 1) Deep Water coring in the Japan Trench and Nankai Trough to unravel paleoseismological records,
- 2) ROV dives to recover seafloor and sub-seafloor instruments in the Kumano Basin mud volcanoes,
- 3) Detailed high resolution seafloor surveys by ROV and accompanied coring on the continental slope and on mud volcanoes, and
- 4) Sedimentological and geotechnical post-cruise analysis and integration of all data, including those from cores, waters, and long-term instruments.

The work program was divided into two parts (Leg 1 conducted mapping and coring along the deep Japan Trench and along the upper slope and forearc escarpment from 36°N to 40°N; and Leg 2 to the Kumano Basin in the NT area to pick up instruments in the mud volcano field by ROV followed by further mapping, coring and detailed video surveying of seafloor in the Kumano Basin, the forearc high and the shallow splay fault area.

Post-cruise science will be coordinated among the international science party. With SO251 we will establish a bathymetric and sedimentary inventory of mass-movements, chronology of extreme-event deposits and their paleoseismologic interpretation. It further will investigate geotechnical aspects of earthquake-triggered mass wasting processes to allow for quantitative interpretation and comparison of the established event catalogue. We also will illuminate the relationship between mud volcanic activity (mudflows, seepage, etc.) and local seismicity by using long-term data, time series samples and additional core/data from the cruise. Anticipated conceptual advance in our understanding of sediment dynamic processes related to subduction zone earthquakes are expected to be transformative and may well apply for other active convergent margins worldwide, not just Japan and the circum-Pacific.

4. Setting of the working area and previous work

Japan Trench

Along the Japan Trench lower Cretaceous (~130 Ma) Pacific oceanic crust subducts below Japan in a west-northwest direction at an average rate of about 8 to 8.5 cm/year (Figure 3.1; DeMets et al., 2010). The bulk of the forearc is composed of Cretaceous accreted strata (Tsuru et al., 2000) discordantly overlain by thick forearc basin fills and thinner slope apron sediments. The sedimentary strata in the upper part of the forearc basin and slope apron Neogene-to-Quaternary stratigraphic succession is mainly composed of diatomaceous-hemipelagic mud and volcanic ash (Scientific Party, 1980; Sacks et al., 2000), reflecting the influence of high oceanic productivity, the interplay between the cool Oyashio and warm Tsugaru and Kuroshio currents, and arc volcanism as main sediment source.

Tectonic history in the convergent margin near the Japan Trench is characterized by tectonic subsidence and erosion: The absence of young accreted strata in the forearc, as well as multichannel seismic records (e.g. Scientific Party, 1980; Tsuru et al., 2000; Kodaira et al., 2012; Nakamura et al., 2013) attest that most of the sediment entering the trench is subsequently subducted. The Scientific Party (1980) demonstrated progressive subsidence of the seafloor by vertically transient benthic biofacies and lithofacies observed in the forearc basin sediments. The subsidence is associated with subduction erosion of the continental slope and forearc wedge related to the subduction of the Pacific Plate, which also caused the trench to retreat an estimated 50-75 km (e.g. von Huene and Lallemand, 1990). Furthermore the Neogene-to-Quaternary sediment sequence is cut by several landward-dipping normal faults spaced ~10 to 15 km apart (Tsuji et al., 2013). As typical for erosive subduction margins characterized by outer-forearc subsidence, extensional features dominate the structural grain, with mass wasting as a consequence. Detailed textural and structural analysis of multibeam bathymetry data by Sasaki (2004), Kawamura et al., (2012), Strasser et al., (2013) and Tappin et al., (2014) shows evidence for both smaller and larger scale submarine landslides and gravitational slope collapse structures. Gravitational mass wasting along the forearc slope, overall, is likely related to the tectonic evolution characterised by tectonic subsidence and erosion (Sasaki 2004; Ogawa 2011) as documented for other erosive subduction margins (von Huene et al., 2004). Individual mass wasting events are often hypothesised to have ultimately been triggered by earthquakes and have also been proposed as a new scenario for amplification of tsunami (e.g. Kawamura et al., 2012; Tappin et al., 2014).

Much of the focus in the JT area is (and has been during cruise SO219A; Wefer et al., 2014) on the consequences of the 2011 Tohoku-oki earthquake and its subsequent tsunami, which hit the Pacific coast of Honshu peninsula with waves up to 38.9m in height, caused 15'883 deaths, 6'145 injured people and 2'671 people that are still listed as missing (National Police Agency of Japan). It is the first destructive event of its kind

whose entire activity was recorded by a modern dense geophysical network located close to the rupture zone. A striking feature common in all data sets is the evidence for co-seismic rupture propagation to the trench (Yokota et al., 2011; Tajima et al., 2013). This shallow slip along the plate boundary fault resulted in co-seismic horizontal displacement of the seafloor, >50 m toward the East and up to 10m vertical (Fujiwara et al., 2011; Ito et al., 2011), and significantly contributed to the generation of the destructive tsunami (Yokota et al., 2011). Prior to the 2011 Tohoku-oki earthquake, such large co-seismic slip at the toe had never been expected from available data sets and from commonly accepted models. Seismicity has been recognized to be highly variable along-strike in the Japan Trench with occasional large-magnitude events with M_w 7 to 8 (Yamanaka and Kikuchi, 2004). The Jogan earthquake of 13 July 869 may be the only documented event to have occurred with a possible magnitude and location similar to that of the 2011 earthquake (Minoura et al., 2001). Similar, but comparably lower-magnitude events, have occurred to the north and south of Tohoku-oki rupture zone, such as the 1896 Sanriku earthquake and ensuing giant tsunami (Tanioka et al., 1996), and the 1454 Kyotoku, 1611 Keicho and 1677 Enpo Boso event to the south (Sawai et al., 2015; 2012; Hatori, 2003). Exact rupture areas and modes of these past events, however, are not well determined.

From the IODP rapid response J-Fast Expedition 343 and other rapid response marine geology research cruises, including S0219A, we learned fundamental characteristics about large slip to the trench: (i) the co-seismic displacement reached all the way to the trench axis with a nearly completed stress-drop (Lin et al., 2013) (ii) the co-seismic megathrust slip was confined to a narrow (<5 m) zone of a very weak clay layer on the Pacific Plate (Chester et al. 2013; Fulton et al. 2013; Ujiie et al., 2013); (iii) trench-fill sediments are deformed by trenchward movement of the overriding block (Kodaira et al., 2012; Strasser et al., 2013). Furthermore, several, submarine landslides were documented on the landward slope of the trench (Fujiwara et al., 2011; Kawamura et al., 2012, Strasser et al., 2013; Fink et al., 2014; Tappin et al., 2014). Slope failures and large scale sediment remobilization and seismoturbidite deposition is also attested by measured turbidity in the bottom waters (Noguchi et al., 2012; Oguri et al. 2013), ocean bottom instruments data (Arai et al. 2013) and comparison of sea-floor images before and after the earthquake (Fujiwara et al., 2011; Strasser et al., 2013; Tappin et al., 2014). In particular, cores document distinct earthquake-related event deposits in the trench, on mid-slope terraces and in fault-bounded basins along the forearc (Figure 4.1; Ikehara et al., 2016; McHugh et al., 2016; Yoshikawa et al., 2016, Usami et al., in press). While earthquake-triggered submarine landslides and/or tsunami back-wash are possible mechanism to generate the sediments transported into basins to form event deposits, also remobilization of surficial sediment (i.e. only a thin veneer of a few cm of the uppermost youngest sediments mobilized over large areas affected by strong seismic shaking) has been recently proposed based on new knowledge gained from studying the Tokoku earthquake to be a potential key mechanism for generating earthquake event deposits (Mc Hugh et al., 2016; Moernaut et al., 2017).

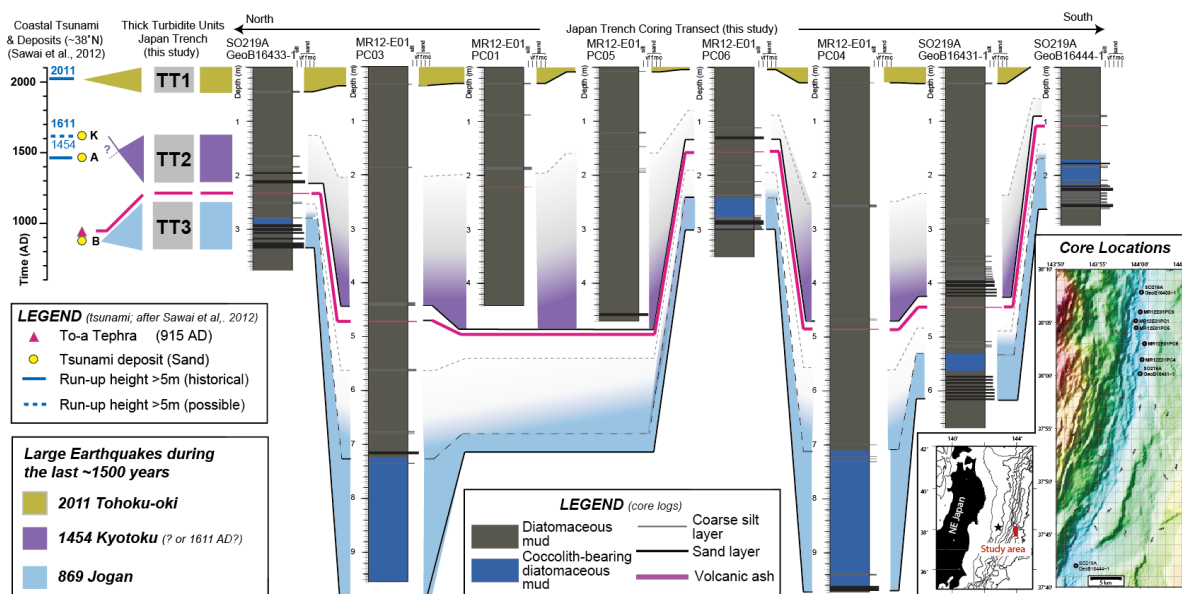


Fig. 4.1: Stratigraphic correlation between cores from two isolated trench-fill basins along the Japan Trench. The records preserve evidence for three major sediment-remobilization events (referred to as thick turbidite units (TT-units)). Also shown is correlation of TT-units to coastal tsunami deposits (Sawai et al., 2012), and inferred occurrence of three earthquakes with similar effects as the 2011 Tohoku earthquake (Ikehara et al., 2016).

High sedimentation rates (5-10 m/kyrs) and most distal sedimentary setting of the Japan Trench indicates high preservation potential of the earthquake-related event deposits in trench-floor basins, which typically have isolated depocentres related to the subducted seafloor morphology (horst-graben structures on the Pacific Plate; Figure 3.1; 4.1 [inset]). More strikingly, the cores further document at least two older turbidite units, which correlate throughout cores taken from separated trench-floor basins 50km apart in central part of the Japan Trench axis (Figure 4.1). Interbedded volcanic ashes provide tephra-chronological age control suggesting that the prominent event deposits correlate to the Jogan tsunami of 869 A.D., and to the 1454 A.D. Kyotoku event (Ikehara et al., 2016); thus, large-scale resedimentation events recorded as widespread turbidites occur less frequent despite the generally high seismicity with M7-8 earthquakes occurring regularly every few tens-to-hundreds of years. This finding supports the hypothesis that the seismo-turbidite record in the trench floor basin is representative for exceptionally large events of a super-earthquake cycle with longer recurrence intervals. However, conclusive interpretation of earthquake recurrence and rupture segmentation remains elusive. During SO251-1 we added important new data and cores that significantly increase the spatial resolution of data coverage along the entire Japan Trench and that provide samples to investigating the source areas and its slope stability conditions during seismic shaking, in order deconvolve the geological record for the source and intensities of earthquake shaking.

Nankai Trough

In the Nankai Trough, the geology of the central and southwestern Japan consists of a series of Mesozoic and early Cenozoic accretionary complexes (Maruyama et al., 1997). The most recent phase of subduction-accretion began approximately 6 Myrs ago (Kamata and Kodama, 1999; Clift et al 2013). Since then, the Nankai Trough is formed by subduction of the Philippine Sea plate to the northwest beneath the Eurasian plate at a rate of ~4.1–6.5 cm/y (Miyazaki and Heki, 2001). The convergence direction is slightly oblique to the trench, and Shikoku Basin sediment is actively accreting at the deformation front. The SW-NE striking accretionary wedge thus mainly consists of scraped-off strata from the incoming trench fill and Shikoku Basin. The upper slope of the Nankai Trough contains several prominent forearc basins (Muroto, Tosa and Kumano), which intercept sediments emanating from small canyons and slope gullies. The Nankai margin has been the target for several DSDP, ODP, IODP and MeBo drillings. The most recent IODP-NanTroSEIZE and previous MARUM-SO222 expeditions focus on the Kumano-nada area. In this area, along a margin-perpendicular transect (i.e. Kumano transect) from SE to NW, the trench zone consists of a thick wedge of Quaternary trench deposits overlies Miocene-Pliocene Shikoku Basin sediments and subducting igneous basement. Landward of the deformation front a series of thrust packages reflecting past in-sequence thrusting and accretion, emplaced within the last ~1.5 Myrs (Strasser et al., 2009) are overlain by Quaternary slope sediments deposited in slope basins within the ridge-basin topography typical of accretionary prisms. Beneath the upper slope and Kumano forearc Basin, a regional splay fault system (Megasplay fault zone; MSFZ), discontinuously cuts across the older part of the accretionary prism (Moore et al., 2007, 2009). The shallow part of the MSFZ is a complex thrust system with backwards breaking branches that truncate the imbricate thrust faults within the accretionary prism and override younger slope basin sediments (Moore et al., 2007). Interpretation of 3D reflection seismic data and geological information from nearby IODP drill document a complex temporal and spatial evolution of the MSFZ and anticline-structures in the underlying accretionary prism since about 2 million years, characterized by alternating periods of high and low structural activity on individual structural segments (Strasser et al., 2009; Kimura et al., 2011).

Landward of the MSFZ and the forearc high, the Kumano forearc basin infill comprises more than 1 km of Quaternary sediment. The seaward portion of the basin section is progressively tilted toward land because of repeated motion on the megasplay fault (Park et al., 2002; Moore et al., 2016). In the landward part of the Kumano-transect about a dozen mud volcanoes have been mapped and sampled during SO222 (Kopf et al., 2013). Interestingly, the active features are characterized by gas-rich mud with variable amounts of gas hydrate chips and clasts of various lithologies. As can be seen from deep seismic reflection data, the origin of these MVs goes back to older accreted series equivalent to the Shimanto Complex onshore.

The Nankai Trough region has a 1300 year historical record of recurring great earthquakes that are typically tsunamigenic, including the 1944 Tonankai M_w 8.2 and

1946 Nankai M_w 8.3 earthquakes (Ando, 1975). The reconstructed record shows that great earthquakes repeated every 100–150 yrs in each segment, and occasionally much greater multisegment earthquakes occurred. The rupture area and zone of tsunami generation for the 1944 event (within the study area) are now reasonably well understood: Seismic waveform and tsunami inversion data suggested that earthquake slip propagated along the megasplay near to the surface (Baba et al., 2005). Co-seismic slip in the shallow megasplay fault zone has also been proposed from vitrinite reflectance and elemental distribution data from IODP cores evidencing past frictional heating by seismic slip (Sakaguchi et al., 2011a; Yamaguchi et al., 2011). Strikingly, similar data sets from the décollement zone near the toe of the prism also suggest that co-seismic slip can propagate to the trench (Sakaguchi et al., 2011a), suggesting that earthquake rupture may have variable modes. Understanding the variable modes of slip propagation near the seabed is essential for assessing the tsunami potential of individual megathrust ruptures, as the resulting tsunami wave hitting the coastline will have different wave parameters if mainly triggered by movement of the megasplay hanging-wall or seaward-shift of the whole outer accretionary prism.

The history and mode of slip (e.g. megasplay rupture vs slip propagation to the toe) of older historic earthquakes and certainly prehistoric earthquakes is very poorly constraint. A promising approach towards filling this gap comes from thin mud-breccia layers that formed during strong ground-shaking in the surficial sediment near the water-sediment interface in the hanging-wall block of the mega-splay fault and which are dated to have occurred frequently but with recurrence intervals significantly longer than the classical 100-150 yrs (Sakaguchi et al., 2011b). However, mud breccia layer in the MSFZ have so far only been investigated in one single IODP core (Site C0004; location see Figure 4.2).

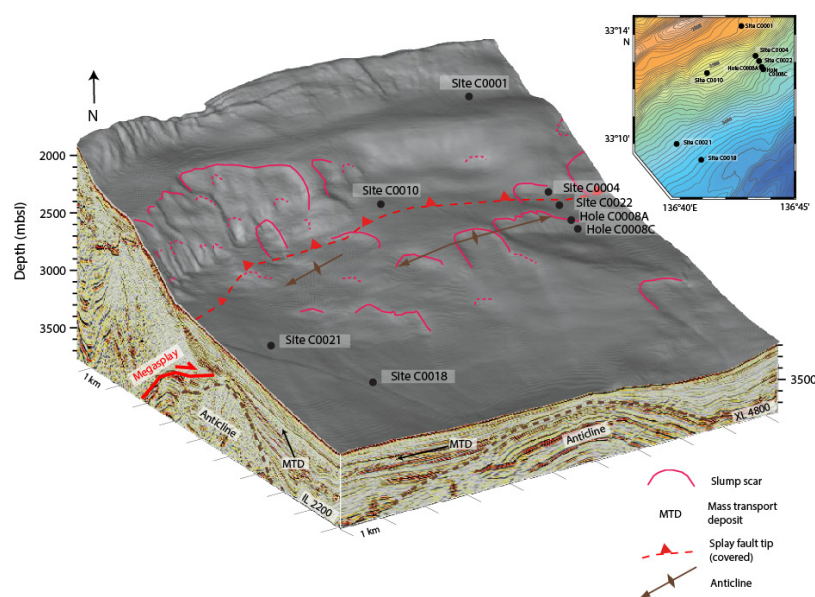


Fig. 4.2: 3D-perspective view of the shallow megasplay fault zone area evidencing landslides scars near the tip of the megasplay fault zone. Black dots indicate IODP Sites (Fig. after Strasser et al., 2011).

Information on recurrence patterns of earthquakes may also come from seismo-turbidite stratigraphy in the Kumano Basin. However, deposition from sediment-gravity flows in the Kumano Basin is also largely influenced by sediment supply by rivers via submarine canyons (Omura and Ikehara 2010). Previous studies have shown that climate and sea level changes take over the first order control on Holocene and Pleistocene turbidite deposition in the main depocentres of the Kumano Basin. Preliminary results from cores of SO222, which recovered the deposits of frequent turbidite events sufficiently energetic to affect the elevated seafloor on top of some inactive mud volcanoes, suggest that the stratigraphy there presents a reliably paleo-seismic archive unaffected by mud extrusion but capturing the most significant events (Kopf et al., 2013). Up to 33 of these turbidites can be found in one core. These turbidites are very regularly spaced and are hypothesised to represent the seismic cycle. The exact recurrence intervals are currently being dated, and expedition SO251 gained more such cores in strategic places in the Kumano Basin area.

In addition to paleoseismology, products of submarine mass movements have been identified in geophysical or core data for slope stability research (see references in Strasser et al. 2011; and more recently Ikari et al 2011; Kawamura et al. 2012; Strasser et al., 2012, Kitamura et al., 2014; Amsler et al., 2014; Alves et al., 2014). In IODP expeditions 333 and 338 two sites were drilled and logged within the slope basin seaward of the megasplay fault to sample stacked mass-transport deposits (MTDs) clearly imaged in the 3D seismic data set (e.g. Strasser et al., 2011, 2012; 2014; Fig. 4.2). The recovered section records ~1 Million years of submarine landsliding history in this active tectonic setting. However, the spacing between individual MTDs suggests submarine slope destabilisation does not occur systematically during subduction earthquakes. In contrast, the landslide recurrence pattern suggests that geological preconditioning factors may exert the first-order control on destabilization processes and MTD formation in the mega-splay fault zone area (Strasser et al., 2012). Another possibility is that the sediments could be consolidated and strengthened during low magnitude events, which do not generate enough seismic shaking induce failure (Lee et al., 2007; Strozyk et al., 2010; Sawyer and DeVore; 2015).

The project Sonne SO222 MEMO, **MeBo** drilling & in situ long-term **Monitoring** offshore Japan (Nankai Trough Accretionary Prism), set out in 2012 to use active mud volcanoes in the northern Kumano Basin as indicators of seismic activity (Tsunogai et al., 2012). These features carry deep-seated fluids, most likely tapping into the seismogenic zone at a depth of several km below seafloor, and are also overlying an area of high strains and a locked plate boundary-thrust. Cruise SO222 sampled both mud volcanoes and background sediments and installed long-term monitoring devices in selected mud domes to use the P and T records as a proxy for strain and fluid flow. Operations at the time included the successful installation of 4 MeBo borehole observatories in a total of six holes drilled in appx. 2 km water depth (Kopf et al., 2013, 2015), and of an additional 6 CAT flowmeters.

5. Narrative of the Cruise

Leg SONNE251-1, Yokohama - Yokohama, 04.10.2016 – 15.10.2016

By September 30, all 29 scientists of the SO251-A science party safely arrived in Yokohama, Japan, and embarked research vessel *Sonne* on Oct 1st. Unfortunately, our scientific equipment, which was shipped from Bremen by a carrier that declared insolvency while the containers were on their way to Yokohama, did not arrive. Nevertheless, and thanks to the great support by our Japanese colleagues from JAMSTEC, the Geological Surveys of Japan, and the University of Tokyo, that kindly provided coring and laboratory equipment for our research cruise on very short notice, we could start our voyage with nearly complete infrastructure and a delay of 2 ½ days to leave the harbor on Tuesday Oct. 4 at 15:00.

The working area of the first part of the SO251 expedition, the Japan Trench, was reached after a transit of 17h. After a first CTD Station and two short multibeam bathymetry and sediment echo sounder mapping surveys, we successfully retrieved a piston core (GeoB21804) from the deepest part of the Japan Trench in more than 8000 m water depth. From Wednesday Oct 5 we conducted detailed mapping and coring along the trench axis from S-N to have arrived in the northern part of the study area by Sunday, Oct 9. Piston coring operation included successful recovery of two nearly 10 m long cores from the very deep trench basins in the >7000 m deep Japan Trench (GeoB21809 and GeoB21812). Furthermore, at stations GeoB21810 and GeoB21815, we sampled two 5 m long cores from the slope.

Starting late evening on Sunday Oct 9 and continuing into Monday Oct 10, we acquired a 175 km long East-West bathymetric profile perpendicular to the margin at 39.3°N. Followed by detailed Multibeam and Parasound mapping along the trench axis to the North, we arrived at the northernmost station (GeoB21817) of our expedition on Tuesday, Oct 11 to take a 10 m long core from the trench basin infill. At the same day, we also managed to obtain a double coring of the slope sediment in the northern part (GeoB21818). On Wednesday, Oct 12, R/V *Sonne* navigated back southwards, while filling small gaps in mapping to eventually succeed in acquiring a complete high-resolution bathymetric map of the trench axis and nearly 2000 km of sub bottom Parasound profiles, covering the entire along-strike extent of the Japan Trench from 36° to 40.3° N. On our voyage back south there remained enough time to take two additional cores in the deep trench (GeoB21821 and GeoB21823). On the early morning of Oct 14, we finished operations of Leg SO251-A, and after transit back to Yokohama, the first leg ended on Saturday October 15 at 8 o'clock in the morning.

A map of the tracks covered is seen in Figure 5.1.

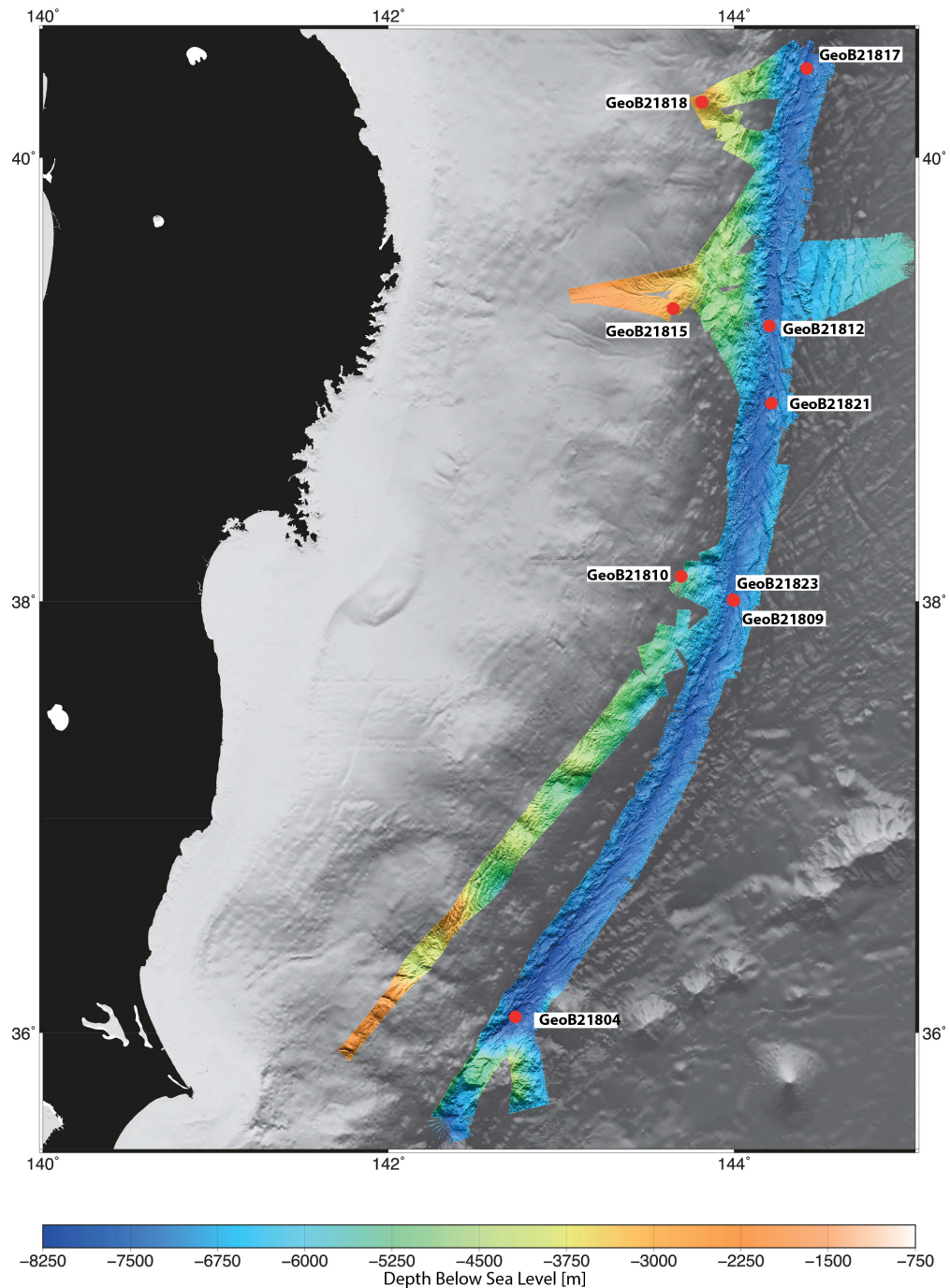


Fig. 5.1: Track chart of R/V SONNE Leg SO251-1 in the Japan Trench, including coring locations.

Leg SO251-2, Yokohama - Yokohama, 18.10.2016 – 02.11.2016

RV Sonne was in Yokohama port from 15-18 October in order to load and mobilize the heat flow probe as well as the remotely operated vehicle PHOCA of our colleagues from GEOMAR Kiel. Despite the delivery of ROV PHOCA on very short notice because of the stranded expedition equipment on HANJIN vessels, the harbour test was successful. In Yokohama we also had visits from several groups from JAMSTEC and CDEX to RV Sonne and discuss scientific strategies. We also had a visit from GOOGLE Culture videographers. The footage will shortly be available as a virtual ship's tour of the RV Sonne via the internet.

The SO251 science party was partly exchanged to meet the requirements in the second study area, the Nankai Trough subduction zone. On 18.10. at 8 o'clock, RV Sonne departed and reached the Kumano forearc basin later the same day. The scientific work started with heat flow measurements across a mud volcano and along a N-S profile across the Kumano Basin, which complements data from cruise SO222 in 2012. During the 3rd week of the expedition, we had three dives with ROV PHOCA on mud volcanoes where we had placed instruments in 2012. In the periods between diving, we carried out hydroacoustic surveys during which we found indications for fluid seepage on mud volcanoes and other topographic features. Cores were taken on a new MV#14, of the Kumano Basin fill, and other MVs (Figure 5.2). On Oct 23 we had bad weather conditions and decided to head for Yokohama again where a Japanese coring technician had to depart.

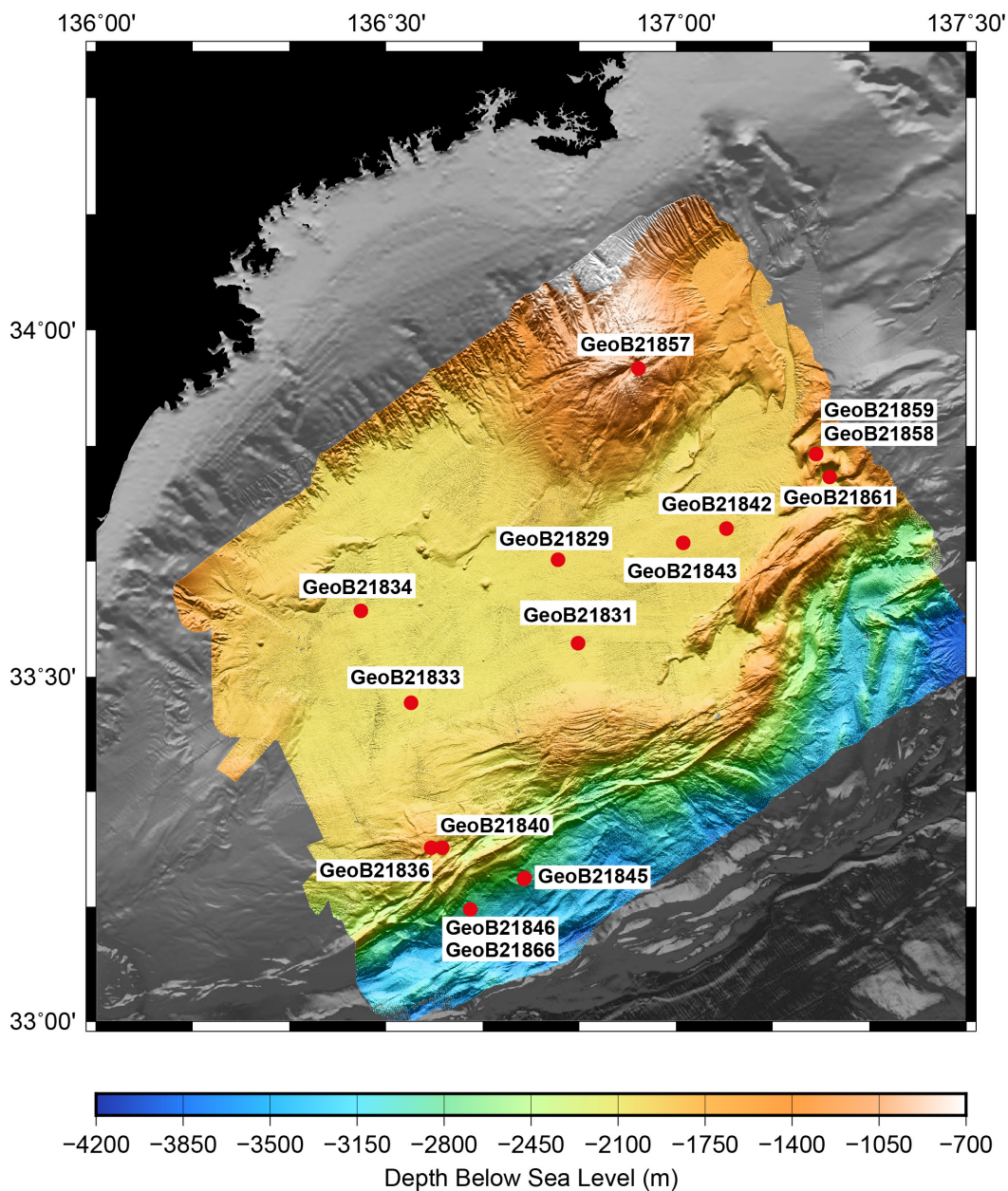


Fig. 5.2: Track chart of R/V SONNE Leg SO251-2 in the Nankai Trough area, including coring locations.

After returning to the study area again on Oct 24, the weather had improved and heat flow, geophysical surveys and ROV operations continued. The final week of SO251 started with the successful recovery of a MeBoPLUG observatory and T-stick (GeoB21853) as well as the recovery of the SmartPlug-piezometer. Since the geophysical acquisition allowed us to identify new, previously unknown sites of flare activity, we also converted the heat flow probe as coring device and from Oct 29 onwards then sampled the seafloor again on suspected MV sites, an isolated pond, and the Nankai slope outboard of the splay fault.

On subsequent dives, we also recovered a second set of MeBoPLUG observatory and T-stick (GeoB21856) as well as the most precious observatory, a MeBoCORK-A by using a second wire. This final dive on Oct 31 terminated the observatory recoveries and shifted the focus towards coring and mapping again. All station work was very successful and the main goals of the cruise were reached. For tracks covered during leg SO251-2, refer to Figure 3.2.

On Nov 01 at appx. 14.30h we finally departed from the study area and steamed towards Yokohama a third and final time. RV Sonne met the pilot at 5 a.m. on Nov 02 and docked about 2.5 hrs later.

6. Methods

6.1. Hydroacoustics

(J. Moernaut, C. Ferreira, M. Asada, A.K. Bachmann, T. Fujiwara, A. Kioka, K. Lange, G. Moore, T. Schwestermann, T. Sun)

RV SONNE is equipped with a suit of hydroacoustic techniques including the KONGSBERG multibeam echosounder EM122 as well as ATLAS PARASOUND P70 sediment echosounder. These techniques provide images of the sub-seafloor, the seafloor, and the water column above the seafloor. The multibeam systems are routinely used to obtain bathymetry of the seafloor, but also include acquisition of acoustic images of the water column. Seafloor properties such as seabed roughness, sediment density, or seafloor inclination may be obtained using the backscatter information of the beams. PARASOUND has the advantage of providing a composite view of the water column (18 kHz signal) as well as the sub-surface (4 kHz signal), in ideal sites up to 150 m below seafloor.

The main intention of using the multibeam system during SO251 was to obtain high-quality bathymetry along the Japan Trench and in the Kuman Basin area to identify mass-wasting and mud-volcano related features. Repeated bathymetric mapping of profiles crossing the trench are performed to compare bottom morphology before the Tohoku earthquake (March 2011), one year after this event (cruise SO219 in March 2012) and nowadays (5.5 yrs after the event). Subbottom profiles were used for accurate core site selection, to obtain general stratigraphic information at the core sites (core-to-seismic integration) and to map the spatial extent of large mass-wasting and mud-volcano related deposits. A summary of all hydroacoustic surveys is given in the Appendix Table 11.1.2.

6.1.1. Bathymetric mapping (multibeam EM122, incl. CTD, XSV and XCTD)

(C. Ferreira, M. Asada, A.K. Bachmann, T. Fujiwara, G. Moore, T. Sun)

The EM 122 KONGSBERG multibeam echosounder operates at 12 kHz. The transducers have a nominal opening of 0.5° in along-track direction and 1° in across track direction. The multibeam echosounder is capable to record up to 433 individual beams across track within a swath of up to 140°. However, due to insufficient data quality in the outer beams, the maximum swath width used during this cruise was 120°.

Actual sound velocity profiles were recorded with the ships CTD and XSV and inserted as basis for optimized performance. Data were recorded in *.all files and processed with software MB-System (Caress and Chayes, 1996) onboard. During the second leg SO251b, we also tested deployment an XCTD probe (eXpendable Conductivity, Temperature and Depth, TSK, <http://www.tsk-jp.com/>) from JAMSTEC. The XCTD probes measures temperature and electrical conductivity of seawater from moving platforms to calculate sound velocity profiles from the drop rate of the probes. However,

unfortunately, the software of the *WinMK-21* system on RV SONNE did not recognize the XCTD-4 probe from JAMSTEC. Therefore, we could not obtain any results from XCTDs during SO251b.

6.1.2. Sediment echo sounding (With Parasound P70)

(J. Moernaut, T., Kioka, A., Lange, K., Moore, G., Schwestermann, T.)

The ATLAS PARASOUND echosounder emits two primary high frequencies (PHF) of ~18 kHz and ~22 kHz. Non-linear interference of the high frequencies produces a secondary low frequency (SLF) of about 4 kHz. This SLF is used for sub-seafloor imaging. Opening angle of the transducer is ~4°, which corresponds to a footprint size of about 7 % of the water depth. The program PARASTORE is used for storing and displaying echographs. The settings applied in PARASTORE for PHF and SLF displaying are variable and dependent on the actual performance influenced by, e.g., water depth and weather conditions. For SLF subbottom imaging filtering was set to: Low pass: on, Iteration: 1, high cut: 6 kHz. The pulse length was set to 1 ms (4 periods per pulse) or 0.25 ms (1 period per pulse) depending on the signal-to-noise ratio. The sampling rate was set to 12.2 kHz and receiver bandwidth to 33% on SO251A, whereas on SO251B we used values 6.6 kHz and 66%, respectively. For the shooting rate, we used “single pulse” in deep areas and areas of complex morphology, whereas “quasi-equidistant” was used in most of the relatively flat and shallow (~2000 m deep) Kumano Basin. Three file formats are recorded during PARASOUND operations: *.asd files (raw data), which contain data of the entire water column as well as the sub-seafloor. PARASTORE produces *.ps3 files and the auxiliary data (navigation files). The depth range of the *.ps3 files was set identical to those of the online display window. In case the recorded window was not positioned optimally (i.e. missing the seafloor), we reproduced the *.ps3 files by replaying the *.asd files in PARASTORE. The option “without phase and carrier” has been selected as the software did not allow us to store the phase and carrier when using a sampling rate of 12.2 kHz or higher. Therefore, the displayed data actually represents the envelope of the seismic trace, and thus only contains positive amplitudes. *.ps3 files were combined and converted into *.sgy files using the software PS32SEGY. We stored the coordinates in the UTM projection (UTM zone 53 for Leg2 and UTM zone 54 for Leg1) within the seg-y header. *.sgy files were imported into IHS KINGDOM SUITE 2015 for quality analysis, core site selection and preliminary mapping.

6.2. Remotely Operated Vehicle (ROV) Deployments

*(F. Abegg, M. Pieper, A. Meier, P. Cuno, H. Huusmann, I. Suck, T. Matthiessen:
ROV-TEAM, GEOMAR Kiel)*

The work class ROV PHOCA was intended to search and recover long-term observatories on various mud volcanoes in the Nankai Trough. The observatories had been deployed by MeBo in 2012 during SO222.

ROV PHOCA is a 3000 m rated deep diving platform of the type Comanche, this is build No. 21. manufactured by SubAtlantic/ FET, Aberdeen, Scotland. As an electric work class ROV of the type Comanche, this is build No. 21. ROV PHOCA.

It is based on commercially available ROVs, but customized to scientific demands, e.g. being truly mobile. ROV PHOCA has previously been operated from the medium sized German research vessels RV POSEIDON and RV ALKOR. It is based at the Helmholtz Centre for Marine Sciences GEOMAR in Kiel, Germany.

The ROV is propelled by 7 SPE-250 Thrusters, four of them for lateral and three for vertical movement. It is equipped with two SD Cameras on pan / tilt units. A still photo camera (15MP) is mounted also on a pan/tilt unit, and is connected to a flash, mounted in the light rack of the ROV. An HD camera is mounted on a tilt unit at the front bottom center of the ROV. Additionally two black and white cameras are monitoring the front of and the cable on top of the ROV, respectively. 4 LED and 4 Halogen lamps are mounted on the front and top of the ROV.

ROV PHOCA (Figure 6.2.1) is furthermore equipped with a Seabird CTD, a SONAR MS 1000, two hydraulically driven manipulators: the starboard manipulator is a position-controlled (using a 'master-arm' as remote control) 7 function ORION (Schilling) while on the portside of the vehicle a rate-controlled 7 function ORION is mounted. Underneath of the ROVs main body the tool skid is located onto which a variety of tools to customers demand can be mounted and which contains to hydraulically driven sample trays /boxes. Hydraulic power is generated by a hydraulic pump of 15kW.

The deep water winch, manufactured by Hatlapa (Germany), contains 2500 m of 19 mm Aramid armoured wire with three copper and 3 fiber optics cables. 3000V by 400 cycles are transmitted to power the ROV.

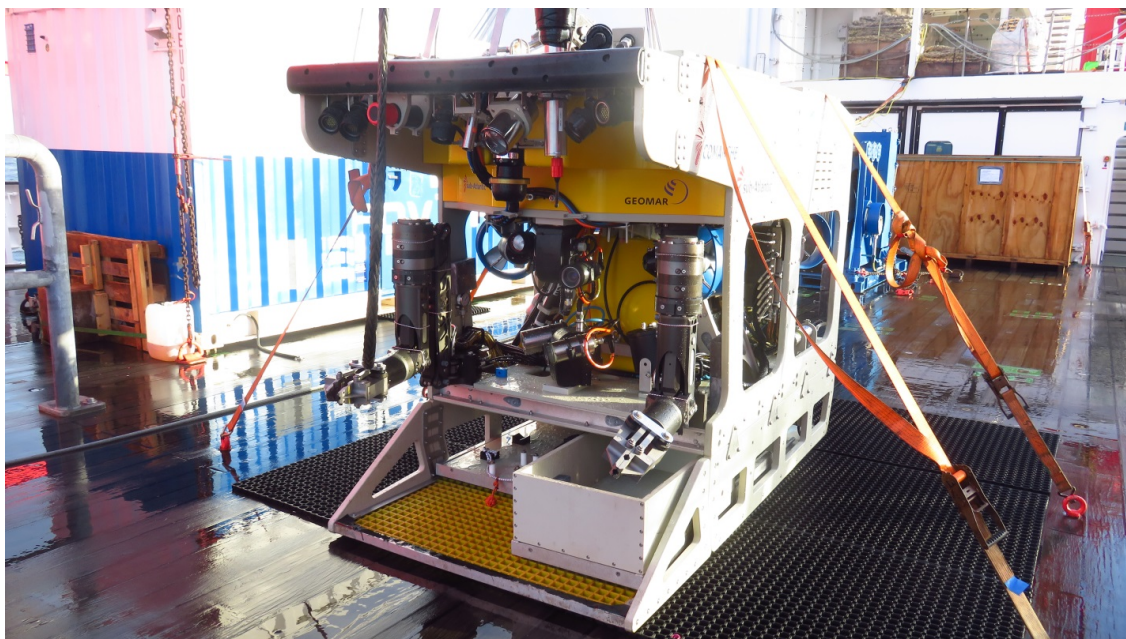


Fig. 6.2.1. ROV PHOCA on the aft deck of RV Sonne.

PHOCA is launched using a Launch and Recovery System mounted on the A Frame of RV SONNE, being lifted by an auxiliary winch/rope. The wire is running through a sheave also mounted on the A Frame.

For underwater navigation, a mobile IXSEA MiniTransponder supplied by RV SONNE was mounted on the ROV, which proved to be problematic as at a certain depth the background noise (including the ROVs own noise) seems to have become too much for the transponders to communicate. For the last dives the navigation has been optimised and worked almost properly.

6.3. Observatories

(A. Kopf, T. Fleischmann)

6.3.1. MeBo CORKs

The general principle of a CORK has to be minimized in case of MeBo, where conical threads and a diameter of only 98-110 mm have to be sealed. Space is hence most seriously governing the design of the CORK, which has to seal the inner borehole from the overlying ocean body, and which also has to host the connection of the borehole tubings to the actual observatory unit. During SONNE cruise SO222 (Kopf et al., 2013), we installed one MeBoCORK observatory. First, the MeBo hole was prepared for long-term instrumentation after coring is completed; for that we left several pieces of MeBo outer drilling rods to act as a casing and stabilize the upper seafloor portion, where the deposits are poorly consolidated and otherwise may close in. Only the lowermost part of the hole is free of “casing” and provides direct access to the formation. A string of 2 armored PTFE tubes is coiled up in the lower part of the MeBo-set observatory unit (termed MeBoCORK A, where A stands for “autonomous”, i.e. MeBo by itself is capable of placing a stand-alone observatory), namely in the lower portion of the “adapter” hosting the receptacle for the hotstab. Once the drilling device has set this

piece, the coil of tubing is unlocked and a dead weight favors the tubing's descent towards terminal depth where the hole is open. The upper end of the individual tubings connects to borings of the hotstab receptacle. The lower unit also hosts battery packs.

The upper portion of the MeBoCORK A hosts the data transmission unit, data logger and transducers, the latter of which are connected to the borings of the male hotstab end (Fig. 6.3.1). The hotstab is mated with its female counterpart, and the two halves of CORK A are further secured by a bayonet connector that allows coupling of the MeBo top drive and hence torque being transmitted (in clockwise direction only!). During installation MeBo fully screws in the entire CORK instrument, which in total is the exact length of a regular MeBo drill rod and which sits on the magazine with the other rods. Once this piece is properly set, MeBo pushes the unit to a depth so that only the titanium part (ca 70 cm long) sticks out of the seafloor and then takes off. In the initial design, this simple, MeBo-set CORK monitors pressure and temperature, which are both indicators for deep-seated fluid flow; pore pressure is additionally valuable as strain proxy (see above). Depending on the sampling rate, the batteries will allow monitoring for many months to a few years (in case of the system deployed during leg SO222A = 7 months).

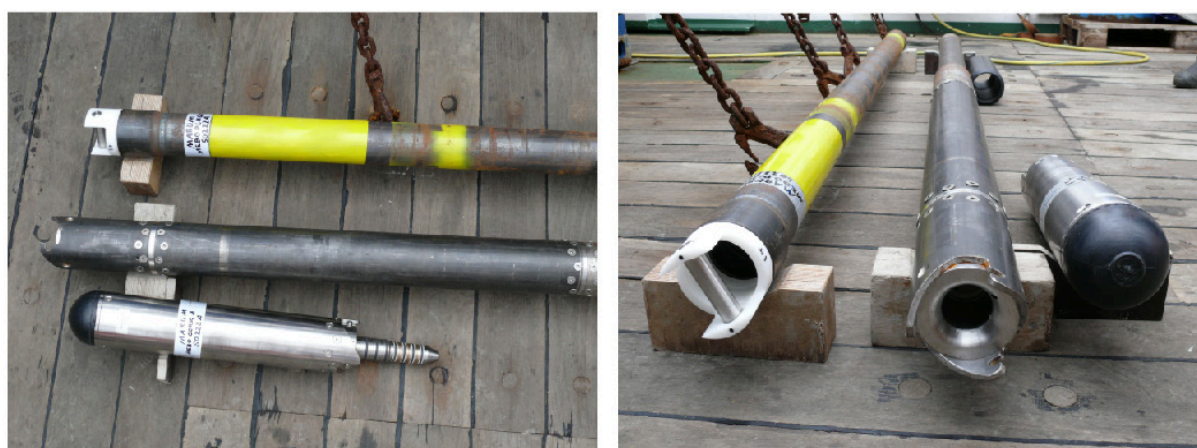


Figure 6.3.1: MeBoCORK A (=autonomous) as well as MeBoPlug for comparison. See text.

6.3.2. MeBo Plugs (and MTL-sticks)

In addition to the MeBoCORK, we used standard RBR data loggers with Keller differential pressure transducers for monitoring strain in the boreholes. For this, plugs from POM were manufactured to seal the conical threads of the uppermost MeBo drill pipes (Fig. 6.3.2). At the top, a handle designed to specification of the ROV *Quest* manipulator was added. In the borehole-facing section, a thermistor as well as the downward-looking P port are situated (Fig. 6.3.2, inset). Given that only one thermistor was fitted into the so-called MeBoPlugs (named in analogy to the so-called SmartPlug terminology in IODP), we are lacking a temperature record from the seafloor (i.e. upward-looking). In order to overcome this shortcoming, a simple self-contained device for seabottom T monitoring was designed and deployed by ROV (see next section). The sampling rate of the MeBoPlugs was set to 10 s on the RBR data loggers, which

is providing them with an estimated lifespan of a few years (anticipated end of recording is Feb. 2016).



Fig. 6.3.2: MeBoPlug prior to being screwed into a MeBo drill pipe (left); right image shows bottom view into the borehole with ports for P [hole at left] and T [little pin at right] monitoring. See text.

Two MTL sticks, named after the Antares mini-temperature logger (MTL) being their key component, were fabricated to be placed next to the MeBo sites containing MeBoPlugs. This was realised during leg SO222B with ROV *Quest*.

The MTL stick is only 70 cm long and comprises a stainless steel rod that has a fin in the lower portion (stuck into the sediment to prevent toppling over, even in strong currents), and a second fin with a pipe welded to it in its upper portion (Fig. 6.3.3). In the pipe, an MTL can be placed securely. At the top of the MTL stick, a small handle to ROV *Quest*'s specifications was mounted. The systems were programmed at a rate of 1 Hz and will monitor transient changes for 2.5 – 3 years.



Fig. 6.3.3: MTL stick to be deployed by ROV; those systems complement the MeBoPlugs at two sites to get high-resolution seafloor temperature variations as reference for the MeBoPlug data. ROV handle is seen left, MTL is hosted in a metal tube; lower portion is stuck into the sediment (with metal shield for stabilisation in case of bottom currents).

6.3.3. SmartPlug piezometer

The SmartPlug borehole observatory belongs, together with the MeBo-CORKs, to a series of recently developed Mini-CORK systems. In contrary to the original borehole observatories, Mini-CORKs are relative simple, self-contained instruments, which can be easily deployed from any ship of opportunity. The SmartPlug instrument package includes a data logger/pressure period counter, a temperature sensor inside the data logger housing, a battery package, and two pressure transducers which are connected to pressure gauges via hydraulic tubing. One pressure gauge is “upward looking”, the other is “downward looking”, monitoring the hydrostatic reference (i.e. seafloor) and formation fluid pressure and temperature, respectively. The formation pressure gauge is isolated from the overlying water column by the bottom seal located at the lower part of the SmartPlug structural outer shell (the “bullnose”) and usually by a mechanically released packer, to which the SmartPlug is attached before being installed in a borehole (for a more comprehensive outline of the technical details, please see Kopf et al., 2011).

During cruise SO222, however, due to the unavailability of a drill ship, the SmartPlug was modified to be installed without the need for a drill string, a packer, or even a borehole. The bullnose was extended by a 1m long steel pipe, which serves not only as stabiliser once the SmartPlug is pushed into the seafloor but also acts as casing protecting the lower pressure gauge inlet and simulating a borehole-like environment (see Fig. 6.3.4). In addition to that, slots were cut into the steel pipe to allow water and sediment to escape during the installation. This is important to allow displacement of water during impact on the seafloor, to prevent overpressurisation within the steel pipe during penetration, and to allow re-equilibration of fluid pressure and temperature with the surrounding formation. The observatory was set to monitor with a sampling frequency of 10 s, which constrains the monitoring period to around 2.5 years (i.e. similar to those of the MeBoPlugs).



Fig. 6.3.4: SmartPlug converted into a piezometer before being mounted to the TV-grab for deployment.

6.4 Sediment sampling

6.4.1. Piston corer (PC)

(T.Fleischmann, D. Jaeger, A. Rösner, E. Hatakeyama, Y. Nakano)

A piston coring system from Jamstec was used to recover sediment cores during cruises SO251A/B. The piston coring system consists of a 1.2 m long pilot/trigger core and a piston core of varying pipe length of 5 or 10 m. The trigger core had a weight of approximately 100 kg, whereas the piston core had a weight of approximately 1200 kg. Weights and core barrel length were adapted to the expected lithology during the cruise. At the bottom of the piston core a piston is inserted close to the core catcher. It creates a vacuum inside the liner supporting sediment recovery by reducing friction between the liner and the sediment. Trigger and piston core are connected via a trigger wire and a deployment wire to a trigger assembly unit; this allows a free fall distance pre-set by the length of the trigger wire (Fig. 6.4.1B). Approaching seafloor the system was lowered with a velocity of $0.2 \text{ m}\cdot\text{s}^{-1}$ until touchdown of the pilot core which releases the piston corer free fall. The deployment wire tightens, ideally at the point the piston inside the barrel is level with the sediment surface (Fig. 6.4.1B, -C). The core barrel sinks into the sediment whereas the piston remains at the sediment surface. Recovery started with an initial velocity of $0.2 \text{ m}\cdot\text{s}^{-1}$ immediately after coring. When MTLs were attached to the core barrel, the piston core stayed for 10 min in the sediment before recovery.

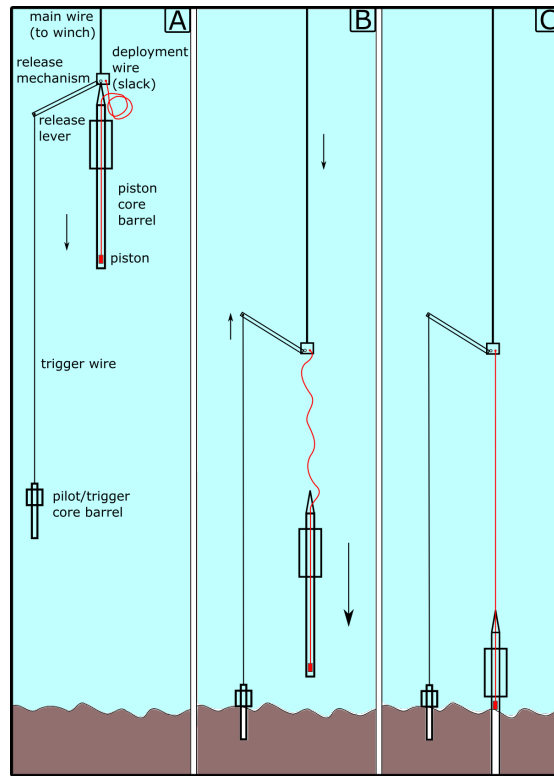


Fig. 6.4.1: Piston coring system. A. shows the initial set up, B. indicates the moment of triggering and C. the ideal final position of core barrel and piston in the sediment.

Trigger core and piston core were loaded with a transparent plastic liner of outer and inner diameter of 78mm and 74mm, respectively. Before loading, the liners were marked with a straight line and arrows for orientation purposes. Once back on board the trigger and piston sediment core was cut into 1 m sections from bottom to top and immediately sampled for gas if needed. The core sections were capped at both ends and labeled according to the GeoB standard scheme (Fig. 6.4.2). Pore water was sampled before the cores were split into work and archive half, which were analyzed and described by the physical properties and sedimentology groups, respectively.

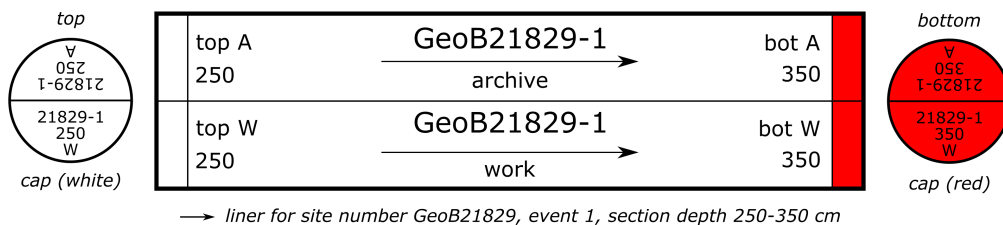


Fig. 6.4.2: Scheme of the inscription for core segments

6.4.2. Gravity Coring (GC) on Heat Flow Probe

(T.Fleischmann, D. Jaeger, A. Rösner)

As a result of the early departure of the Japanese technician, we were not in a position to use the JAMSTEC piston corer beyond Oct 24, 2016. Thus we improvised and mounted a core barrel equipped with an empty liner and core catcher to the heat flow probe (Fig. 6.4.3). First, the heat flow probe penetrates the seafloor and somewhat later the corer eases its way to the sediment. The assembly was kept in the seafloor for 15 m for a heat flow measurement and then the HF probe and corer were retrieved back on deck. With this set up we successfully recovered subseafloor samples from five sites. Core quality in the upper part was compromised by this coring technique but intact and good quality cores could be recovered from deeper subsurface section, although exact subsurface depth of cored section cannot be assessed conclusively from the penetration depth of the HF probe.



Fig. 6.4.3 The new „Heat flow corer“, an improvised sampling device developed on board, on deck before being deployed in the Kumano Basin.

In total 23 piston with 19 trigger cores and 6 gravity cores (HF-corer) were successfully recovered during SO251A/B. These cores have a total length of 149.4 m (Table 6.4_T1).

GeoB-Nr.	Corer typ	Liner Length [m]	Recovery [m]	Split/WR	CC	Headspace Samples	Pore Water Samples	Temperature Measurement
GeoB 21804-1	PC	10,00	9,76	split	yes	yes	yes	
GeoB 21804-2	pilot-PC	1,20	1,20	split	yes	no	yes	
GeoB 21809-1	PC	10,00	9,13	split	yes	yes	yes	
GeoB 21809-2	pilot-PC	1,20	0,86	split	no	no	yes	
GeoB 21810-1	PC	5,00	4,62	split	no	no	yes	
GeoB 21810-2	pilot-PC	1,20	0,81	split	no	no	yes	
GeoB 21810-3	PC	5,00	4,44	WR	no	no	no	
GeoB 21810-4	pilot-PC	1,20	0,52	WR	yes	no	no	
GeoB 21812-1	PC	10,00	9,06	split	no	yes	no	
GeoB 21812-2	pilot-PC	1,20	0,83	split	yes	no	no	
GeoB 21815-1	PC	5,00	4,67	split	yes	yes	yes	
GeoB 21815-2	pilot-PC	1,20	empty	empty	no	empty	empty	
GeoB 21815-3	PC	5,00	3,66	WR	yes	no	no	
GeoB 21815-4	pilot-PC	1,20	empty	empty	no	empty	empty	
GeoB 21817-1	PC	10,00	9,71	split	yes	yes	yes	
GeoB 21817-2	pilot-PC	1,20	0,74	split	no	no	yes	
GeoB 21818-1	PC	5,00	4,63	split	no	yes	yes	
GeoB 21818-2	pilot-PC	1,20	0,15	WR	yes	no	no	
GeoB 21818-3	PC	5,00	4,60	WR	yes	no	no	
GeoB 21818-4	pilot-PC	1,20	0,15	WR	no	no	no	
GeoB 21821-1	PC	10,00	9,70	split	no	no	no	
GeoB 21821-2	pilot-PC	1,20	1,20	split	no	no	no	
GeoB 21823-1	PC	10,00	8,78	split	no	yes	yes	
GeoB 21823-2	pilot-PC	1,20	1,20	split	yes	no	yes	
GeoB 21829-1	PC	5,00	4,46	split	yes	yes	yes	
GeoB 21829-2	pilot-PC	1,20	0,72	split	yes	no	no	
GeoB 21831-1	PC	5,00	4,08	split	yes	yes	yes	
GeoB 21831-2	pilot-PC	1,20	0,60	split	no	no	no	
GeoB 21833-1	PC	5,00	4,30	split	yes	yes	yes	
GeoB 21833-2	pilot-PC	1,20	0,41	split	yes	no	no	
GeoB 21834-1	PC	5,00	4,17	split	yes	no	yes	
GeoB 21834-2	pilot-PC	1,20	0,48	split	no	no	no	
GeoB 21836-1	PC	5,00	4,28	split	yes	yes	yes	MTL
GeoB 21836-2	pilot-PC	1,20	empty	empty	yes	empty	empty	
GeoB 21840-1	PC	5,00	4,57	split	yes	yes	yes	MTL
GeoB 21840-2	pilot-PC	1,20	empty	empty	yes	empty	empty	
GeoB 21842-1	PC	10,00	0,95	split	yes	yes	yes	MTL
GeoB 21842-2	pilot-PC	1,20	empty	empty	no	empty	empty	
GeoB 21843-1	PC	5,00	4,60	split	yes	yes	yes	MTL
GeoB 21843-2	pilot-PC	1,20	0,75	split	yes	no	no	
GeoB 21845-1	PC	5,00	4,49	split	yes	yes	yes	
GeoB 21845-2	pilot-PC	1,20	0,17	WR	no	no	no	
GeoB 21845-3	PC	5,00	4,44	WR	no	no	no	
GeoB 21845-4	pilot-PC	1,20	0,68	split	yes	no	yes	
GeoB 21846-1	PC	5,00	4,54	WR	no	no	yes	
GeoB 21846-2	pilot-PC	1,20	0,38	split	yes	no	yes	
GeoB21858-2	GC-HF	5,00	2,55	split		no	yes	HF
GeoB21860-2	GC-HF	5,00	0,77	split		yes	yes	HF
GeoB21861-2	GC-HF	5,00	2,02	split		no	yes	HF
GeoB21864-2	GC-HF	5,00	1,72	split		no	yes	HF
GeoB21866-2	GC-HF	5,00	2,85	split		no	no	HF
Sum		202,6	149,4					

Table 6.4-T1. Core summary table

6.4.3. Sediment description

(C. McHugh, M. Strasser, K. Ikehara, W. Menapace, A. Yamaguchi, K. Usami, W. Szczuciński, A. Molenaar, T. Schwestermann, S. Trütner, D. Jaeger, K. Mochizuki)

The archive halves of split piston cores were first cleaned (split surface smoothing) and then photographed onboard using a static camera framework with constant-intensity light source. Three to four overlapping photos were taken per section. Using a white marker point at constant section depth, the photos then were manually stitched using photo-editing software packages. For the visual description of sediment core sections, we followed the conventional Ocean Drilling Program (ODP) and IODP procedures for recording sedimentologic information (Mazzullo and Graham, 1988). The colour of the material was determined visually using Munsell color charts (Munsell 2012). Sediment texture (defined by the relative proportions of sand, silt, and clay) was determined using a simple hand-lens and smear-slide analysis (see below) and follows the classification of Shepard (1954). The classification scheme for siliciclastic and pelagic lithologies follows Mazzullo et al. (1988). In practice, it was difficult to discriminate between the dominant lithologies of silty clay and clayey silt without undertaking quantitative grain size analyses on board. Where siliceous (mainly diatomaceous) or calcareous (mainly calcareous nannofossils) sediment occur (i.e. cores from the Japan Trench and from Kumano Basin mud volcano site) we used the term “diatomaceous mud” and “calcareous mud”, respectively, for mud deposits that contain 10%–50% siliceous and calcareous biogenic components (following the classification of Dunham, 1962). Smear slides of both dominant and minor lithologies were analyzed under a cross-polarizing microscope in accordance with Rothwell (1989) and Marsaglia et al., (2012). Smear slides were taken when there were changes in lithology, color, and sedimentary structures such as those associated with sand beds and laminae. Smear slides are useful for identifying and reporting basic sediment attributes (texture and composition), and especially for the identification of tephra intervals that were sampled onboard for developing a chronology. Results are only semiquantitative. Errors can be large, especially for textural estimates of the fine silt and clay-size fractions. Smear slide analysis also tends to underestimate the amount of sand-size grains because they are difficult to incorporate evenly onto the slide. We estimated the texture of the sediments with the help of a visual comparison chart (Rothwell, 1989). The various sediment components were divided into several categories (major minerals such as clay, quartz, pyrite, and accessory minerals; biogenic components such as, calcareous nannofossils, foraminifera, spicules, diatoms, radiolaria; and rock fragments such as volcanic and sedimentary or metamorphic lithic fragments. For Leg A (Japan Trench) semi-quantitative estimates were conducted. The sand, silt and clay components of texture were estimated as representing 100% of the grain size fraction and described as grain size percentages. A similar estimation was used for minerals (accessory, calcite, clay, quartz, volcanic glass), biogenic (calcareous nantoplankton, foraminifera, spicules, diatoms, radiolarian and plant) and rock (pumice, lithic fragments) components that were grouped to represent 100% and described as percentages. The accessory minerals when possible were identified and named on the core logs and

plots at their respective depth intervals. The dominant, common and rare components were described on the core logs but these attributes were not included as part of the percent calculations. For Leg B we used descriptive categories according to the following classification

- ++ = dominant (>50% of total grains).
- + = common to abundant (>5%–50% of total grains).
- (+) = rare to only traces (<5% total grains).

Smear Slide description sheets with semi-quantitative information on texture and composition are shown in Appendix Table 11.4.1.

Visual Core Description (VCD) forms were compiled on a section-by-section basis. The position of each Smear Slide sample is shown on the VCD sample column as SS. Hand-written core descriptions were transferred to digitized one-page composite core logs compiled for each piston core with depths in meters and centimeters below sea-floor. The core logs show the graphical lithology, and give information on major and minor lithologies, primary sedimentary structures, accessories, bioturbation, coring disturbance, and smear slide samples, which are indicated by patterns and symbols in the graphic logs. A key to the full set of patterns and symbols used is shown in Appendix Figure 11.3.1 page 1. The symbols are schematic, but they are placed as close as possible to their proper stratigraphic position on the composite core log. All core descriptions are provided in the Appendix Figure 11.3.1.

6.5. Physical properties

(G. Wiemer, J. Hillman, M. Höhne, M. Ikari, T. Kanamatsu, M. Rex, A. Rösner, S. Trütner)

6.5.1. Magnetic Susceptibility

(T. Kanamatsu)

During the first leg of SO251 (Leg A – Japan Trench), the magnetic susceptibility (MS) of split sediment cores (piston and pilot cores from sites GeoB218-04, -09, -10, -12, -15, -17, -18, -21, and -23) was routinely measured every 1cm using a Bartington point sensor (MS2E). The sensor measures magnetic field response signal of the flat split core surface and the underlying sediment to about 10mm depth. For split core surface roughness less than 1mm, and by individual calibration to compensate for temperature-induced drift, this method reveals high-resolution true volumetric magnetic susceptibility data, which is reported as dimensionless [SI] results.

6.5.2. Undrained shear strength and sampling

(G. Wiemer, Hillman, J., Höhne, M., Rösner, A., Trütner, S.)

During cruises SO 251 undrained shear strength measurements were conducted directly after core splitting using the cone penetrometer test and the vane shear test on the working halves of the retrieved sediment cores. Piston cores GeoB21810-3, GeoB21815-3, GeoB21818-3, GeoB21845-1, GeoB21846-1, and pilot cores GeoB21810-4, GeoB21818-4, GeoB21845-2, and GeoB21846-2 remained as whole round cores for shore-based, post-cruise advanced geotechnical experiments. Therefore shipboard measurements exclude these sediment cores. As shipboard measurements naturally take place after disturbance of sediment due to coring and splitting, the measurement generally underestimates the true in situ undrained peak shear strength (Lee et al., 1979).

Cone penetrometer test:

The undrained shear strength (s_u) along the sediment cores was determined according to the British Standards Institutions (BS1377, 1975) with a *Wille Geotechnik* cone penetrometer (Figure 6.5.1A). The metal cone has a defined weight of 79.8 g and an opening angle of 30°. The cone tip was brought to a point exactly on the split core surface and was then released to penetrate the sediment in free-fall for 5 seconds. A displacement transducer was used to measure the penetration depth of the cone with a precision of 0.01 mm. The standard measurement spacing was 5 cm, however for the correlation of pilot cores with the upper most segment of the piston cores, the interval was reduced to 1 cm.

The undrained shear strength was then calculated following $S_u = (m \cdot g \cdot k) / d^2$, where m is the cone mass, g is the gravitational acceleration - ignoring variations due to ship motions, d is the penetration depth and k is the cone factor chosen as 0.85 for a 30° cone (Hansbo, 1957; Wood 1985).

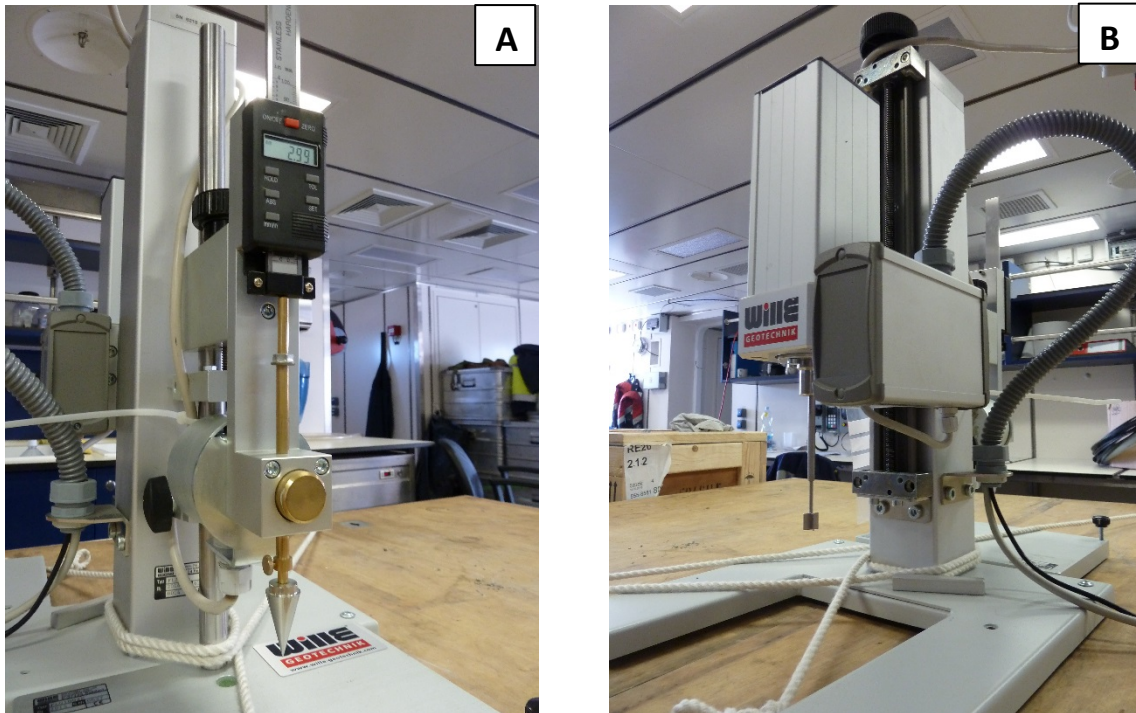


Fig. 6.5.1: (A) Fall cone penetrometer and (B) vane shear device for determining undrained shear strength.

Vane shear testing:

A fully automated vane shear apparatus manufactured by *Wille Geotechnik* (Figure 6.5.1B) was used for further sediment stress-strain behavior and residual shear strength analysis. A four-bladed Vane was inserted into the core face in fine grained sediment in ~ 25 cm intervals. The vane was rotated at a constant rate of 8°/min. The torque required shearing the sediment along the vertical and horizontal edges of the vane as well as the rotation angle were logged with a frequency of 4 Hz. A complete vane shear test consisted of two test phases: (1) measurement of maximum shear strength and (2) measurement of residual shear strength. The first test phase was stopped at a shear strength decrease of 30%. Subsequently, i.e. prior to the second test phase the vane was rotated five times with 1200°/min in order to entirely remold the sediment for residual strength determination. The second test phase was stopped once the residual shear strength was reached, i.e. at constant shear strength or rotation angle reached 25-30°. This measurement allows for the determination of the sediment sensitivity which is defined as the ratio of undrained shear strength (s_u) and residual shear strength ($s_{u,res}$). Data were logged via an interface module and the test-point software package *GEOsys 8.7.8.10*, both provided by *Wille Geotechnik*. Undrained and residual shear strength values were determined by post-processing using *Matlab*.

S_u is a function of the maximum torque (T) required to shear the sediment, and the geometry of the vane which is defined by the vane-constant $K=3/(7*\pi*(D^2/4)*H)$, where D is the vane diameter (12.7 mm) and H is the vane height (12.7 mm). S_u is then calculated as the product of the maximum torque and K.

6.5.3. Electrical resistance

(M. Ikari)

Electrical resistivity can be used to estimate the water content and/or porosity of marine sediments, due to the conductive nature of saline fluid (Archie, 1942). Resistivity may also be used as a proxy for quantities that depend on water content such as permeability or mechanical strength (Jackson et al., 1978). Measurements of electrical resistance were made on the working halves of piston cores using a Fluke 179 True RMS multimeter (ohmmeter setting). A spacer was constructed out of styrofoam to keep the two needle probes parallel with a constant separation distance of 30 mm (Figure 6.5.2). For testing, the probes were inserted 16 mm into the sediment. Measurements were made in two orientations; perpendicular to the core axis and parallel to the core axis. Paired measurements in both orientations were made at a frequency of 20-25 cm. For consistency, during all measurements the positive node was to the right for core-perpendicular measurements, and to the top in core-parallel measurements. In many cases, the resistance measurement exhibited time-dependent drift, and therefore the probe was held in the core samples for up to 300 seconds before taking a record of the measurement. Initial measurements (for core GeoB21804-1) were made with an automatic range function; however complications in the measurement were observed when time-dependent changes in resistance caused the range to switch between 0-60 and 0-600 k Ω . For all subsequent cores, measurements were mostly made in a fixed range of 0-600 k Ω , with a smaller number of measurements made at a fixed range of 0-60 k Ω for sediment with high water content.

Electrical resistance measurements are typically obtained from well logs (Archie, 1942), on discrete samples with a well-defined geometry (Jackson et al., 1978; Expedition 343/343T Scientists, 2013), or with a four-electrode Kelvin Bridge (Samouëlian et al., 2005) and reported as the scale-independent electrical resistivity (in Ω m). However, our use of the paired needle probes likely presents geometrical complications and therefore we report here electrical resistance (in k Ω) as a raw measurement. Calibration measurements on a sample of seawater from just above the sediment-water interface in core GeoB21809-1 exhibited resistance values of ~5-7 k Ω . Assuming a mean value of 6 k Ω and a typical seawater value of 2 Ω m implies a conversion factor from resistance to resistivity of ~0.0003 m for our measurements.

The use of paired core-perpendicular and core-parallel resistance measurements allows calculation of vertical resistance anisotropy on the split core surfaces. Anisotropy α is calculated by expressing the difference between the core-perpendicular (R_x) and core-parallel (R_z) resistances as a percentage of the mean value (Expedition 343 Scientists, 2013):

$$\alpha(\%) = 200 * \frac{R_x - R_z}{R_x + R_z}$$

We report here the absolute value of vertical resistivity, due to the possibility of fine-scale variations associated with using the small-dimension needle probes.

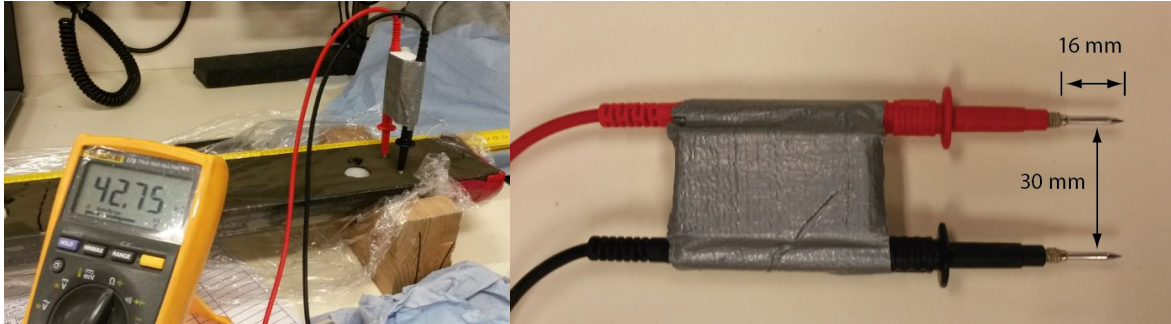


Fig. 6.5.2: Example of a measurement using the Fluke 179 multimeter on the ohmmeter setting (left) and dimensions of the needle probes (right).

6.5.4. Thermal Conductivity

(Norbert Kaul, Marie Rex)

Needle probe measurements were performed on recovered sediment core material during cruise SO251 in order to determine thermal conductivity and calculate the heat flow. Detecting and quantifying thermal conductivity and possible temperature anomalies give some information on ascent of warm fluids and mud at mud volcanoes and along faults as well as the extent of the gas hydrate stability zone in the sub-seabed. During cruise SO251 in situ thermal conductivity and needle probe measurements were conducted.

The needle probe measurements were performed using the KD2 Thermal Properties Analyzer produced by Decagon Devices Inc (Fig. 6.5.3). The KD2 consists of a display device combined with a single-needle sensor. At the start of the measurement the entire needle has to be inserted into the sediment. The instrument first equilibrates for 30 seconds to ensure temperature stability before starting a 30 second heating and measurement cycle. The microprocessor calculates the amount of power supplied to the heater. The probe's thermistor measures the changing temperature for 30 seconds and afterwards the rate of cooling for 30 seconds. In the end, thermal conductivity is computed using the change in temperature vs. time data.

Thermal conductivity is measured in available archive half sections of the sediment cores. Measurement frequency is usually every 10 cm for the 5 m cores and every 20 cm for the 10 m cores with one measuring cycle at each point. This includes 50 points in all sediment cores. However, spacing has to be adapted where a void or crack is observed. Sediment cores are brought into the laboratory at least 6 h before start of measurement, allowing the sediment to equilibrate to room temperature. Sediment

cores GeoB21818-1, GeoB21829-1, and GeoB21831 were not warmed up due to time constraints but were analyzed in a climate laboratory of 4°C. Those values are adjusted using the formulas:

$$(1) \quad k = k_w^\Phi k_M^{(1-\Phi)}$$

$$(2) \quad k_{(20^\circ\text{C})} = k_{w(20^\circ\text{C})}^\Phi k_M^{(1-\Phi)}$$

$$k_{(4^\circ\text{C})} = k_{w(4^\circ\text{C})}^\Phi k_M^{(1-\Phi)}$$

$$(3) \quad \frac{k_{(4^\circ\text{C})}}{k_{w(4^\circ\text{C})}^\Phi} = \frac{k_{(20^\circ\text{C})}}{k_{w(20^\circ\text{C})}^\Phi}$$

$$k_{(20^\circ\text{C})} = k_{(4^\circ\text{C})} \frac{k_{w(20^\circ\text{C})}^\Phi}{k_{w(4^\circ\text{C})}^\Phi}$$

(Lovell 1985)

$k_{(20^\circ\text{C})}$: thermal conductivity of sample at 20°C

$k_{(4^\circ\text{C})}$: thermal conductivity of sample at 4°C

Φ : porosity (65 %)

$k_{w(4^\circ\text{C})}$: thermal conductivity of water at 4°C (0.57 W/(m°C))

$k_{w(20^\circ\text{C})}$: thermal conductivity of water at 20°C (0.6 W/(m°C))

k_M : thermal conductivity of sediment matrix; k_M is assumed to be constant within this temperature range.



Fig. 6.5.3: Needle probe applied to a split core. A Decagon KD2 physical property analyzer is used for measurements.

6.5.5. Sampling for shore-based analyses

Samples of about 10 cm³ were taken for further laboratory analyses (e.g. water content, grain size, grain density etc.), at the positions where vane shear measurements had been conducted.

6.6. Geochemistry

(M. Kölling, N. Lübber, P. Töchterle)

Gas sampling

Sediment samples for gas analytics were taken on the work deck directly after taking off the core catcher and recovering the liner from the piston corer. 5mL cut syringes were used to sample 5 ml of sediment from the lower end of the core segment immediately after cutting the liner into 1m segments. The sediment sample was transferred to a 20mL headspace vial with a septum cap and a 10 mL saturated NaCl brine (~350 g L⁻¹) receiver.

DNA (and µBio sampling)

(W. Szczucinski)

For core GeoB21810-3, whole core rounds were cut at the lower ends of core segments, stored in a zip-lock bags and frozen at -80 °C in a lab super froster. In addition, 5 cm³ sediment samples were taken from the working half of core GeoB21809-1 immediately after splitting, pore water sampling (see below) and surface cleaning using sterilized spatula. These samples were also stored at -80 °C before being sent by frozen sampling shipping to the laboratory for DNA analyses at University of Geneva.

Pore water sampling

The 1m core segments were transferred to the geo lab and curated followed by pore water extraction from the closed liner within the first three hours after retrieval (before opening and description; Figure 6.6.1). Pore waters were sampled using rhizon samplers (Dickens et al, 2007). Before use, rhizons were placed in a beaker with MilliQ water. A standard 3.8 mm diameter drill bit was used to drill a hole in the plastic liner. A spacer on the drill bit prevented it from going into the core material. If necessary, a 2.5 mm wide stainless steel stick was used to prepare a hole in the sediment. A rhizon sampler was carefully pushed into the sediment and connected to a 20 mL disposable syringe. Vacuum was established by pulling the syringe plunger and keeping it open with a wooden spacer. After a few minutes, the syringes were taken off and the first 0.5 mL of sample was discarded.

The vacuum was then reattached and sampling continued until either the syringe was filled or sampling was stopped. The sampling intervals were generally decreasing

between 1.5 cm at the core top and 100 cm in the lower part of the core. For cores GeoB21829-1, GeoB21831-1, GeoB21833-1, GeoB21834-1, GeoB21836-2, GeoB21840-1, GeoB21842-1, GeoB21843-1, GeoB21858-2, GeoB21860-2 and GeoB21861-2 resolution was changed to regular intervals of 20 cm throughout the entire core beginning at 10 cm from liner top. If necessary, samples were taken from the working half of the open core to further increase the resolution of the data. The pore water flow was generally good, so that most sample volumes were between 5 and 18 mL after a maximum of three hours. If compatible with the core flow, rhizon samplers were taped to the core segments and left overnight at 4°C in a refrigerated storage room. At sample volumes over 15 mL (or after a reasonable time) the vacuum was released, the syringes were disconnected from the samplers and capped.

The syringe was stored cool (4°C) until sample splitting. For sample splitting, the syringe was emptied into a 20 mL scintillation vial (Greiner, polypropylene). Sample splits were taken from this master sample if feasible. Filtering was not necessary because the maximum pore width of the rhizons is 0.2 µm (thus the samples are sterile filtrated by the rhizon). Broken rhizons could easily be detected, as the vacuum cannot be maintained when the porous tube is damaged. These rhizons were replaced.

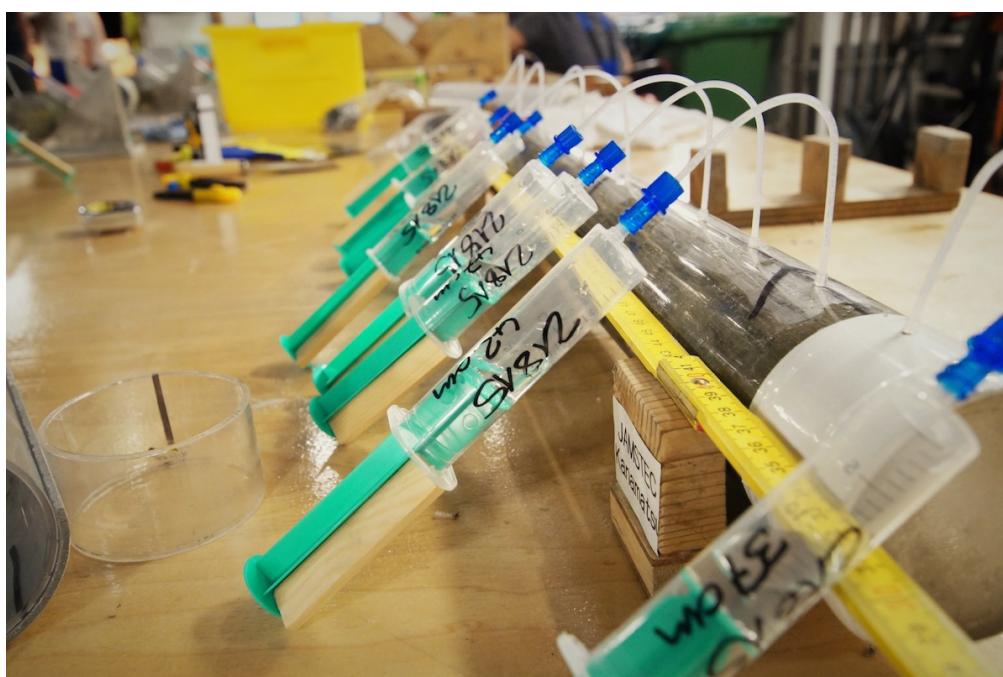


Fig. 6.6.1. Rhizon pore water sampling from closed liners. (photo P. Töchterle)

Labelling

The syringes were first hand-labeled with core and sampling depth information. Additionally, all samples and all sample splits were labelled with a circled sequential number. This sequential number is useful to quickly label temporary sample containers in the lab and for sorting samples. Samples were collected in the hangar and measured for pH and alkalinity and in "dry lab one". The results were entered into a worksheet to calculate alkalinities.

Sample splitting

Table 6.6.1 summarizes the splitting scheme for all samples by core. Splits were taken from the pore water master sample if not specified otherwise. Where exact amounts were needed adjustable pipettes (Eppendorf 2500 µL, Eppendorf 1000 µL, Eppendorf 200 µL, Eppendorf 100 µL) were used to transfer samples from the primary sample vial. Sample splits for δ¹⁸O analysis of cores GeoB21833-1, GeoB21834-1, GeoB21836-2, GeoB21840-1, GeoB21842-1, GeoB21843-1, GeoB21858-2, GeoB21860-2 and GeoB21861-2 were taken directly from the syringes. Afterwards, a leftover volume of 15 mL (syringe reading) was emptied into the master containers whereas 5 mL were retrieved for additional sample splits and shipboard measurements.

Table 6.6.1. Geochemistry sample split overview

seq	split	analysis	amount	preserv	vial	GeoB21804	GeoB21809	GeoB21810	GeoB21811	GeoB21812	GeoB21815	GeoB21817	GeoB21818	GeoB21822	GeoB21823	GeoB21829	GeoB21831	GeoB21833	GeoB21834	GeoB21836	GeoB21840	GeoB21842	GeoB21843	GeoB21858	GeoB21860	GeoB21861	GeoB21862						
						x	-	x	-	-	-	5x	x	5x	-	x	5x	-	5x	5x	5x	5x	-	5x	5x	x	5x	x	-	-	-	-	
0	gas	onshore	5 mL fresh sediment	20 mL satur. NaCl soln	crimp glass 20 mL	x	-	5x	-	-	-	5x	x	5x	-	x	5x	-	5x	5x	5x	-	5x	5x	x	5x	x	-	-	-	-	-	-
1	anions 1:50	onshore	0.039 mL PW	1.911 mL pure water (MilliQ)	Eppendorf PE 2 ml	x	x	x	x	x	-	x	x	x	x	x	x	-	-	-	-	-	-	x	x	x	x	-	-	-	-	-	-
2	alkalinity / pH / salinity	offshore	0.5 mL PW	-	Eppendorf PE 2 ml	x	-	x	x	x	-	x	x	x	x	x	-	-	x	x	x	x	x	x	x	x	x	-	-	-	-	-	-
3	NH4	onshore	2 mL PW	-	Eppendorf PE 2 ml	x	x	x	x	x	-	x	x	x	x	x	x	x	x	x	x	x	x	x	x	x	x	x	x	x	x	x	x
4	cations	onshore	1 mL PW	4 / 9 mL 0.65% HNO3	Nalgene vial HDPE 8 ml	x	x	x	x	x	-	x	x	x	x	x	x	-	-	-	-	-	-	x	x	x	x	x	x	x	x	x	x
5	δ13C δ34S δ18O / δD	onshore	1.9 mL PW	no headspace	twist cap glass 2 ml / crimp glass 1.5 ml	x	-	x	x	x	-	x	x	x	x	x	x	x	x	x	x	x	x	x	x	x	x	x	x	x	x	x	x
6	plain	onshore	1.9 mL PW	no headspace	twist cap glass 2 ml	x	-	x	x	x	-	x	x	x	x	x	x	-	-	-	-	-	-	-	-	-	-	-	-	-	-	-	-
7	residual of master sample	backup	1-12 mL PW	-	Scintillation vial PP 20ml	x	x	x	x	x/-	x	-	x	x	x	x	x/-	x/-	x	x	x	x	x	x	x	x	x	x	x	x	x	x	x

Pure water

18 MOhm water was generated in the dry lab from the ship's desalinated water with a MilliQ Integral 10 water purifier with an integrated A10 TOC monitor. The conductivity of the water was controlled to be <0.05 µS (>18.2 MOhm) by the built in conductivity detector. Both pure water for laboratory use and pure water for standards and for dilutions of original samples was prepared fresh from the MilliQ purifier.

Sample temperature

In situ temperatures of the sample could not be measured. Temperatures in the clean lab were constantly kept between 22.0 and 24.5 °C. For pH measurement, the temperature compensation was set manually according to an external temperature sensor that reacted to the room temperature. Since pH measurements were performed in 2 mL Eppendorf vials, sample temperatures were expected to equilibrate with room temperatures.

pH value

The pH value was measured with a Fisherbrand micro volume glass body microcombination glass electrode with a 6 mm tip connected to a WTW pH 3210 pH meter. In 2 mL Eppendorf cups, the pH value and the alkalinity were determined from 0.5 mL of sample. A constant reading was achieved by turning the vial around the electrode with a special magnetically driven vial holder rather than stirring the sample with a stir bar. The pH meter was calibrated at least once a day using AppliChem colour coded NBS scale pH buffer solutions (pH = 4.01 and 7.00). Slope and offset of the sensor were recorded. Temperatures were monitored with a pt1000 T-sensor next to the sample vial. The instrument shows the pH with a resolution of 0.001 pH units. The measurement has an accuracy of better than ± 0.02 pH units. The titration was performed using HCl at concentrations of 0.01M, 0.02M, 0.05 M and 0.1M, prepared from dilutions of a Merck certipur 1M HCl stock solution. MilliQ water was used for dilution. The 2 mL vial could hold 0.5 mL of sample and a maximum 0.7 mL of titrant, so we switched to higher concentration titrants as the titration volume exceeded 500 μL :

1	to	10 mM	0.01 M HCl	10	to	20 mM	0.02
M HCl							
20	to	50 mM	0.05 M HCl				
50	to	100 mM	0.1 M HCl				

Alkalinity

Alkalinity was determined by titration with HCl. The equivalence point was detected by titrating 0.5 mL of sample with an HCl of an exactly known concentration while controlling the pH value. Titration was stopped at pH < 3.9. The algorithm used to calculate alkalinity accounts for the activity of seawater and dilution by the titration solution so that the results are stable for different endpoint pH values. The measurement has an accuracy of better than 0.2 mmol/L. The algorithm is a corrected version of the algorithm in Grasshoff et al. (1983).

$$Alk [mol \cdot L^{-1}] = 10^{-pH_{initial}} \cdot f_{H^+_{initial}}^{-1} \cdot V_0^{-1} + c_{HCl} \cdot V_{HCl} \cdot V_0^{-1} - 10^{-pH_{final}} \cdot f_{H^+_{final}}^{-1} \cdot (V_0 + V_{HCl}) \cdot V_0^{-1}$$

pH initial - original pore water pH

pH final - pH at endpoint of titration between pH 4 and pH 3.5

fH+ - activity coefficient of H+ for standard seawater this is 0.755

c HCl - concentration of titration solution, usually 0.01 or 0.05 mol/L

vHCl - titration volume depending on Alkalinity of sample

v0 - initial volume of sample usually 0.0005 L (500 μL)

Salinity

Offshore measurements of pore water salinity were performed on a Krüss DR301-95 digital refractometer for cores GeoB21829-1, GeoB21831-1, GeoB21833-1,

GeoB21834-1, GeoB21836-2, GeoB21840-1, GeoB21842-1, GeoB21843-1, GeoB21846-1, GeoB21846-2, GeoB21858-2, and GeoB21861-2. For measurements 500 μ L were taken directly from the master sample container using an Eppendorf 1000 μ L pipette. The instrument was calibrated on a daily basis using MilliQ water. Instrument stability was monitored by measurements of MilliQ water and inhouse seawater standard before and after every batch of samples corresponding to one core. Product specifications recommend a sample temperature between 18 and 20°C. This recommendation could not be met due to lacking means for temperature regulation on board. The derived values for salinity of pore water have an accuracy of 0.1‰_{Salinity}.

Headspace gas sampling

Headspace samples were taken on the work deck when the core liner was cut into 1m segments upon recovery from the piston corer. Using a cut-off disposable 5 mL syringe, 5 mL of fresh sediment were sampled from the core catcher and from the bottom of the 1m segments as the core was cut into segments on deck. Samples were taken regularly from each core (typically 5 samples in the lower half of a 10m piston core), corresponding to sampled segments from bottom upwards. The sample was immediately transferred into a 20 mL septum crimp cap vial containing 10 mL of saturated NaCl brine. The vials were sealed, labelled and stored cool in a padded box. When possible the headspace gas samples were frozen at -18°C (onboard and after arrival in the MARUM) while samples were transported in the reefer at 4°C. All headspace samples were labelled with a sequential number. After sediment sampling for gas analysis the core was capped and transferred to the GeoLab for labelling and further processing. The headspace samples were noted in the lab book and entered into the DIS.

Geochemistry Offshore Measurements

On SO-251, a total of 479 porewater samples were taken from 18 piston cores, 7 pilot cores and 3 gravity cores and analysed for pH and alkalinity and in part also salinity. The trench core alkalinities indicate high production sediments reaching alkalinities up to 70 mM at depths of 8 to 10 mbsf. Alkalinities are generally increasing with depth starting with seawater concentrations at the sediment surface (alkalinity 2.4 mM/L).

In some of the cores on the slope (sites GeoB 21815, 21818) and in some of the Kumano Basin cores of leg B (sites GeoB 21833, 21834, 21836, 21858 and 21861) sulfide smell was detected from a certain depth (typically below 1 to 3 mbsf. PH-values are in the range of 7.4 to 8.2, which is normal for marine sediments. Single values are significantly higher and might correlate with ash layers in the sedimentary sequences.

6.7. Heat flow determination

(N. Kaul, B. Heesemann, M. Rex, M. Yoshimura, E. Hatakayma and M. Asada)

Thermal gradients for heat flow determinations are sampled by two different methods, a) temperature loggers, mounted on a core barrel and b) a heat flow probe, which delivers subbottom temperature and thermal conductivity values.

6.7.1. MTL temperature measurement

Miniaturised Temperature Loggers (MTL) are mounted onto the core barrel of the JAMSTEC piston corer (Figure 6.7.1), which was kept in seafloor-penetrated position after coring for about 12 minutes for in continuous situ temperature measurements. MTLs are single channel temperature data logger, produced by ANTARES, Germany. They are rated at 1 mK resolution and 600 bar pressure resistance. Three or five loggers, mounted at app. 1.5 m distance, yield up to two temperature gradient values. Four attempts were made (GeoB21836, GeoB21840, GeoB21842 and GeoB21843), three of them successful. Data reduction and gradient calculation was done by Masa Kinoshita onshore.



Fig. 6.7.1: Photo of MTL sensors mounted onto the core barrel

6.7.2. Heat flow probe

During cruise SO251B, we conducted heat flow measurements at a local scale in order to assess the activity of selected mud volcanoes in the Kumano basin. From the 2012 SO222 cruise, the regional geothermal background and the different activity of mud

volcanoes is known since the ascent of warm fluids and mud at mud volcanoes creates temperature anomalies at the seabed. This cruise gives us the unique opportunity to do a monitoring meaning a comparison of the thermal expression of mud volcanoes after a four year time lap. Furthermore, in situ sediment temperature measurements are crucial for determining the extent of the gas hydrate stability zone (GHSZ) in the sub-seabed.

In situ sediment temperature and thermal conductivity measurements are carried out using a 6 m-long heat flow probe (Fig. 6.7.2). It has a Lister-type violin bow design of FIELAX brand, lent from GEOMAR, Kiel. The sensor strings contain 22 thermistors spaced at an interval of 26 cm and a heater wire along the entire length of the string. The electronics are integrated into the head of the probe. Four 8-channels 22-bit A/D converters are used to record temperature readings at a sampling interval of 1 s. The probe is operated in an autonomous mode on this cruise.



Fig. 6.7.2: 6 meter heat flow probe, from GEOMAR, Kiel

Measurements are conducted in so called ‘pogo-style’, performing several penetrations in a row at small distances. Each penetration consisted of raising the probe some hundred meters above the sea floor from the previous penetration, slowly moving the ship to the next penetration site and letting the wire angle become nearly

vertical before dropping the probe into the sediment for the next penetration. The USBL system POSIDONIA is used to control the instrument's position. The transponding pinger is mounted 50 or 100 m above the probe. Due to the intermediate water depth of 2000 m, USBL performance is good. The probe is left undisturbed in the seafloor for 7 minutes for the sediment temperature measurement and another 7 minutes, in case a thermal conductivity measurement is conducted. Transit between measurements took between 30 and 75 minutes. Transit speed was governed by the trade-off between keeping the wire angle small and minimizing the time between measurements, usually 1 – 2 knots.

Winch speed during veering and hoisting is 1 m/s. Deployment of the instrument is from amid ship on the starboard side, employing a beam crane and assistance crane. This procedure ensures safe operation even during medium sea state. Heat flow stations stretching across mud volcanoes consist of individual penetration sites at a variable spacing of 100 - 200 m, up to 1000 m outside the actual volcano.

Full processing of the measurements includes calibration of thermistor sensors, calculation of sediment temperatures and temperature gradients, correction for probe tilt during penetration, and calculation of thermal conductivities. Prior to each series of measurements, the probe was halted 200 m above the seabed for approximately five minutes to inter-calibrate the temperature sensors. The software MHFRED (based on Villinger & Davis, 1987) is used to extrapolate the equilibrium sediment temperatures from the recorded time series at each station and to determine the thermal conductivity of the seabed.

Additionally, thermal conductivity measurements are carried out on split cores. An industry standard Decagon KD2 needle probe device is used. Detailed information on this topic is listed in Chapter 6.5.4, physical properties.

7. Initial shipboard results

7.1. Hydroacoustics

(J. Moernaut, C. Ferreira, M. Asada, A.K. Bachmann, T. Fujiwara, A. Kioka, K. Lange, G. Moore, T. Schwestermann, T. Sun)

7.1.1. Bathymetry

(C. Ferreira, M. Asada, A.K. Bachmann, T. Fujiwara, G. Moore, T. Sun)

The quality of the multibeam was very good despite many days with bad weather in leg 1 and 2. The higher resolution of the multibeam installed on RV Sonne provided us many examples of mass slides (Figure 7.1.1) that were quite visible in the EM122 data, but never really clear in the EM120 acquired 4 years before in the Japanese Trench. For the Nankai Trough the level of details of EM122 bathymetry again show us small mud volcanoes or topographic features that were not detectable with the EM120 sonar. The water column data from EM122 opened another chapter of our knowledge of the Nankai Trough since we detected more than 40 flares never ever seen before SO251 (Figure 7.1.2). The distribution of the flares could not be easily explained since it happened basically everywhere (at mud volcanoes, on top/flank of ridges, slopes or at spots in the flat basin).

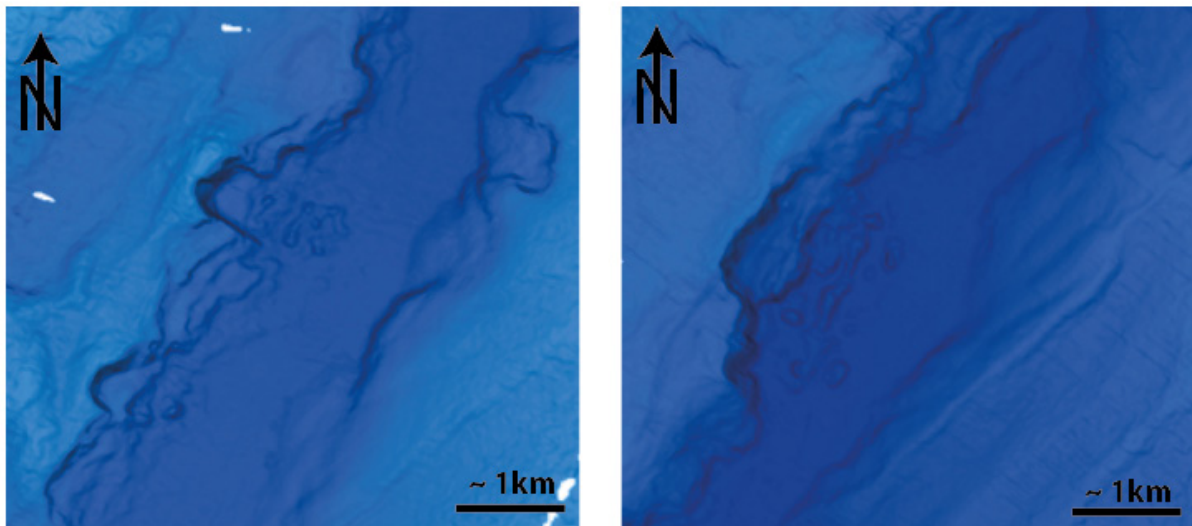


Fig. 7.1.1: Bathymetric maps acquired with the Kongsberg EM122 multibeam system during SO251 in the Japan Trench, showing submarine landslides features on the landward slope into the deep (> 7km deep) trench axis. This features were either not yet present, or not resolved in the lower-resolution bathymetric dataset acquired before 2011

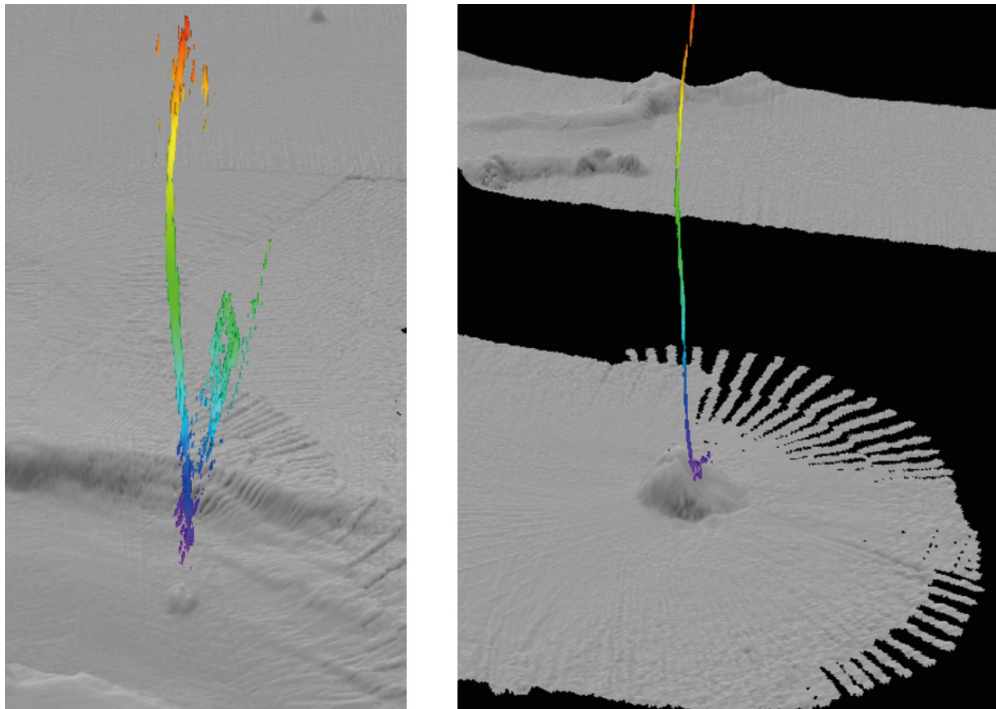


Fig. 7.1.2: Shaded relief of bathymetric data (gray-scale) and flares (colored) imaged in the water column data acquired with the Kongsberg EM122 multibeam system during SO251 in the Kumano Basin, Nankai Trough study area.

7.1.2. Subbottom Profiles

(J. Moernaut, A. Kioka, K. Lange, G. Moore, T. Schwestermann)

The overall quality of the Parasound data is very good in depths of 2-5 km whereas signal-to-ratio in the deep Japan Trench is significantly lower. The multibeam emitted signals and reflections produce noise on the Parasound data (see Fig 7.1.3), which does not significantly hamper the visualization and interpretation of subsurface data. The *.slf data reveal subseafloor stratification down to ~70 m within sedimentary basins whereas mud volcanoes or slopes steeper than ~5 degrees consist of reflection hyperbolae and poor signal penetration. Preliminary seismic-stratigraphic interpretation identified the existence of a.o. normal faults, sediment waves, mass-transport deposits and megaturbidites in different study areas. The *.phf files were evaluated above mud volcanoes in order to identify gas flares. No evidence for flares was found even though the multibeam water column data identified several. Post-cruise work will include further processing and seismic-stratigraphic mapping in order to put the other shipboard data (cores, heat flow, etc.) in its spatial and stratigraphic context.

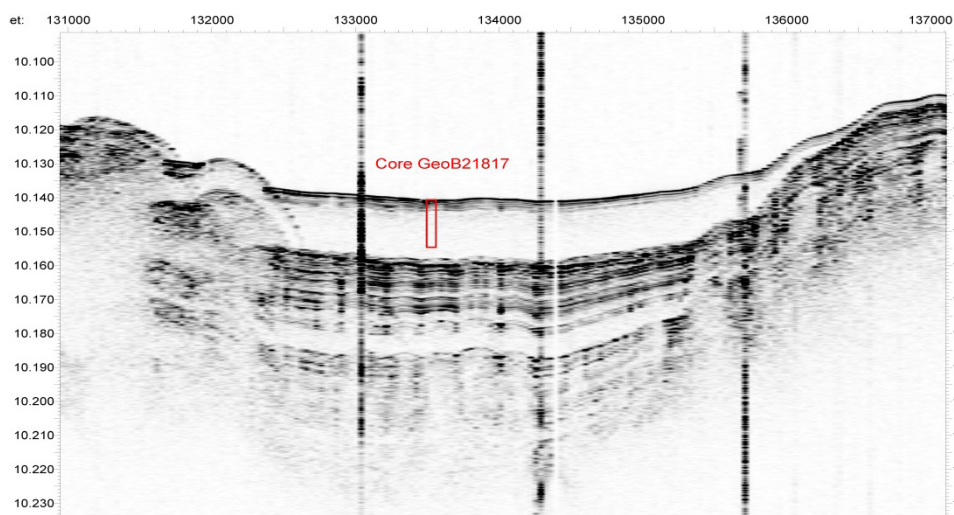


Fig. 7.1.3. Parasound profile in the Japan Trench and projection of core site GeoB21817 (10 m long), taken within an acoustically-transparent unit. Horizontal scale in meters; vertical scale in seconds. Core projection using an assumed P -wave velocity of 1500 m/s.

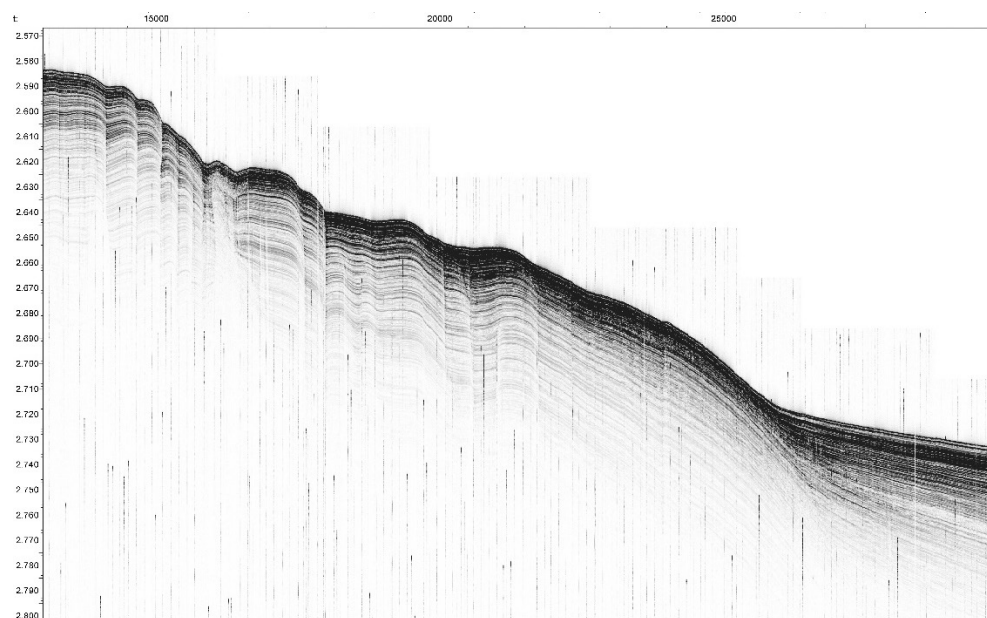


Fig. 7.1.4: Parasound seismic profile (south-to-north oriented) of the southern edge of the Kumano Basin illustrating normal faults within stratified sedimentary sequences. The vertical high-amplitude noise mainly results from the multibeam system. Horizontal scale in meters; vertical scale in seconds.

7.2. Remotely Operated Vehicle (ROV) dives

(A. Kopf, W. Menapace and the ROV Team)

During Leg 251-2, the ROV PHOCA from GEOMAR dove seven times in two weeks, with the foremost goal to recover observatory instruments installed on different mud volcanoes during Sonne cruise SO222 in 2012. Maximum diving depth was approximately 2070 m and maximum bottom time was 06:40 hours. In total, bottom time accumulated to approx. 35 hours (total dive time 53 hours). Targets were mud volcanoes MV#2 (GeoB212828), MV3 (GeoB21838, -53) and MV4 (GeoB21841, -50, -55, and -63). We describe the main operations in this chapter and also show photos. The exact track of the vehicle on the bathymetric map as well as the protocol can be found in Appendix Table 11.5.1.

Dive #1 on MV #2 (GeoB21828)

This dive served to search and recover the two CAT flowmeters that were deployed in 2012, but were not recovered owing to time constraints on the Japanese cruise in 2013 led by Juichiro Ashi. After having tried to activate the flowmeters acoustically, no answer was received. We hence lowered the ROV on 19.10. at 1:30h UTC and dove down to the summit of the MV in appx. 1990 m water depth.

At about 3:00h UTC we arrived at the seafloor and started to systematically search in short, somewhat offset N-S-transects. By doing so, we discovered numerous fields of clams, sometimes shells and shell fragments, and rarely also living organisms (Calyptogena; Fig. 7.2.1A). There were fish on the summit of the MV and bacterial mats of dm-diameter in various places. Parts of the seafloor showed small sediment mounds, almost like those of moles, and large crabs were seen twice. Occasionally, pieces of wood (trunks of trees) and clasts of several decimeters were sighted. From 5:30h onwards, we gave up the search, which was severely hampered by problems with the very unstable Posidonia pinger system. Instead of looking for the CAT meters, we aimed at a systematic NW-SE oriented T-stick profile. A total of five measurements

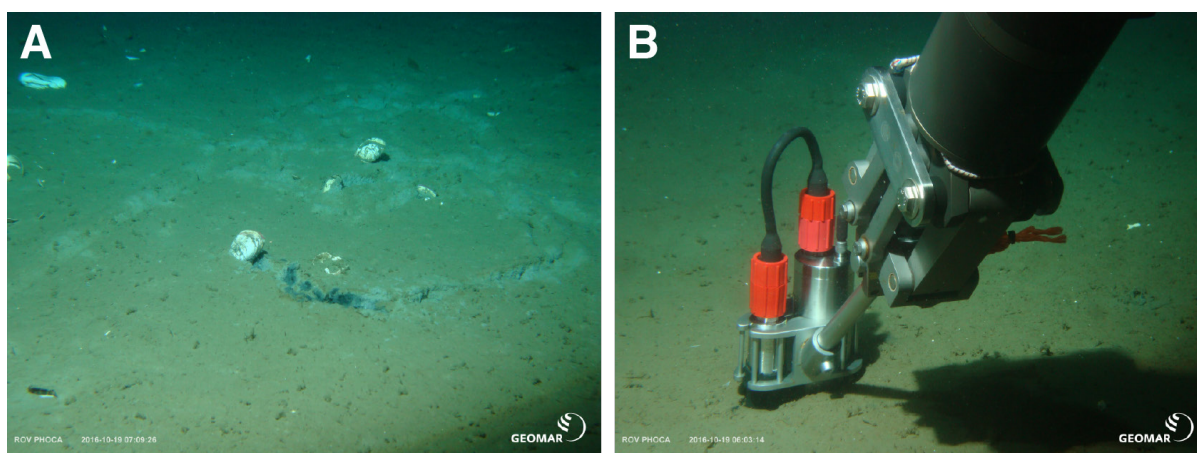


Fig. 7.2.1: a) Living *Calyptogena* clams and the traces they leave on the seafloor; b) T-stick deployed on the summit of MV#2. Photos ROV PHOCA, GEOMAR.

were carried out (Fig. 7.2.1B) and showed the highest thermal gradients in the crestal area in the SW. Notably this is the region where we also observed a change in sediment to soft, greenish colours, parts of which appeared to be grown over by microorganisms; indicating fresh mudflows and warmer or nutrient-rich substrates.

Dive #2 on MV #3 (GeoB21838)

In 2012, we left one MeBo hole uninstrumented (only protection cap attached) and one with a MeBoPLUG (Kopf et al., 2013). During this second PHOCA dive we tried to find the two borehole strings. During this dive, which reached ground on 21.10. at 1:50 UTC, we had even worse problems with positioning and were only able to find one MeBo drill string. As a result of the growth on it (Fig. 7.2.2), we falsely identified it as MeBoPLUG and unscrewed the end cap of the former MeBoCORK-B (Kopf et al., 2013). Other than that, no gear was recovered or deployed.

When surveying the region, we noticed numerous fish, coral, sea stars, sea cucumbers and debris of mollusc shells. On occasion large clasts were found on the surface of MV#3. Part of the summit area shows a rough, hummocky surface, which hampered our search for the MeBoPLUG.



Fig. 7.2.2: Former MeBo hole with end cap once CORK-B was recovered in 2012 (Kopf et al., 2013).

Dives #3 and 4 on MV #4 (GeoB21841 and -50)

The first dive on MV#4 took place on 22.10, when we deployed the vehicle at 2:34 UTC and arrived at the seafloor at 4:51 UTC. At 5:16h we sighted the MeBoCORK-A observatory with plenty of overgrowth and attempted to loosen the hotstab connector by attaching a clamping device (Fig. 7.2.3A, -B), however, that was apparently too tight to be pulled by ROV. As an alternate plan, we then tried to unscrew the MeBo drill rod underneath and succeeded by maybe 2 full turns. The rod and observatory started to rotate along their long axis with significant tilt, so we were under the impression that the hole assembly is loose (7:33h). It was, however, impossible to lift it with PHOCA so that we started our ascent 15 minutes later and arrived safely on deck at 8:48 UTC.

PHOCA dive #4 revisited the same MV four days later. In the meantime we had prepared a few recovery devices in the ROV drawer (Homer beacon for orientation, rope for catching the drill string) and on deck (second wire with dummy weight and Homer beacon). We dove on MV#4 again on 26.10. and arrived on the seafloor at 3:33 UTC. Only 6 minutes later we sighted the MeBoCORK-A and placed the beacon south of it. We then started to lay the rope around the drill string, tightened it, and ordered the second wire with the dummy weight from the vessel. That was finally sighted in 30 m distance at 5:41 UTC. We detached the hook and rope from the weight and flew back to the CORK-site to attach the hook to the rope at the drillstring (6:06h). We then connected a safety line to the clamp on top of CORK-A and started to pull by using the ship winch.

Even at strong pulling forces, nothing moved, and first the safety line, then a knot in the black rope assembly burst and we lost the opportunity to recover CORK-A.

We then tried further north by searching for the MeBoPLUG and T-stick observatories. These were found at 8:58h and recovered first the T-stick (9:15h), then the PLUG (9:40h) and put both into PHOCA's drawer. Very unfortunately, we failed to observe that the MTL in the T-stick was missing and actually lay on the seafloor unnoticed. We departed instead (9:43h) and arrived safely on deck at 11:03 UTC.

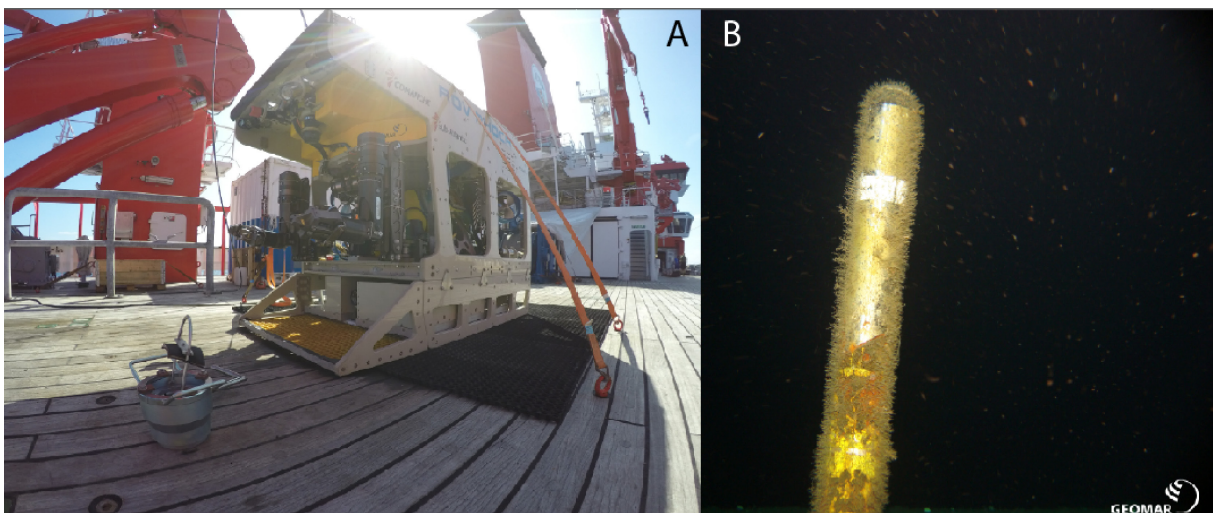


Fig. 7.2.3: a) PHOCA with recovery device (Backenklemme); b) sighting of MeBoCORK-A overgrown with organisms.

Dive #5 on MV #3 (GeoB21853)

In splendid weather and calm seas, we set out to dive #5 on 27.10. at 9:17 UTC. We lowered the vehicle to the summit area of MV#3 (10:42h) where we successfully redeployed the end cap to the MeBoCORK-B string (11:51h; see Fig. 7.2.4A, -B). We then flew further and sighted the MeBoPLUG assembly only shortly afterwards (11:55h). We first grasped to the MeBo rod with one manipulator and unscrewed the observatory plug with the other arm. We then recovered the T-stick, this time with MTL in it, and stored both devices in the ROV's drawer (Fig. 7.2.4C, -D). We started our return to the vessel at 12:22 UTC and brought PHOCA safely back to SONNE after a short and successful dive.

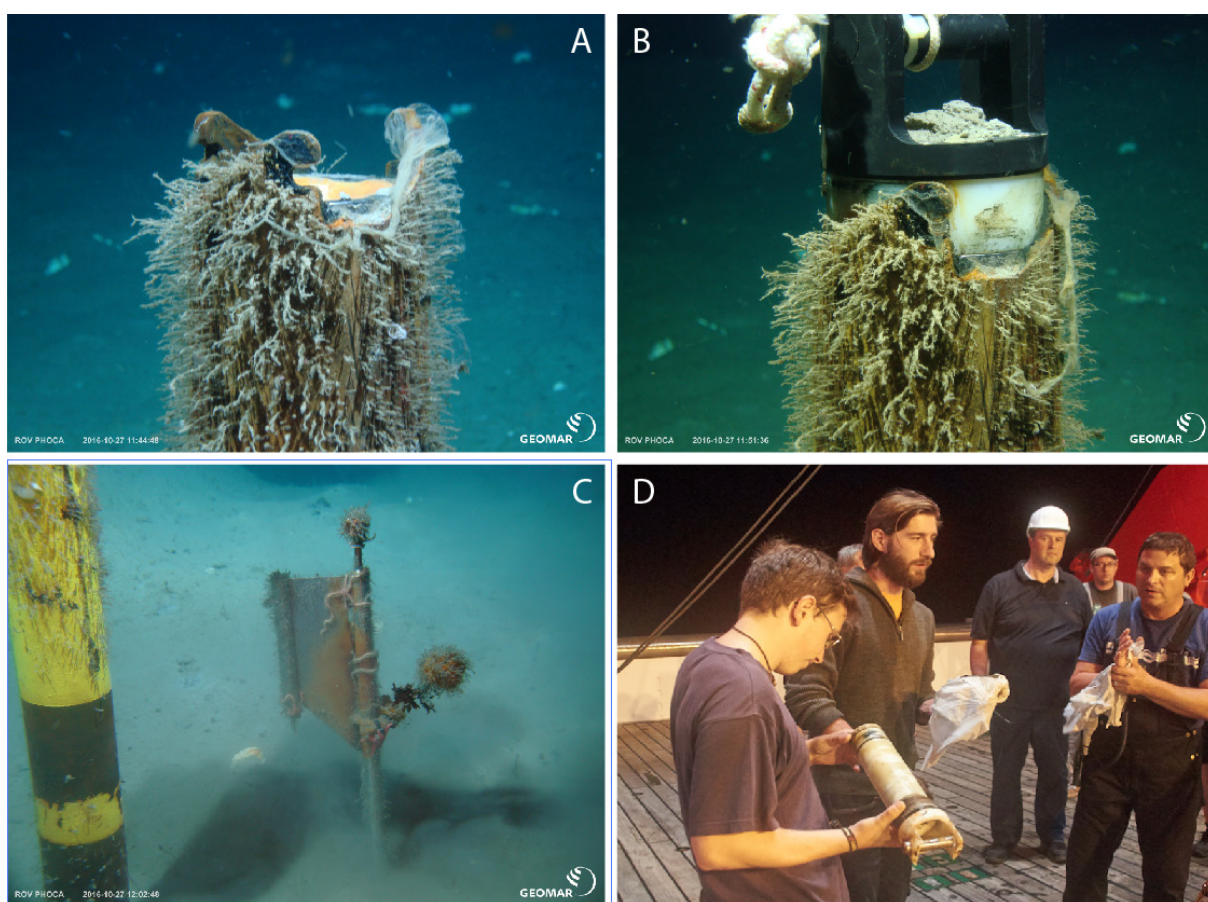


Fig. 7.2.4: a) open drill string with bajonet; b) end cap mounted for protection; c) T-stick with MTL next to MeBo drill string; d) MeBoPLUG is handed to scientists after the dive.

Dive #6 on MV #4 (GeoB21855)

On 28.10. we had another fair weather window and dove once more on MV#4. This time the SmartPlug piezometer was our target. The device was deployed by TV-grab in 2012 (Kopf et al., 2013) and was left with some flotation and fluorescent tape. After arrival on the seafloor at appx. 1:00h UTC PHOCA located the device 20 minutes later (Fig. 7.2.5A). We received a second wire with dummy weight from the ship and manoeuvred that to the SmartPlug. At 3:34h, the hook from the ship's wire was connected to lines of the SmartPlug (Fig. 7.2.5B). The ship heaved heavily and

unlocked the instrument from the seafloor at 3:58 UTC. The SmartPlug was recovered on deck some 45 minutes later (Fig. 7.2.5C).

We then tried our luck and flew down the northern slope of MV#4 to the T-stick site where the MTL was missing. Unbelievably, we sighted the MTL, which is only 15 cm long (Fig. 7.2.5D). Very unfortunately, however, the ORION manipulator failed to grip it with its claw and all attempts to catch it with a net failed afterwards. Given that the weather was getting worse, we left the seafloor at 7:37 UTC and arrived with an intact vehicle, but damaged umbilical on deck at around 9h UTC.

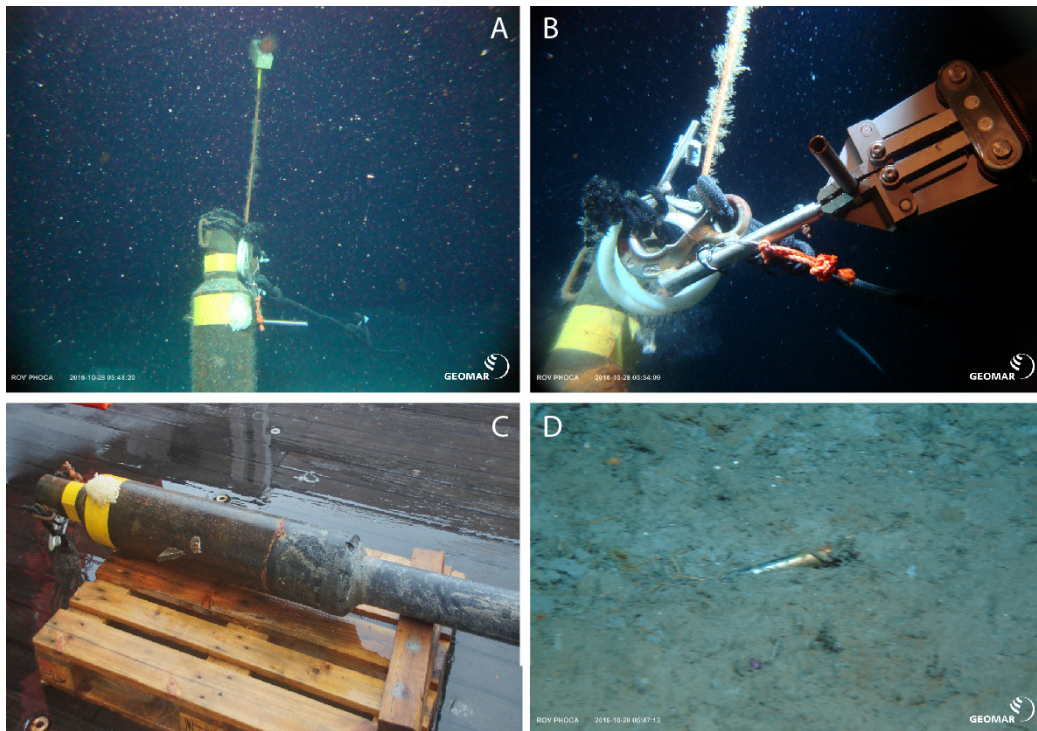


Fig. 7.2.5: a) SmartPlug piezometer on the seafloor; b) ship's wire connected by PHOCA; c) SmartPlug on deck; d) MTL found, but not recovered in the very soft mud.

Dive #7 on MV #4 (GeoB21863)

The final dive of cruise SO251-2 was again on MV#4 in order to finally recover the MeBoCORK-A. We set out on 31.10. and reached the seafloor at UTC and immediately located the instrument. While the ship was lowering the dummy weight, PHOCA unscrewed the MeBo drill rod by another 4 turns. After having located the weight bar, we flew and there and unlatched the recovery hook on the rope at 3:32h. Half an hour later, the hook was connected to the black rope around the CORK-A instrument. The ship started to heave the wire, however, the CORK-A got locked in the bajonet (4:18h) so that PHOCA had to fly to the drill string again in order to turn the CORK-A and unlock the pins one more time at 4:26 UTC. We then placed PHOCA 12 m away from the site and watched the ship heaving the wire. Instead of releasing the CORK-A at the hotstab, the entire first MeBo rod got free at 1.6 tons pulling force and shot up in the water column, leaving us in a suspension cloud at 4:33h. While the instrument was

safely brought to deck and disassembled (Fig. 7.2.6), ROV PHOCA spend some more time at the ground to collect a beacon before finally ascending at appx. 6.30 UTC.

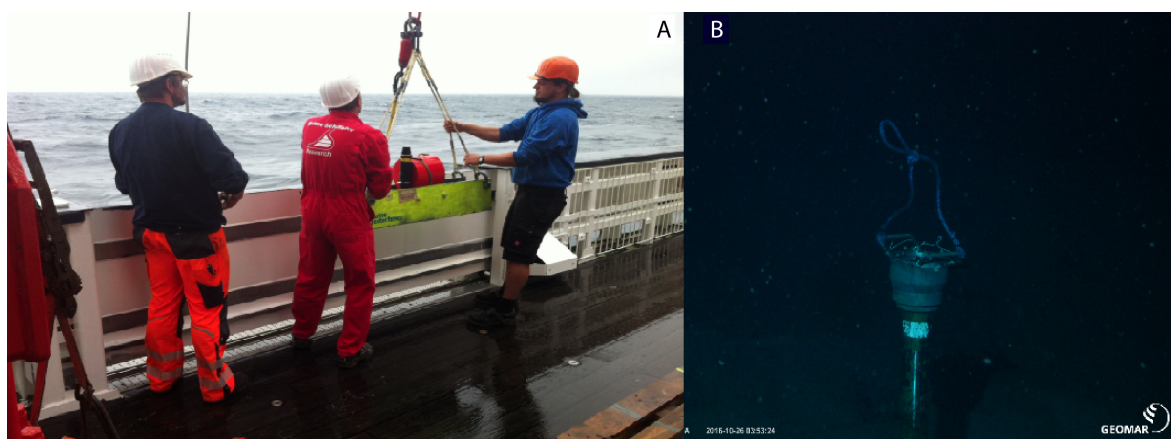


Fig. 7.2.6: a) CORK-A assembly upon its arrival on deck; b) intact observatory with hotstab.

7.3. Observatories

(W. Menapace, A. Kopf, A. Rösner, T. Fleischmann)

During the course of leg SO251B different types of long-term observatories have been recovered with a high degree of success, using the ROV Phoca from Geomar, Kiel and supporting winch cables from the R/V Sonne. Operations began with dive GeoB21828 on MV#2, which, due to malfunctioning of the onboard navigation systems, failed to find the CAT meters, which was the main purpose of this first mission.

Table 7.3.1 Basic information about the observatories and their locations

Name	Type of deployment	Latitude N	Longitude E	Location	Measured parameters	Recovered
CAT Meter #7	Seafloor	33°40.540	136°55.280	MV#2	fluid flow/water samples	NO
CAT Meter #9	Seafloor	33°40.530	136°55.280	MV#2	fluid flow/water samples	NO
MeBo Plug 1	Borehole	33°38.028	136°40.257	MV#3 Summit	temperature/differential pressure	YES
MTL Logger	Seafloor	33°38.028	136°40.257	MV#3 Summit	temperature	YES
MeBo CORK A	Borehole	33°39.355	136°38.037	MV#4 Summit	temperature/pressure	YES
MeBo Plug 2	Borehole	33°39.541	136°38.015	MV#4 Flank	temperature/differential pressure	YES
MTL Logger	Seafloor	33°39.541	136°38.015	MV#4	temperature	NO
SmartPlug	Seafloor	33°39.384	136°38.043	MV#4	temperature/differential pressure	YES

Same problems affected the subsequent dive, GeoB21838, which was focused on the recovery of the instruments deployed on MV#3 and just found the borehole casing where the MeBo CORK B was installed, a seafloor unit deployed and retrieved during SO222.

Eventually, before dive GeoB21841 on MV#4, the positioning systems were repaired and the ROV located the MeBo CORK A, trying to unscrew it from the borehole casing in order to rescue the whole instrument package. That did not produce any results, since the instrument seemed stuck and the ROV was not able to retrieve it during the same mission.

On the next dive, GeoB21850, the ROV could immediately find and successfully retrieve the MeBo Plug 2 on MV#4. The MTL temperature stick near the borehole was also rescued but unfortunately the logger itself slipped away from the casing, fact we just realized once the ROV came on deck. After a thorough cleaning of the MeBo Plug 2 logger casing, the logger electronics were found damaged from infiltrating seawater to an extent that reparation onboard was not possible. The logger will be then professionally cleaned and an attempt to retrieve its data will be made once onshore.

During dive GeoB21853 on top of MV#3 was first recovered the borehole part (with the hotstab connection) of MeBo CORK B, whose seafloor logger was retrieved already during SO222. The ROV proceeded then towards the MeBo Plug 1 location and was able to quickly retrieve the instrument as well as the MTL logger near it. The MeBo Plug 1 logger was intact and about 700 MB of data could be downloaded. The data series recorded by MeBo Plug 1 consists of differential pressure and temperature values with a sampling rate of 1 sample per 10 s and a continuous recording from 16/06/2012 to 24/02/2016 (Fig.7.3.1).

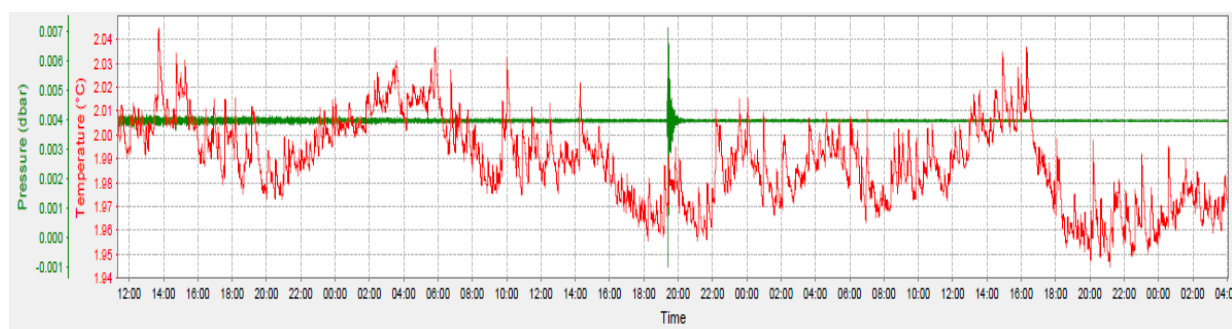


Fig. 7.3.1. Extract of the data from the MeBo Plug 1. An earthquake signal can be seen at the differential pressure spike in the middle of the image.

The MTL temperature data have a lower resolution of 1 sample per hour and a continuous recording from 07/07/2012 to 07/07/2015 was downloaded (Fig. 7.3.2).

Dive GeoB21855 was spent on MV#4 trying initially to retrieve the MTL lost near the MeBo Plug 2, unsuccessfully, and then heading towards the SmartPlug location. Once found, the SmartPlug was safely pulled on deck, but, even if structurally intact, it was not making able any download of the data, due to low battery power (Fig. 7.3.3). The battery pack will be replaced once onshore, due to the lack of components on the ship.

During the last dive on MV#4, GeoB21856, the MeBo CORK A instrument package was unscrewed and retrieved after some struggling on the seafloor (see ROV dives chapter below). The MeBo CORK A logging unit was not opened onboard because of safety concerns about its pressurized conditions and will be taken apart once onshore and the data analyzed.

Basic information concerning all dives is summarised in Table 7.3.1.

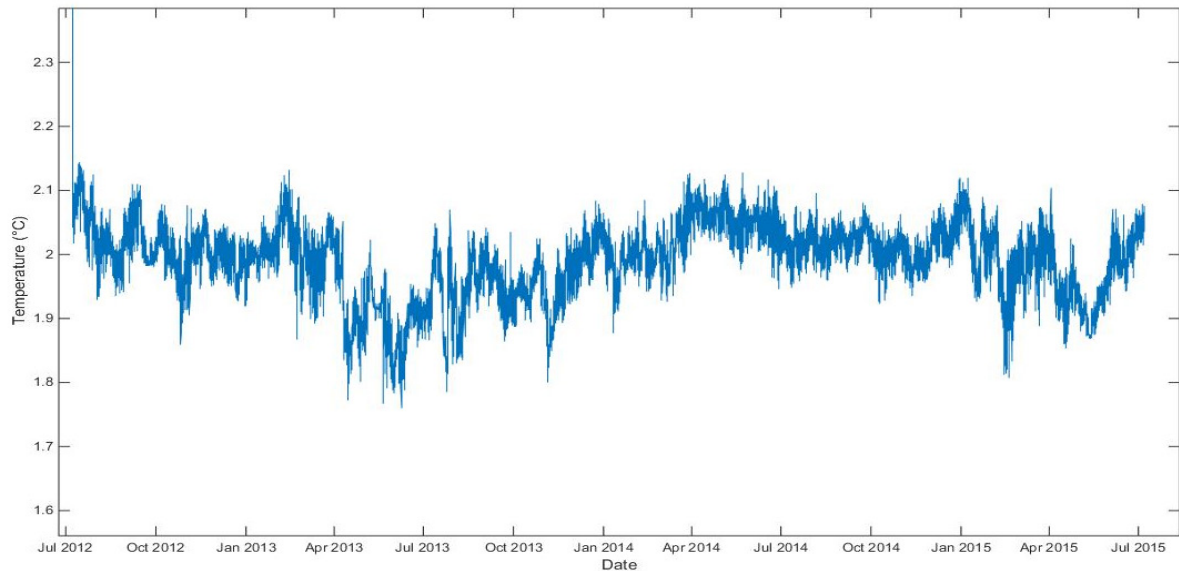


Fig. 7.3.2. Whole dataset of temperatures from the MTL near the MeBo Plug 1.



Fig. 7.3.3. MeBo CORK A borehole rod and SmartPlug deployment configuration once safe on deck.

7.4 Sedimentology

(C. McHugh, M. Strasser, K. Ikehara, W. Menapace, A. Yamaguchi, Kazuko Usami, Witold Szczuciński, J. Molenaar, T. Schwestermann, S. Trütner, D. Jaeger, K. Mochizuki)

7.4.1. Japan Trench

(C. McHugh, K. Ikehara, A. Yamaguchi, K. Usami, W. Szczuciński, J. Molenaar, T. Schwestermann)

The lithology is mainly composed of biosiliceous muds (Fig. 7.4.1A). Smear slides revealed that the biosiliceous components are mainly tests and fragments of diatoms, silicoflagellates, sponge spicules and minor radiolarians. Calcium carbonate components are minor and when present they are tests and fragments of foraminifera and coccoliths. The diatomaceous muds commonly contain black bands, laminae and patches that may represent FeS chemical alterations (Fig. 7.4.1B). A better understanding of these reactions will require future and more in depth geochemical analyses

The diatomaceous muds are interbedded with silt and sand laminae and beds. These transported deposits interpreted as turbidites, generally have sharp basal scoured contacts and are normally graded with gradual upper contacts. The sand ranges from very fine to medium size. Coarser sand beds can be as thick as 5 cm. Intervals of fine sand laminae can be 10's of centimeters thick (Fig. 7.4.1C, -D). Notable are intervals of homogeneous mud present above sandy turbidites (Fig. 7.4.1C). These homogenous muds lack bioturbation and can be up to 1 m thick. Intervals of homogeneous mud revealed in the cores generally correlate with homogenous intervals observed on Parasound images (See Hydroacoustics Section). These turbidite-homogenite units have been initially interpreted as resedimentation events triggered by earthquakes or "seismo-turbidites". More in depth studies will better identify the triggering mechanism and sediment transport processes linked to these deposits.

Ash beds are present in both slope and trench sediments (Fig. 7.4.1E). Generally, ash beds were noted by their light greenish gray color, sharp boundaries and fine grain size. Although intervals of coarse silt-sized volcanic glass shards and pumice are also found as minor lithological components within the diatomaceous muds. Smear slide studies reveal that characteristic mineral assemblages composed of orthoclase, plagioclase, amphibole and other clinopyroxenes are present in association with ash beds and ash rich intervals. An approximately 30 cm thick sand bed and pumice layer above, were recovered. The pumice is up to gravel size and poorly sorted (Fig. 7.4.1G). The identified minerals and possibly others contained in the ash bed and pumice rich intervals will be further analysed for correlations with known volcanic eruptions and tephra chronology for age correlations.

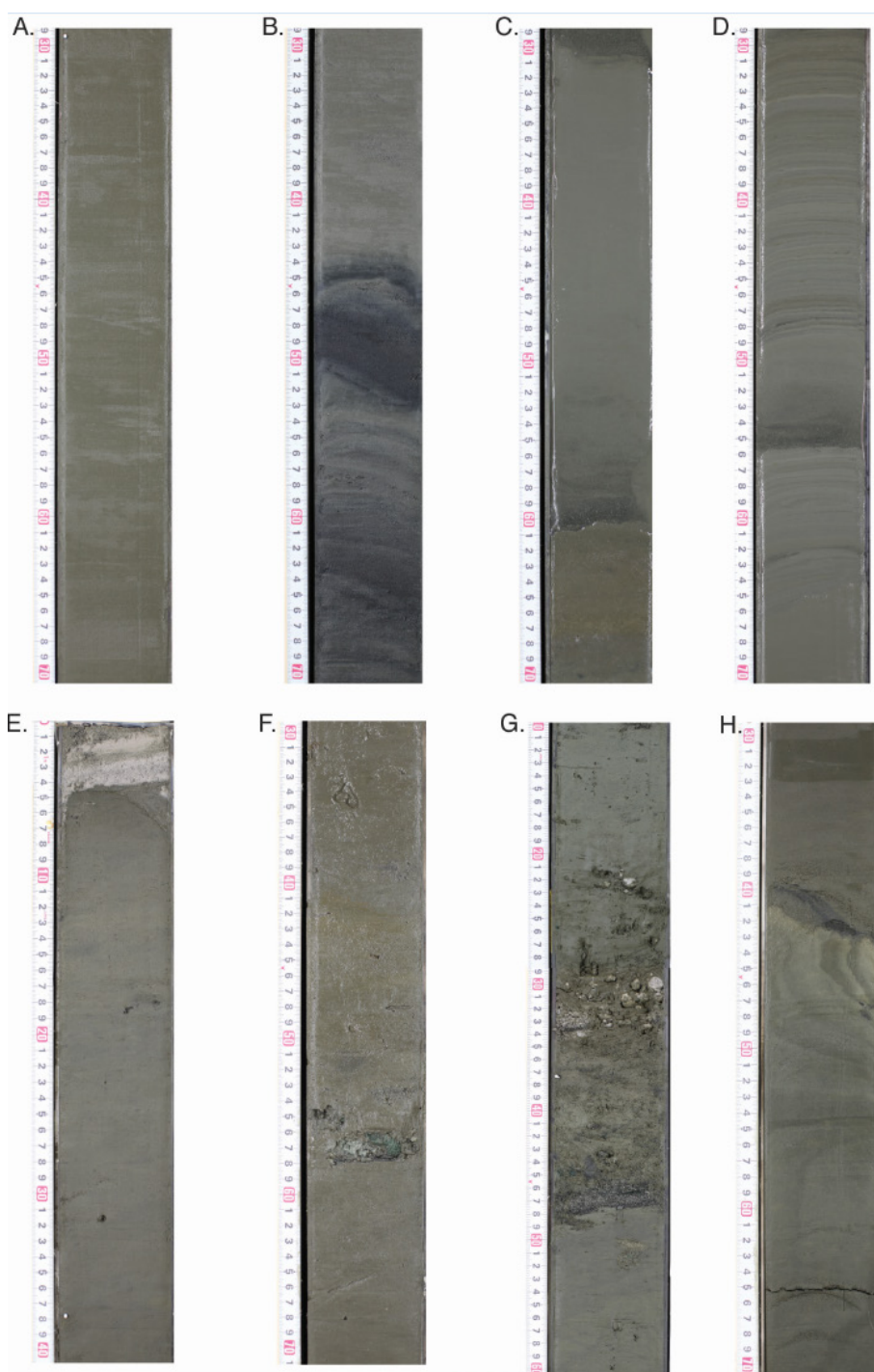


Fig. 7.4.1. Core Photographs: A. GeoB21817-1, 300-340 cm. Olive grey diatomaceous mud is the dominant lithology of the cores. B. GeoB21823-1, 608-648 cm. The diatomaceous mud commonly contains black bands; laminae and patches that in some instances reveal sedimentary structures such as scour surfaces. C. GeoB21812-1, 30-70 cm. The diatomaceous mud is interbedded with fine to medium sand beds up to 5 cm thick, with scoured basal contacts and normal grading. Intervals (10's of centimeters thick) are commonly present above the sand beds. D. GeoB21812-1, 136-176 cm, showing intervals of multiple, stacked, silt and fine sand laminae and beds with sharp basal contacts, cross bedding and normal grading. E. GeoB21810-1, 362-402 cm. Light greenish grey volcanic ash layer, 5 cm thick, with sharp basal and upper contacts. F. GeoB21810-2, 30-70 cm. Diagenetic clast could be easily disaggregated. Contains chlorite as accessory mineral. G. GeoB2818, 174-224 cm. Sand bed and pumice layer above. The sand is medium grained, black to light grey and forms an erosional contact with the lithology beneath. The pumice is up to gravel size and poorly sorted. H. GeoB21804, 900-970 cm. Slump identified by its recumbent, isoclinal and drag folds noted by their color and grain size variability. A sharp, steeply dipping contact separates the slump from the lithology above.

Mass-transport deposits were rarely recovered. A slump about 0.5 m thick, was identified from its recumbent and isoclinal folds with parasitic drag folds. These structures were noted by their slight grain size (fine sand and mud) and color variability (different shades of gray and olive gray) (Fig. 7.4-1H). The slump is likely larger in size and not all of its structures are evident in the 7 cm wide core. Magnetic susceptibility measurements, smear slide analyses and visual core descriptions reveal a correlation between a strong magnetic susceptibility signal and sand beds and laminae (See MS Section). The strongest magnetic susceptibility measurements were correlated with an interval of black bands beneath calcareous diatomaceous mud (Fig. 7.4-1B). However, the grain size in this interval is not coarse grained. More analyses need to be conducted to better understand the relation between magnetic susceptibility, grain size and composition.

These interpretations are preliminary and future analyses will better constrain the major and minor lithological components, diagenesis and geochemical reactions, transported sediment intervals and ash beds-tephra correlations for age determinations.

7.4.2. Nankai Trough / Kumano Basin

(M. Strasser, W. Menapace, J. Molenaar, T. Schwestermann, S. Trütner, D. Jaeger, K. Mochizuki)

The dominant lithology of cores recovered during SO251-2 is mainly greenish grey to olive grey silty clay to clayey silt with abundant siliceous and calcareous biogenic components. Minor lithologies include ash beds (or more commonly intervals with dispersed ash) and coarse silt and/or fine sand beds. Yet, lithology and stratigraphic succession varies in place according to the location of the coring site ranging from (i) silty clay and interbedded silty clay with sand laminae and beds in the Kumano Basin (“background” cores GeoB218-29, -31, -33, -34, 43; Figure 7.4-2A), (ii) structureless mixture of calcareous mud, sandy silty clay and/or clayey silt with mudstone pebbles, and/or interbedded sequence (dm-scale) between layers containing hard pieces with mm-scale incrustation and clayey silt with sand at Mud Volcano coring sites GeoB218-36; -42 -60 (Figure 7.4-2B & C); (iii) slightly mottled (bioturbated) dark greenish gray clay with black staining in cores recovered from slightly inclined slopes of the lower Nankai Accretionary wedge seaward of the Megasplay fault Zone (GeoB218-45, 46, and 66).

The lithostratigraphic succession of the Kumano Basin “background” cores are apparently nicely correlatable across the entire basin, tentatively correlated by a prominent ash bed / interval with dispersed ash at 1.5-2.5 mbsf, and the distinct lithological change from interbedded silty clay with sand beds below and more homogenous silty clay above at 2.6-3.1 mbsf. This stratigraphic success has been previously described for the Latest Pleistocene transgressive and Holocene sea-level high-stand sequence, as dated by radio-carbon ages and tephrochronology (Omura et

al., 2012). SO251-B onboard smear slide analyses of sand beds reveal distinct differences in the amount and nature of lithic components (sedimentary lithic vs. metamorphic and volcanic lithic fragments), suggesting distinct sedimentary provenance.

The three cores from the mud volcano sites show large variability with respect to mudstone pebbles (greenish gray to dark gray mudstone to sandy mudstones pebbles of different sizes) mixed in a sandy clayey silt matrix (-> interpreted a mud breccias from mudvolcano mudflows) and may also contain intervals encrusted authigenic calcite precipitation encrusted with *Calypptogena sp* shell fragments (GeoB218-42; Figure 7.4-2B). All three cores retrieved from the mud volcano sites show mud breccia occurring at the top of the core suggesting (very) recent activity of respective mud volcanoes.

Differences in lithology and sedimentary structures are further noted for cores retrieved from (i) an isolated basin in the eastern part of the working area, revealing silty clay interbedded with cm-scale beds with mostly homogeneous upper parts and a sandy to silty, fining upward basal part, suggesting deposition from recurrent submarine sediment remobilization events (GeoB 21861-2) (ii) a northern Kumano Basin filled subbasin at the toe of a slope with several small canyons, revealing silty clay interbedded with slightly coarser slightly darker beds with sharp lower and diffuse upper contact (lower part) and dm-scale beds with 1-2 cm fine sand to coarse silt basal layer and upper mostly homogeneous bed (upper part), suggesting deposition from recurrent turbidity flow within small canyons and gully systems feeding the basin (GeoB 21864-2); (iii) a coring site near the fore arc high /Kumano Basin Edge Fault Zone area (GeoB218-40), revealing silty clay interbedded with cm-scale partly amalgamated beds of mixed clayey silt with sand and mud clasts, tentatively interpreted as deposits from gravitational mass movement processes; (iv) a core from the high of a prominent bathymetric hill (GeoB 21858) revealing mostly homogenous clayey silt remains enigmatic to interpret mostly due to coring disturbance by the HF coring device.



Fig.7.4.-2. Core Photographs: D. GeoB21829-1, 355-397 cm. showing intervals of multiple, stacked, silt and fine sand laminae and beds with sharp basal contacts, and normal grading. E: GeoB21842-1, 60-95cm, Interbedded sequence between mud containing abundant autigenic calcite and layer with calcite cemented mud chips, shell fragments (*calyptogena*) and mudstone pebbles. F: GeoB21860-2, 0-34cm. structureless mixture of clayey silt with pebbles consisting of mudstone, sand patches and nanofossils.

7.5. Physical properties

7.5.1. Magnetic Susceptibility

(T. Kanamatsu)

Magnetic susceptibility measurements range between -1.1×10^{-4} and 1.3×10^{-2} (SI). A very good correlation was found between magnetic susceptibility measurements and coarser sand grain size fractions (Figure 7.5.1). The highest measurements are correlated with a scour surface and thick interval of black mud above in Core GeoB21823-1, at 614-678 cm. However, grain size in this interval is not coarse grained.

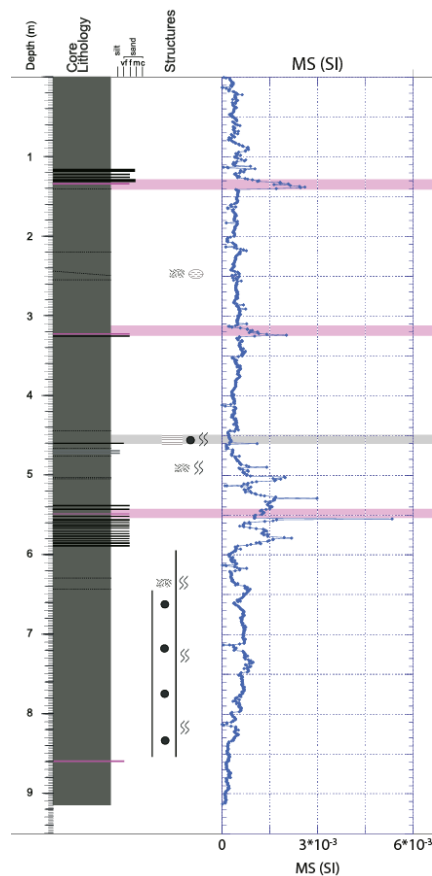


Figure 7.5.1. Example of magnetic susceptibility data of core GeoB21809-1. The comparison with the lithology log (see appendix Figure 11.3.1 page for symbol legend) indicates very good correlation between magnetic susceptibility measurements and coarser sand grain size fractions.

7.5.2. Undrained shear strength

(G. Wiemer, J. Hillman, M. Höhne, A. Rösner, S. Trütner)

Undrained shear strength values from the fall cone penetrometer tests and vane shear test are overall coherent. However, fall cone data locally reveal higher values of s_u , which are related to higher resolution and the testing of also coarser grained layers, e.g. clayey silt or sandy silt. Vane shear tests were only performed in fine-grained sediments. Figure 7.5.2 exemplarily presents a typical shear strength measurement,

conducted with the vane shear device. It is shown that the shear stress increases drastically to a peak value within 8° of vane rotation. Following the peak, shear stress decreases almost constantly. The undrained shear strength is the peak in shear stress. The measurement is stopped once the shear stress is reduced by 30% of the undrained shear strength. Subsequently the residual shear strength measurement starts, which is exemplarily presented in figure 1B. Here, the shear stress increases with the rotation angle up to a constant value, which corresponds to the residual shear strength.

Undrained shear strength values of each measurement are plotted with core depth in the composite data logs attached in the appendix Figure 11.6.1.

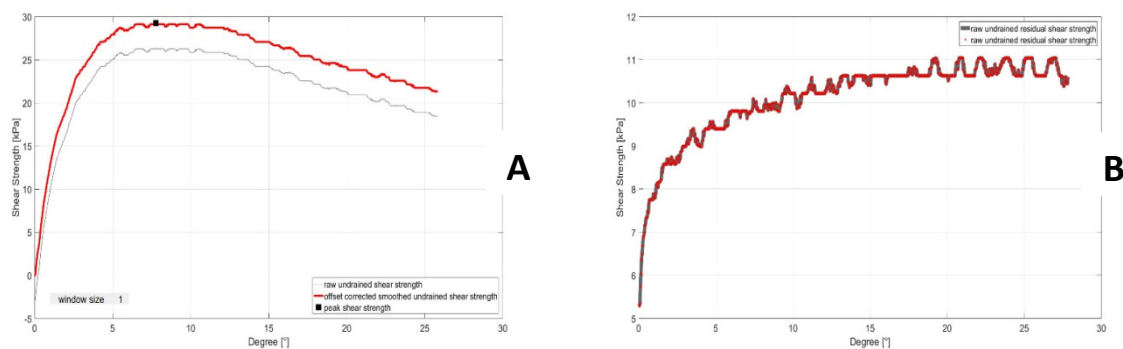


Figure 7.5.2: Example of shear strength measurement with the automated vane shear device: (A) shear stress as a function of rotation angle and (B) residual shear stress as a function of rotation angle.

Japan Trench:

Slope Cores:

In general, the sediment shear strength of the three ~5 m long slope cores (GeoB21810-1, GeoB21815-1, GeoB21818-1) is very high relative to the burial depth of the sediment.

Undrained shear strength values acquired from vane shear testing range from 0-20 kPa in the upper ~80 cm and increases with depth to 35-80 kPa. Peaks displayed in fall cone data reach a maximum of ~160 kPa but are generally around 80-140 kPa. GeoB21810-1 (Figure 7.5.3) presents peak values as high as 160 kPa only at depth >300 cm. Sediment from core GeoB21815-1 presents peak values of 140 kPa at 200 cm depth downwards and are more frequent whereas highest shear strength values of 160 kPa already exist in 100 cm depth in sediment core GeoB21818-1. Hence, there may be an increasing trend of sediment undrained shear strength from south to north along the slope.

The undrained shear strength of the upper 75 cm in the pilot core GeoB201810-2 varies between 0.5 and 8 kPa. At ~45 cm depth the s_u values are as low (~2 kPa) as in ~3 cm depth

Trench cores:

The five ~10 m long cores from the Japan Trench (GeoB21804-1, GeoB21809-1, GeoB21812-1, GeoB21817-1, GeoB21823-1) generally present undrained shear strength values which increase with depth and rarely exceed 30 kPa. Yet, in detail, the trends in s_u may be quite variable in different cores and over certain depth intervals. The most southern core GeoB21804-1 (figure 7.5-3) reveals a very low gradient of increasing undrained shear strength from 1 – 3 kPa in the depth interval 0 - 350 cm below seafloor. From ~350 cm – 950 cm depth, undrained shear strength increases near linearly with a slightly steeper gradient and reaches shear strength values of ~20 kPa at depth. Cores further north in the trench (GeoB21809-1, GeoB21812-1, GeoB21823-1) locally show a decreasing trend in shear strength with depth. Most prominently, shear strength in core GeoB21817-1 (furthest north) decreases almost linearly from ~20 kPa to ~10 kPa in the depth range of ~500 cm to 950 cm. Shear strength values are relatively constant (0-5 kPa) in the upper 250-350 cm of the sediment cores taken in the trench and then range from 5-20 kPa in the lower parts of the sediment cores. A few peaks in shear strength ($s_u=20-40$ kPa) are observed, which increase in abundance towards the north. There is significantly less scatter in the data of cores GeoB21804-1, GeoB21821-1, and GeoB21817-1 than in the other trench cores which might be evidence for less input of silt or sand size particles in the sediment.

The pilot cores reach at maximum 120 cm below sea floor (GeoB21821-2) and present increasing shear strength values from ~1 kPa to maximum ~7.5 kPa. Note that the fall cone measurements were performed in 5 cm intervals on cores GeoB21804-2 and GeoB21823-2, which gives a biased impression of less scatter in the data. However, it can be seen in the data that the undrained shear strength at depth (~25-75 cm) may be as low (2-4 kPa) as in the upper 0-25 cm.

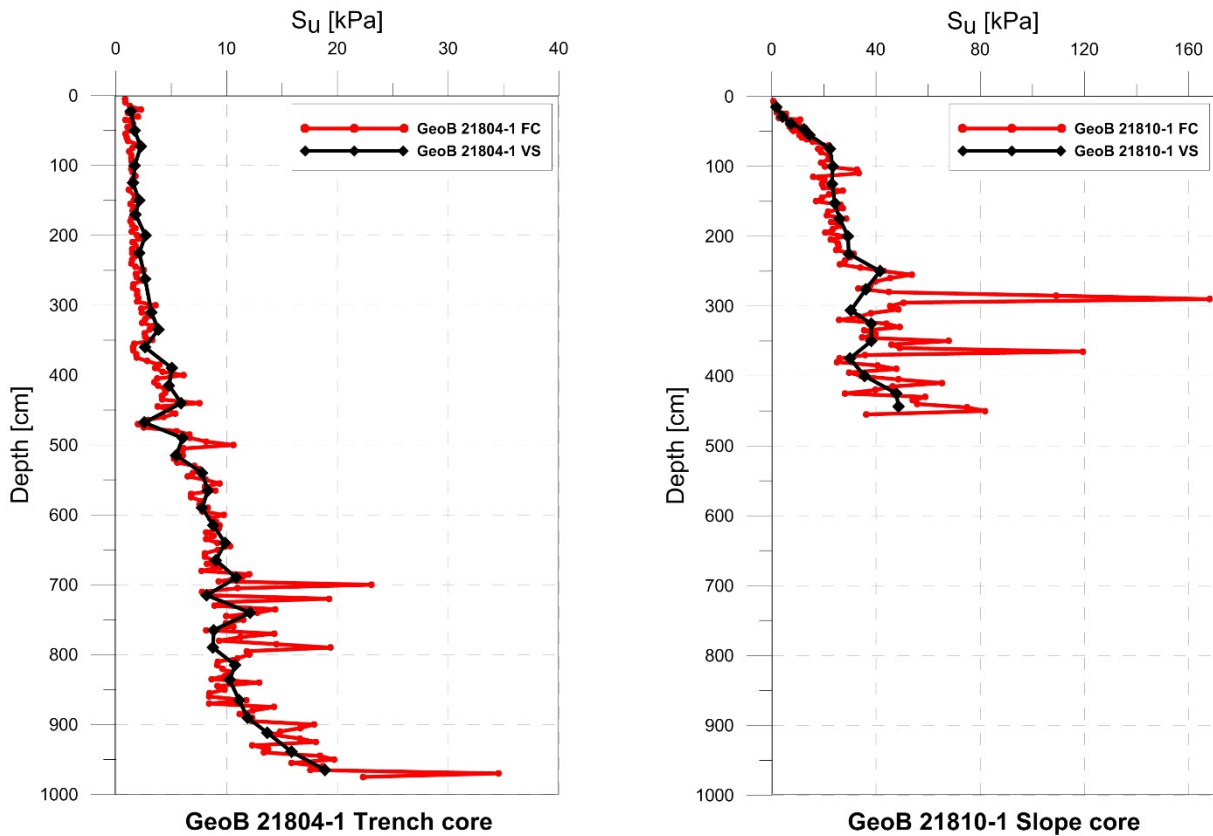


Figure 7.5.3: Exemplary shear strength's trend and value range of a trench and slope core in the Japan Trench study area.

Nankai Trough:

Within the Nankai Trough study area, several sites were sampled for diverse scientific purposes. Samples were taken where there is evidence for deep-seated fluids (e.g. mud volcanoes), in areas with no evidence for any sort of activity (Kumano basin background sediment), within an isolated basin located in the eastern part of the Kumano basin, and at a site where a good record of Holocene turbidites is expected, and on the Nankai slope. Moreover, two different coring systems were deployed: i) the conventional piston coring system provided by JAMSTEC, and ii) an improvised gravity core system which consisted of a rod, liner and core catcher mounted to the heat flow probe. In the following the undrained shear strength results are presented in dependence of geological setting.

Kumano Basin background sediment:

The cores GeoB21829-1, GeoB21831-1, GeoB21833-1, GeoB21834-1, GeoB21843-1 and GeoB21864-1 were taken in areas with no obvious evidence of fluid or mud flow from deeper down in the formation. Again, s_u values from vane shear and fall cone testing are consistent and show an increasing trend of undrained shear strength with depth (Figure 7.5.4). In the eastern part of the basin (sites GeoB21831, GeoB21831) the shear strength increases with a lower gradient than in the western part of the basin (sites GeoB21833, GeoB21834). For instance, at site GeoB21843, s_u increases from 1 kPa to ~20 kPa within the depth interval of 0-350 cm depth. From 350-450 cm depth

the scatter increases drastically and s_u fluctuates from 20 – 100 or even up to 130 kPa. At site GeoB21833, s_u values reach up to 20 kPa already at 100 cm depth. At ~375cm depth values reach up to 250 kPa. The scatter in the fall cone data is generally significantly larger in the sediment coming from the western part of the Kumano Basin than in the sediment from the eastern part.

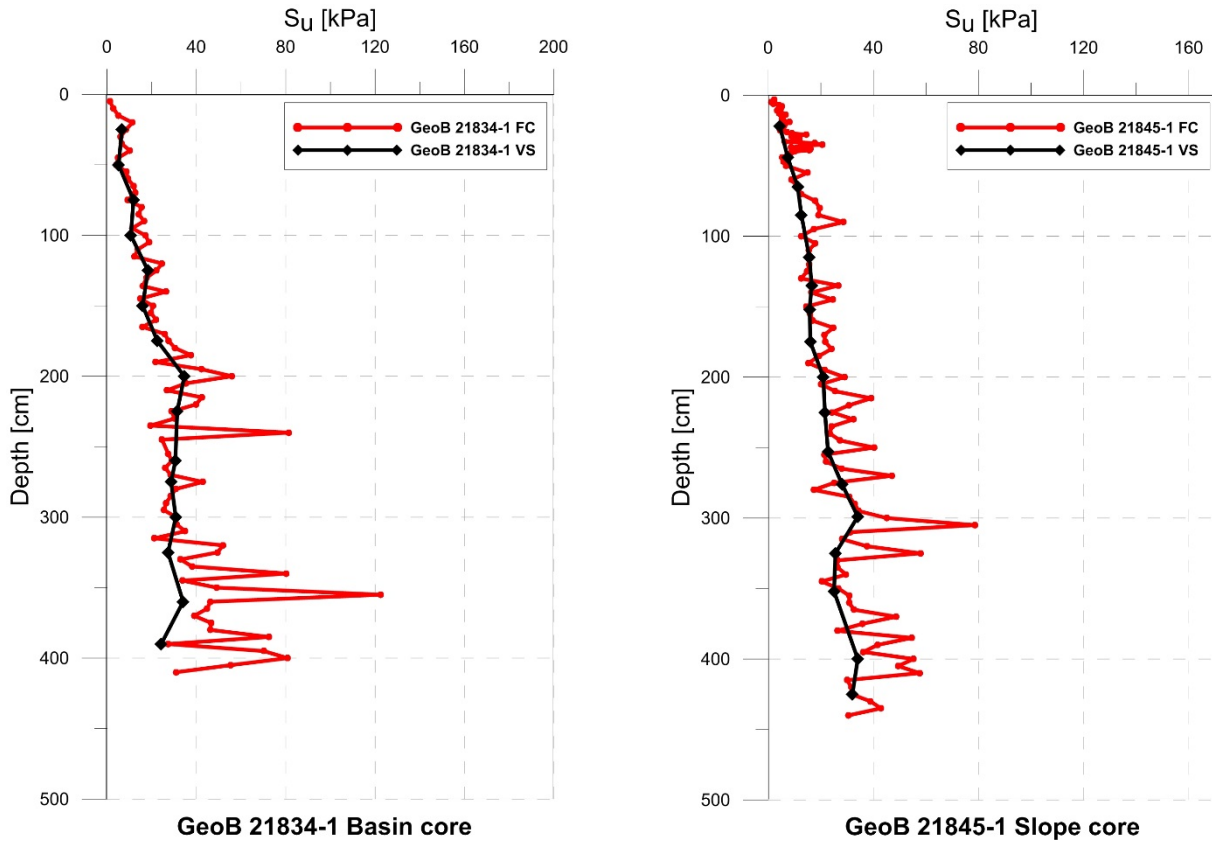


Figure 7.5.4: Exemplary shear strength's trend and value range of a basin and slope core in the Nankai Trough study area.

Kumano Basin - Mud Volcanos (MVs):

Cores taken on MVs (GeoB21836, GeoB21840, GeoB21842, GeoB21858, GeoB21860) with good recovery (>4m), show unusual undrained shear strength trends with depth. Core GeoB21836 presents s_u values of ~ 20 kPa from 0 ~350cm depth. From 350-400cm depth shear strength increases from 20-80kPa. Sediment in core GeoB21858 presents an increase in shear strength from ~1- 10 kPa from 0 – 250 cm depth. In core GeoB21860-1, s_u increases from ~2 – 10 kPa or more at 80 cm depth. A maximum value of 37 kPa is reached at 70cm depth. Generally, there is significant scatter in the fall cone data, which is believed to be related to the fall cone hitting mud clasts or rocks superficially covered in fine-grained sediment.

Kumano Basin – isolated basin:

Core GeoB21861-1 was taken in an isolated basin located in the north eastern part of the Kumano Basin. This core aimed at a good paleoseismic turbidite record, since the basin may be isolated from sediment supply other than through rapid sedimentation processes providing sediment from the basin walls. The sediment shear strength in core GeoB21861-1 increases linearly from ~1-10 kPa from 0-100cm depth. From ~100-200 cm below seafloor shear strength values present more scatter and reach up to 45 kPa.

Nankai – slope:

The cores GeoB21845-1 and GeoB21860.1 were taken on the slope for shear strength comparison with Japan Trench slope sediments. At site GeoB21845, s_u increases near linearly from ~1 to ~50 kPa from 0-450 cm depth. Core GeoB21866-1 reached only 280 cm below seafloor and s_u increases linearly to ~20 kPa at 250 cm depth. Scatter is notably low in the fall cone data of these cores.

7.5.3. Electrical Resistance

(M. Ikari)

Electrical resistance ranges from 3 to 311 k Ω , and values generally increase with depth. The trench cores GeoB21804-1 and GeoB21812-1 exhibit consistently low (< 60 k Ω) resistance values in the uppermost ~300 cm, before clearly increasing in the deeper sediments (Figure 7.5.5). Despite significant scatter, resistance values clearly and consistently increase with depth for trench cores GeoB21809-1 and GeoB21821-1 for the entire cored interval; the largest overall resistances tend to occur in core GeoB21809-1. Trench cores GeoB21817-1 and GeoB21823-1 exhibit broadly increasing resistance values, but also intervals of decreasing resistance; below ~700 cm for GeoB21817-1 and from ~300-600 cm for GeoB21823-1. Downhole resistance trends are highly variable in the slope cores (Figure 7.5.6). Core GeoB21810-1 shows steeply increasing resistance in the upper 100 cm, with no discernible trend deeper in the section. Core GeoB21805-1 exhibits a relatively constant range of values downhole, and resistance value decrease with depth in core GeoB21818-1.

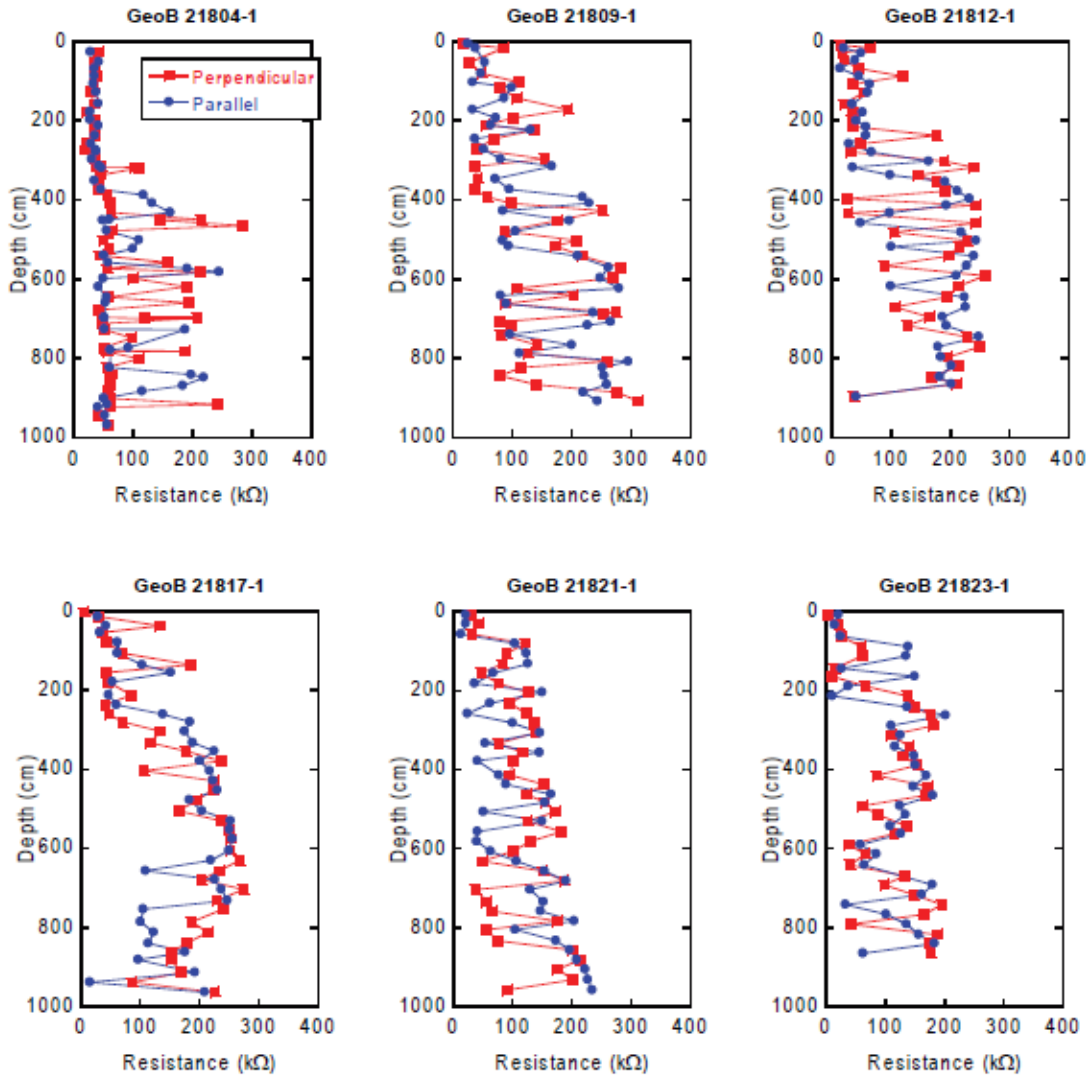


Figure 7.5.5: Electrical resistance as a function of depth for trench cores.

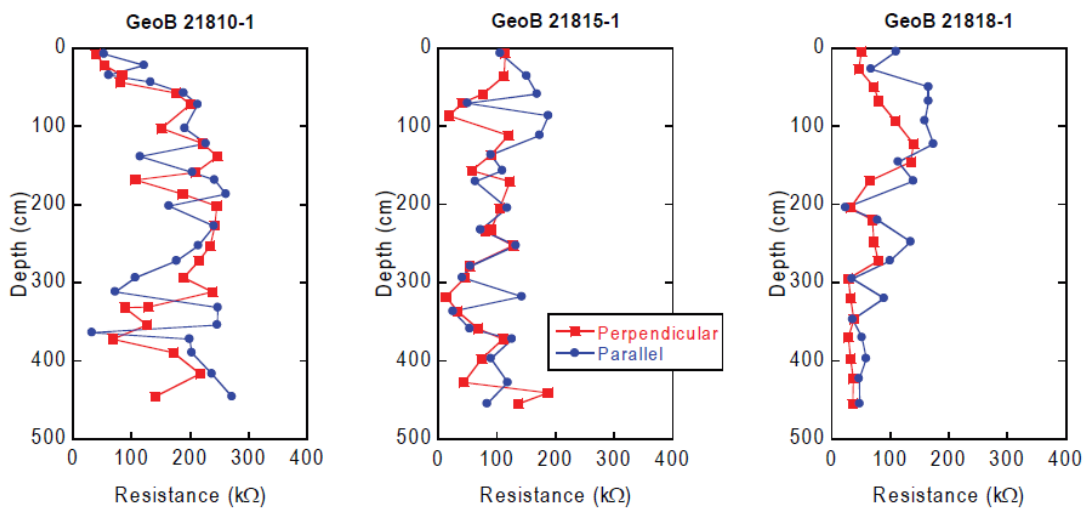


Figure 7.5.6: Electrical resistance as a function of depth for slope cores.

Resistance anisotropy values range from 0 (fully isotropic) to 175%. In general, anisotropy values show large scatter and downhole trends are difficult to identify. However, several zones of low anisotropy (isotropic zones) appear in the trench cores. Specifically, isotropic zones can be seen in the upper 200 cm of core GeoB21804-1, below 800 cm in core GeoB21812-1, from ~400-600 cm in core GeoB21817-1, and from ~200-400 cm in core GeoB21823-1 (Figure 7.5.7). Resistance anisotropy in the slope cores shows large scatter, a lack of downhole trends and also a lack of clear isotropic zones (Figure 7.5.8).

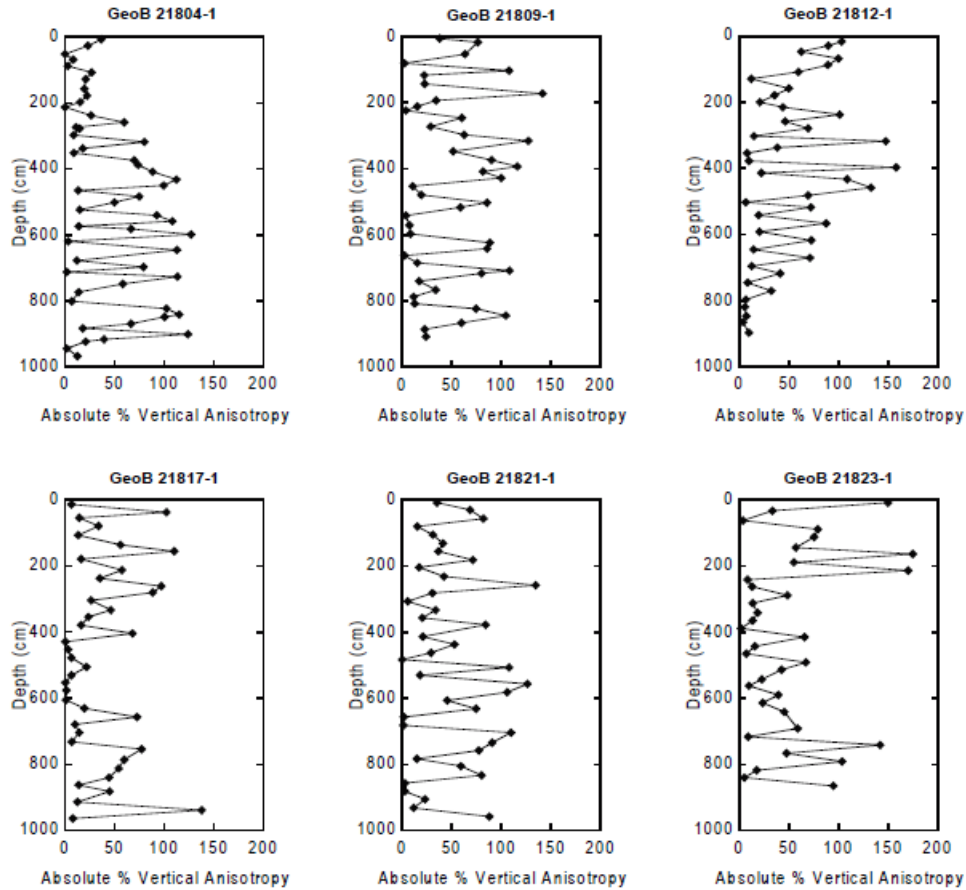


Figure 7.5.7: Absolute value of % vertical resistance anisotropy for trench cores.

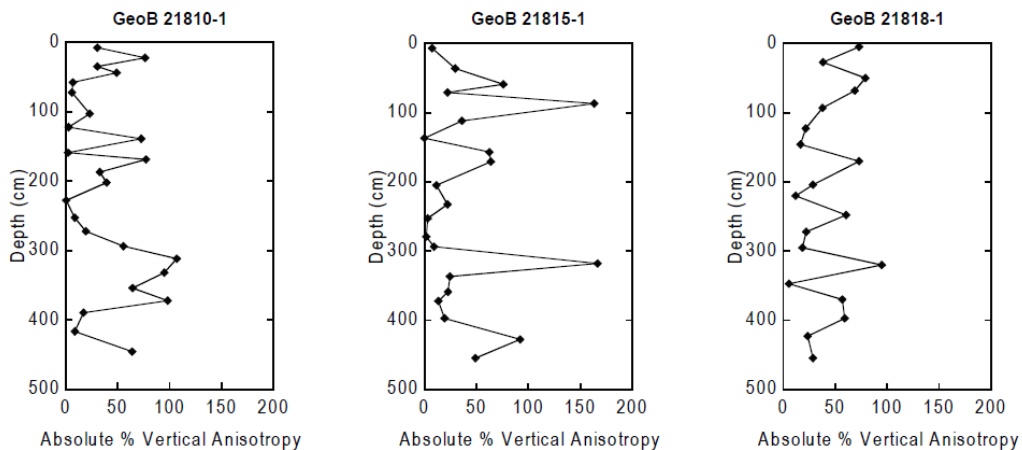


Figure 7.5.8: Absolute value of % vertical resistance anisotropy for slope cores.

7.5.4. Thermal Conductivity

(N. Kaul, M. Rex)

Thermal conductivity is mainly determined by the mineralogy and water content of the sediment. In general, high values are associated with sands and gravels, whereas low values may reflect fine-grained material with higher water contents. Quartz and carbonate mineralogy show particularly high thermal conductivity values and clay mineralogy particularly low values. Thermal conductivity generally increases with depth as porosity decreases due to compaction.

Japan Trench:

Not all sediment cores retrieved during SO251 Leg A were analyzed due to time constraints. However, thermal conductivity is measured on two trench cores (GeoB21804-1 and GeoB21809-1) and three slope cores (GeoB21810-1, GeoB21815-1, and GeoB21818-1). They show values ranging from 0.65 W/(m°C) to 0.9 W/(m°C). The mean thermal conductivity value of the trench cores is around 0.7 W/(m°C) and for the slope cores 0.8 W/(m°C).

Both trench cores reveal similar development of thermal conductivity with depth displayed by relatively stable low thermal conductivity values in the upper 6 m (particularly remarkable in GeoB21804-1; Figure 7.5.9). Furthermore, a sawtooth pattern is recognized in the lower part of the sediment cores with slightly higher values (0.7 W/(m°C) - 0.72 W/(m°C)). No distinct pattern is detected in the slope cores. Thermal conductivity ranges from 0.7 W/(m°C) to 0.9 W/(m°C) with several increasing and decreasing intervals in each of the cores. In general the five sediment cores recovered from the Japan Trench present relatively constant thermal conductivity values with only a few extreme values and a relatively small variation of 0.2 W/(m°C).

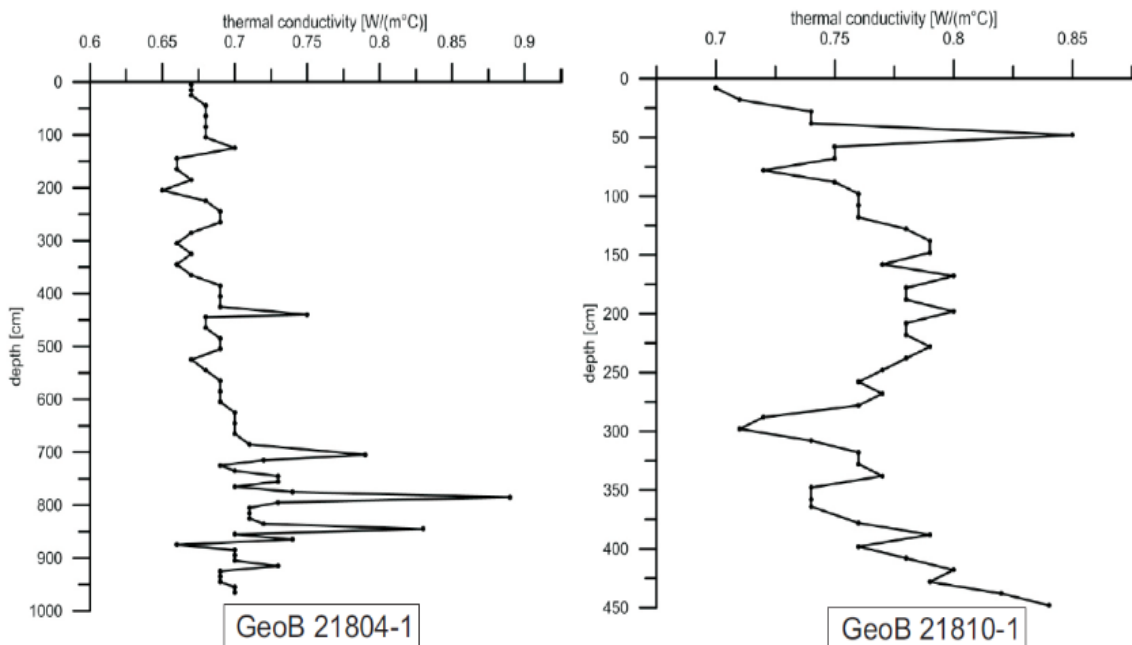


Figure 7.5.9: Exemplary thermal conductivity of a trench core (GeoB21804-1) and a slope core (GeoB21810-1) in the Japan Trench study area

Nankai Trough:

Thermal conductivity of sediment cores from the Nankai Trough study area lies between 0.67 W/(m°C) and 1.4 W/(m°C). A general rise in thermal conductivity with increasing depth exists in most of the sediment cores. Values rise relatively linear about 0.4 W/(m°C) over the total core length of 5 m. Peaks occur more frequently in the lower part of the sediment cores, indicating coarser layers.

The sediment cores GeoB21829-1, GeoB21831-1, GeoB21833-1, GeoB21834-1, GeoB21843-1, GeoB21858-1, GeoB21861-2, GeoB21864-2, and GeoB21866-2 show a similar development (Figure 7.5.10). Thermal conductivity is very constant in the upper 2.5 m without any major fluctuations. These low values reflect fine grained materials. Nevertheless, values rise relatively steady from 0.7 W/(m°C) to 0.9 W/(m°C). Thermal conductivity generally increases with depth as porosity decreases due to compaction.

The lower part from 3 mbsf downwards is dominated by frequent extreme values up to 1.4 W/(m°C). The large scatter results from high conductivity in sandy layers. However, in the western most cores of the study area (GeoB21833-1 and GeoB21834-1) thermal conductivity also reaches peak values in the upper part, indicating coarser layers with higher quartz content.

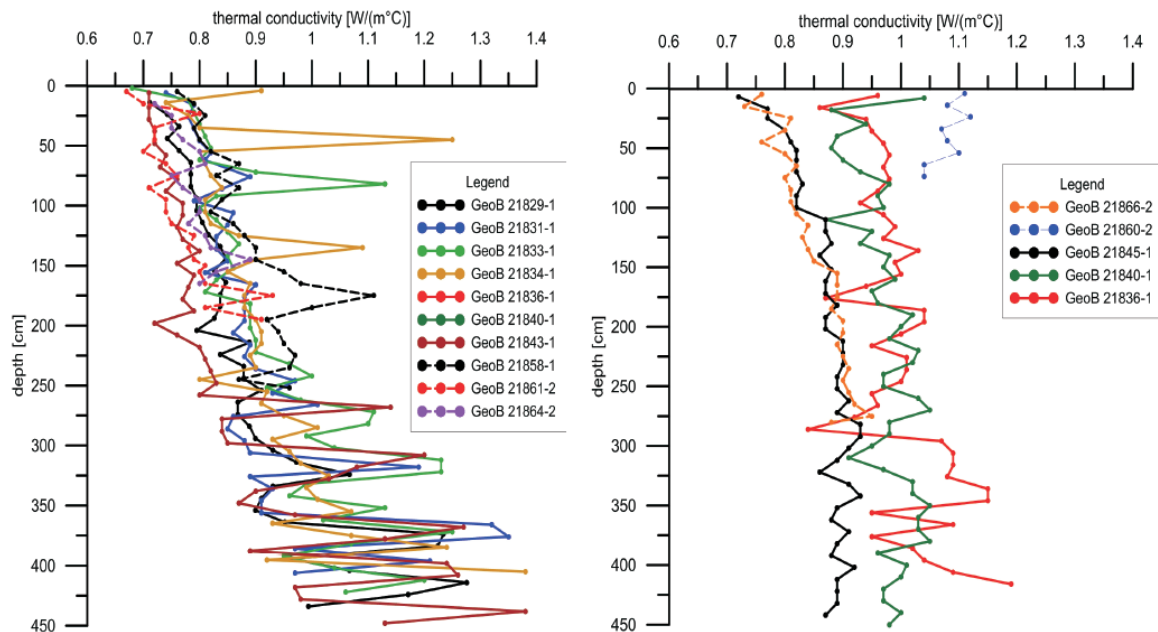


Figure 7.5.10: Left graph shows sediment cores in the Nankai Trough study area with similar thermal conductivity development; Right graph shows sediment cores located at the southern edge of the Nankai Trough study area and sediment core GeoB21860-2 retrieved on mud volcano number 2

Sediment cores GeoB21836-2, GeoB21840-1, GeoB21845-2, and GeoB21866-2 display different trends regarding thermal conductivity. Values slightly increase in sediment cores GeoB21866-2 and GeoB21845-1 from 0.7 W/(m°C) to 0.85 W/(m°C) within the first 1.5 m. Thermal conductivity is constant with increasing depth and no peak values occur.

Thermal conductivity values of sediment cores GeoB21836-1 and GeoB21840-1 belong to one of the highest measured values in the Nankai Trough study area with $0.95 \text{ W}/(\text{m}^\circ\text{C})$. No significant changes or peak values appear in these cores except for low values around 3 m depth, which are caused by ash depositions (information from sediment core descriptions).

Coarser material did not reach the core location of these four cores because of their location at the southern edge of the study area. This results in a rather homogenous thermal conductivity contribution.

Sediment core GeoB21860-1 was recovered on mud volcano number 2 and has a length of less than 1 m. Thermal conductivity values of this core vary between $1 \text{ W}/(\text{m}^\circ\text{C})$ and $1.1 \text{ W}/(\text{m}^\circ\text{C})$. These high values are probably caused by carbonate depositions on the mud volcano.

7.6. Geochemistry

(M. Kölling, N. Lübben, P. Töchterle)

Japan Trench Preliminary Results

Pore water samples from 7 piston cores were taken from locations within and from the slope of the Japan Trench. Samples were analysed offshore for alkalinity and pH. Alkalinity generally increases with depth (Figure 7.6.1). In the long piston cores (GeoB21804-1, GeoB21809-1, GeoB21817-1 and GeoB21823-1, all approximately 9.50 m), alkalinities reach 50 to over 70 mM/L, which is generally indicative of very high production areas. In the special case of the Japan Trench we suspect it shows the high fraction of relatively fresh organic material being trapped in the trench. The shallower shorter (approximately 4.5m) slope cores still show increasing alkalinities with maxima of 16 mM/L (GeoB21810-1 and GeoB21815-1) and 23 mM/L (GeoB21818-1). PH values are generally increasing from around pH 7.5 to pH 7.9 in the upper part of the cores and stabilize around 8.0 to 8.2 further downcore. Two of the slope cores smell of H₂S below 2 or 3 mbsf. Given the high production rates indicated by the alkalinity data, in most of the cores the sulfide seems to be fixed as iron sulfides that are highly abundant in the cores. Since the source rock for the terrigenous fraction in the recovered sediments is mostly of vulcanoclastic origin, a high abundance of iron minerals is likely and it will keep the formation of sulfide minerals sulfur limited rather than iron limited, keeping the free sulfide concentrations low.

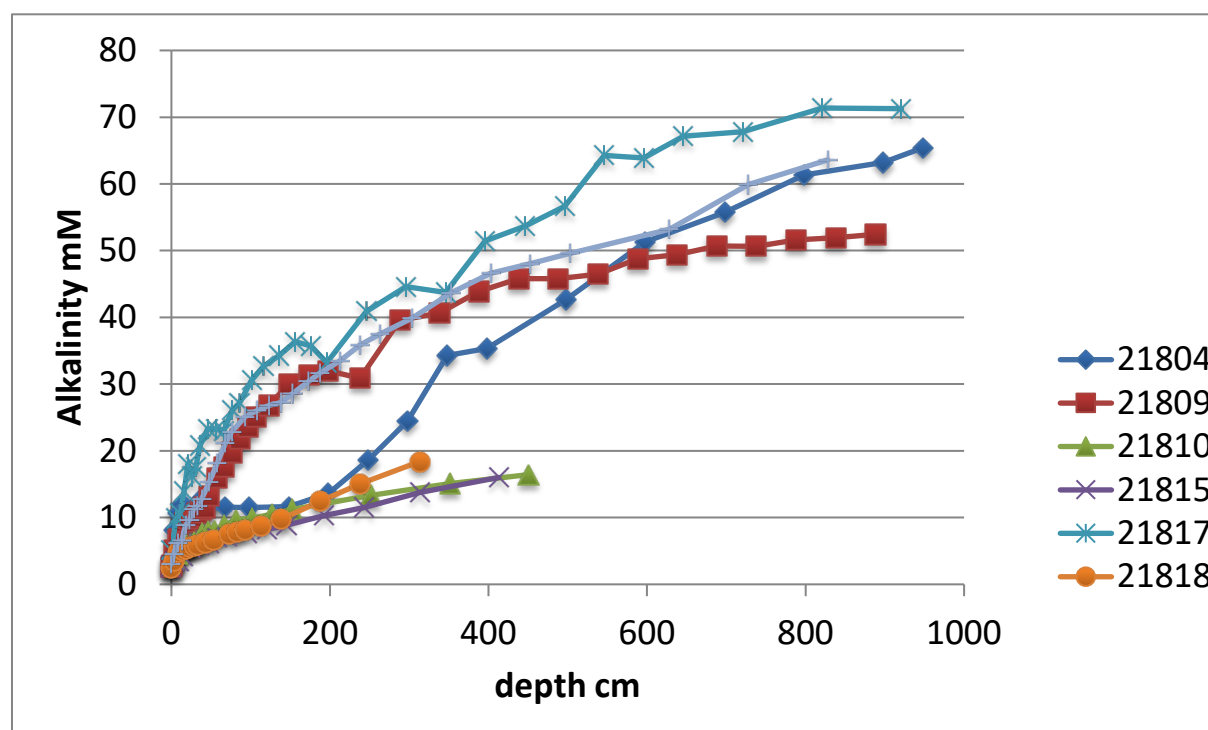


Fig. 7.6.1 Alkalinity measurements of interstitial water from cores recovered at several sites in the Japan Trench study area. For complete label and details, see station list in Appendix 11.1.1.

Nankai Trough / Kumano Basin Preliminary Results:

Pore water samples from 10 piston cores and 4 gravity cores taken from various locations within the Kumano Basin were analysed offshore for alkalinity, pH and in part also salinity. Analytical uncertainties (2σ) derived from in-house standard measurements at regular intervals amount to ± 0.10 mM in terms for alkalinity, ± 0.160 for pH and 0.2% salinity for salinity measurements. However, test runs on in-house salinity standards give reason to believe that the salinity values reported hereafter are affected by instrument drift related to lacking temperature regulation of sample material that cannot be quantified at this point. We therefore advise to handle these data with care and rather rely on offshore salinity data.

Alkalinities of most cores show a generally increasing trend with depth (Figure 7.6.2). However, as depicted in Figure 7.6.1 the gradients of this increase show large variations. GeoB21833-1, GeoB21834-1, GeoB21836-2 and GeoB21840-1 are characterised by a strong increase in alkalinity up to values of > 35 mM, featuring a drop in alkalinity values towards the lowermost sample point. GeoB21829-1, GeoB21831-1, GeoB21843-1 and GeoB21846-1 illustrate lower peak alkalinity values (< 11 mM), showing a nearly linear trend. GeoB21845-1 and GeoB21858-2 exhibit alkalinity values in between the previous mentioned groups (< 15 mM). GeoB21861-2 shows higher alkalinity values and a steep gradient culminating at 25.84 mM. GeoB21842-1, GeoB21845-4 and GeoB21846-2 feature alkalinities, which are only slightly increasing to 3 mM throughout the core.

A H_2S smell was detected throughout sites GeoB21833, GeoB21834, GeoB21836 (all western Kumano Basin) and in cores GeoB21858, GeoB21860 and GeoB21861 (easternmost edge of Kumano Basin).

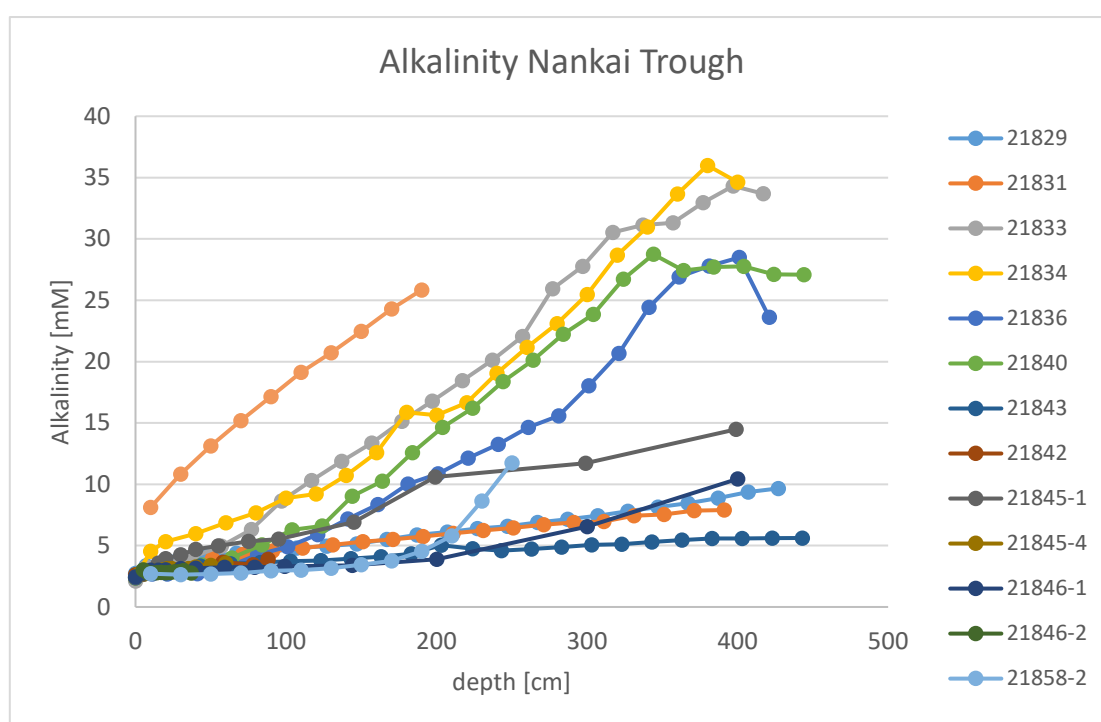


Fig. 7.6.1. Alkalinity measurements of interstitial water from cores recovered in the Nankai Trough study area

The salinity values span a range from 3.1 to 4.2 ‰_{salinity}. With the exception of GeoB21829-1, GeoB21843-1 and GeoB21846-1, all cores are characterised by a slight decrease. GeoB21829-1 and GeoB21843-1 exhibit a flat trend with values of 3.7 ‰_{salinity}, whereas GeoB21846-1 ranges between 2.8 and 3.9 ‰_{salinity}. GeoB21831-1 occupies the highest values with up to 4.2 salinity ‰. GeoB21833-1, GeoB21834-1, GeoB21836-2, GeoB21840-1, GeoB21842-1, GeoB21846-2, GeoB21858-2, and GeoB21861-2 fluctuate between 3.8 and 3.1 ‰_{salinity}. However, these data are likely biased by instrument drift due to changes in sample temperature. The observed trends are therefore not to be attributed to a salinity signal unambiguously. The main motivation to use the relatively unprecise Krüss optical refractometer for salinity measurement was to be able to detect massive changes in salinity related to mud volcanoes or gas hydrates.

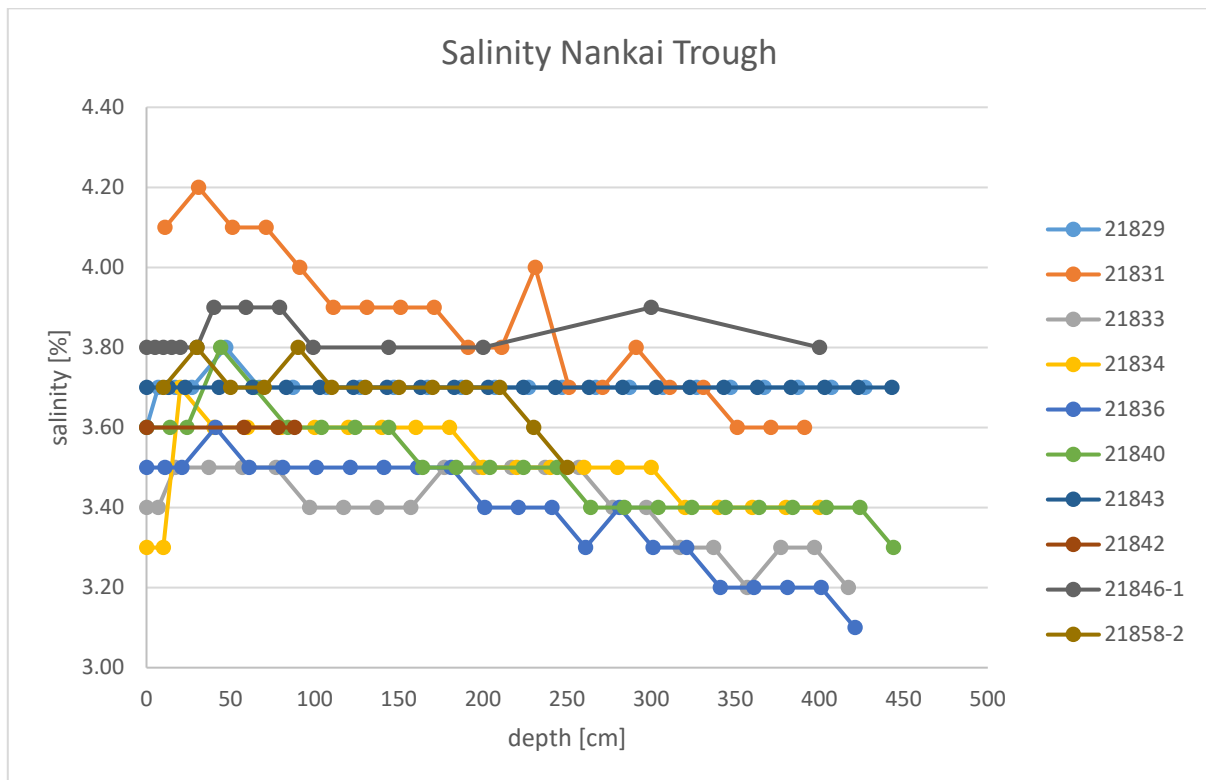


Fig. 7.6.2. Salinity measurements of interstitial water from cores recovered in the Nankai Trough study area

7.7. Heat Flow determination

(N. Kaul, B. Heesemann, M. Rex, M. Yoshimura, E. Hatakayma and M. Asada)

4 piston core deployments carried temperature sensors. Preliminary data analysis by Prof. Masa Kinoshita (Earthquake Research Institute, University of Tokyo) I) reveal in situ temperature gradient of 60, 66 +/- 1.5 and 79 +/- 3 at sites GeoB21836, GeoB21840 (Figures 7.7.1 and 7.7.2), and GeoB21843, respectively). No data were obtained from Site GeoB21842, because the probe did not penetrate into the subsurface.

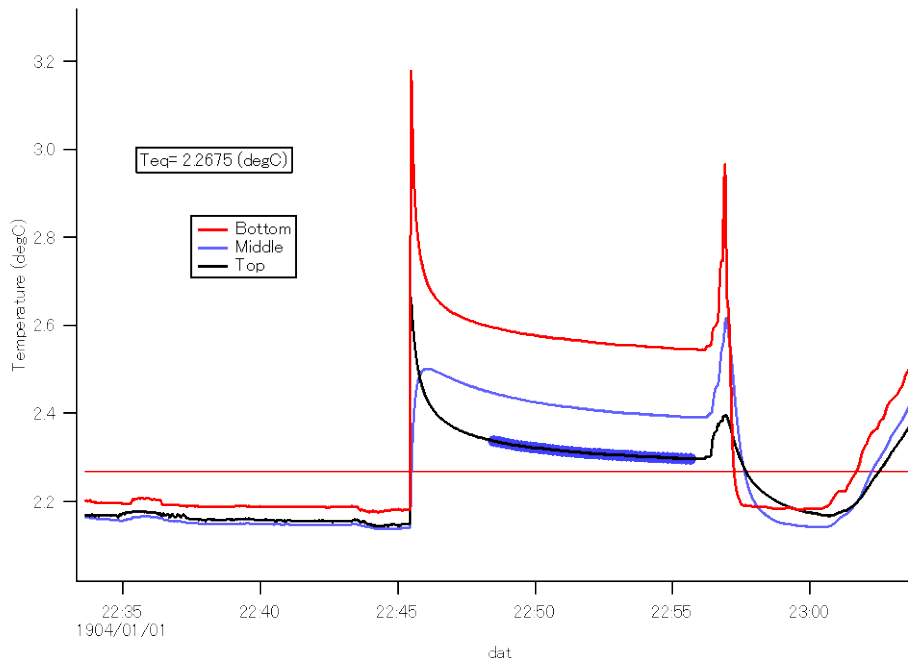


Fig. 7.7.1. Temperature vs. time plot for 3 MTL at site GeoB21836. T_{eq} (equilibrium temperature) is estimated by least-squares fitting of $(1/T)$ vs. time.

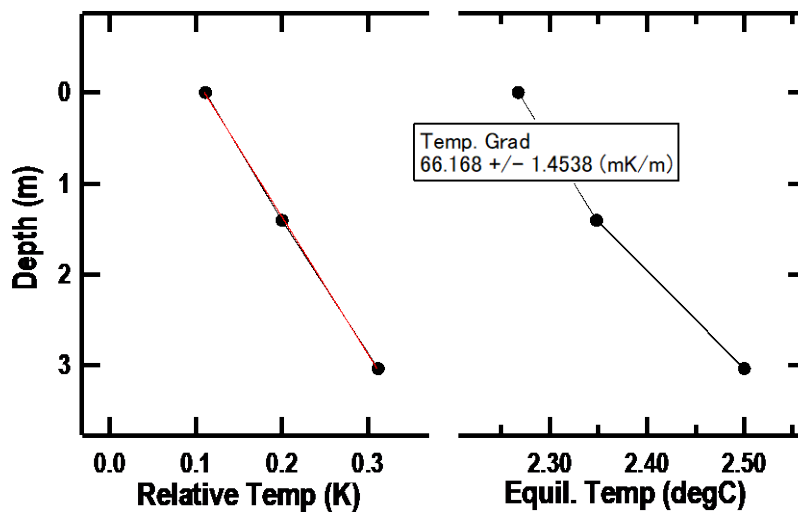


Fig. 7.7.2. Equilibrium temperature vs. depth at site GeoB21836. 'Relative temperature' on the left panel is the difference between T_{eq} and bottom water temperature prior to penetration.

46 sites were tested for temperature gradients by the 6 m heat flow probe, 38 of them successful. Those, which failed, had almost no penetration, probably due to carbonate crusts. A common penetration depth was 3 – 4 mbsf, depths greater than 5 mbsf were rarely achieved (Table 7.7.1).

Most of the mud volcanoes appear to be dormant, deduced from the thermal gradient which only slightly exceeds the background values of 0.03 and 0.06°C/m.

The following data example of the 22 channel heat flow probe is taken from a transect across KK13 (see Figure 7.7.3).

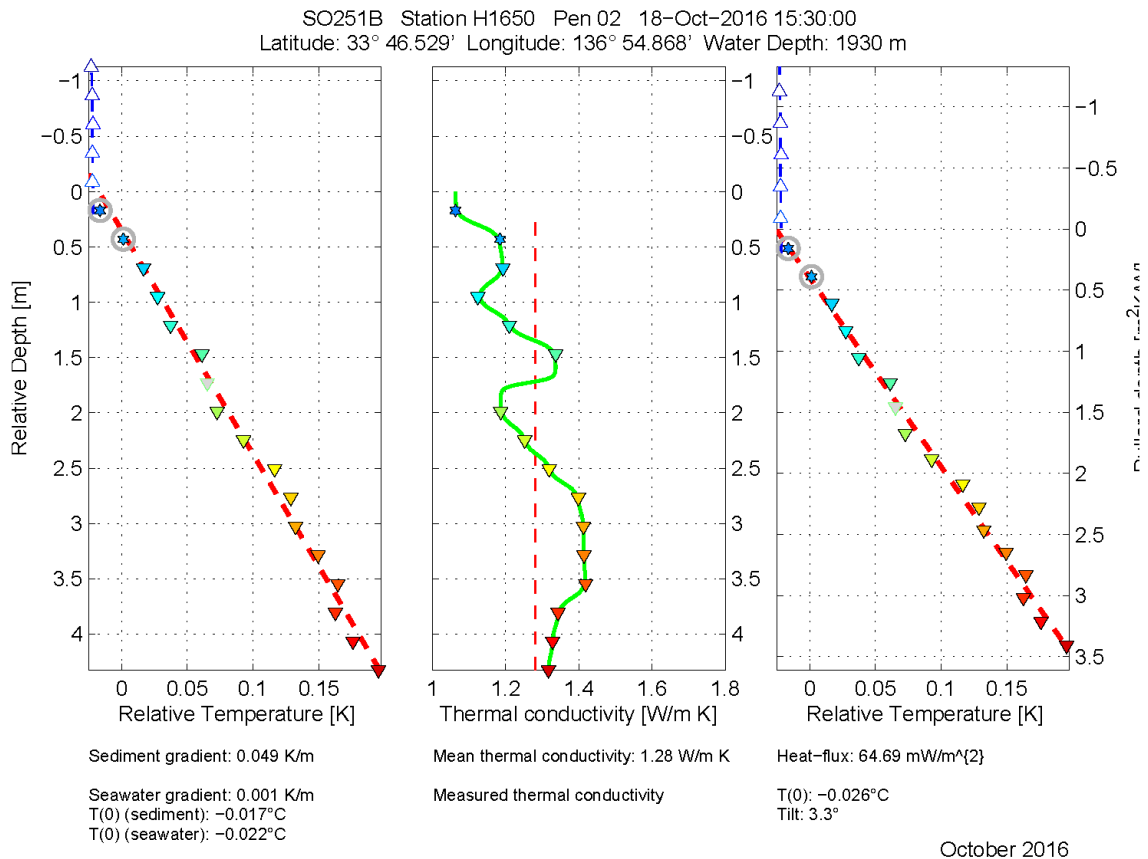


Fig. 7.7.3: Data example from GeoB21825, a profile across KK13 by the 22 channel heat flow probe. Left hand side: temperature gradient with temperatures relative to the calibration point, middle: in situ thermal conductivities, right hand side: Bullard plot

Table 7.7.1: Results of temperature gradient measurements

GeoB-Name	HF-Name	Depth	Date (UTC)	Latitude N	Longitude E	Grad. [mK/m]	Pen. Depth [mbsf]	Quality		
GeoB218-25	H1650P01	1918	18.10.2016	33	46,722	136	54,860	47	4,3	++
GeoB218-25	H1650P02	1930	18.10.2016	33	46,529	136	54,868	49	4,3	++
GeoB218-25	H1650P03	1936	18.10.2016	33	46,355	136	54,859	50	5	++
GeoB218-25	H1650P04	1927	18.10.2016	33	46,212	136	54,883	58	5,7	++
GeoB218-25	H1650P05	1880	18.10.2016	33	46,119	136	54,868	36	2,1	-
GeoB218-25	H1650P06	1889	18.10.2016	33	46,079	136	54,861	67	2	-
GeoB218-25	H1650P07	1928	18.10.2016	33	45,912	136	54,868	50	2,6	+
GeoB218-25	H1650P08	2015	18.10.2016	33	45,405	136	54,929	61	4,1	+
GeoB218-25	H1650P09	2015	18.10.2016	33	44,862	136	54,957	58	5,2	++
GeoB218-32	H1651P01	2016	19.10.2016	33	29,931	136	49,301	31	1,5	+
GeoB218-32	H1651P02	2019	19.10.2016	33	30,354	136	48,911	29	2,1	+
GeoB218-32	H1651P03	2027	19.10.2016	33	30,785	136	48,520	33	2,9	+
GeoB218-32	H1651P04	2034	19.10.2016	33	31,217	136	48,134	43	3,3	+
GeoB218-32	H1651P05	2040	19.10.2016	33	31,645	136	47,736	40	2,7	++
GeoB218-32	H1651P06	2041	20.10.2016	33	32,086	136	47,353	43	3,1	++
GeoB218-32	H1651P07	2044	20.10.2016	33	32,525	136	46,962	43	3,3	++
GeoB218-36		1919	20.10.2016	33	15,174	136	35,071	60	3,1	+
GeoB218-40		1862	21.10.2016	33	15,134	136	34,893	66	3,1	++
GeoB218-42		1830	22.10.2016	33	42,867	137	5,224	NaN	NaN	--
GeoB218-43		1987	22.10.2016	33	41,621	137	0,739	79	2,6	++
GeoB218-55	H1652P01	1966	25.10.2016	33	43,253	137	6,208	53	2,8	++
GeoB218-55	H1652P02	1959	25.10.2016	33	43,152	137	5,931	50	2,8	++
GeoB218-55	H1652P03	1983	25.10.2016	33	42,630	137	4,485	56	3,1	++
GeoB218-55	H1652P04	1982	25.10.2016	33	42,682	137	4,776	47	2,5	++
GeoB218-55	H1652P05	1913	25.10.2016	33	42,783	137	5,008	30	3,3	-
GeoB218-55	H1652P06	1837	25.10.2016	33	42,820	137	5,127	69	2,8	+
GeoB218-55	H1652P07	1822	25.10.2016	33	42,860	137	5,220	NaN	NaN	--
GeoB218-55	H1652P08	1823	25.10.2016	33	42,884	137	5,285	NaN	NaN	--
GeoB218-55	H1652P09	1848	25.10.2016	33	42,906	137	5,353	NaN	NaN	--
GeoB218-55	H1652P10	1909	25.10.2016	33	42,948	137	5,443	NaN	NaN	--
GeoB218-55	H1652P11	1907	25.10.2016	33	42,948	137	5,443	NaN	NaN	--
GeoB218-55	H1652P12	1936	25.10.2016	33	42,989	137	5,624	NaN	2,4	--
GeoB218-52	H1653P01	2006	27.10.2016	33	39,515	136	55,266	64	3,5	+
GeoB218-52	H1653P02	2009	27.10.2016	33	40,070	136	55,241	59	3,6	+
GeoB218-52	H1653P03	2007	27.10.2016	33	40,229	136	55,237	36	4,7	GH
GeoB218-52	H1653P04	1998	27.10.2016	33	40,372	136	55,250	54	4,3	GH
GeoB218-52	H1653P05	1992	27.10.2016	33	40,480	136	55,236	303	5,4	++
GeoB218-52	H1653P06	1993	27.10.2016	33	40,590	136	55,228	270	6,1	++
GeoB218-52	H1653P07	1995	27.10.2016	33	40,837	136	55,229	144	5,4	GH
GeoB218-52	H1653P08	2002	27.10.2016	33	40,754	136	55,207	-22	4,3	GH
GeoB218-57	H1654P01	740	30.10.2016	33	56,688	136	56,128	NaN	NaN	--
GeoB218-58	H1655P01	1961	30.10.2016	33	49,298	137	1,442	61	4,4	+
GeoB218-60	H1656P01	2000	30.10.2016	33	40,675	156	55,129	62	3,3	GH
GeoB218-61	H1657P01	2160	30.10.2016	33	47,382	137	16,037	68	4,3	++
GeoB218-64	H1658P07	2038	31.10.2016	33	46,609	136	29,07	48	3	-
GeoB218-66	H1659P01	2889	31.10.2016	33	9,732	136	38,805	67	3,6	+

8. Data and Sample Storage and Availability

All sediment cores and samples are stored in the MARUM GeoB core repository. All data produced can be obtained from the respective research groups on request. Data sets, which are part of publications in international peer-reviewed journals will automatically be made publically available on www.pangaea.de.

9. Acknowledgements

We want to thank Captain Oliver Meyer and the entire crew for their friendly and helpful collaborative approach, in particular when we had to improvise as a result of the missing equipment and containers.

We also want to thank our colleagues onshore and offshore in Japan, without whom we would have not been able to set up the seagoing equipment or laboratories on RV Sonne. The following institutions provided tremendous help with this: JAMSTEC, AORI, Geological Survey of Japan.

We further are grateful for the help by GEOMAR, Kiel, who mobilized both ROV PHOCA and the violin bow HF probe at very short notice in a very collaborative way.

A number of outreach activities, mainly three ship logs, were published over the course of the cruise on three websites: MARUM Bremen, Univ. Innsbruck, and Planet Erde. We thank those who provided the shore based support and posted the news in the respective locations.

Last but not least, we acknowledge receipt of initial funding for this cruise from BMBF via grant 03G0251A, and additional financial help after the HANJIN bankruptcy took its course and resulted in no equipment showing up on time for cruise SO251.

10. References

- Alves, T., et al., 2014. Erosional features as indicators of thrust fault activity (Nankai Trough, Japan), *Marine Geology*, 356, 5-18
- Amsler et al., 2014. Elemental distribution and microfabric characterization across a buried slump scar: New insights on the long-term development and reactivation of scar surfaces from a microscopic perspective. *Advances in Natural and Technological Hazard Research*, 37, 23-32.
- Ando, M., 1975, Source mechanisms and tectonic significance of historical earthquakes along the NT, Japan: *Tectonophysics*, v. 27, no. 2, p. 119-140.
- Arai, K., et al, 2013, Tsunami-generated turbidity current of the 2011 Tohoku-Oki earthquake: *Geology*. v. 41, p. 1195– 1198
- Archie, G. E. 1942. The electrical resistivity log as an aid in determining some reservoir characteristics. *Transactions of the AIME*, 146(01), 54-62.
- Baba, T., et al., 2005, Contiguous rupture areas of two Nankai Trough earthquakes revealed by tsunami waveform inversion: *Geophys. Res. Lett.*, v. 32.
- British-Standard-Institute 1977. *Methods of testing soil for civil engineering purposes*, BS 1377. BSI, London. BSI, London
- Chester, F.M., et al., 2013. A thin and weak plate-boundary décollement in the region of maximum slip, 2011 Tohoku-oki earthquake. *Science*, Vol. 342, Issue 6163, pp. 1208-1211,
- Clift, P. et al., 2013, Zircon and apatite thermochronology of the Nankai Trough accretionary prism and trench, Japan: *Tectonics*, v. 32, no. 3, p. 377-395.
- DeMets, C., et al., 2010. Geologically current plate motions. *Geophys. J. Int.* 181, 1
- Dunham, R.J., 1962. Classification of carbonate rocks according to depositional texture. *In* Ham, W.E. (Ed.), *Classification of Carbonate Rocks*. AAPG Mem., 1:108–121.
- Expedition 343/343T Scientists, 2013. *Methods*. In Chester, F.M., Mori, J., Eguchi, N., Toczko, S., and the Expedition 343/343T Scientists, *Proc. IODP, 343/343T: Tokyo (Integrated Ocean Drilling Program Management International, Inc.)*, doi:10.2204/iodp.proc.343343T.102.2013.
- Fink, H.G., et al., (2014): Evidence for Mass Transport Deposits at the IODP JFAST-Site in the Japan Trench, *Advances in Natural and Technological Hazards Research* 37. 33-43
- Fujiwara, T., et al., 2011, The 2011 Tohoku-Oki Earthquake: Displacement Reaching the Trench Axis: *Science*, v. 334, no. 6060, p. 1240.
- Fulton, P. M., et al., 2013. Low Coseismic Friction on the Tohoku Fault Determined from Temperature Measurements. *Science*, Vol. 342, Issue 6163, pp. 1214-1217
- Hansbo, S., 1957. A new approach to the determination of the shear strength of clay by the fall-cone test. *Proceedings Swedish Geotechnical Institute* 14: 1-47.
- Hatori, T, 2003. Irregular height deviation of the 1677 Enpo Boso-Oki tsunami, Eastern Japan, *Historic Earthquake*, 19, 1-7 (in Japanese).
- Ikari et al., 2011. Submarine landslide potential near the megasplay fault at the Nankai subduction zone *Earth and Planetary Science Letters*, 312, 453-462
- Ikehara, K., et al., 2016. Documenting large earthquakes similar to the 2011 Tohoku-oki earthquake from sediments in the Japan Trench over the past 1500 years, *EPSL*, 445, 48-56,
- Ito, Y., et al., 2011, Frontal wedge deformation near the source region of the 2011 Tohoku-Oki earthquake: *Geophys. Res. Lett.*, v. 38, no. 15, p. L00G05.
- Jackson, P. D., et al, 1978. Resistivity-porosity-particle shape relationships for marine sands. *Geophysics*, 43(6), 1250-1268.
- Kamata, H. & Kodama, K., 1999. Volcanic history and tectonics of the southwest Japan arc. *Island Arc*, Volume 8, pp. 393-403.
- Kanamatsu et al., 2013, Characterization of event deposits induced by Tohoku-oki Earthquake in the Japan Trench using paleo-magnetic techniques. *AGU Fall Meeting*, Abstract T23C-2603
- Kato, A., et al. 2012, Propagation of Slow Slip Leading Up to the 2011 Mw 9.0 Tohoku-Oki Earthquake: *Science*, v. 335, no. 6069, p. 705-708.
- Kawamura, K., et al., 2012, Submarine landslides in the Japan Trench: A new scenario for additional tsunami generation: *Geophys. Res. Lett.*, v. L05308.
- Kimura et al., 2011. Spatial and temporal evolution of the megasplay fault in the Nankai Trough. *Geochemistry, Geophysics, Geosystems*, 12, Q0A008
- Kodaira, S., et al., 2012, Coseismic fault rupture at the trench axis during the 2011 Tohoku-oki earthquake: *Nature Geosci*, v. 5, no. 9, p. 646-650.
- Kopf, A., Araki, E., Toczko, S., and the Expedition 332 Scientists, 2011. *Proc. IODP, 332: Tokyo (Integrated Ocean Drilling Program Management International, Inc.)*. doi:10.2204/iodp.proc.332.2011

- Kopf et al., 2013: REPORT AND PRELIMINARY RESULTS of RV Sonne CRUISE SO222: MEMO – MeBo drilling and in situ Long-term Monitoring in the Nankai Trough accretionary complex, Japan. *Berichte des Fachbereich Geowissenschaften der Univ. Bremen*, 297: 121pp.
- Kopf et al., 2015, Simple, affordable, and sustainable borehole observatories for complex monitoring objectives, *Geosci. Instrum. Method. Data Syst.*, 4, 99-109,
- Lee, H. J., et al. 2007, Submarine mass movements on continental margins, in Nittrouer, C. A., et al, eds., *Continental Margin*, p. 213-273.
- Lin, W., et al. 2013, Stress State in the Largest Displacement Area of the 2011 Tohoku-Oki Earthquake: *Science*, v. 339, no. 6120, p. 687-690.
- Lovell, M. A., 1985. Thermal conductivities of marine sediments. *Quarterly Journal of Engineering Geology and Hydrogeology*, 18, 437-441.
- Marsaglia, K., Milliken, K., Doran, L. (2012) Smear Slides of Marine Mud for IODP Core Description: PART I Methodology and Atlas of slioclastic & volcanogenic components, (Maruyama et al., 1997) Paleo-geographic maps of the Japanese Islands: Plate tectonics synthesis from 750 Ma to the present. *Island. Arc*, 6, 121-141
- Mazzullo, J.M., Meyer, A., and Kidd, R.B., 1988. New sediment classification scheme for the Ocean Drilling Program. In Mazzullo, J.M., and Graham, A.G. (Eds.), *Handbook for shipboard sedimentologists*. ODP Tech. Note, 8:45–67.
- McHugh, et al., 2016. Remobilization of surficial slope sediment triggered by the A.D. 2011 Mw 9 Tohoku-Oki earthquake and tsunami along the Japan Trench. *Geology*, 44, 387-390,
- Miller, M.S., 2008. Breaking the slab. *Nature Geoscience*, 1, 730-731 (2008)
- Minoura, K, F. et al. 2001. The 869 Jogan tsunami deposit and recurrence interval of large-scale tsunami on the Pacific coast of northeast Japan. *J. Natural Disaster Sci.* 23, 83 (2001)
- Miyazaki, S. i., and Heki, K., 2001, Crustal velocity field of southwest Japan: Subduction and arc-arc collision: *J. Geophys. Res.*, v. 106.
- Moore, G. F., et al., 2007, Three-Dimensional Splay Fault Geometry and Implications for Tsunami Generation: *Science*, v. 318, no. 5853, p. 1128-1131.
- Moore, G. F., et al., 2009, Structural and Seismic Stratigraphic Framework of the NanTroSEIZE Stage 1 Transect: *Proc. IODP*, 314/315/316
- Moore, et al., 2016. Evolution of Tectono-Sedimentary Systems in the Kumano Basin, Nankai Trough Forearc. *Marine and Petroleum Geology*, 67, 604-616
- Moernaut et al., 2017. Lacustrine turbidites produced by surficial slope sediment remobilization: A mechanism for continuous and sensitive turbidite paleoseismic records. *Marine Geology*. Doi: 10.1016/j.margeo.2015.10.009
- Munsell. (2012). *Munsell Soil Color Charts 2009*.
- Nakamura, Y., et al., 2013, High-resolution seismic imaging in the Japan Trench axis area off Miyagi, N-Japan: *Geophys Res Lett*, 40, 1713–1718.
- Noguchi, T., et al., 2012, Dynamic process of turbidity generation triggered by the 2011 Tohoku-Oki earthquake: *G-cubed* 13, no. 11, p. Q11003.
- Ogawa, Y., 2011: Erosional Subduction Zone in the Northern Japan Trench: Review of Submersible Dive Reports Modern App. in *Solid Earth Sci.* 8,
- Oguri, K., et al., 2013, Hadal disturbance in the Japan Trench induced by the 2011 Tohoku–Oki Earthquake: *Sci. Rep.*, v. 3.
- Omura, A., and Ikehara, K., 2010, Deep-sea sedimentation controlled by sea-level rise during the last deglaciation, *Mar Geol*, v. 274, no. 1-4, p. 177-186.
- Park et al., 2002, Splay fault branching along the Nankai subduction zone, *Science*, 297 (5584), 1157 – 1160
- Rothwell, R. G. (1989), *Minerals and mineraloids in marine sediments an optical identification guide*, XIV, 279 pp., Elsevier Applied Science, London etc.
- Sacks S. et al. 2000. *Proceedings of the Ocean Drilling Program, Initial Reports* 186
- Sakaguchi, A., et al. 2011a, Seismic slip propagation to the updip end of plate boundary subduction interface faults: *Geology*
- Sakaguchi A., et al., 2011b, Episodic seafloor mud brecciation due to great subduction zone earthquakes *Geology*, 39, 919-922,
- Samouëlian, A., et al. 2005. Electrical resistivity survey in soil science: a review. *Soil and Tillage research*, 83(2), 173-193.
- Sasaki T 2004 Subduction tectonics of the northern Japan trench based on the regional seabeam mapping. PhD Theses, University of Tokyo, 159 pp
- Sawyer, D. E., and J. R. DeVore. 2015. Elevated shear strength of sediments on active margins: Evidence for seismic strengthening, *GRL.*, 42, GL066603.

- Sawai et al., 2012. Challenges of anticipating the 2011 Tohoku earthquake and tsunami using coastal geology, *GRL*, 39, L21309
- Sawai et al., 2015. Shorter intervals between great earthquakes near Sendai: scour ponds and a sand layer attributable to A.D. 1454 overwash. *GRL*, 42, 4785-4800
- Scientific Party. 1980. Initial Reports of the Deep Sea Drilling Project 56/57. U.S. Government Printing Office, Washington, DC.
- Shepard, F.P., 1954. Nomenclature based on sand-silt-clay ratios. *J. Sediment. Petrol.*, 24(3):151–158.
- Strasser et al., 2009: Origin and Evolution of a spaly fault in the Nankai accretionary prism *Nature Geoscience*, 2, 648-652
- Strasser et al., 2011 Slumping and mass-transport deposition in the Nankai forearc: Evidence from IODP drilling and 3-D reflection seismic data *Geochemistry, Geophysics, Geosystems*, 12, Q0AD13,
- Strasser et al., 2012 Scientific Drilling of Mass-Transport Deposits in the Nankai accretionary wedge: First Results from IODP Expedition 333. *Adv. Nat. and Tech. Hazard Research*, 31, 671-681,
- Strasser, M., et al., 2013, A Slump in the Trench: Tracking the impact of the 2011 Tohoku-Oki earthquake. *Geology* 41 (8): 935-938. doi:10.1130/g34477.1
- Strasser et al., 2014. **Proc. IODP**, 338: Yokohama (Integrated Ocean Drilling Program). [doi:10.2204/iodp.proc.338.2014](https://doi.org/10.2204/iodp.proc.338.2014)
- Strozyk et al., 2010 Slope failure repetition in active margin environments – constraints from submarine landslides in the Hellenic forearc, eastern Mediterranean. *Journal of Geophysical Research – Solid Earth*, 115, B08103
- Tajima, F., et al. 2013, A review of the 2011 Tohoku-Oki earthquake: Large-scale rupture across heterogeneous plate coupling: *Tectonophysics*, 586, 15-34.
- Tappin et al., 2014. Did a submarine landslide contribute to the 2011 Tohoku tsunami? *Marine Geology*, 357. 344-361
- Tanioka, Y. Satake, K. 1996. Fault parameters of the 1896 Sanriku Tsunami earthquake estimated from tsunami numerical models, *GRL* 23, 1549-1552.
- Tsuji, T., et al., 2013, Extension of continental crust by anelastic deformation during the 2011 Tohoku-oki earthquake: *Earth Plan Sci Lett*, 364, 44-58.
- Tsunogai, U. et al. 2012, Coseismic massive methane release from a submarine mud volcano: *Earth Plan Sci Lett*, 341–344, p. 79-85.
- Tsuru T., et al. 2000. Tectonic features of the Japan Trench convergent margin off Sanriku northeastern Japan, revealed by multichannel seismic reflection data. *Journal of Geophysical Research* 105, 16 403–13.
- Usami et al., in press Usami, K., et al., Benthic foraminiferal evidence of deep-sea sediment transport by the 2011 Tohoku-oki earthquake and tsunami, *Marine Geology*, <http://dx.doi.org/10.1016/j.margeo.2016.04.001>
- Ujiié, K. et al., 2013. Large shallow slip on the 2011 Tohoku-Oki megathrust as a result of low shear strength. *Science*, Vol. 342, Issue 6163, pp. 1211-1214
- von Huene and Lallemand, 1990. Tectonic erosion along the Japan and Peru convergent margins. *GSA Bulletin*. 102. 704-720
- von Huene, et al., 2004, Generic model of subduction erosion: *Geology*, v. 32, p. 913–916, doi: 10.1130/G20563.1..
- Wefer et al., 2014, Report and preliminary results of R/V SONNE Cruise SO219A, Tohoku-Oki Earthquake – Japan Trench, Yokohama – Yokohama, 08.03.2012 – 06.04.2012. *Berichte, MARUM – Universität Bremen*, No. 301, 83 pages. Bremen, 2014. ISSN 2195-7894).
- Wood, D.M., 1985, Some fall-cone tests. *Géotechnique*, 38: 64-68
- Yamaguchi, A., et al., 2011, Progressive illitization in fault gouge caused by seismic slip propagation along a megasplay fault *Geology*, 39, 995-998.
- Yamanaka, Y., & Kikuchi, M., 2004, Asperity map along the subduction zone in northeastern Japan inferred from regional seismic data, *JGR*. B07307.
- Yokota, Y., et al. 2011, Joint inversion of strong motion, teleseismic, geodetic, and tsunami datasets for the rupture process of the 2011 Tohoku earthquake: *Geophys. Res. Lett.*, v. 38, p. L00G21.
- Yoshikawa et al., 2016 Small-scale spatial variation in near-surface turbidites around the JFAST site near the Japan Trench, *Geochem. Geophys. Geosyst.*, 17, 1238–1246,

11. Appendix

11.1 Station Lists

Table 11.1.1: Station list coring sites

Table 11.1.2: Station list hydroacoustic profiles, ROV, HF & CTD

11.2 Core photos,

Figure 11.2.1 Core photos

11.3 Core Logs,

Figure 11.3.1 Core lithology logs

11.4 Table SmearSlide:

Table 11.4.1: Smear slide description

11.5 ROV Dive Protocols

Table 11.5.1: ROV dive protocols

11.6 Composite core logs

Figure 11.6.1 Composite core logs and core-parasound-correlation with compiled shipboard results of SO251 cores

Station List (Coring Sites)

GeoB	Ships Station	Device	Bottom Contact Date Time	Latitude	Longitude	Depth (m)	Recovery	Comment
21804	SO251/1_4-1	PC	05/10/2016 07:38:28,000	36° 4,256' N	142° 44,045' E	8025	976	SL max 8053m No Posidonia
21809	SO251/1_10-1	PC	07/10/2016 08:31:15,000	38° 0,428' N 38° 0,409' N	143° 59,634' E 143° 59,636' E	7540,4	913	SL max 7573 m Posidonia SL1800m
21810-1	SO251/1_11-1	PC	07/10/2016 14:36:23,000	38° 6,788' N 38° 6,776' N	143° 41,662' E 143° 41,684' E	5216,6	462	SL max 5239m Posidonia SL50m
21810-3	SO251/1_12-1	PC	07/10/2016 18:54:01,000	38° 6,795' N 38° 6,777' N	143° 41,670' E 143° 41,673' E	5215,1	444	SLmax 5239m Posidonia SL50m
21812	SO251/1_14-1	PC	09/10/2016 00:07:30,000	39° 14,908' N 39° 14,897' N	144° 12,230' E 144° 12,189' E	7743,9	906	SL max 7499m Posidonia SL1600m
21815-1	SO251/1_18-1	PC	10/10/2016 06:40:42,000	39° 19,535' N 39° 19,575' N	143° 38,859' E 143° 38,874' E	3105,5	467	SLmax 3117m Posidonia SL50m
21815-3	SO251/1_19-1	PC	10/10/2016 10:18:45,000	39° 19,563' N 39° 19,606' N	143° 38,885' E 143° 38,894' E	3107,3	366	SLmax 3118m Posidonia SL50m
21817	SO251/1_21-1	PC	10/10/2016 23:58:58,000	40° 23,743' N 40° 23,743' N	144° 25,226' E 144° 25,226' E	7607,8	971	SL max 7632m Posidonia SL1700m
21818-1	SO251/1_23-1	PC	11/10/2016 07:19:39,000	40° 14,767' N 40° 14,789' N	143° 48,783' E 143° 48,807' E	3138,9	463	SLmax 3142m Posidonia SL50m
21818-3	SO251/1_25-1	PC	11/10/2016 10:56:10,000	40° 14,786' N 40° 14,784' N	143° 48,830' E 143° 48,820' E	3136,9	460	SLmax 3141m Posidonia SL50m
21821	SO251/1_27-1	PC	12/10/2016 15:07:04,000	38° 53,963' N	144° 12,972' E	7664	970	SLmax 7433m No Posidonia
21823	SO251/1_29-1	PC	13/10/2016 03:58:19,000	38° 0,180' N 38° 0,204' N	143° 59,972' E 143° 59,989' E	7555,6	878	SLmax 7577m Posidonia SL1800m
21829	SO251/2_34-1	PC	19/10/2016 11:24:46,000	33° 40,141' N 33° 40,159' N	136° 47,792' E 136° 47,802' E	2029,9	450	SL max 2032m Posidonia SL50m
21831	SO251/2_36-1	PC	19/10/2016 16:19:09,000	33° 32,904' N 33° 32,915' N	136° 49,878' E 136° 49,892' E	2038,2	408	SLmax 2042m Posidonia SL50m
21833	SO251/2_38-1	PC	20/10/2016 06:10:15,000	33° 27,739' N 33° 27,746' N	136° 32,604' E 136° 32,614' E	2055,5	430	SLmax 2059m Posidonia SL50m
21834	SO251/2_39-1	PC	20/10/2016 09:17:39,000	33° 35,725' N 33° 35,732' N	136° 27,406' E 136° 27,409' E	2043,2	417	SL: 2046m Posidonia SL50m

Station List (Coring Sites)

GeoB	Ships Station	Device	Bottom Contact Date Time	Latitude	Longitude	Depth (m)	Recovery	Comment
21836-2	SO251/2_42-1	PC/MTL	20/10/2016 15:43:25,000	33° 15,131' N	136° 35,820' E	1916,8	428	SLmax 1952m No Posidonia
21840	SO251/2_47-1	PC	21/10/2016 22:46:14,000	33° 15,136' N 33° 15,148' N	136° 34,663' E 136° 34,743' E	1818,8	457	SL: 1868m Posidonia SL50m
21842	SO251/2_49-1	PC/MTL	22/10/2016 12:26:24,000	33° 42,853' N 33° 42,850' N	137° 5,225' E 137° 5,232' E	1829,2	95	SL max 1828 m Posidonia SL50m
21843	SO251/2_50-1	PC/MTL	22/10/2016 16:04:54,000	33° 41,621' N 33° 41,625' N	137° 0,738' E 137° 0,753' E	1985	460	SLmax 1989m Posidonia SL50m
21845-1	SO251/2_52-1	PC	23/10/2016 00:37:01,000	33° 12,488' N 33° 12,512' N	136° 44,350' E 136° 44,368' E	2863,4	449	SL max 2894 m Posidonia SL50m
21845-3	SO251/2_52-2	PC	23/10/2016 03:48:48,000	33° 12,418' N 33° 12,454' N	136° 44,265' E 136° 44,357' E	2863,5	444	SLmax 2893m Posidonia SL50m
21846	SO251/2_53-1	PC	23/10/2016 06:51:03,000	33° 9,760' N 33° 9,773' N	136° 38,716' E 136° 38,790' E	2882,3	454	SLmax 2916m Posidonia SL50m
21857-2	SO251/2_64-1	HF / GC	30/10/2016 00:10:43,000	33° 56,694' N 33° 56,688' N	136° 56,120' E 136° 56,128' E	740,2	0	SLmax 757 m Posidonia SL50m
21858-2	SO251/2_65-1	HF / GC	30/10/2016 02:53:02,000	33° 49,296' N 33° 49,298' N	137° 1,450' E 137° 1,442' E	1918,4	258	SL max 1945m Posidonia SL50m
21860-2	SO251/2_67-1	HF / GC	30/10/2016 07:56:10,000	33° 40,679' N 33° 40,675' N	136° 55,133' E 136° 55,129' E	2001,2		SLmax: 2026m Posidonia SL50m
21861-2	SO251/2_68-1	HF / GC	30/10/2016 11:32:18,000	33° 47,323' N 33° 47,382' N	137° 15,883' E 137° 16,097' E	2160,9	81	SL max 2188m Posidonia SL50m
21864-2	SO251/2_71-1	HF / GC	31/10/2016 09:38:36,000	33° 46,624' N 33° 46,623' N	136° 29,078' E 136° 29,075' E	2034,6	171	BOKO, SLmax: 2058m Posidonia SL50m
21866-2	SO251/2_73-1	HF / GC	31/10/2016 23:30:20,000	33° 9,731' N 33° 9,732' N	136° 38,805' E 136° 38,805' E	2890,8	281	SLmax 2935m Posidonia SL50m

Station List (hydroacoustic profiles, ROV, HF, and CTD)

GeoB	Station	Device	Date Time	Latitude	Longitude	Depth (m)	Comment	Action
21801	SO251/1_1-1	CTD	04/10/2016 21:00:02.000	35° 35,997' N	142° 21,712' E	7448,6		station start
	SO251/1_1-1	CTD	04/10/2016 22:03:21.000	35° 36,230' N	142° 23,752' E	7265,8	SL max 2000m	max depth
	SO251/1_1-1	CTD	04/10/2016 22:46:00.000	35° 36,675' N	142° 25,054' E	6990,1		station end
21801-2	SO251/1_1-2	CTD	04/10/2016 21:32:35.000	35° 35,930' N	142° 22,721' E	7377,5		Station start
	SO251/1_1-2	CTD/XSV	04/10/2016 21:43:24.000	35° 35,974' N	142° 23,052' E	7344	SL max 1200m	station end
21802	SO251/1_2-1	EM122	04/10/2016 23:41:11.000	35° 35,503' N	142° 20,987' E	7960,7		station start
	SO251/1_2-1	EM122	05/10/2016 01:15:07.000	35° 43,872' N	142° 26,548' E	6640,4		station end
21803	SO251/1_3-1	EM122	05/10/2016 02:49:03.000	36° 2,800' N	142° 42,894' E	7976,3		station start
	SO251/1_3-1	EM122	05/10/2016 03:52:11.000	36° 8,043' N	142° 47,292' E	7912,3		station end
21805	SO251/1_5-1	EM122	05/10/2016 11:01:24.000	36° 2,848' N	142° 46,739' E	7775,6		station start
	SO251/1_5-1	EM122	05/10/2016 13:00:00.000	36° 3,325' N	142° 45,798' E	7902,4		station end
21806	SO251/1_6-1	EM122	06/10/2016 04:55:35.000	36° 4,109' N	142° 44,092' E	8030,7		station start
	SO251/1_6-1	EM122	06/10/2016 23:24:41.000	38° 0,441' N	144° 0,273' E	0		station end
21807	SO251/1_7-1	CTD	06/10/2016 23:30:22.000	38° 0,444' N	144° 0,276' E	7562,6		station start
	SO251/1_7-1	CTD	07/10/2016 00:34:30.000	38° 0,449' N	144° 0,271' E	0	SL max 2000m	max depth
	SO251/1_7-1	CTD	07/10/2016 01:14:24.000	38° 0,407' N	144° 0,182' E	7552,8		station end
21808	SO251/1_9-1	EM122	07/10/2016 02:12:44.000	38° 4,635' N	143° 52,575' E	6825,4		station start
	SO251/1_9-1	EM122	07/10/2016 04:08:37.000	38° 2,997' N	144° 7,125' E	6858,5		station end
21811	SO251/1_13-1	EM122	07/10/2016 22:11:02.000	38° 10,601' N	144° 0,091' E	7461,5		station start
	SO251/1_13-1	EM122	08/10/2016 19:35:40.000	39° 20,294' N	144° 15,393' E	7424,7		station end
21813	SO251/1_15-1	CTD	09/10/2016 02:49:42.000	39° 14,409' N	144° 9,629' E	6938,3		station start
	SO251/1_16-1	CTD	09/10/2016 04:41:09.000	39° 15,335' N	144° 8,570' E	6705,9		station end
21814	SO251/1_17-1	EM122	09/10/2016 08:23:04.000	39° 34,651' N	144° 56,122' E	5680,3		station start
	SO251/1_17-1	EM122	10/10/2016 02:42:09.000	39° 23,291' N	143° 3,018' E	1897,2		station end
21816	SO251/1_20-1	EM122	10/10/2016 15:31:08.000	39° 58,541' N	144° 17,969' E	7508,1		station start
	SO251/1_22-1	EM122	11/10/2016 03:22:51.000	40° 24,350' N	144° 23,135' E	7262,5		station end
21819	SO251/1_24-1	CTD/XSV	11/10/2016 08:57:48.000	40° 15,345' N	143° 50,124' E	3163,9	XVS	information
	SO251/1_24-1	CTD/XSV	11/10/2016 08:58:19.000	40° 15,323' N	143° 50,171' E	3167,2		in the water
	SO251/1_24-1	CTD/XSV	11/10/2016 09:05:46.000	40° 15,042' N	143° 50,239' E	3180,4	SL max 1500m	deployed
21820	SO251/1_26-1	EM122	11/10/2016 12:33:36.000	40° 16,419' N	143° 47,375' E	2999,5		station start
	SO251/1_26-1	EM122	12/10/2016 11:32:59.000	38° 53,584' N	144° 11,908' E	7302,6		station end
21822	SO251/1_28-1	EM122	12/10/2016 18:33:40.000	38° 50,266' N	144° 19,757' E	6720		station start
	SO251/1_28-1	EM122	13/10/2016 01:08:14.000	38° 0,086' N	144° 0,931' E	7406,9		station end
21824;21825	SO251/1_30-1	EM122	13/10/2016 07:50:43.000	37° 42,129' N	143° 54,419' E	7420,4		station start
	SO251/1_30-1	EM122	13/10/2016 15:45:51.000	37° 39,108' N	143° 31,179' E	5239,3		station end

Station List (hydroacoustic profiles, ROV, HF, and CTD)

GeoB	Station	Device	Date Time	Latitude	Longitude	Depth (m)	Comment	Action
21826	SO251/2_31-1	HF	18/10/2016 14:00:55,000	33° 46,724' N	136° 54,755' E	1919,2	HF_1650	station start
	SO251/2_31-1	HF	18/10/2016 14:47:08,000	33° 46,721' N	136° 54,832' E	1917,8	WP1;GeoB16784-1	max depth Posidonia SL100m
21828-1	SO251/2_31-1	HF	18/10/2016 15:29:26,000	33° 46,722' N	136° 54,858' E	1929,5	WP2;GeoB16784-2	max depth Posidonia SL100m
	SO251/2_31-1	HF	18/10/2016 16:09:12,000	33° 46,529' N	136° 54,868' E	1936,8	WP3;GeoB16784-3	max depth Posidonia SL100m
21830	SO251/2_31-1	HF	18/10/2016 16:48:34,000	33° 46,364' N	136° 54,825' E	1927,6	WP4;GeoB16784-4	max depth Posidonia SL100m
	SO251/2_31-1	HF	18/10/2016 17:23:23,000	33° 46,212' N	136° 54,883' E	1882,2	WP5;GeoB16784-5	max depth Posidonia SL100m
21827	SO251/2_31-1	HF	18/10/2016 17:51:53,000	33° 46,123' N	136° 54,835' E	1886,3	WP6;GeoB16784-6	max depth Posidonia SL100m
	SO251/2_31-1	HF	18/10/2016 18:35:48,000	33° 46,083' N	136° 54,861' E	1930,5	WP7;GeoB16784-7	max depth Posidonia SL100m
21828-2;21828-3	SO251/2_31-1	HF	18/10/2016 19:42:02,000	33° 45,912' N	136° 54,845' E	2015,7	WP8;GeoB16784-8	max depth Posidonia SL100m
	SO251/2_31-1	HF	18/10/2016 20:48:47,000	33° 45,398' N	136° 54,913' E	2015,5	WP9;GeoB16784-9	max depth Posidonia SL100m
21828-1	SO251/2_31-1	HF	18/10/2016 22:00:05,000	33° 44,862' N	136° 54,957' E	2017,1		station end
	SO251/2_32-1	CTD	18/10/2016 22:04:25,000	33° 44,854' N	136° 54,944' E	2016,6		station start
21828-1	SO251/2_32-1	CTD	18/10/2016 23:46:07,000	33° 44,860' N	136° 54,942' E	2011,5		station end
	SO251/2_33-1	MOOR	19/10/2016 00:35:15,000	33° 39,786' N	136° 55,447' E	2005,9	MV#2	station start
21828-2;21828-3	SO251/2_33-1	MOOR	19/10/2016 00:36:53,000	33° 39,788' N	136° 55,449' E	2006,8	Hydrophone z/W	information
	SO251/2_33-1	MOOR	19/10/2016 01:04:54,000	33° 39,786' N	136° 55,445' E	0	CAT release failed	information
21830	SO251/2_33-2	ROV	19/10/2016 01:29:46,000	33° 40,554' N	136° 55,290' E	1991,5		station start
	SO251/2_33-2	ROV	19/10/2016 09:34:34,000	33° 40,608' N	136° 55,299' E	1994,5		station end
21830	SO251/2_35-1	EM122	19/10/2016 12:22:45,000	33° 40,147' N	136° 47,793' E	2029,5		station start
	SO251/2_35-1	EM122	19/10/2016 14:39:58,000	33° 28,450' N	136° 51,072' E	1922,3	CAT Recovery failed, T-Stick NE-SW transect	station end

Station List (hydroacoustic profiles, ROV, HF, and CTD)

GeoB	Station	Device	Date Time	Latitude	Longitude	Depth (m)	Comment	Action
21832	SO251/2_37-1	HF	19/10/2016 17:54:24,000	33° 29,871' N	136° 49,392' E	2014	HF_1651	station start
	SO251/2_37-1	HF	19/10/2016 18:44:41,000	33° 29,931' N	136° 49,286' E	2013,5	WP1	max depth Posidonia SL100m
21833	SO251/2_37-1	HF	19/10/2016 19:48:35,000	33° 29,931' N	136° 49,301' E	2020,1	WP2	max depth Posidonia SL100m
	SO251/2_37-1	HF	19/10/2016 20:58:55,000	33° 30,354' N	136° 48,894' E	2027,1	WP3	max depth Posidonia SL100m
21834	SO251/2_37-1	HF	19/10/2016 22:05:34,000	33° 30,785' N	136° 48,503' E	2034,6	WP4	max depth Posidonia SL100m
	SO251/2_37-1	HF	19/10/2016 23:09:18,000	33° 31,217' N	136° 48,121' E	2039,8	WP5	max depth Posidonia SL100m
21835	SO251/2_37-1	HF	20/10/2016 00:21:20,000	33° 31,647' N	136° 47,723' E	2040,2	WP6	max depth Posidonia SL100m
	SO251/2_40-1	EM122	20/10/2016 11:16:50,000	33° 31,649' N	136° 47,738' E	2041,1	WP7	max depth Posidonia SL100m
21836	SO251/2_40-1	EM122	20/10/2016 12:56:12,000	33° 32,089' N	136° 47,340' E	2056,2		station start
	SO251/2_43-1	EM122	20/10/2016 17:15:09,000	33° 32,086' N	136° 47,353' E	2024		station end
21837	SO251/2_43-1	EM122	20/10/2016 17:15:09,000	33° 32,525' N	136° 46,963' E	1984,7		station start
	SO251/2_44-1	EM122	21/10/2016 00:25:51,000	33° 32,517' N	136° 46,962' E	1948		station end
21838	SO251/2_44-1	ROV	21/10/2016 00:30:39,000	33° 38,083' N	136° 40,199' E	1948,1	MV#3	station start
	SO251/2_44-1	ROV	21/10/2016 01:49:55,000	33° 38,084' N	136° 40,195' E	1946	BOSI	max depth
21839	SO251/2_44-1	ROV	21/10/2016 09:40:04,000	33° 38,081' N	136° 40,209' E	1940,3		station end
	SO251/2_45-1	EM122	21/10/2016 11:11:10,000	33° 38,024' N	136° 40,280' E	1986,8		station start
21839-2	SO251/2_45-1	EM122	21/10/2016 16:13:34,000	33° 24,460' N	136° 35,017' E	2101,8		station end
	SO251/2_46-1	EM122	21/10/2016 16:51:25,000	33° 22,645' N	136° 42,284' E		Profil Beginn rwk 150° , d 9,35nm	station start
21841	SO251/2_46-1	EM122	21/10/2016 20:46:31,000	33° 16,418' N	136° 41,838' E	2311,5		station end
	SO251/2_48-1	ROV	22/10/2016 02:26:46,000	33° 15,244' N	136° 35,005' E	1876		station start
21844	SO251/2_48-1	ROV	22/10/2016 08:52:21,000	33° 39,332' N	136° 38,124' E	1986,9		station end
	SO251/2_51-1	EM122	22/10/2016 17:20:38,000	33° 39,369' N	136° 38,045' E	1971,2		station end
21847	SO251/2_51-1	EM122	22/10/2016 22:26:16,000	33° 41,624' N	137° 0,754' E	1987,1	Beginn Profil, rwk 200° , d 2,54nm	station start
	SO251/2_54-1	EM122	24/10/2016 10:26:03,000	33° 12,557' N	136° 44,427' E	2858,2		station end
21847	SO251/2_54-1	EM122	25/10/2016 03:09:53,000	34° 0,652' N	137° 10,474' E	1822,7		station start
	SO251/2_54-1	EM122		33° 42,490' N	137° 4,342' E	1982		station end

Station List (hydroacoustic profiles, ROV, HF, and CTD)

GeoB	Station	Device	Date Time	Latitude	Longitude	Depth (m)	Comment	Action
21848	SO251/2_55-1	HF	25/10/2016 03:39:06,000	33° 43,103' N	137° 5,955' E	1959,2	HF_1652	station start
	SO251/2_55-1	HF	25/10/2016 04:31:12,000	33° 43,256' N	137° 6,209' E	1966,3	WP1	max depth Posidonia SL100m
	SO251/2_55-1	HF	25/10/2016 05:15:30,000	33° 43,253' N	137° 6,208' E	1958,6	WP2	max depth Posidonia SL100m
	SO251/2_55-1	HF	25/10/2016 07:26:31,000	33° 43,135' N	137° 5,920' E	1981,8	WP3	max depth Posidonia SL100m
	SO251/2_55-1	HF	25/10/2016 08:12:26,000	33° 43,152' N	137° 5,931' E	1981,8	WP4	max depth Posidonia SL100m
	SO251/2_55-1	HF	25/10/2016 08:58:23,000	33° 42,516' N	137° 4,495' E	1904,2	WP5	max depth Posidonia SL100m
	SO251/2_55-1	HF	25/10/2016 09:29:14,000	33° 42,532' N	137° 4,488' E	1836	WP6	max depth Posidonia SL100m
	SO251/2_55-1	HF	25/10/2016 10:02:02,000	33° 42,670' N	137° 4,791' E	1825	WP7	max depth Posidonia SL100m
	SO251/2_55-1	HF	25/10/2016 10:36:19,000	33° 42,677' N	137° 4,78' E	1824,9	WP8	max depth Posidonia SL100m
	SO251/2_55-1	HF	25/10/2016 11:17:53,000	33° 42,771' N	137° 5,037' E	1846	WP9	max depth Posidonia SL100m
	SO251/2_55-1	HF	25/10/2016 11:50:20,000	33° 42,781' N	137° 5,014' E	1905,6	WP10	max depth Posidonia SL100m
	SO251/2_55-1	HF	25/10/2016 11:55:09,000	33° 42,822' N	137° 5,157' E	1902,9	WP11	max depth Posidonia SL100m
21849	SO251/2_56-1	EM122	25/10/2016 12:48:28,000	33° 42,820' N	137° 5,236' E	1932,6	WP12	max depth Posidonia SL100m
	SO251/2_56-1	EM122	25/10/2016 13:50:02,000	33° 42,849' N	137° 5,219' E	1932,2		station end
21850	SO251/2_57-1	ROV	25/10/2016 14:11:02,000	33° 42,860' N	137° 5,295' E	1988		station start
	SO251/2_57-1	ROV	25/10/2016 14:11:02,000	33° 42,875' N	137° 5,278' E	1949,1		station end
	SO251/2_57-1	ROV	25/10/2016 23:44:47,000	33° 42,885' N	137° 5,361' E	1979	MV #4	station start information
	SO251/2_57-1	ROV	25/10/2016 23:44:47,000	33° 42,900' N	137° 5,353' E	2049,8	0 Obs. Recovered	station end

Station List (hydroacoustic profiles, ROV, HF, and CTD)

GeoB	Station	Device	Date Time	Latitude	Longitude	Depth (m)	Comment	Action
21851	SO251/2_58-1	EM122	26.10.2016 11:16:59,000	33° 39,351' N	136° 38,357' E	2054,1		station start
	SO251/2_58-1	EM122	26.10.2016 22:38:06,000	33° 38,831' N	136° 37,594' E	2056,9		station end
21852	SO251/2_59-1	HF	27.10.2016 00:28:27,000	33° 39,485' N	136° 55,298' E	2006	HF_1653	station start
	SO251/2_59-1	HF	27.10.2016 01:20:13,000	33° 39,515' N	136° 55,265' E	2005,7	WP1	max depth
	SO251/2_59-1	HF	27.10.2016 02:36:28,000	33° 39,515' N	136° 55,266' E	2009,3	WP2	Posidonia SL100m
	SO251/2_59-1	HF	27.10.2016 03:23:24,000	33° 40,075' N	136° 55,233' E	2007,6	WP3	max depth
	SO251/2_59-1	HF	27.10.2016 04:07:44,000	33° 40,070' N	136° 55,241' E	1999,8	WP4	Posidonia SL100m
	SO251/2_59-1	HF	27.10.2016 04:49:59,000	33° 40,231' N	136° 55,235' E	1994,3	WP5	max depth
	SO251/2_59-1	HF	27.10.2016 05:32:50,000	33° 40,22' N	136° 55,237' E	1992,5	WP6	Posidonia SL100m
	SO251/2_59-1	HF	27.10.2016 06:07:58,000	33° 40,362' N	136° 55,251' E	1995	WP7	max depth
	SO251/2_59-1	HF	27.10.2016 06:47:18,000	33° 40,372' N	136° 55,250' E	2003,4	WP8	Posidonia SL100m
	SO251/2_59-1	HF	27.10.2016 08:00:00,000	33° 40,481' N	136° 55,233' E	2005		station end
21853	SO251/2_60-1	ROV	27.10.2016 09:28:01,000	33° 38,022' N	136° 40,270' E	1942,8	MV#3; MeBo Plug #1 and T-Stick Rec.	station start
	SO251/2_60-1	ROV	27.10.2016 12:15:53,000	33° 38,061' N	136° 40,258' E	1941,5	Borehole sealed	information
	SO251/2_60-1	ROV	27.10.2016 13:47:40,000	33° 38,056' N	136° 40,266' E	1941,5		station end
21854	SO251/2_61-1	EM122	27.10.2016 13:51:32,000	33° 38,037' N	136° 40,296' E	1940,9		station start
	SO251/2_61-1	EM122	27.10.2016 23:00:04,000	33° 39,077' N	136° 37,807' E	2059,2		station end
21855	SO251/2_62-1	ROV	27.10.2016 23:20:58,000	33° 39,342' N	136° 38,037' E	1968,1	MV # 4	station start
	SO251/2_62-1	ROV	28.10.2016 03:57:26,000	33° 39,420' N	136° 38,054' E	0	Smartplug Recovered	information
	SO251/2_62-1	ROV	28.10.2016 09:08:43,000	33° 39,334' N	136° 38,319' E	2053,1		station end
21856	SO251/2_63-1	EM122	28.10.2016 09:09:03,000	33° 39,333' N	136° 38,325' E	2050,9		station start
	SO251/2_63-1	EM122	29/10/2016 23:49:46,000	33° 56,693' N	136° 56,103' E	737,5		station end
21857-1	SO251/2_64-1	HF/GC	29/10/2016 23:50:08,000	33° 56,694' N	136° 56,102' E	739,2		station start
	SO251/2_64-1	HF/GC	30/10/2016 00:10:43,000	33° 56,694' N	136° 56,120' E	740,2		max depth
	SO251/2_64-1	HF/GC	30/10/2016 00:50:57,000	33° 56,688' N	136° 56,128' E	730,8		Posidonia SL50m
	SO251/2_64-1	HF/GC		33° 56,701' N	136° 56,087' E			station end

Station List (hydroacoustic profiles, ROV, HF, and CTD)

GeoB	Station	Device	Date Time	Latitude	Longitude	Depth (m)	Comment	Action
21858-1	SO251/2_65-1	HF/GC	30/10/2016 02:08:23,000	33° 49,303' N	137° 1,431' E	1920,9		station start
	SO251/2_65-1	HF/GC	30/10/2016 02:53:02,000	33° 49,296' N	137° 1,450' E	1918,4		max depth Posidonia SL50m
	SO251/2_65-1	HF/GC	30/10/2016 04:01:38,000	33° 49,298' N	137° 1,442' E	1914,8		station end
21859	SO251/2_66-1	EM122	30/10/2016 05:02:33,000	33° 41,282' N	136° 56,004' E	2001,5		station start
	SO251/2_66-1	EM122	30/10/2016 06:42:07,000	33° 40,529' N	136° 56,102' E	2005,7		station end
21860-1	SO251/2_67-1	HF/GC	30/10/2016 07:10:23,000	33° 40,668' N	136° 55,128' E	1998,7		station start
	SO251/2_67-1	HF/GC	30/10/2016 07:56:10,000	33° 40,679' N	136° 55,133' E	2001,2		max depth Posidonia SL50m
	SO251/2_67-1	HF/GC	30/10/2016 09:00:01,000	33° 40,675' N	136° 55,129' E	2001,3		station end
21861-1	SO251/2_68-1	HF/GC	30/10/2016 10:46:14,000	33° 47,310' N	137° 15,845' E	2160,5		station start
	SO251/2_68-1	HF/GC	30/10/2016 11:32:18,000	33° 47,323' N	137° 15,883' E	2160,9		max depth Posidonia SL50m
	SO251/2_68-1	HF/GC	30/10/2016 12:36:54,000	33° 47,382' N	137° 16,097' E	2157,2		station end
21862	SO251/2_69-1	EM122	30/10/2016 12:37:08,000	33° 47,307' N	137° 15,870' E	2159,2		station start
	SO251/2_69-1	EM122	30/10/2016 23:00:07,000	33° 39,187' N	136° 38,005' E	2061,9		station end
	SO251/2_70-1	ROV	30/10/2016 23:00:24,000	33° 39,207' N	136° 38,002' E	2041,2		station start
21863	SO251/2_70-1	ROV	31/10/2016 04:33:37,000	33° 39,382' N	136° 38,034' E	0	0 MeBo Plug #2 Rec.	information
	SO251/2_70-1	ROV	31/10/2016 07:43:49,000	33° 39,377' N	136° 38,041' E	0		station end
	SO251/2_71-1	HF/GC	31/10/2016 08:53:11,000	33° 46,600' N	136° 29,051' E	2034,7		station start
21864-1	SO251/2_71-1	HF/GC	31/10/2016 09:38:36,000	33° 46,624' N	136° 29,078' E	2034,6		max depth
	SO251/2_71-1	HF/GC	31/10/2016 10:44:35,000	33° 46,420' N	136° 29,038' E	2038		station end
	SO251/2_72-1	EM122	31/10/2016 10:45:12,000	33° 46,323' N	136° 29,042' E	2038,2		station start
21865	SO251/2_72-1	EM122	31/10/2016 22:09:24,000	33° 9,809' N	136° 38,912' E	2889,8		station end
	SO251/2_73-1	HF/GC	31/10/2016 22:30:10,000	33° 9,754' N	136° 38,839' E	2888,8		station start
	SO251/2_73-1	HF/GC	31/10/2016 23:30:20,000	33° 9,731' N	136° 38,805' E	2890,8		max depth
21866-1	SO251/2_73-1	HF/GC	01/11/2016 00:49:59,000	33° 9,732' N	136° 38,805' E	2957,4		station end
	SO251/2_74-1	EM122	01/11/2016 01:14:16,000	33° 10,456' N	136° 38,550' E	2789,3		station start
	SO251/2_74-1	EM122	01/11/2016 05:40:25,000	33° 34,626' N	137° 30,138' E	3896,1		station end

SO251a

GeoB21804-1

1

10

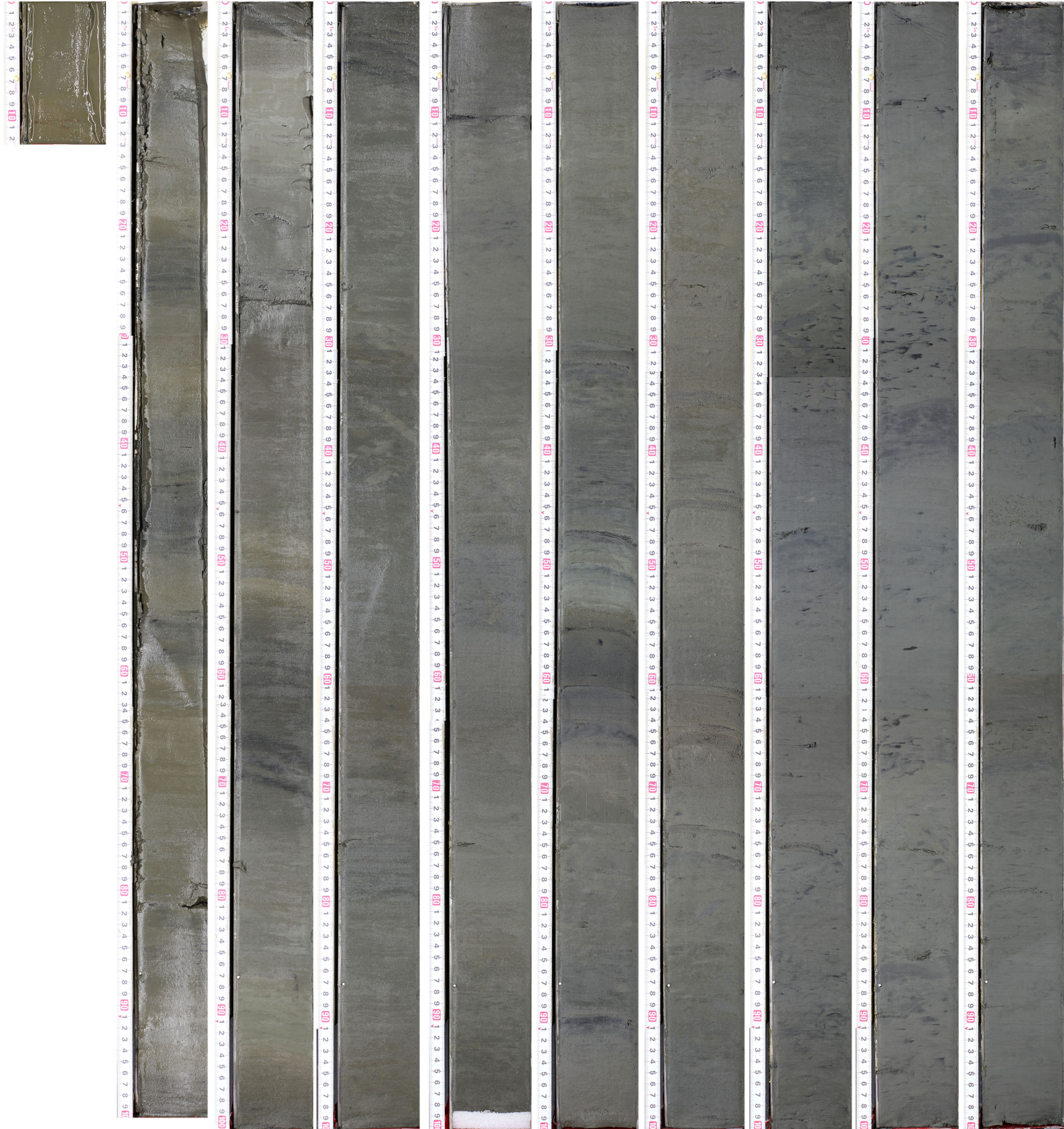


SO251a

GeoB21809-1

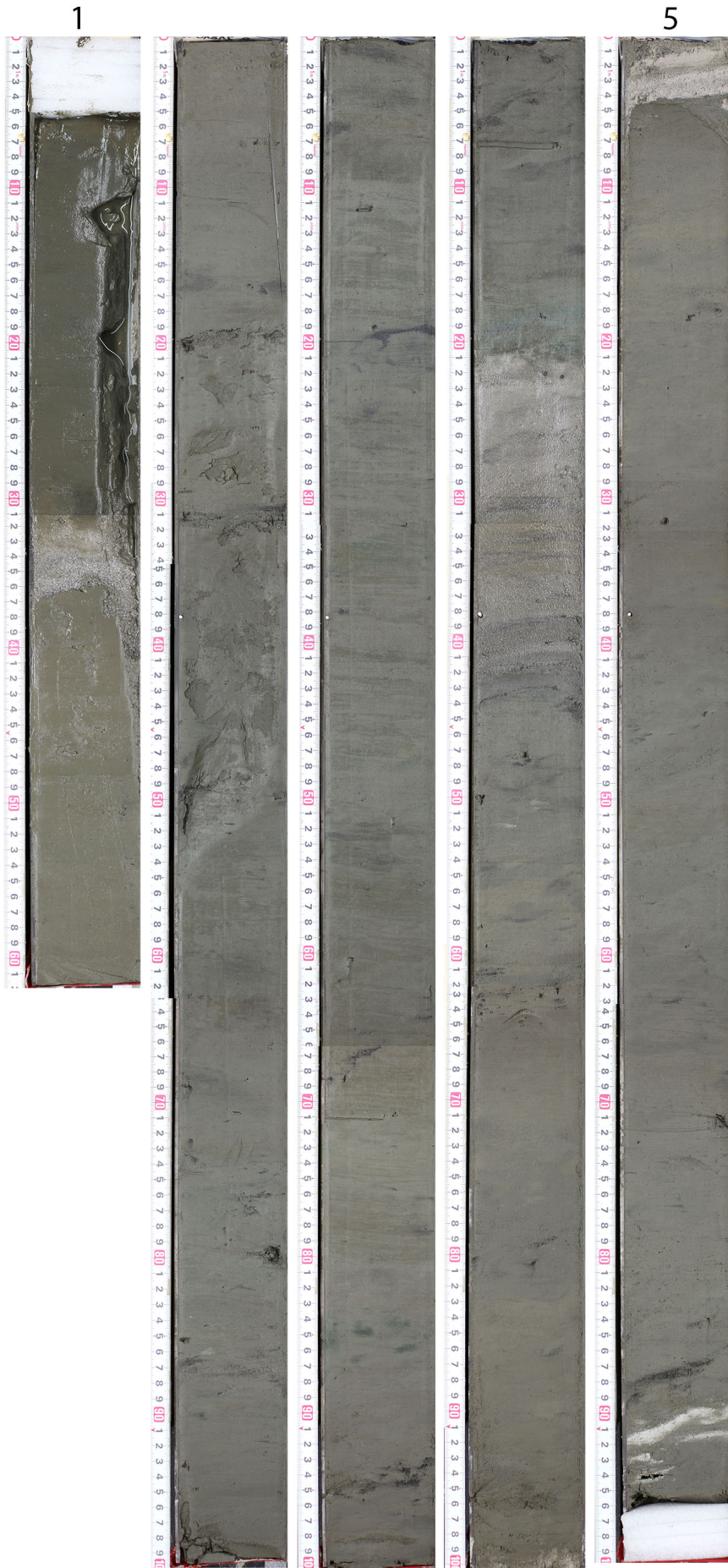
1

10



SO251a

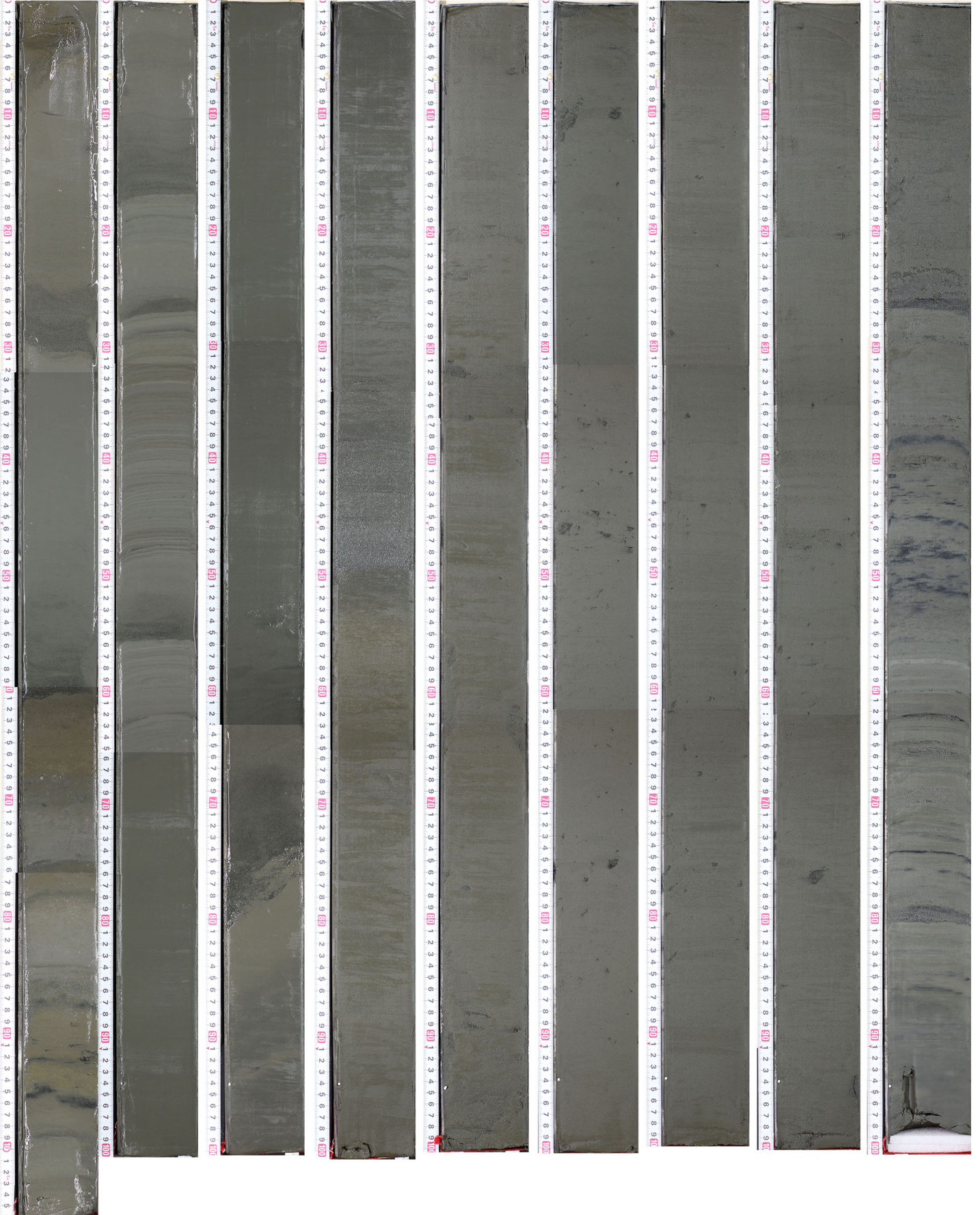
GeoB21810-1



SO251a

GeoB21812-1

1



9

SO251a

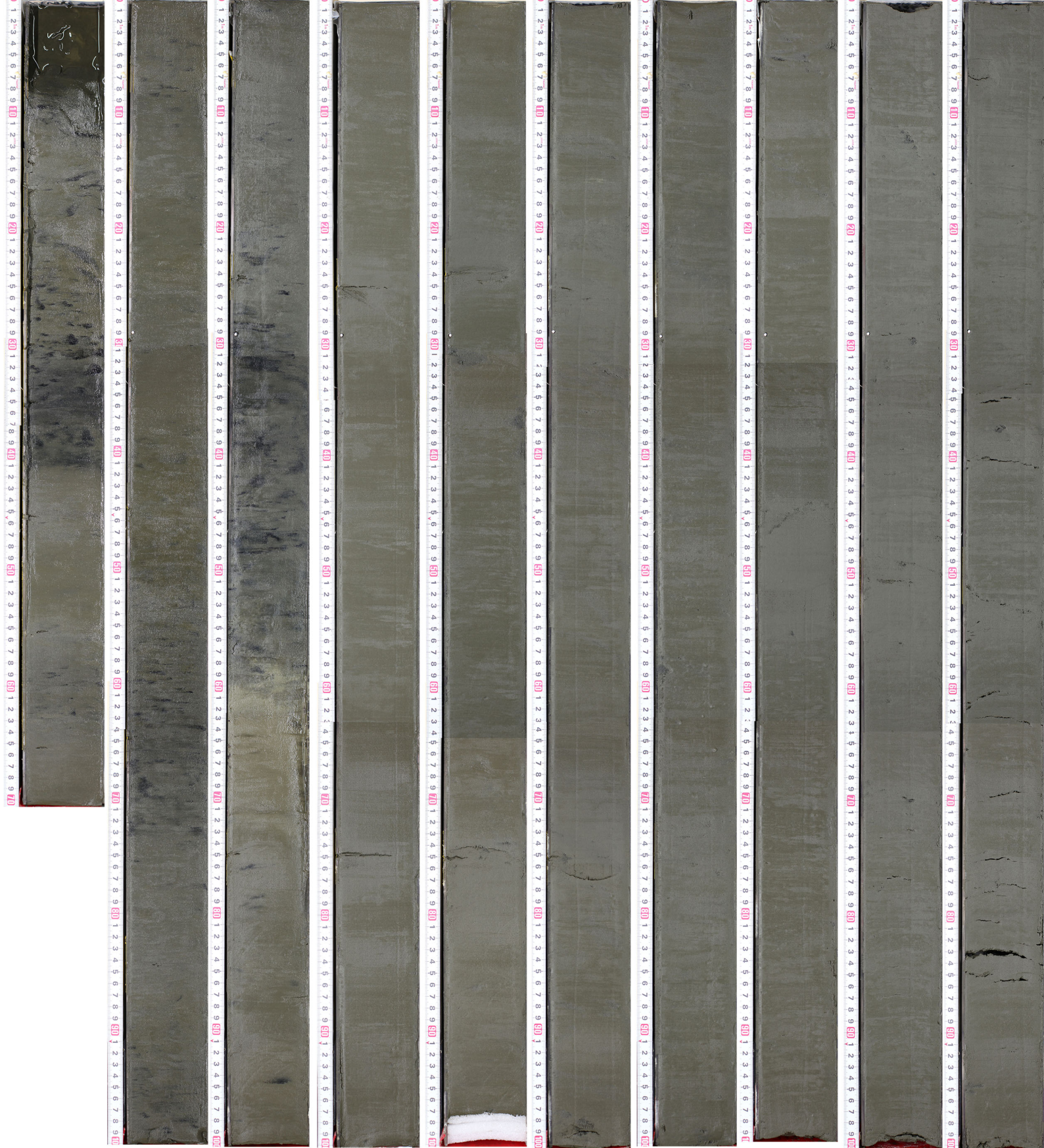
GeoB21815-1



SO251a

GeoB21817-1

1



10

SO251a

GeoB21818-1

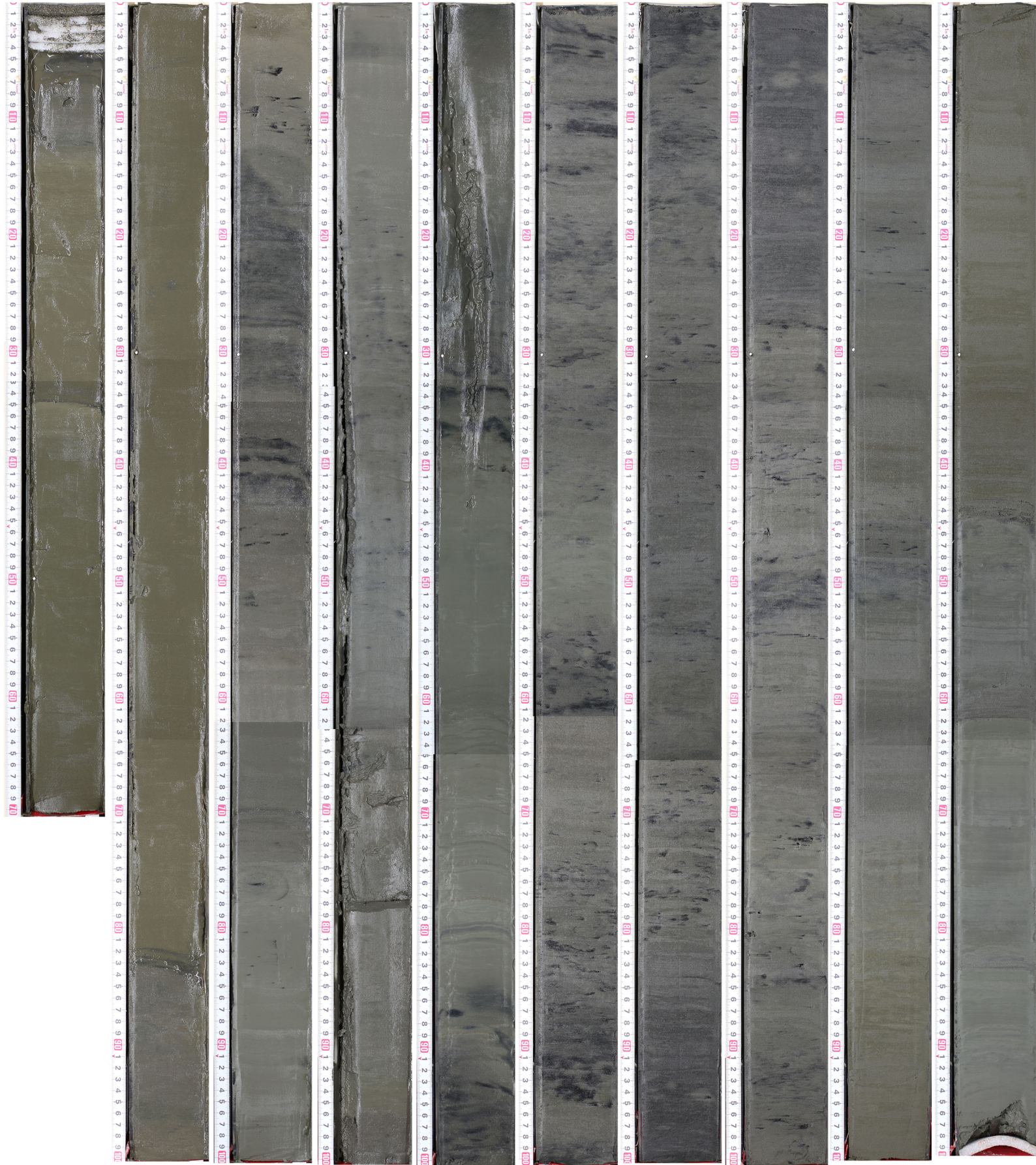


SO251a

GeoB21821-1

1

10



SO251a

GeoB21823-1

1









9














Legend core logs SO251

Lithology

	JT*: diatomaceous mud N***: silty clay / clayey silt
	JT*: sandy diatomaceous mud N***: sandy silty clay
	mixed sediment
	coccoliths bearing diatomaceous mud
	sand bed
	ash bed







Structures

	parallel lamination
	cross bedding
	mixed/chaotic sediment
	convolut / contorted bedding
	fining upwards
	fining upwards with sharp base
	bioturbation
	diffuse boundary, colour change
	syn-sedimentary fault
	ripple marks
	flame structures

Coring disturbance

	coring disturbance
	slightly fractured (coring disturbance)

Samples

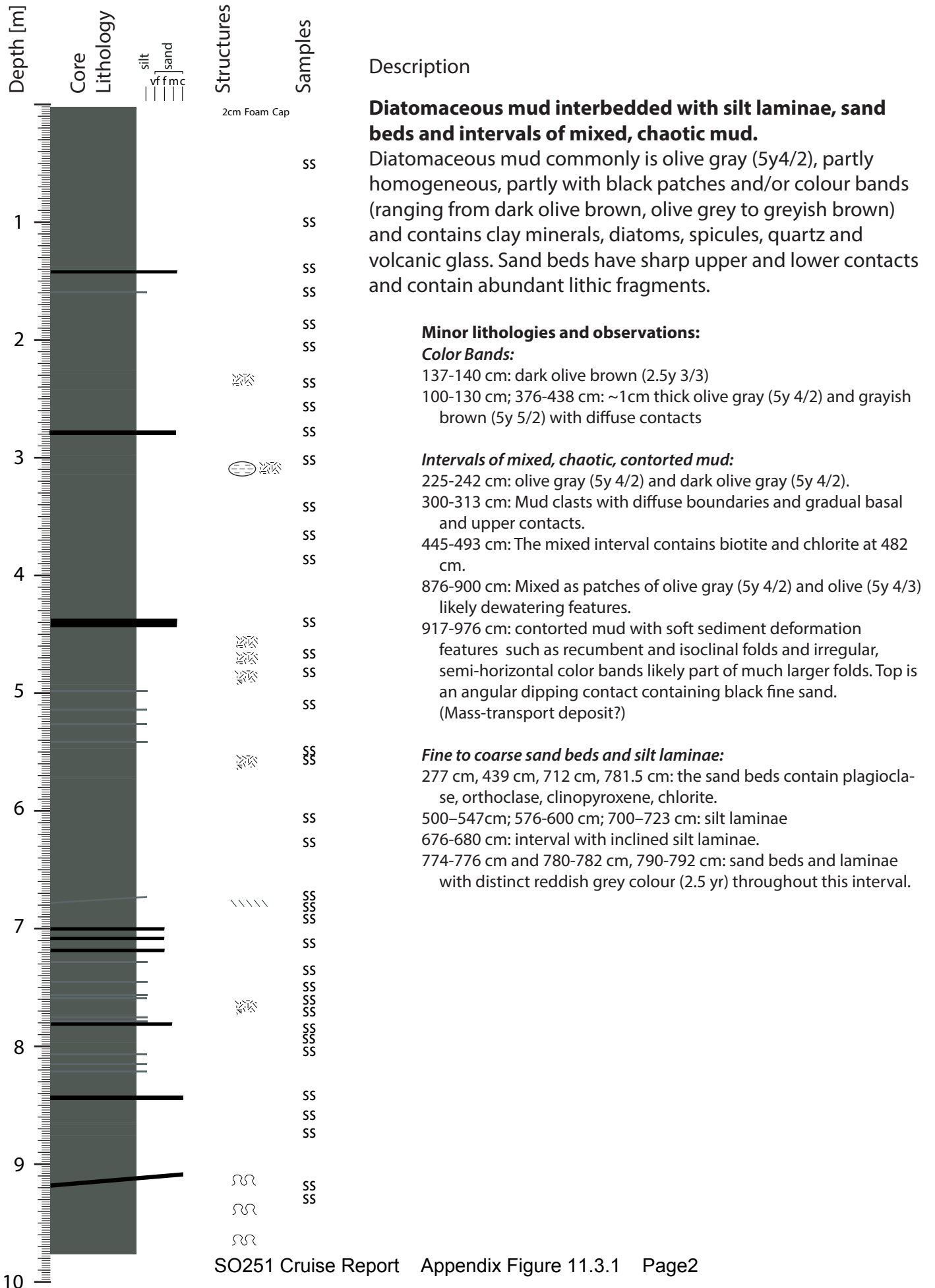
	shell fragment	SS	smear slide
	plant remains		
	sponge spicules		
	organic / monosulfide spot		
	pyrite nodule		
	diagenetic clast		

*JT=Japan Trench (leg a)

**N=Nankai trough, Kumano basin (leg b)

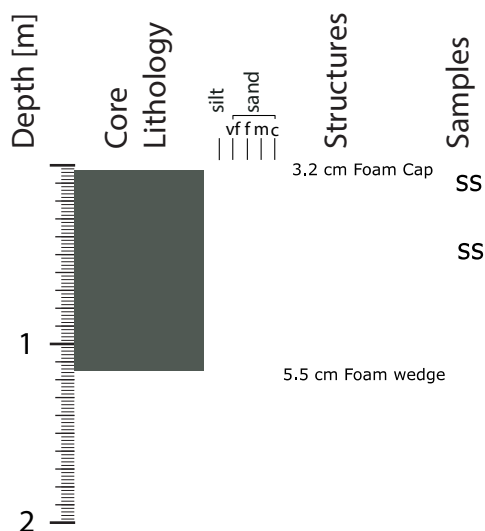
GeoB 21804-1

Latitude: 36°N 04.256 Longitude: 142°E 44.045
 Waterdepth: 8025 m Recovery: 9.76 m



GeoB 21804-2

Latitude: 36°N 04.256 Longitude: 142°E 44.045
 Waterdepth: 8025 m Recovery: 1.20 m



Description

Diatomaceous mud interbedded with silt laminae, sand beds and intervals of mixed, chaotic mud.

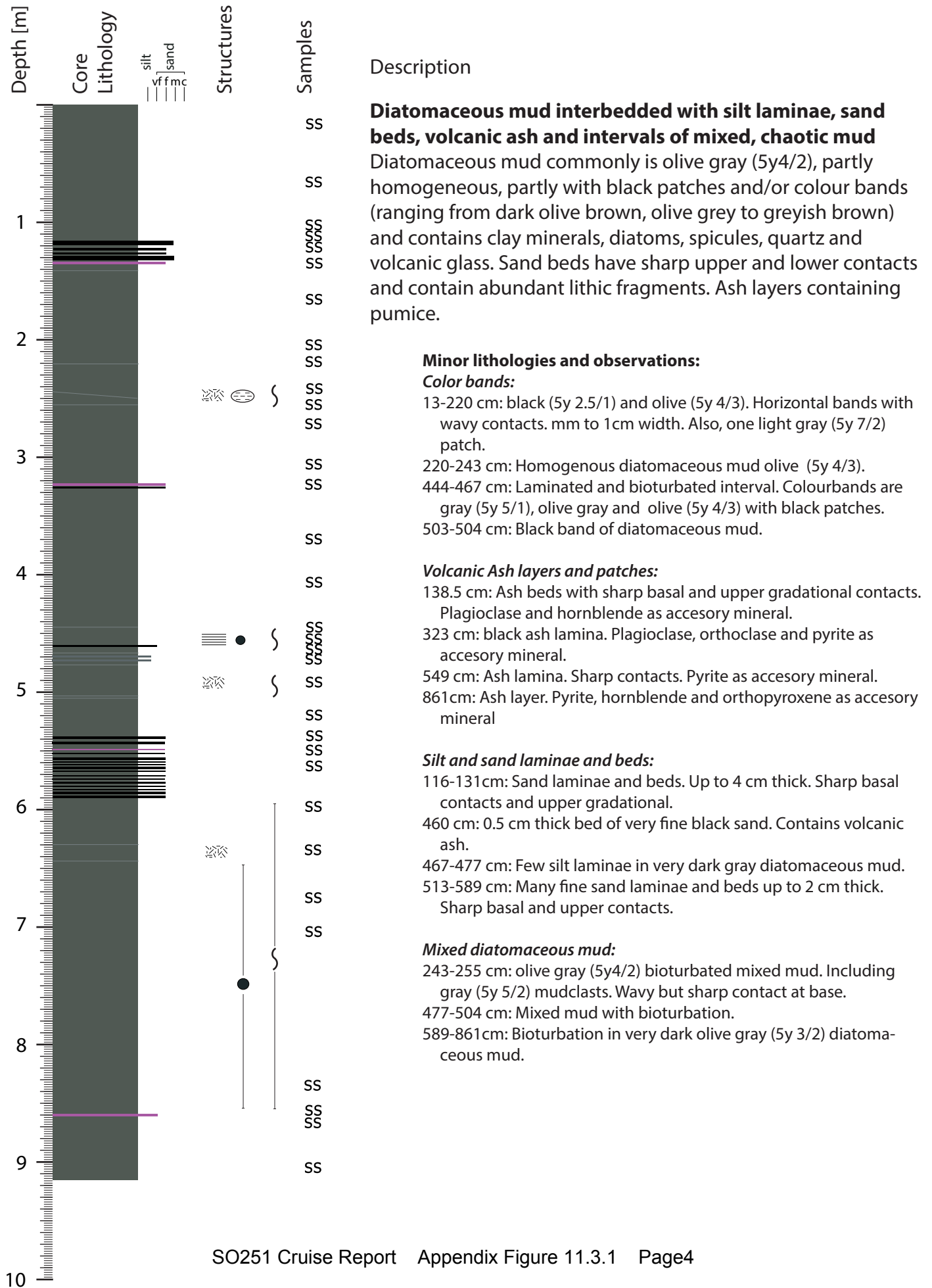
Diatomaceous mud commonly is olive gray (5y4/2), partly homogeneous, partly with black patches and/or colour bands (ranging from dark olive brown, olive grey to greyish brown) and contains clay minerals, diatoms, spicules, quartz and volcanic glass. Sand beds have sharp upper and lower contacts and contain abundant lithic fragments.

Minor lithologies and observations:

Diatomaceous silt. 34.5-36 cm
 Diatomaceous silty clay with some lighter coloured (544/1 - 4/2) bands (more diatomaceous?). Boundaries sometimes sharp, usually irregular.

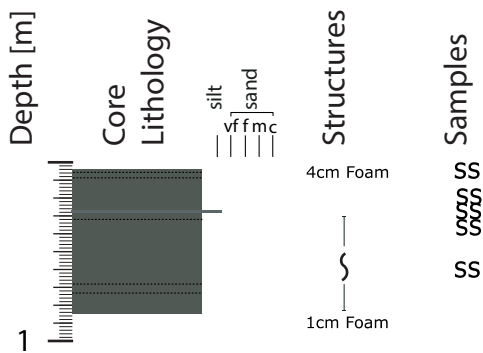
GeoB 21809-1

Latitude: 38°N 00.427 Longitude: 143°E 59.636
 Waterdepth: 7540 m Recovery: 9.13 m



GeoB 21809-2

Latitude: 38°N 00.427 Longitude: 143°E 59.636
 Waterdepth: 7540 m Recovery: 0.86 m



Description

Diatomaceous mud interbedded with silt laminae, sand beds, volcanic ash and intervals of mixed, chaotic mud

Diatomaceous mud commonly is olive gray (5y4/2), partly homogeneous, partly with black patches and/or colour bands (ranging from dark olive brown, olive grey to greyish brown) and contains clay minerals, diatoms, spicules, quartz and volcanic glass. Sand beds have sharp upper and lower contacts and contain abundant lithic fragments. Ash layers containing pumice.

Minor lithologies and observations:

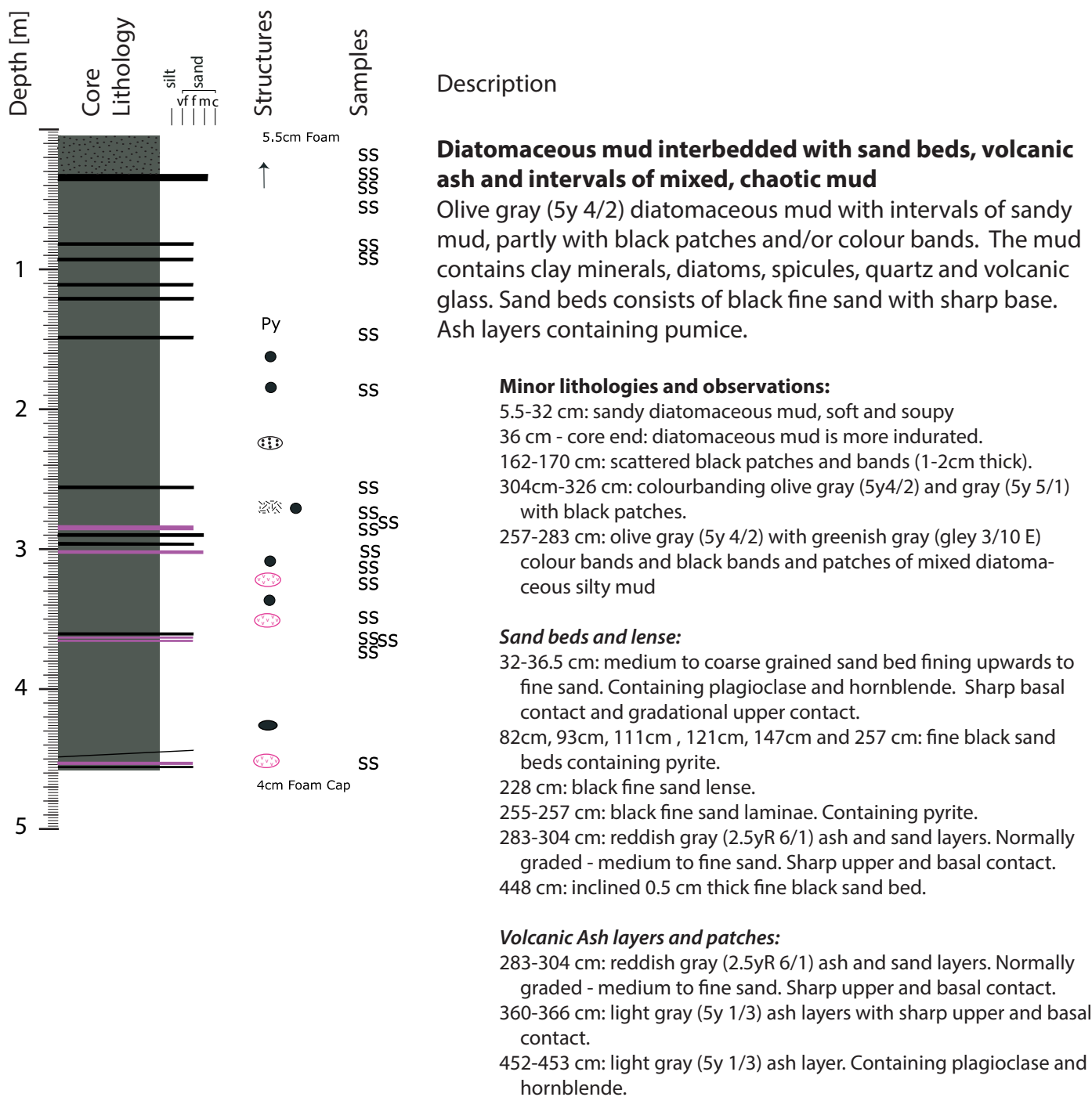
- 4-5.3 cm: grayish olive (7.5y 4/2) with dark grayish yellow (2.5y 4/2) oxidized layer at top
- 5.3-5.4 cm, 7.0-7.3 cm and 8.2-8.8 cm: gray (7.5y 4/1) diatomaceous ooze band
- 8.8-27 cm: grayish olive (7.5y 4/2)
- 27-27.25 cm: coarse gray (7.5y 4/1) silt bed

Bioturbation:

- 27.5-32 cm: Bioturbated dark grayish yellow (2.5y 4/2) diatomaceous silty clay with grayish yellow brown (10yR 4/2) band at 28-29cm.
- 32-68 cm and 73.5-85 cm: Olive black (7.5y 3/2) bioturbated diatomaceous silty clay.
- 68-73.5 cm: Grayish olive (7.5y 3/1) bioturbated diatomaceous silt

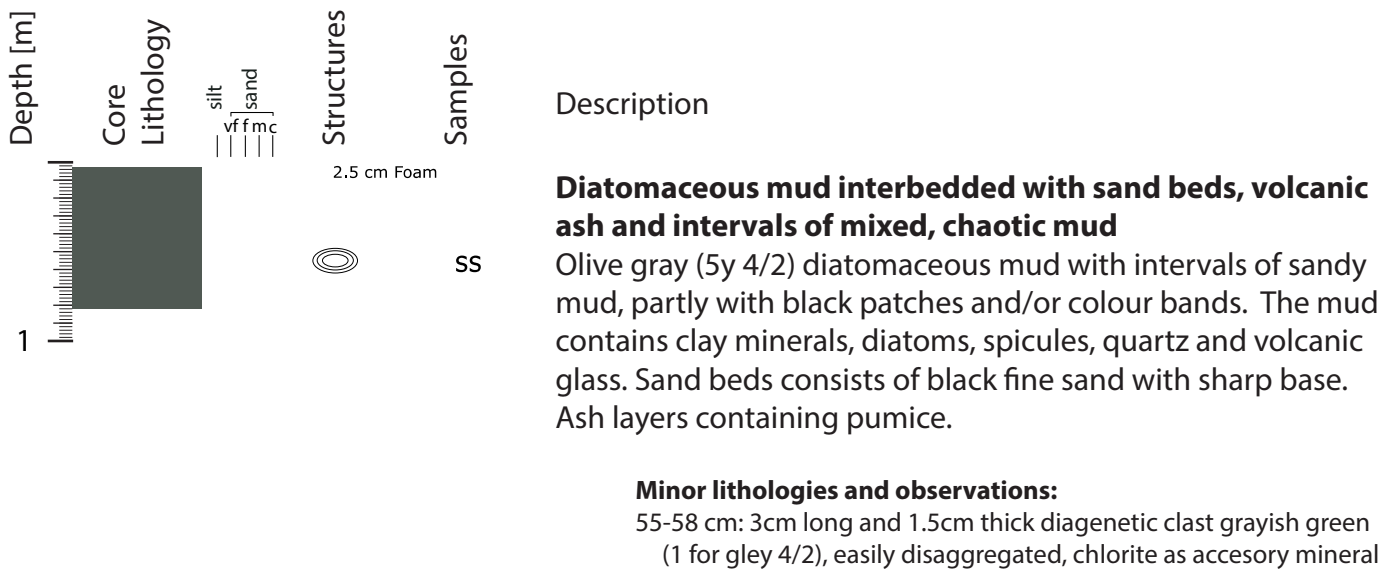
GeoB 21810-1

Latitude: 38°N 06.787 Longitude: 143°E 41.662
 Waterdepth: 5216 m Recovery: 4.62 m



GeoB 21810-2

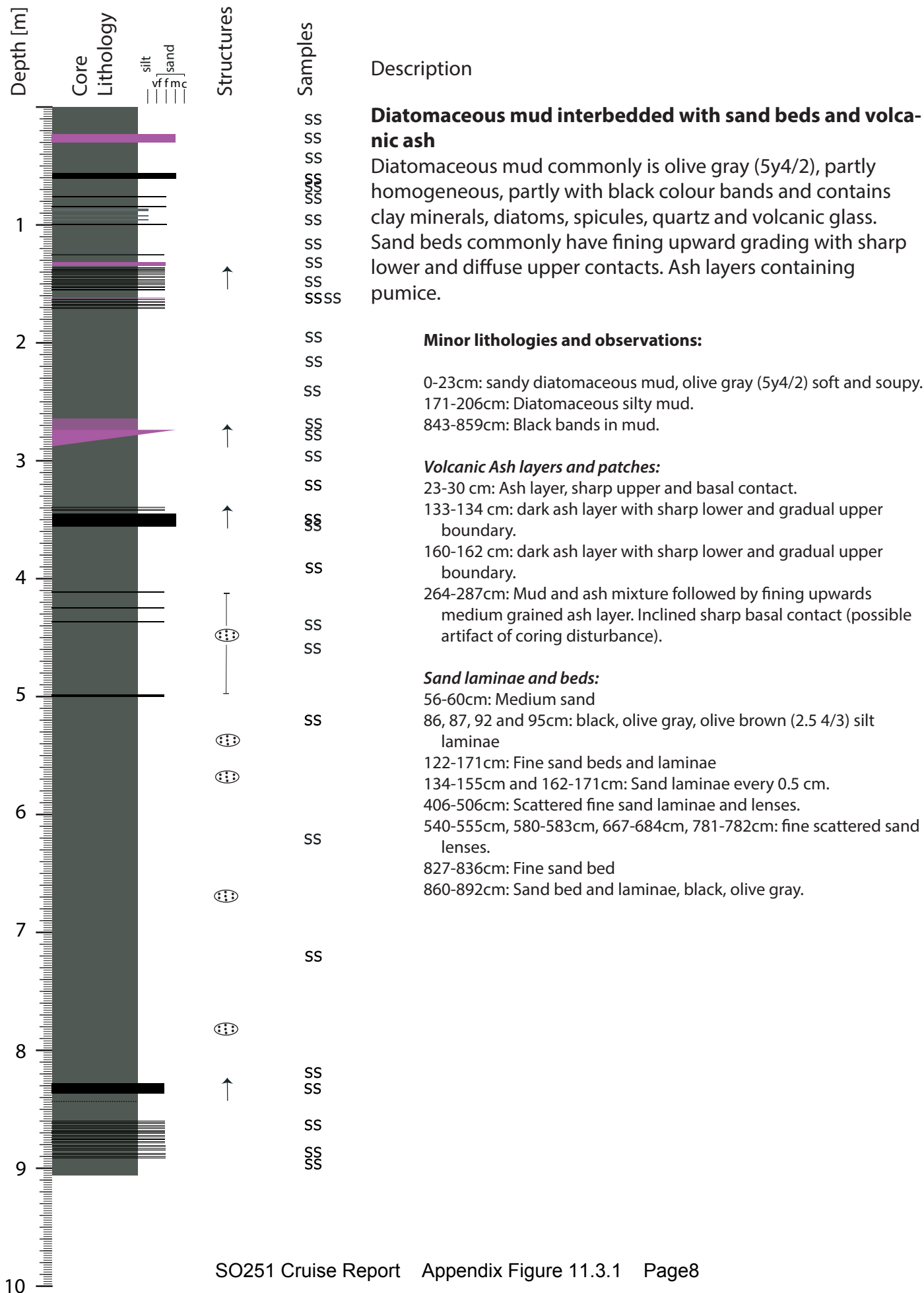
Latitude: 38°N 06.787 Longitude: 143°E 41.662
 Waterdepth: 5216 m Recovery: 0.81 m



GeoB 21812-1

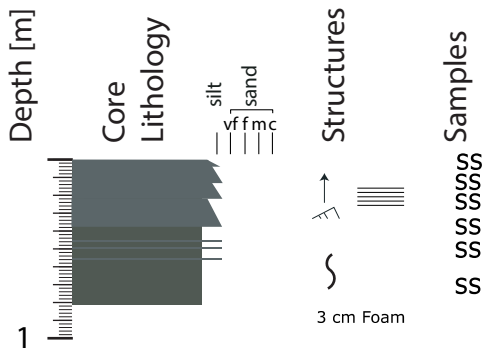
Latitude: 39°N 14.908 Longitude: 144°E 12.230

Waterdepth: 7744 m Recovery: 9.06 m



GeoB 21812-2

Latitude: 39°N 14.908 Longitude: 144°E 12.230
 Waterdepth: 7744 m Recovery: 0.81 m



Description

Diatomaceous mud interbedded with sand beds and volcanic ash

Diatomaceous mud commonly is olive gray (5y4/2), partly homogeneous, partly with black colour bands and contains clay minerals, diatoms, spicules, quartz and volcanic glass. Sand beds commonly have fining upward grading with sharp lower and diffuse upper contacts. Ash layers containing pumice.

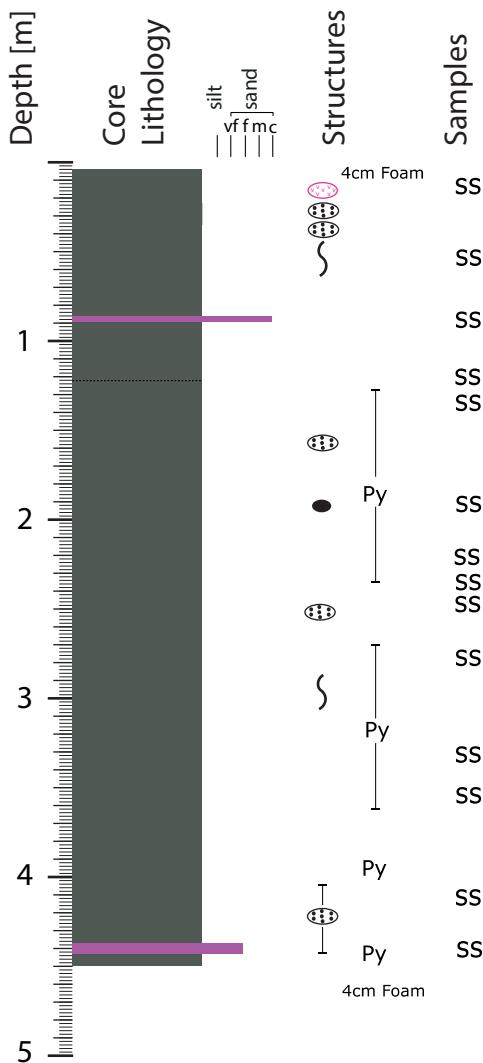
Minor lithologies and observations:

Silt:

- 0-1 cm: Gray (7.5 Y 4/1) silt.
- 4 cm: coarse silt layer
- 10.5-12.22 cm: Black (7.5 Y 2/1) coarse silt with sharp base.
- 12.2-21 cm: Gray (7.5 Y 4/1) silt laminated except for 16-20 cm interval.
- 21-21.7 cm: Black (7.5 Y 2/1) coars silt with sharp base.
- 32.5-37.5: Black (7.5 Y 2/1) coarse silt with upper part ripple and lower part laminated.
- 37.5-62.5 cm: Gray (7.5 Y 4/1) to olive black silty clay to silt interbedded with irregular black coarse silt beds.
- 62.5-80 cm: Gray (7.5 Y 4/1) homogenous clayey silt.

GeoB 21815-1

Latitude: 39°N 19.575 Longitude: 143°E 38.874
 Waterdepth: 3104 m Recovery: 4.67 m



Description

Diatomaceous mud interbedded with volcanic ash and intervals with sand lenses and pyrite concretions

Olive gray (5y 4/2) diatomaceous mud partly varies in place between different olive hues. The mud contains clay minerals, diatoms, spicules, quartz and volcanic glass. Ash layers containing pumice and lithic fragments.

Minor lithologies and observations:

- 54-67 cm: Dark olive gray (5y 3/2)
- 122 cm: Contact to colour change from olive gray to olive.
- 140 cm: Grayish green (1 for GLEY 4/5 G) patch

Volcanic ash lense and layers:

- 11-14 cm: Ash patch
- 86-89 cm: Coarse gray (5y 5/1) ash layer, sharp basal and upper contact.
- 439.5-443.5cm: fine gray (5y 5/1) ash layer with sharp basal contact and top discontinuous.

Sand lenses and beds:

- 28-31cm and 31-38cm: sand patches
- 149, 152, 156, 165, 226-238 and 400-440 cm: scattered fine black sand lenses

Pyrite Concretions:

- 126, 383, 393 and 459cm: 1 cm long
- 133, 156 and 280-292cm: mm long
- 178-180, 197-198, 207, 243, 249, 255, 383

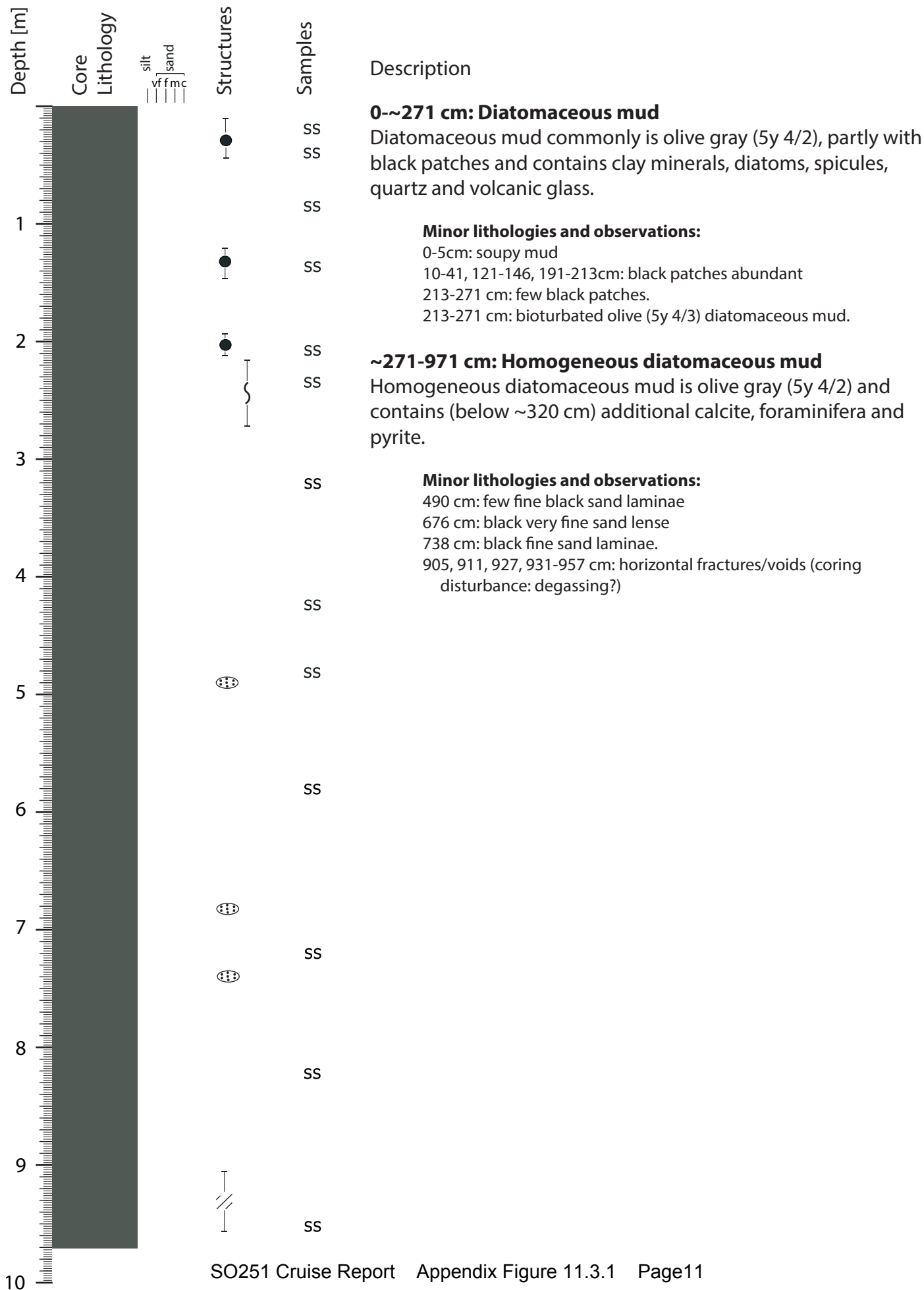
Lithic Clast:

- 198cm: Subrounded lithic clast gray with white patches 0.5 cm long

GeoB 21817-1

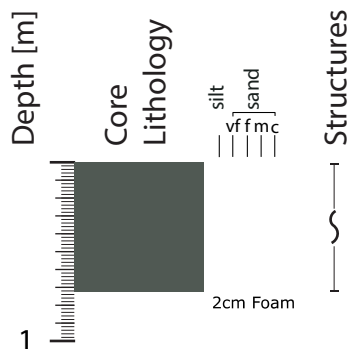
Latitude: 40°N 23.735 Longitude: 144°E 25.256

Waterdepth: 7607 m Recovery: 9.71 m



GeoB 21817-2

Latitude: 40°N 23.735 Longitude: 144°E 25.256
 Waterdepth: 7607 m Recovery: 0.74 m



Samples
 SS
 SS
 SS

Description

Diatomaceous mud

Diatomaceous mud commonly is olive gray (5y 4/2), partly with black patches and contains clay minerals, diatoms, spicules, quartz and volcanic glass.

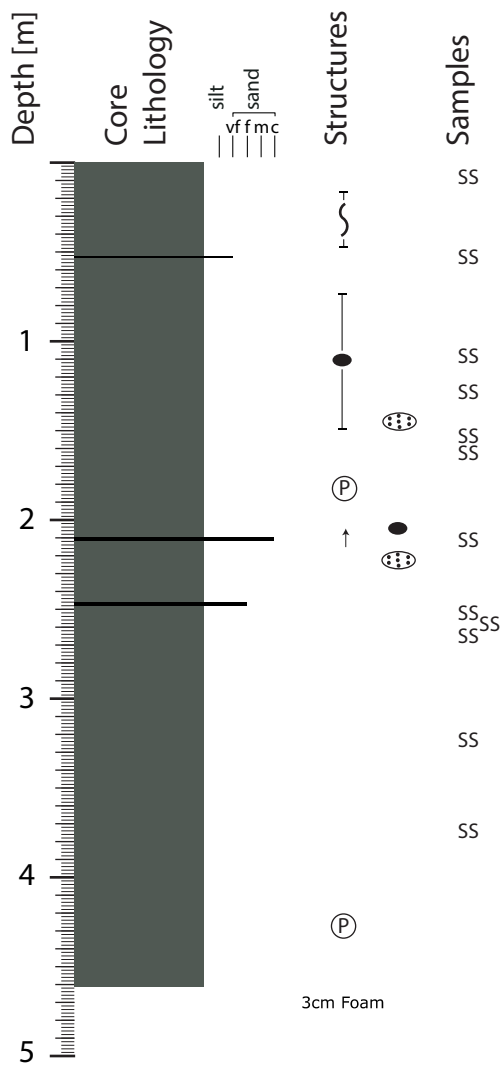
Minor lithologies and observations:

- 0-1 cm: brownish black (2.5y 3/2)
- 1-5.5 cm: olive black (5y 3/1)
- 5.5-34 cm: olive black (5y 3/1) - black (7.5y 2/1) diatomaceous silt
- 34-64.5 cm: grayish olive (7.5y 4/2) - gray (7.5y 4/1)
- 64.5 cm-end: Gray (7.5y 4/1), homogenous with a few burrows

GeoB 21818-1

Latitude: 40°N 14.789 Longitude: 143°E 48.807

Waterdepth: 3138 m Recovery: 4.63 m



Description

Diatomaceous mud interbedded with sand beds and intervals with lithic clasts and pumice

Olive gray (5y 4/2) diatomaceous mud with intervals of sandy mud, partly with black patches and/or colour bands, and/or lithic clasts. The mud contains clay minerals, diatoms, spicules, quartz and volcanic glass. Sand beds contain pumice and lithic fragments. Ash layers containing pumice

Minor lithologies and observations:

199-209 cm: sandy diatomaceous mud.

Lithic clasts:

70-71 cm: Greenish black subrounded lithic clast with white lines on surface.

89-91 cm: Angular to subrounded brown lithic clast.

111-112 cm: subrounded brown lithic clast.

113-115cm: angular, jagged black lithic clast (volcanic?)

143 cm and 147-148cm: mm-scale angular, brown lithic clast.

206-208 cm: 3cm long subrounded green lithic clast.

Sand beds and patches:

152-155 and 160-161cm: medium black and gray sand patch.

209-211cm: Gray and black sand bed. Fining upwards from coarse to fine. Sharp contacts.

213-216cm: Sand patch.

246-248cm: Fine black sand bed.

Pumice:

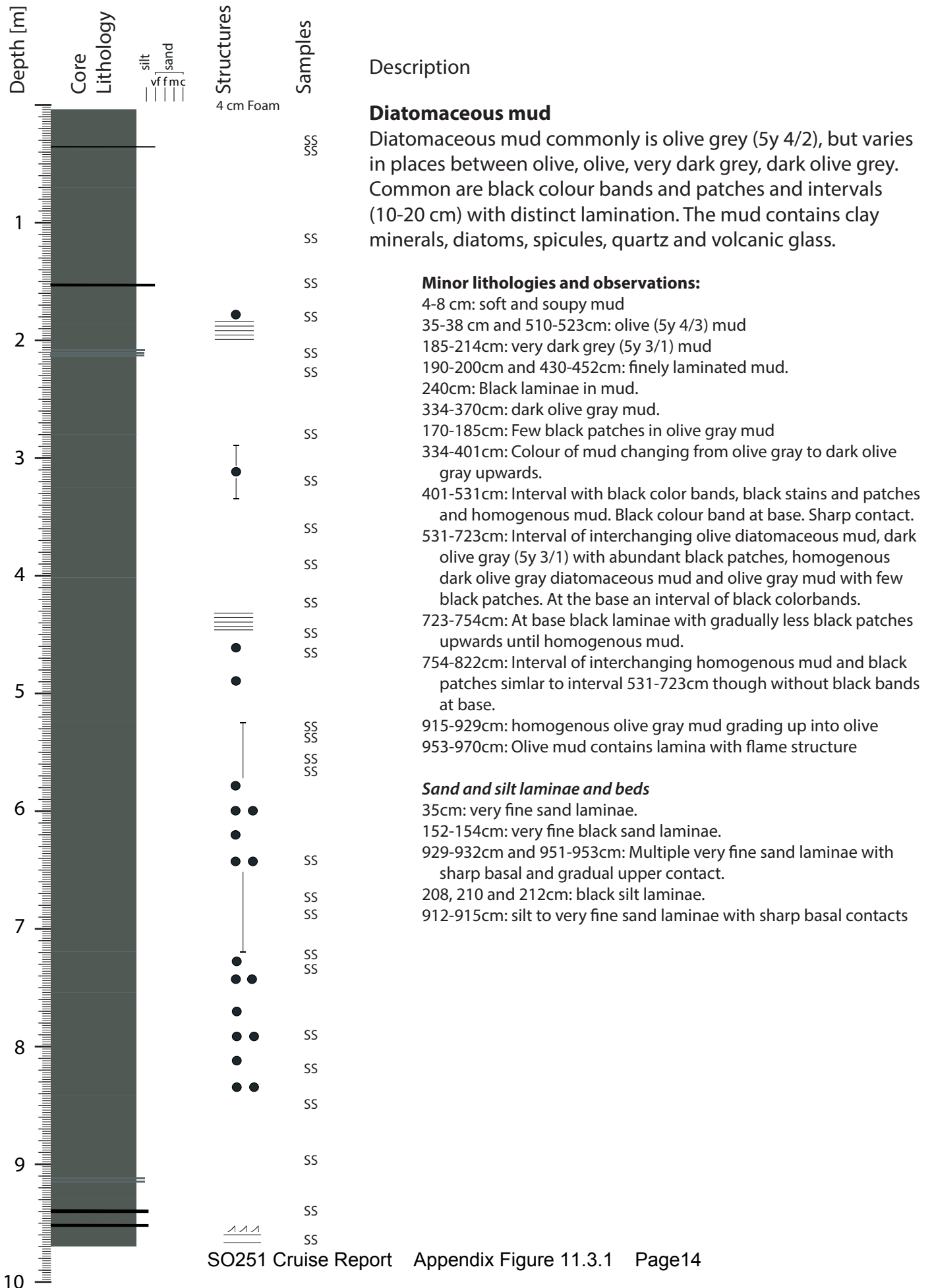
167-169 cm: elongated, angular pumice clast (2cm)

184-197cm: Unsorted pumice bed composed of angular, white, not sorted clasts (mm- to cm-scale).

422cm: Angular pumice clast (1 cm)

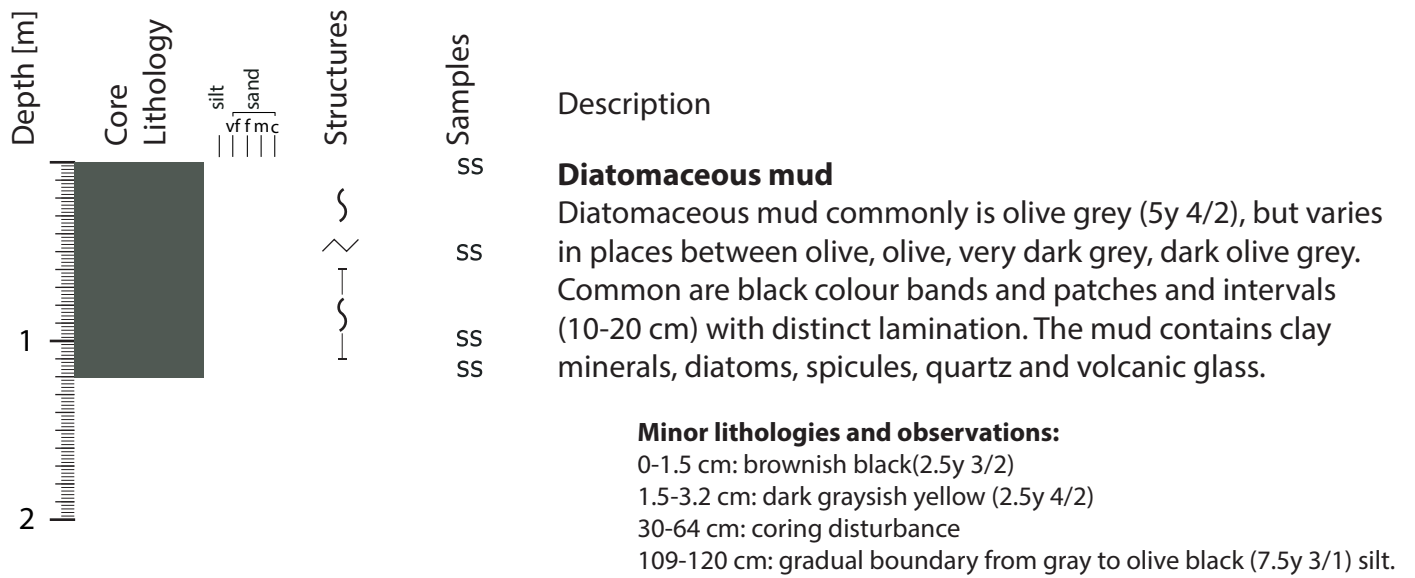
GeoB 21821-1

Latitude: 38°N 53.963 Longitude: 144°E 12.972
 Waterdepth: 7405 m Recovery: 9.70 m



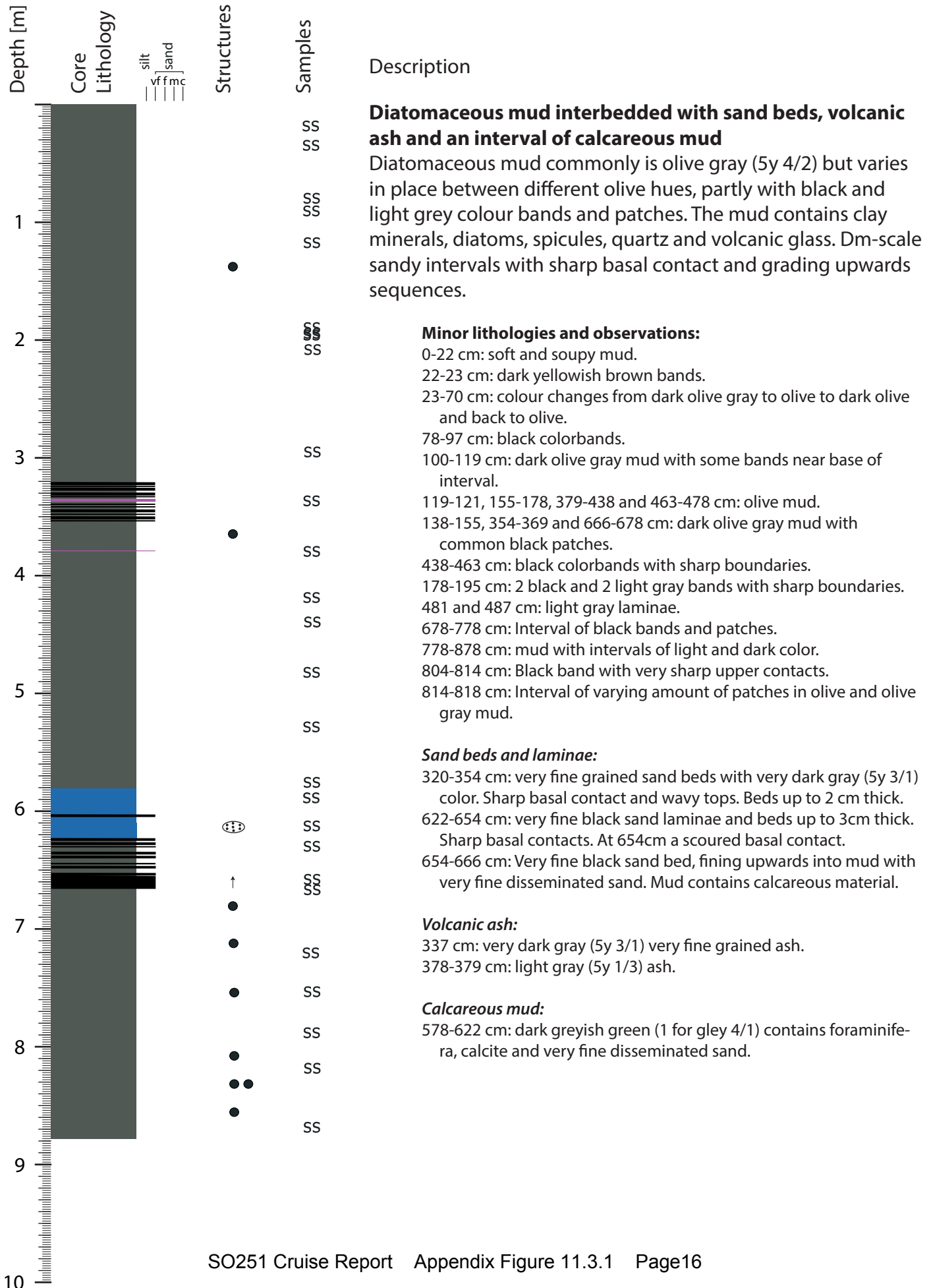
GeoB 21821-2

Latitude: 38°N 53.963 Longitude: 144°E 12.972
 Waterdepth: 7405 m Recovery: 1.20 m



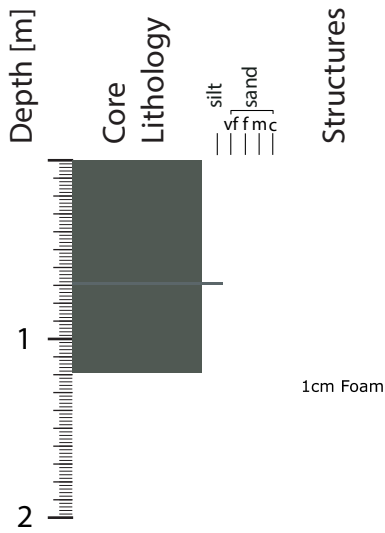
GeoB 21823-1

Latitude: 38°N 00.204 Longitude: 143°E 59.989
 Waterdepth: 7555 m Recovery: 8.78 m



GeoB 21823-2

Latitude: 38°N 00.204 Longitude: 143°E 59.989
 Waterdepth: 7555 m Recovery: 1.20 m



Samples

Description

SS

Diatomaceous mud interbedded with sand beds, volcanic ash and an interval of calcareous mud

SS

SS

SS

SS

Diatomaceous mud commonly is olive gray (5y 4/2) but varies in place between different olive hues, partly with black and light grey colour bands and patches. The mud contains clay minerals, diatoms, spicules, quartz and volcanic glass. Dm-scale sandy intervals with sharp basal contact and grading upwards sequences.

Minor lithologies and observations:

Oxidized at top of core

0.5-69.3cm: olive black (7.5y 3/2)

2.7-3.2 cm, 5.8-6.2 cm, 8.7-9.2 cm, 28.8-29.3 cm, 30.4-31 cm,

32.3-32.8 cm: gray (7.5y 4/1) silty clay

silty clay layers with sharp upper and gradual lower boundaries:

69.5 cm: brownish black (2.5y 3/2) silty clay (oxidized)

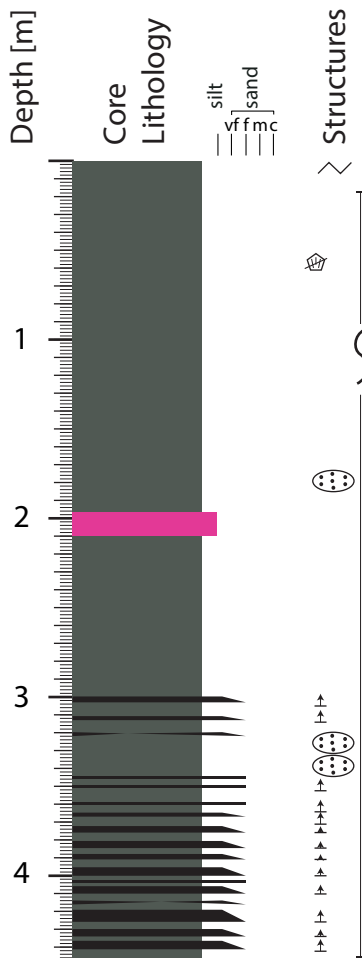
69.5-82, 97.5-119 cm: bioturbated grayish olive silty clay.

82-97.5 cm: olive black bioturbated silt.

69.3 cm: medium to coarse silt, sharp contact.

GeoB 21829-1

Latitude: 33°N 40.159 Longitude: 136°E 47.802
 Waterdepth: 2031 m Recovery: 4.46 m



Samples

Description

0-300 cm: Silty clay

Dark greenish grey (GLEY-1 4/1), homogeneous to slightly mottled (bioturbated) silty clay, containing foraminifera, spicules, diatoms, calcareous nannofossils. Detrital silt fraction composed of qtz, volcanic glass, lithic fragments, accessory minerals.

Minor lithologies and observations:

- 20 cm: partly slightly mottled and patchy (-->bioturbated)
- 49 cm: plant fragment
- 178 cm: patch of black coarse silt with sand, mostly detrital with FeS framboïd --> black colour and volcanics and biogenics (mixed -->bioturbated)
- 197-210 cm: dispersed ash with patch at 210 cm

300-446 cm: Interbedded silty clay with sand laminae and beds

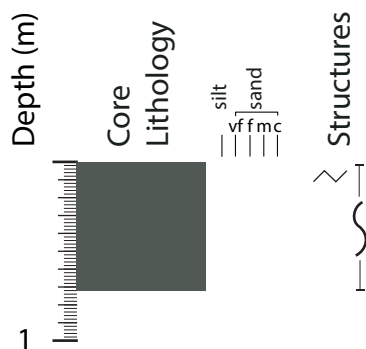
Silty clay as above, sandy silt to fine sand beds containing abundant qtz, mica and lithic fragments (metamorphic and sedimentary rock fragments)

Sand laminae and beds:

- 300-303 cm: sharp base and diffuse upper boundary (bioturbated), graded sand bed (coarse silt with sand)
- 311-313 cm: sharp base and diffuse upper boundary (bioturbated), graded sand bed (coarse silt with sand)
- 320-322 cm: disrupted sand bed
- 346 cm: thin graded sand layer
- 349-351 cm: thin graded sand layer
- 359-360 cm: graded sand layer with sharp base and diffuse upper contact (bioturbated); same at 365-367 cm, 372-376 cm, 381-385 cm, 388-391 cm
- 395-400 cm: possible two overlaying sand layers / or bioturbated diffusio upper contact
- 403 cm: thin sand layer
- 406-410 cm: sand layer, clear erosional contact with plant remains at the base
- 414-416 cm: dispersed sand bed
- 419-426 cm: sand bed with plant remains in interlayer 425 cm
- 430-434 cm: sand bed
- 436-441 cm: sand bed

GeoB 21829-2

Latitude: 33°N 40.159 Longitude: 136°E 47.802
 Waterdepth: 2031 m Recovery: 0.72 m



Samples

Description

Silty clay

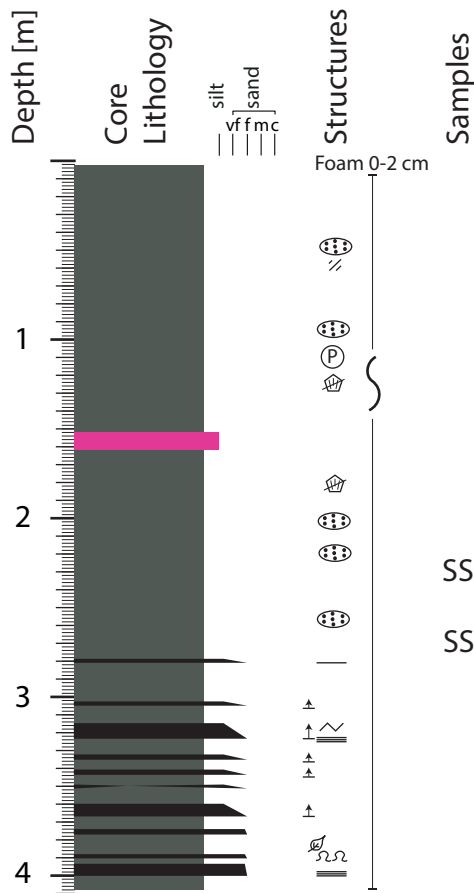
Dark greenish grey (GLEY-1 4/1), homogeneous to slightly mottled (bioturbated) silty clay, containing foraminifera, spicules, diatoms, calcareous nannofossils. Detrital silt fraction composed of qtz, volcanic glass, lithic fragments, accessory minerals.

Minor Lithologies

- 0-0.5 cm: oxidised layer
- ~7-9 cm: two ~0.5 cm thick, oxidised layers, slight convolute bedding (coring disturbance?)
- ~40 cm: inclined band with subtle darker colour hue (bioturbation?)
- 66 cm: patch (darker colour hue) --> bioturbation

GeoB 21831-1

Latitude: 33°N 32.915 Longitude: 136°E 49.892
 Waterdepth: 2039 m Recovery: 4.08 m



Description

0-280 cm: Silty clay

Dark greenish grey (GLEY-1 4/1), homogeneous to slightly mottled (bioturbated) silty clay, containing foraminifera, spicules, diatoms, calcareous nannofossils. Detrital silt fraction composed of qtz, volcanic glass, lithic fragments, accessory minerals.

Minor lithologies and observations:

- 2-3cm: soupy core
- 46 cm: silt patch
- 152-162 cm: subtle dispersed ash (greenish grey mottled)
- 222 cm: silty patch
- 257 cm : silty patch

280-408 cm: Interbedded silty clay with sand laminae and beds

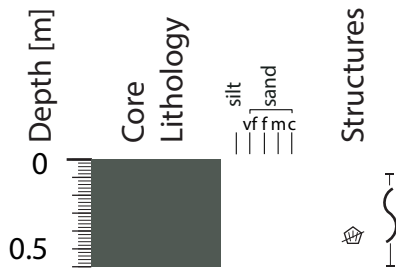
Silty clay as above, sandy silt to fine sand beds containing abundant qtz, mica and lithic fragments (metamorphic and sedimentary rock fragments)

Sand laminae and beds:

- 97 cm: fine sand patch
- 118 cm: fine sand patch
- 204 cm: coarse silt to fine sand patch
- 280 cm: sand bed with sharp base
- 304 cm: sand bed with sharp base
- 315-322 cm: „mushy“ coarse silt and fine sand layers (partly coring disturbed), base with subtle parallel lamination.
- 332-335 cm: fine sand bed, graded, sharp base same at 341-343 cm, 360-367 cm, 374-377 cm, 380-384 cm (plant remains interbedded within sand bed)
- 349-351 cm: disrupted (bioturbated) sand layer
- 388-390 cm: sand bed with convolute base

GeoB 21831-2

Latitude: 33°N 32.915 Longitude: 136°E 49.892
Waterdepth: 2039 m Recovery: 0.6 m



Samples

Description

Silty clay

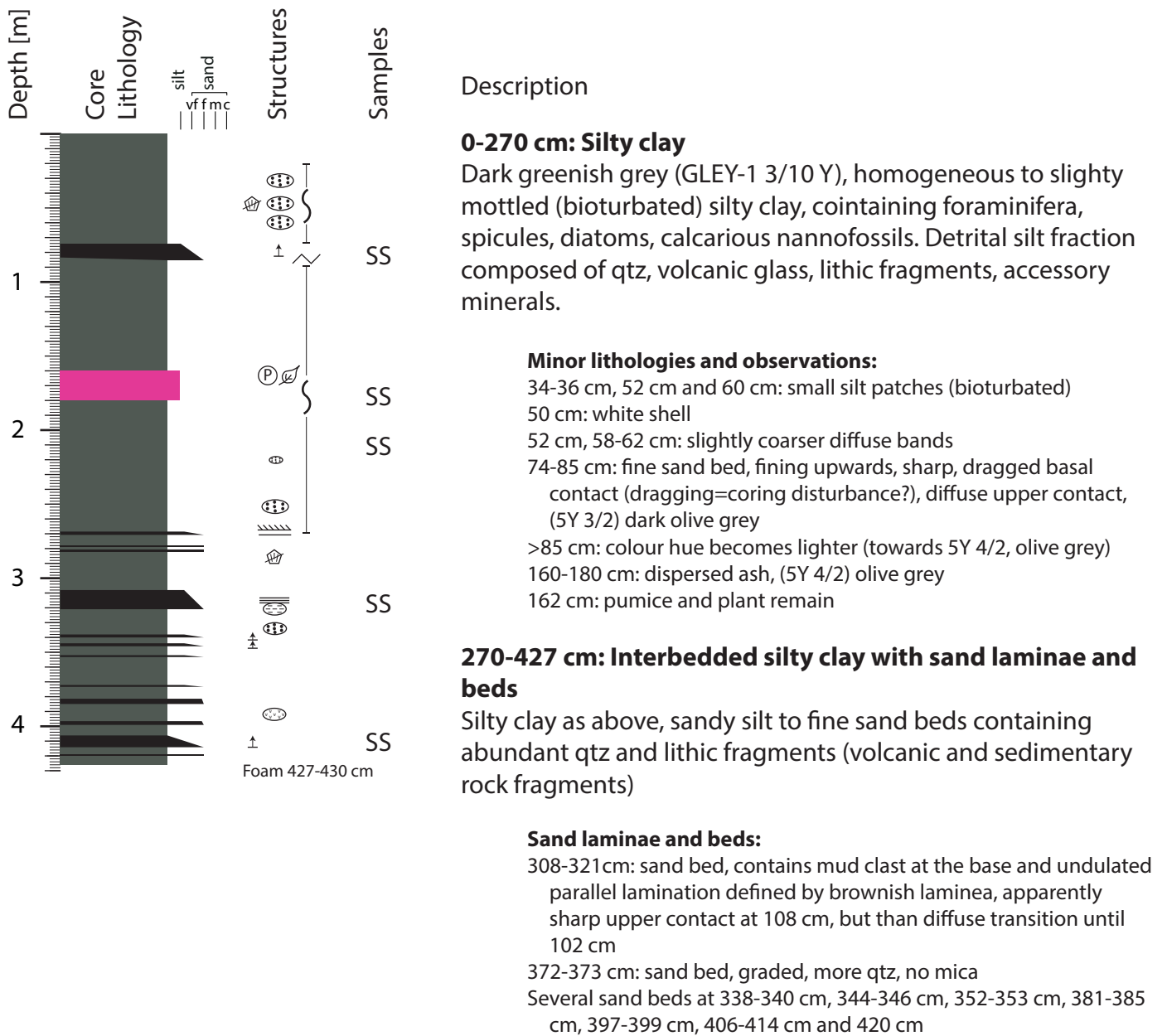
Dark greenish grey (GLEY-1 4/1), homogeneous to slightly mottled (bioturbated) silty clay, containing foraminifera, spicules, diatoms, calcareous nannofossils. Detrital silt fraction composed of qtz, volcanic glass, lithic fragments, accessory minerals.

Minor lithologies and observations:

0-0.5 cm: slightly oxidised top layer

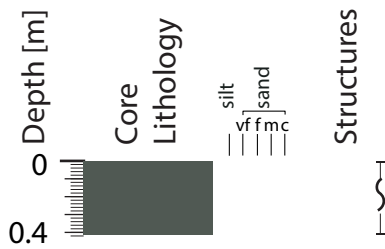
GeoB 21833-1

Latitude: 33°N 27.746 Longitude: 136°E 32.614
 Waterdepth: 2054 m Recovery: 4.27 m



GeoB 21833-2

Latitude: 33°N 27.746 Longitude: 136°E 32.614
Waterdepth: 2054 m Recovery: 0.41 m



Samples

Description

Silty clay

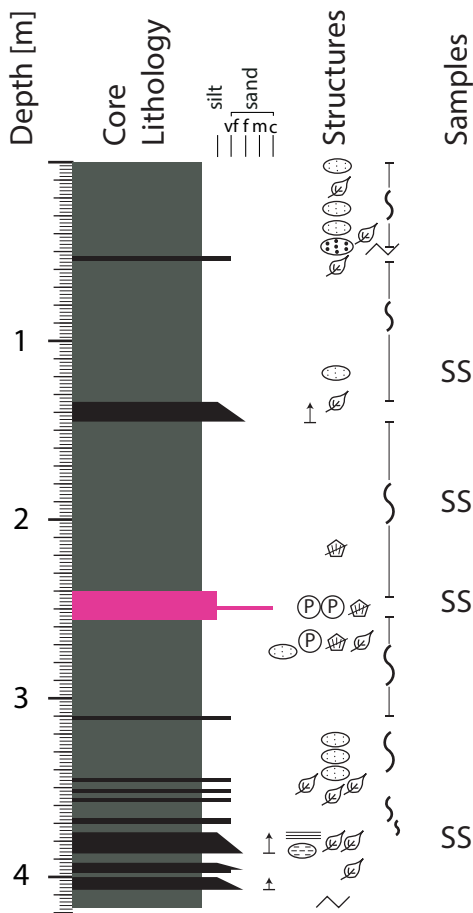
Dark greenish grey (GLEY-1 3/10 Y), homogeneous to slightly mottled (bioturbated) silty clay, containing foraminifera, spicules, diatoms, calcareous nannofossils. Detrital silt fraction composed of qtz, volcanic glass, lithic fragments, accessory minerals.

Minor lithologies and observations:

0-2 cm: slightly oxidised top layer

GeoB 21834-1

Latitude: 33°N 35.732 Longitude: 136°E 27.409
 Waterdepth: 2041 m Recovery: 4.17m



Description

0-310 cm: Clayey silt

Dark greenish grey (GLEY-1 3/10 Y), homogeneous to slightly mottled (bioturbated) silty clay containing foraminifera, spicules, diatoms, calcareous nannofossils. Detrital silt fraction composed of qtz, volcanic glass, lithic fragments, accessory minerals and plant remains

Minor lithologies and observations:

- 134-145 cm: sand bed with erosional base, graded with distinct foraminifera layer at 140 cm
- 240-250 cm: dispersed ash
- 250-251 cm: well sorted, subrounded, pumice pebbles (0.5 cm), parallel oriented, darker grey, 1.5 cm thick layer
- 251-256 cm: ash layer
- 268 cm: shell fragment and 0.5 cm wood fragment

310-417 cm: Interbedded clayey silt with sand laminae and beds

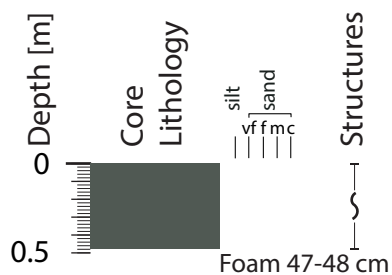
Clayey silt as above, sandy silt to fine sand beds containing abundant qtz and lithic fragments (volcanic and sedimentary rock fragments) and common plant remains

Sand laminae and beds:

- 346 cm, 352 cm and 357 cm: sand beds interbedded with silty clay rich in plant remains
- 367-370 cm: sand beds (possible multi layer and/or bioturbated)
- 375-387 cm: sand bed, graded, including small (mm-scale) mud clasts near the base and a 1 cm thick, well-defined layer with organic material, plant remains, 10YR 2/2 very dark brown at 380 cm
- 392-398 cm: sand bed, graded
- 400-407 cm: sand bed, graded

GeoB 21834-2

Latitude: 33°N 35.732 Longitude: 136°E 27.409
Waterdepth: 2041 m Recovery: 0.48 m



Samples

Description

Clayey silt

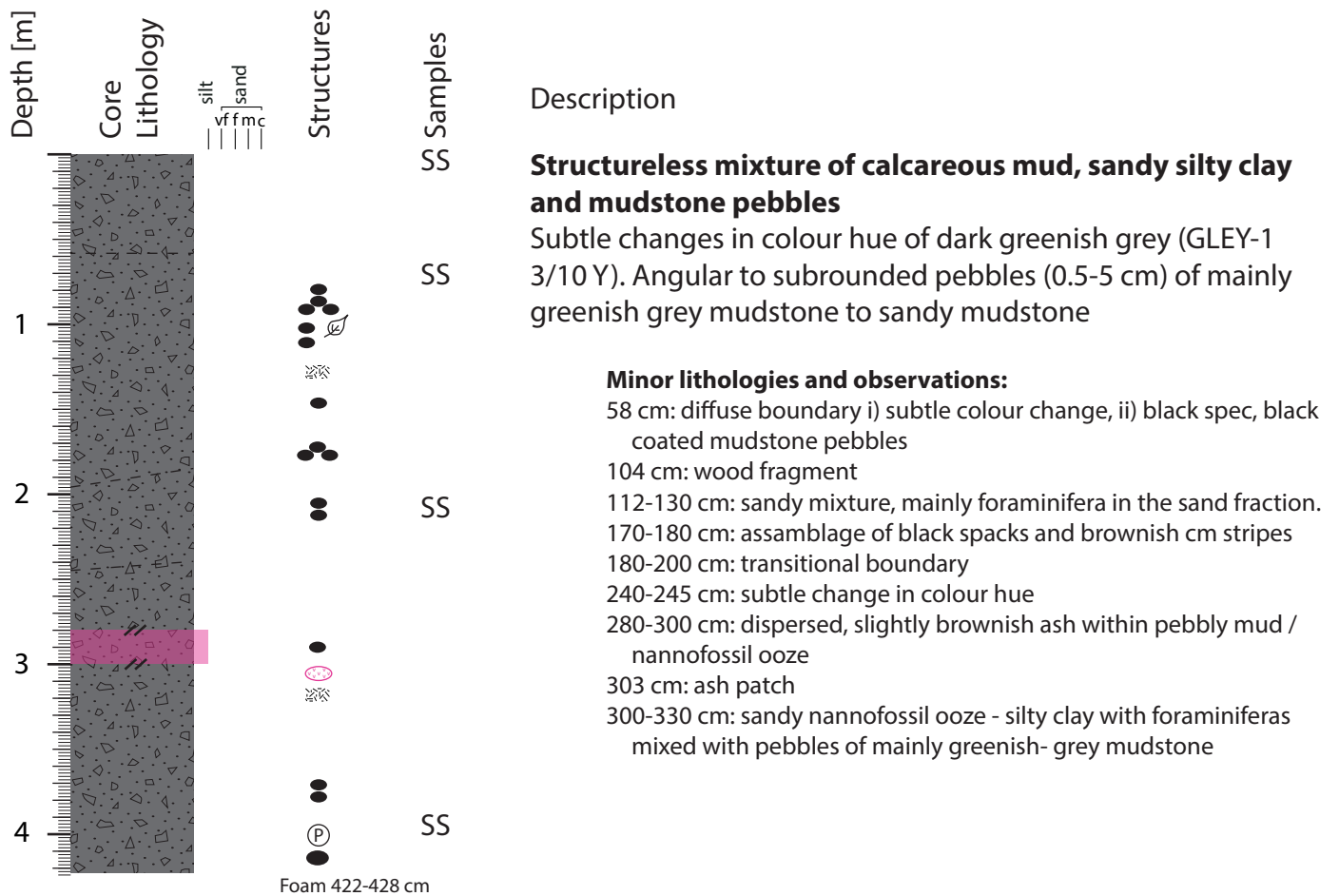
Dark olive grey, homogeneous to mottled (bioturbated) clayey silt with siliceous and calcareous biogenic components and occasional occurrence of mm-scale plant remains

Minor lithologies and observations:

0-2 cm: oxidised top layer

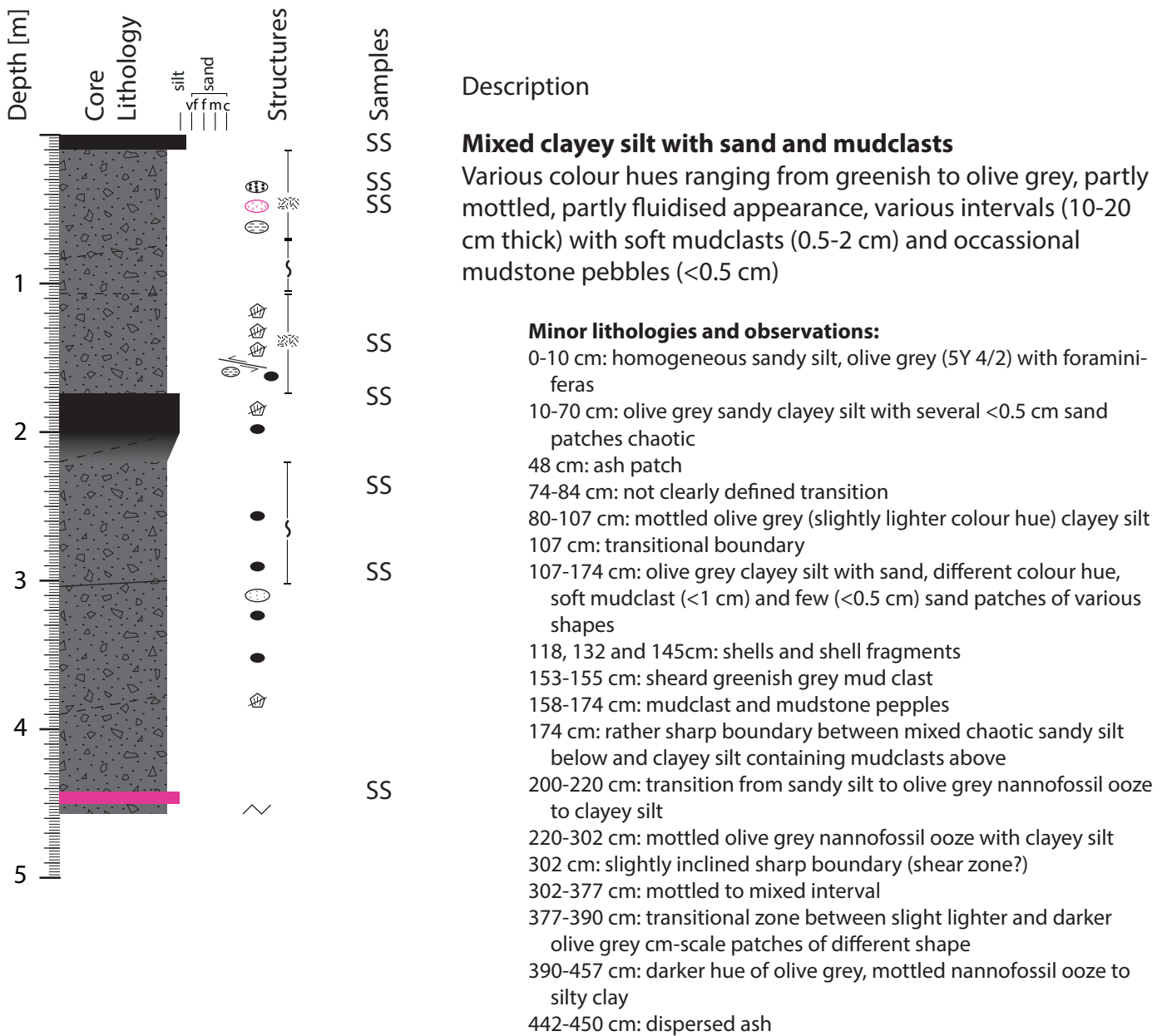
GeoB 21836-1

Latitude: 33°N 15.131 Longitude: 136°E 35.820
 Waterdepth: 1919 m Recovery: 4.28 m



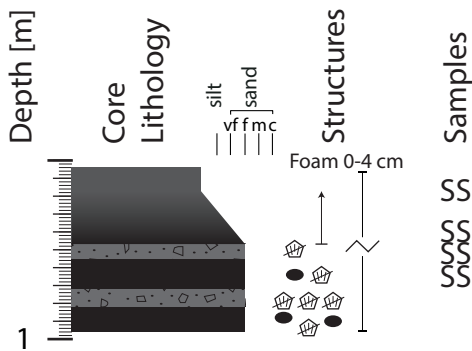
GeoB 21840-1

Latitude: 33°N 15.148 Longitude: 136°E 34.743
 Waterdepth: 1823m Recovery: 4.57 m



GeoB 21842-1

Latitude: 33°N 42.854 Longitude: 137°E 05.226
 Waterdepth: 1830 m Recovery: 0.96m



Description

Interbedded sequence (dm-scale) between layers containing hard pieces with mm-scale incrustation and clayey silt with sand

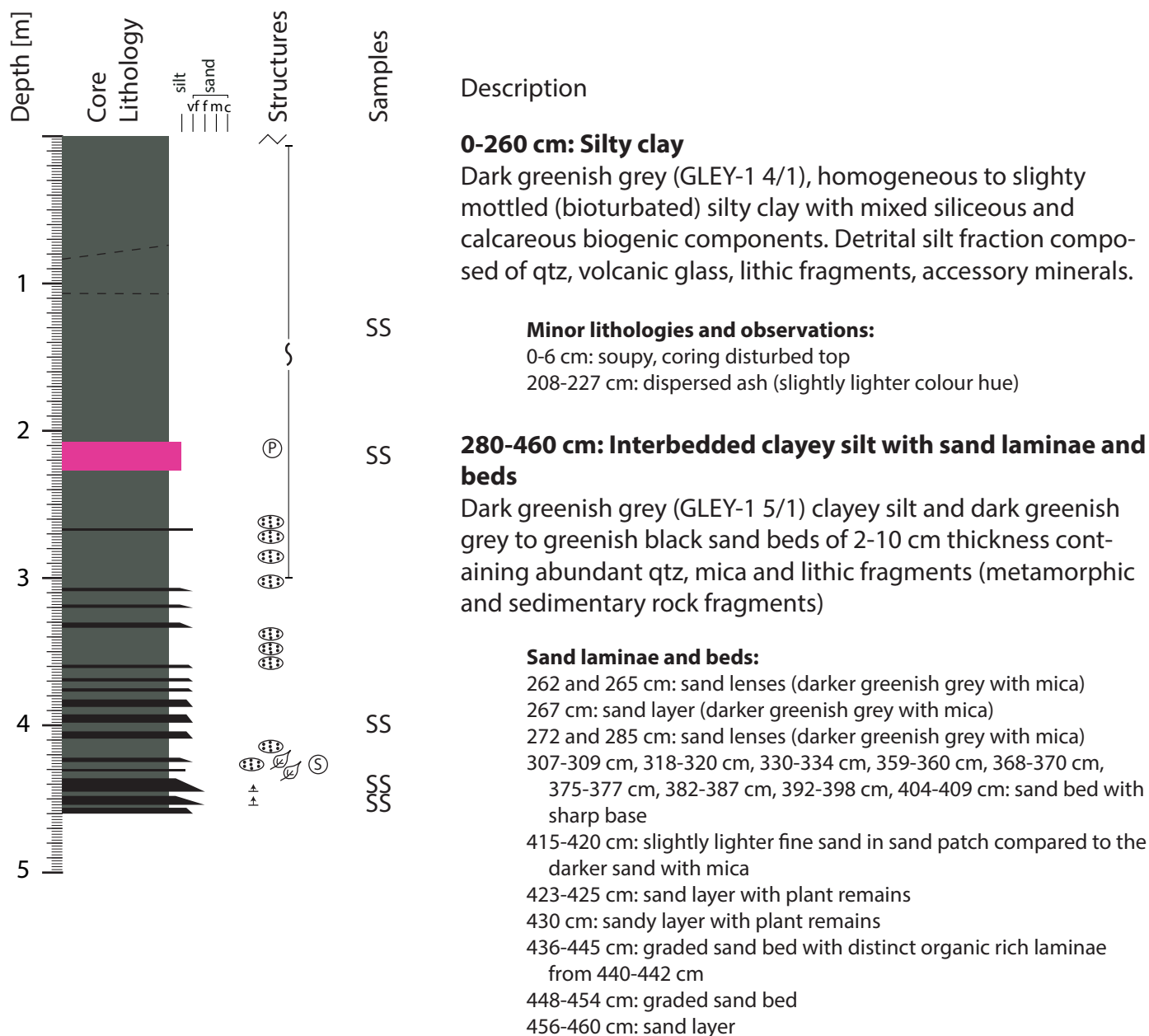
Dark greenish grey fine fraction contains abundant autigenic calcite and pale brown hard pieces appear to be calcite cemented. Abundant occurrence of shell fragments (calyptogena) and greenish grey mudstone pebbles.

Minor lithologies and observation:

- 4-17 cm: liquid mud
- 17-47 cm: graded sequence from fine sand to silty clay --> settled out from suspended material in the liner upon coring
- 47-50 cm: hard piece (pale brown) with upper side mm-scale incrustation of black to reddish crust with <1 cm deep unregular hole with fauna (tube worms?)
- 50-55 cm: hard piece without incrustation
- 64 cm: Calyptogena (shell fragment) and greenish grey mudstone pebble
- 73-82 cm: hard pieces 2-3 cm as 50-55 cm, but no black curst, many broken calyptogena (shell fragments)
- 82-95 cm: 3 cm half tube shaped calcite- cemented pale brown mudstone piece (--> concrete fluid conduit?) and <1 cm greenish grey mudstone pebble

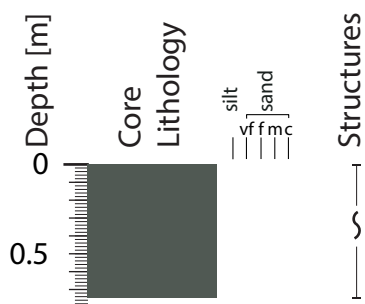
GeoB 21843-1

Latitude: 33°N 41.620 Longitude: 137°E 00.739
 Waterdepth: 1987m Recovery: 4.60 m



GeoB 21843-2

Latitude: 33°N 41.620 Longitude: 137°E 00.739
 Waterdepth: 1987m Recovery: 0.75 m



Samples

Description

Silty clay

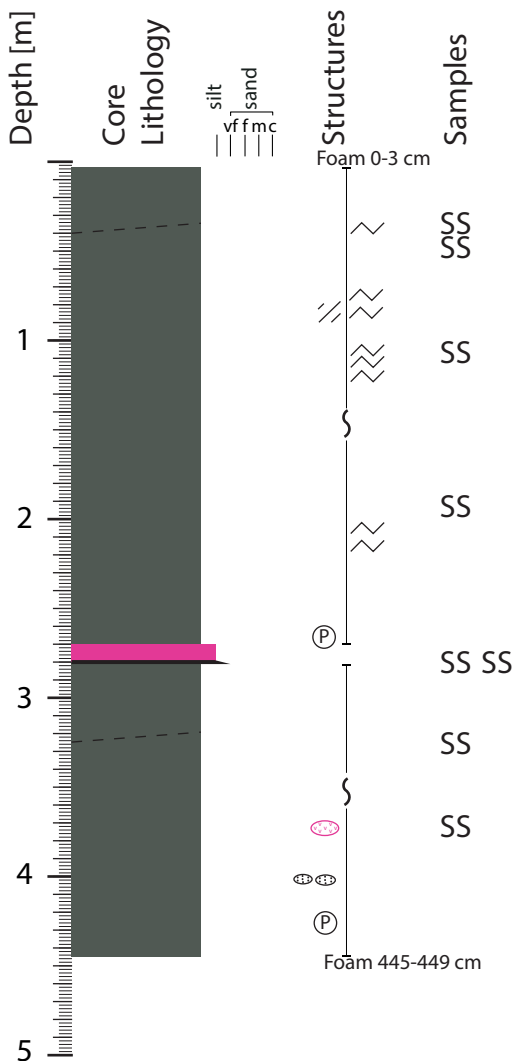
Dark greenish grey (GLEY-1 4/1), homogeneous to slightly mottled (bioturbated) silty clay with mixed siliceous and calcareous biogenic components. Detrital silt fraction composed of qtz, volcanic glass, lithic fragments, accessory minerals.

Minor lithologies and observations:

0-1cm: oxidized top layer, bioturbation of oxidised sediment down to 10 cm.

GeoB 21845-1

Latitude: 33°N 12.489 Longitude: 136°E 44.349
 Waterdepth: 2860 m Recovery: 4.49 m



Description

Silty clay

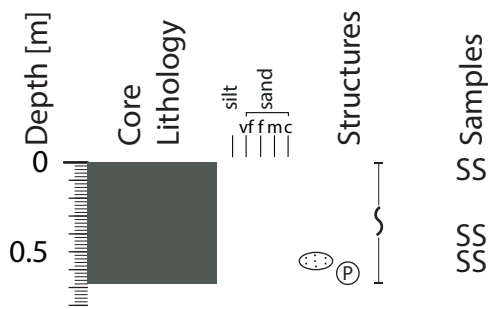
homogeneous to slightly mottled, dark greenish grey (GLE Y-1 4/10Y) silty clay with mixed siliceous and calcareous biogenic components, with faint (mm scale) black staining (FeS) and white specs (foraminifera, sponge spicules)

Minor lithologies and observations:

- 35-40 cm: subtle change in colour hue (to lighter colour) and slightly more silty not distinguishable in SS
- 76-100 cm: cracks (mm-scale, inclined) likely due to coring opening and/or pore water sampling
- 140 +/- 5 to 10 cm: transition from slightly darker colour hue (above) to lighter colour hue (below) of greenish grey
- 266 cm: <1 cm pumice piece
- 278-280 cm: basal 0.5 cm thick fine sand with dark volcanic and white foraminifera components; overlain by 0.5 cm well sorted, rounded pumice in coarse sand fraction: overlain vitric ash patch
- 307 cm: FeS staining patch
- 320-325 cm: dispersed slightly coarse transition
- 325 cm: faint patch of lighter grey silty clay
- 327 cm: fine sand patch with dark volcanoclastic and white foraminiferas.
- 373 cm: ash patch, vitric ash
- 401 and 402: 0.5 cm silty patches

GeoB 21845-2

Latitude: 33°N 12.419 Longitude: 136°E 44.264
 Waterdepth: 2860 m Recovery: 0.68 m



Description

Silty clay

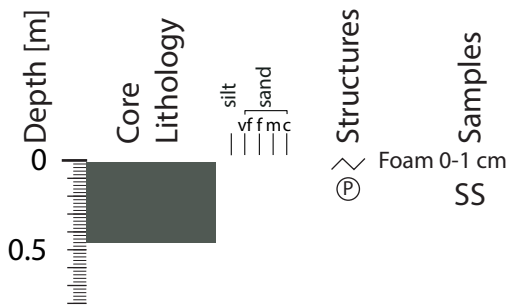
homogeneous to slightly mottled, dark greenish grey (GLEY-1 4/10Y) silty clay with mixed siliceous and calcareous biogenic components

Minor lithologies and observations:

0-3 cm: dark greyish brown oxidised top layer
 55 cm: patch slightly more silty

GeoB 21846-2

Latitude: 33°N 09.773 Longitude: 136°E 38.790
Waterdepth: 2888 m Recovery: 0.46 m



Description

Silty clay

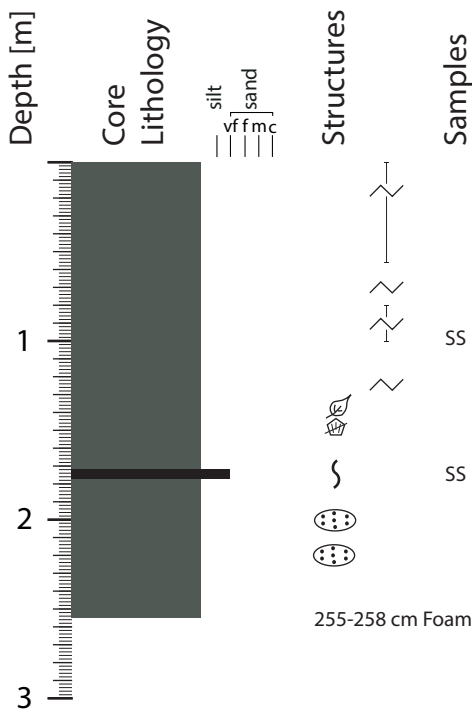
homogeneous to slightly mottled, dark greenish grey (GLEY-1 4/10 6Y) silty clay with mixed siliceous and calcareous biogenic components

Minor lithologies and observations:

- 1-4 cm: soupy and oxidised (greyish brown) top layer
- 4 cm: sharp contact

GeoB 21858-2

Latitude: 33°N 49.298 Longitude: 137°E 01.442
 Waterdepth: 1920 m Recovery: 2.55 m



Description

Clayey silt

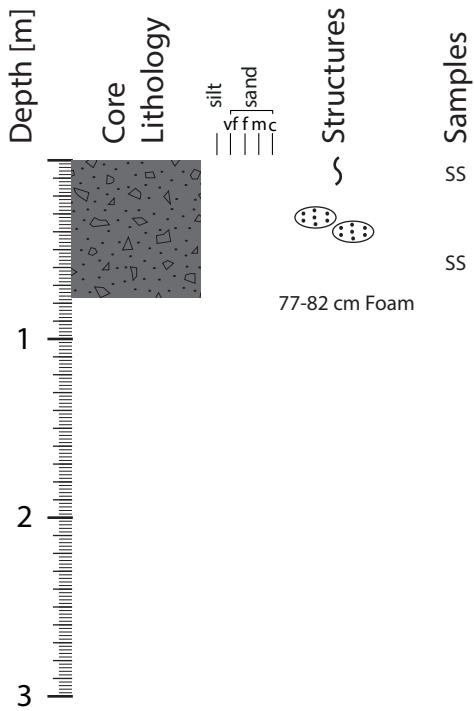
Clayey silt is homogeneous to only partly very subtle mottled and slight patches of darker colour hues. Mud contains few faint black staining specs and very few sub mm white components (shell fragments, foraminifera?). Clayey silt consists of clay minerals, quartz, volcanic glass, foraminifera, calc. nanofossils, pyrite.

Minor lithologies and observations:

- 9 cm: patch of darker colour
- 75-76 cm: patch of darker colour
- 122-124 cm: slight colour hue patch
- 130 cm: slightly more coherent appearance with less deformation (only along liner)
- 134 cm: <1cm plant remain (black coated wood?)
- 171-176 cm: interval with sandy clayey silt, bioturbated, mica visually present
- 201-202 cm: sandy-silty lense
- 219-256 cm: bottom of core with slightly higher sand content

GeoB 21860-2

Latitude: 33°N 40.675 Longitude: 136°E 55.129
 Waterdepth: 2003 m Recovery: 0.77 m



Description

Structureless mixture of clayey silt with pebbles

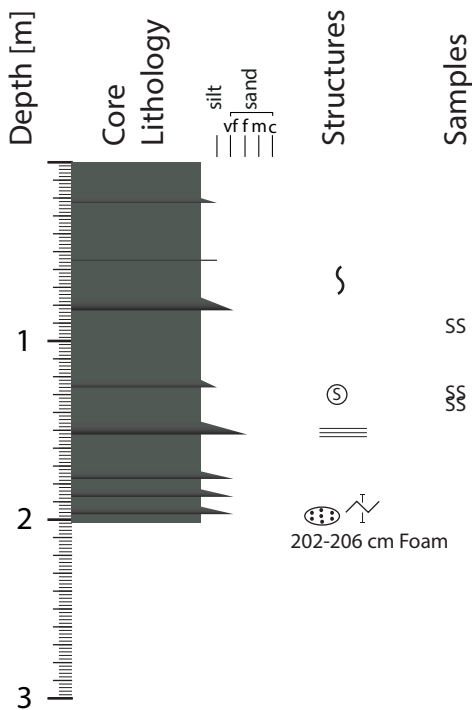
Stucked deposits of structureless mixture of clayey silt (with pebbles consisting of mudstone, sand patches and nanofossils. Pebbles are indurated but not completely lithified.

Minor lithologies and observations:

- 0-5 cm: patches of black and brownish bioturbation traces
- 12 cm: 0.5 cm greenish mudstone
- 20 cm: 1 cm greenish mudstone
- 26-29 cm: 4 cm sandy mudstone (grey)
- 32 cm: 1 cm sand patch
- 34 cm: 0.5 cm mudstone
- 38 cm: 1 cm mudstone
- 40 cm: 1 cm sand patch
- 48 cm: 2 cm mudstone
- 51 cm: 1 cm mudstone
- 57-59 cm: sharp upper contact, diffuse lower contact, slightly darker colour and containing more siliceous biogenic components (--> dispersed (bioturbated) back ground sediment)
- 59 cm - end of core: slightly darker structureless mixture of clayey silt with nanofossils and pebbles (more

GeoB 21861-2

Latitude: 33°N 47.382 Longitude: 137°E 16.097
 Waterdepth: 2162 m Recovery: 2.02 m



Description

Silty clay interbedded with dm-scale beds

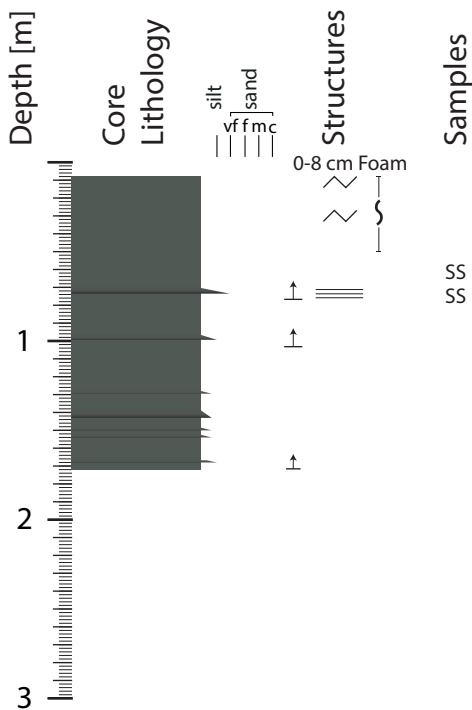
Silty clay is olive grey (SY 4/2) partly homogenous, partly dark grey (SY 4/1). The mud consists of clay minerals, quartz, volcanic glass, and various biogenic components. The beds have a mostly homogeneous upper part and a sandy to silty, fining upward basal part and are partly amalgamated.

Minor lithologies and observations:

- 0.5 cm: faint dark grey lamina
- 20-23 cm: slightly coarser (fining upward) dark silt lamina at the base at 23 cm.
- 28-31 cm: dark grey interval with sharp base and diffuse top
- 41-44 cm: interval with apparent slightly higher occurrence of foraminifera
- 45-48 cm: wavy, mottled (diffuse crossbedding?, coring disturbance?, bioturbation?)
- 48-55 cm: homogeneous with gradual change from darker to lighter colour hue
- 56 cm: <0.5 cm patch of slightly higher grey colour hue
- 56-66 cm: slightly mottled, olive grey, gradual lower contact
- 66-81 cm: homogeneous with gradual colour hue, change from darker grey to olive.
- 81 cm: mm-scale fine sand lamina
- 83 cm: 3 to 5 mm-scale lamination of dark grey and olive grey clayey silt and silty clay.
- 126 cm: sharp darker grey base and subtle upward colour hue change to olive grey at ~100 cm. Base slightly coarser, apparently fining upward but mostly homogeneous
- 126-133 cm: olive grey interval, apparently slightly coarser
- 133 cm: white patch of sponge spicules
- 133-149 cm: homogeneous with apparent shift in colour to lighter hue upward
- 150-152 cm: parallel laminated, foraminifera-bearing fine sand bed with sharp base and upward fining
- 154 cm: slightly darker
- 160-177 cm: same kind of sequence as 33-52 cm, 60-76 cm homogeneous and 76-77 cm foram-bearing sand layer...
- 77-80 cm: slightly darker
- 80-86 cm: same as sequence 33-52 cm (foram-bearing sand at 86 cm)
- 88-90 cm: slightly darker
- 90-96 cm: same as sequence 33-52 cm (foram-bearing sand at 96 cm)
- 96 cm to end of core: slightly coarser.

GeoB 21864-2

Latitude: 33°N 46.599 Longitude: 136°E 29.057
 Waterdepth: 2036 m Recovery: 1.72 m



Description

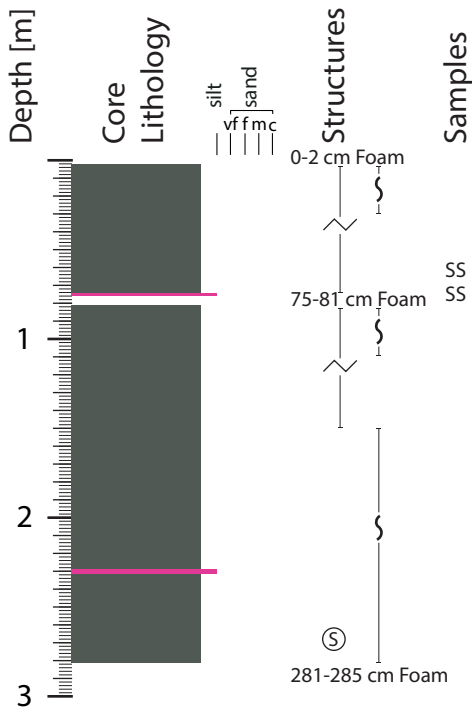
Silty clay interbedded with slight coarser and darker beds
 Slightly mottled olive grey (5Y 4/1) silty clay interbedded with 1-3 cm slightly coarser slightly darker beds with sharp lower and diffuse upper contact (lower part) and dm-scale beds with 1-2 cm fine sand to coarse silt basal layer and upper mostly homogeneous bed (upper part).

Minor lithologies and observations:

- 8-17 cm: interval with faint black staining lamina/patches
- 26 cm: black patch (FeS staining?)
- 50-71 cm: mostly homogeneous, slightly darker (gradual) colour hue towards base and slightly coarser towards the base (71-73 cm fine sand base)
- 73-80 cm: mottled with faint black staining and patches
- 80-99 cm: homogeneous slight darker (gradual) towards dark grey (5Y 4/1), silty base with sharp low contact.
- 100 cm: 0.5 cm black colour band
- 101 cm: 0.5 cm silt patch
- 103 cm: 1.5 cm black colour patch
- 105-109 cm: slightly coarser slightly darker interval
- 109-116 cm: slightly mottled with faint black stainings
- 116- 120 cm: slightly coarser and slightly darker with shiny mica
- 128-129, 139-143, 149-150, 153-154 cm: 1-3 cm beds of slight coarser and slight darker colour hue intervals within slightly mottled silt clay.
- 168 cm: black (FeS coated?) fine sand lamina with fining upward and diffuse (bioturbated?) upper boundary at ~160 cm

GeoB 21866-2

Latitude: 33°N 09.752 Longitude: 136°E 38.805
 Waterdepth: 2890 m Recovery: 2.85 m



Description

Silty clay

Silty clay is dark greenish grey (GLEY1 4/10y), heavily coring disturbed, apparently homogeneous to mottled. The mud contains both siliceous and calcareous biogenic components, some detrital silt and dominant clay, sand fraction are foraminifera (<5%)

Minor lithologies and observations:

- 0-25 cm: slight brownish colour hue, mottled (bioturbated near oxic top?)
- 26-60 cm: voids: round partly void partly soupy sediment (coring disturbance? degassing?)
- 35 cm +: below 35 cm: mm-scale faint, black staining
- 74 cm: 0.5 cm thick lamina of light tephra
- 140-145 cm: 1 cm thick elongated patch with more soupy sediment (coring disturbance?)
- 150 cm +: below 150 cm: apperantly more intact, less disturbed
- 165 cm: two small (0.3 cm) black patches
- 198 cm: another 0.5 cm hole (still coring disterbed)
- 229-230 cm: diffuse ash
- 230-231 cm: 1 cm vitric (light) ash layer
- 268 cm: white sponge spicule patch

GEOB - SMEAR SLIDES DESCRIPTION

R/V	Leg				GeoB-Number								
S	O	2	5	1	/	A	2	1	8	0	4	-	2

Observer	Asuka Yamaguchi
----------	-----------------

Section No.	Smear Slide No.	Depth in section (cm)	Lithology	Texture		Minerals							Biogenic				Rock		Comments														
				Sand	Silt	Clay	Accessory Minerals	Calcite	Clay	Dolomite	Inorganic calcite	Pyrite	Quartz	Volcanic glass	Clacar. Nannopl.	Foraminifera	Spicules	Diatoms		(Radiolaria)	Plant	Pumice	Volcanic Ash										
1	SS1	10				Clay																											
1	SS2	48					1	2	2	7	3																						quartzite fragments?

GEOB - SMEAR SLIDES DESCRIPTION

R/V		Leg				GeoB-Number				Observer																												
S	O	2	5	1	/	A	2	1	8	0	9	-	1	Asuka Yamaguchi																								
Section No.	Smear Slide No.	Depth in section (cm)	Lithology	Texture				Minerals					Biogenic				Rock		Comments																			
				Sand	Silt	Clay	Accessory Minerals	Calcite	Clay	Dolomite	Inorganic calcite	Pyrite	Quartz	Volcanic glass	Clacar. Nannopl.	Foraminifera	Spicules	Diatoms		(Radiolaria)	Plant	Pumice	Volcanic Ash															
1	SS1	16		1	15	2					2	3				2	7	+																				
		65		0	10	2		1			3	1				2	5	+																				
		108,5		0	10	5		3			2	2				3	8	+																				
		115		2	10	3		2			2	1				2	4	+																				
		121		0	6	4		0,5			1	1				0,5	2	+																				
		138,5	volcanic ash	20	10	0	2				7	5					2	+																				
		165		0	5	1		1			+ 0,5	1				2	3																					
		204		0	4	2	+	2			1	5				1	2																					
		218		0	4	4		2			1	1,5				2	1	+																				
		241		0	2	2		1,5			+ 0,3	0,5				0,5	1	+																				
		255		0	2	2	+	2			0,5	1				0,5	1,5																					
		271		1	5	3		3			+ 2	2				2	2																					
		306		0	6	3		2			+ 2	1				1	3	+																				
		323	volcanic ash	9	7	3	0,5	2			2	2				2	4	+																				
		369		0	8	4		2			+ 2	2				2	4	+																				
		406		0,5	9	3		2			+ 0,5	1				2	6																					
		444		0	4	4		4			+ 0,5	2				1	2																					
		460		0,5	6	3		2			+ 1	3				1	2																					
		464		0	2	4		2			+ 0,5	3				0,2	0,5																					
		472		0	7	8		4			+ 0,5	1				2	7																					
		491		2	8	10	1	7			3	4				1	3	+																				
		519		0,5	5	6		4			15	1				0,5	2	+																				
		537		3	2	5		5			1	2				0,2	1																					
		549	volcanic ash	5	3	2		2			+ 1	2				+	0,5																					
		563		4	6	4	0,5	2			1,5	4				+	1	3																				
		597		2	9	5		4			+ 2	4				2	4	+																				
		634		0	5	5		4			+ 0,33	3				0,5	2																					
		675		0	7	10		10			+ 1	4				1	3	+																				
		704		0	5	10		7			+ 1	2				0,5	1	+																				
		835		0	3	10		7			+ 1	1				+	1																					
		860	volcanic ash	2	10	2	3	2			5	5				+	0,5																					
		861		0	4	3	+	2			1	3				+	+																					
		905		0	2	2	+	2			0,5	1				+	1	+																				

GEOB - SMEAR SLIDES DESCRIPTION

R/V	Leg										GeoB-Number				
S	O	2	5	1	/	A	2	1	8	1	0	-	1		

Observer												
Asuka Yamaguchi												

Section No.	Smear Slide No.	Depth in section (cm)	Lithology	Texture			Minerals						Biogenic					Rock		Comments					
				Sand	Silt	Clay	Accessory Minerals	Calcite	Clay	Dolomite	Inorganic calcite	Pyrite	Quartz	Volcanic glass	Clacar. Nannopl.	Foraminifera	Spicules	Diatoms	(Radiolaria)		Plant	Pumice	Volcanic Ash		
1	SS1	18,5		7	7	3	2		3							2	1				3		plagioclase and hornblende as accessory minerals (A.M.)		
1		32		5	15	3	1		3							2	5				2		hornblende as A.M.		
1		36,5		30	10	0	8									8	8				8		plagioclase and hornblende as A.M.		
1		56		2	25	3	1		3							3							hornblende as A.M.		
2		82,5		10	15	5			4							5	7				5				
2		93,5		2	15	2			2							2	4								
3		147		0	13	3			2							1	4								
3		186		0	7	10			3							3	1							abundant clay sized diatom fragments	
4		257		2	15	3			2							1	10								
4		274		1	6	1			1							2	1								
4		282		0	15	3			1							2	10								
4		286	volcanic ash	30	10	0										2	20							mostly composed of angular volcanic glass fragments	
4		301,5	volcanic ash	20	10	0										1	20								
4		313		2	20	2	1		1							2	4							plagioclase, hornblende and chlorite as A.M.	
4		324,5	volcanic ash	0	20	0			0,5							1	7								
4		349	volcanic ash	0	5	5			2							1	5								
5		364	volcanic ash	5	20	0	1									3	20								
5		365,5	volcanic ash	4	20	0										1	20								
5		369		0	5	1											4								
5		453,5	volcanic ash	5	20	0	1									2	20								plagioclase and hornblende as A.M.

GEOB - SMEAR SLIDES DESCRIPTION

R/V	Leg							Geob-Number						
S	O	2	5	1	/	A	2	1	8	1	7	-	1	

Observer	Asuka Yamaguchi
----------	-----------------

Section No.	Smear Slide No.	Depth in section (cm)	Lithology	Texture							Minerals							Biogenic							Rock		Comments												
				Sand	Silt	Clay	Accessory Minerals	Calcite	Clay	Dolomite	Inorganic calcite	Pyrite	Quartz	Volcanic glass	Clacar. Nannopl.	Foraminifera	Spicules	Diatoms	(Radiolaria)	Plant	Pumice	Lithic Fragments																	
		19		0	7	3	+			2					1	3					0,5	5							biotite as A.M.										
		39		0	7	7	+			5					1	1						1	5	+					biotite as A.M.										
		84		0	6	4				3					2	2						0,5	3	+	+														
		136		0	5	5				0,5	3				1	2						+	2																
		207		0	15	15					10				2	5						2	15	+															
		234		0	8	3				+	2				0,33	2						2	5																
		320		0	6	4	+			+	2				2	2						0,5	3																
		423		0	10	7	+			0,33	5				2	3						2	7																
		481		0	3	3				+	2				1	2						0,5	1																
		580		0	6	4	+			+	2				1	3						0,5	3	+	+														
		720		1	4	4				+	3				1	2						+	2																
		821		6	9	6				0,33	5				3	5						1	7																
		952		10	15	7				1	0,5	5			10	5						+	2	10															

GEOB - SMEAR SLIDES DESCRIPTION

R/V	Leg	GeoB-Number
S O 2 5 1 / A 2 1 8 1 7 - 2		

Observer
Asuka Yamaguchi

Section No.	Smear Slide No.	Depth in section (cm)	Lithology	Minerals										Biogenic					Rock		Comments															
				Sand	Silt	Clay	Accessory Minerals	Calcite	Clay	Dolomite	Inorganic calcite	Pyrite	Quartz	Volcanic glass	Clacar. Nannopl.	Foraminifera	Spicules	Diatoms	(Radiolaria)	Plant		Pumice	Lithic Fragments													
		1		0	5	2	+	1								0,5	3																			
		30			8	3	+	2			+				1	2														1						
		50			8	4	+	3							1	3														1						

GEOB - SMEAR SLIDES DESCRIPTION

R/V	Leg				GeoB-Number				Observer					
S	O	2	5	1	/	A	2	1	8	1	8	-	1	Asuka Yamaguchi

Section No.	Smear Slide No.	Depth in section (cm)	Lithology	Texture							Minerals								Biogenic						Rock		Comments			
				Sand	Silt	Clay	Accessory Minerals	Calcite	Clay	Dolomite	Inorganic calcite	Pyrite	Quartz	Volcanic glass	Clacar. Nannopl.	Foraminifera	Spicules	Diatoms	(Radiolaria)	Plant	Pumice	Lithic Fragments								
		7																											hornblende as A.M.	
		52,5																											1 plagioclase, biotite and hornblende as A.M.	
		109																											15 cpx, hornblende and biotite as A.M.	
		128																											opx, hornblende and biotite as A.M.	
		154																											5 biotite and hornblende as A.M.	
		160																											5 hornblende and biotite as A.M.	
		210																											5 plagioclase and hornblende as A.M.	
		254																											biotite and glauconite as A.M.	
		258																											biotite and chlorite as A.M.	
		262																												
		322																												
		373																												

GEOB - SMIEAR SLIDES DESCRIPTION

R/V	GeoB-Number								Observer					
S	0	2	5	1	/	A	2	1	8	2	1	-	1	Asuka Yamaguchi

Leg	GeoB-Number								Observer					
S	0	2	5	1	/	A	2	1	8	2	1	-	1	Asuka Yamaguchi

Section No.	Smear Slide No.	Depth in section (cm)	Lithology	Texture			Minerals							Biogenic					Rock			Comments	
				Sand	Silt	Clay	Accessory Minerals	Calcite	Clay	Dolomite	Inorganic calcite	Pyrite	Quartz	Volcanic glass	Clacar. Nanopl.	Foraminifera	Spicules	Diatoms	(Radiolaria)	Plant	Pumice		Lithic Fragments
		33		4	4	3	+	2	2	2	2	+	0,5	3	1	1	1	1	1	1	1	Lithic = crystalline rock fragments. Plagioclase, biotite and glauconite as A.M.	
		35		0	7	3				0,33	1		1	5									
		113		1	4	3	+			0,5	1	+	0,5	3									
		153		4	6	4	+			2	3	0,33	+	7								1	zeolite(?) as A.M.
		181		0	6	7	+			1	4		+	3									
		211		2	8	8		0,5	6	2	4			0,5	5	+							
		228		0	5	4				1	2			0,5	2								
		280		0	5	3	+			2	2	+	+	2	+								hornblende, chlorite, biotite as A.M.
		320		0,5	7	7	+	0,33	5	3	3		+	2	+								plagioclase, cpx and opx
		360		1	5	10				+	0,5	1	+	5	+						+		
		391		0	6	4				+	2	3	+	2									
		423		0	3	5				+	0,5	2	+	1									
		448		0	3	7					0,33	1		3	1								
		466		2	4	4				+	2	2		0,5	2	+							1
		529		0	7	2					0,33	1		+	5	+							
		538,5		0	6	8				7	0,5	0,5		1	5						+		
		556		0	4	6	+				0,33	0,5		0,5	4	+							
		566		0	6	4				+	0,33	0,33		0,5	5								
		643		0	6	4	+			3	1	0,5		+	5								chlorite and biotite as A.M.
		674		0	10	7	+			7	1	1		2	10								plagioclase as A.M.
		687		2	5	5	+			5	1	2		+	2								plagioclase as A.M., Black stuff should be carbonaceous material.
		722		0	5	9	+			8	1	1		1	3	+							
		735		1	6	8	+			7	2	3		1	2	+							
		791		0	6	3				2	1	1		0,5	5	+							
		820		2	9	7	+			7	2	3		+	5	+					1		
		850		0	5	6				5	1	1		0,5	3								
		897		3	9	5	+	1	4	+	4	2	+	1	5								glauconite and zeolite(?) as A.M.
		941		0	6	7				3	0,5	7		0,5	2	+							
		964,5		0	5	6	+			2	0,5	5		0,5	3								

GEOB - SMEAR SLIDES DESCRIPTION

R/V	Leg							GeoB-Number					Observer	
S	0	2	5	1	/	A	2	1	8	2	3	-	1	Asuka Yamaguchi

Section No.	Smear Slide No.	Depth in section (cm)	Lithology	Texture			Minerals							Biogenic					Rock		Comments		
				Sand	Silt	Clay	Accessory Minerals	Calcite	Clay	Dolomite	Inorganic calcite	Pyrite	Quartz	Volcanic glass	Clacar. Nannopl.	Foraminifera	Spicules	Diatoms	(Radiolaria)	Plant		Pumice	Lithic Fragments
		17		0	7	5	+	2					1	3				+	4	+	0,5	1	glauconite, biotite as A.M.
		34		0	4	3		0,5	2				0,5	1				+	2			1	
		79		0	10	3	+	3										1	7		0,5		
		90		0	18	7		2				0,5	2					1	6	+	+		opx and biotite as A.M.
		117		0	5	4		0,5	3					2				0,5	3				
		189		0	6	4		2						3				2	3				
		193		0	10	4	+	3					2	3				0,5	5				
		195		4	6	3	+	2					5	3				0,5	2	+			
		208		6	8	6		0,5	5				5	4				1	5				
		295		3	10	7		0,5	5				4	5				+	5	+		1	
		337	volcanic ash	25	10	0	2	1					20	5				+	+		2	15	plagioclase, hornblende, biotite as A.M.
		379		15	10	3		2					0,5	20				+	3	+	2		
		418		0	9	4	+	3					2	3				0,5	4				
		439		3	5	7	+	6					2	3				+	3	+		1	
		481,5		3	5	0	1	+					2	2				+	+			3	lithic-microcrystalline rock fragments. Cpx, hornblende, biotite, plagioclase as A.M.
		528		0	2	6		5					0,5	2				+	+	1			
		575		7	2,5	1	+	1					2	15				1	+			5	biotite and plagioclase as A.M.
		588		3,5	4	4		0,5	3				1	3				0,5	0,5	1	+	1	1
		612		3	7	6		0,33	5				1	2				+	+	1	+	4	3
		628,5		15	7	0	2	+					5	2				0,5	+			8	5
		658		2	4	2	+	15					2	1,5				+	+	1	+	0,5	2,5
		666		15	3	0	1	+					3	3				1,5			5	5	hornblende, biotite, cpx, zeolithe as A.M.
		720		0	8	12		10					0,5	2					1	7			
		753		0	7	9	+	7						1					1	7			
		788		0	8	5		4					1	5				+	3				
		818		0	8	7		5					1,5	2					1	7	+	+	
		868		0	8	6	+	5					1	2					1	5	+		cpx as A.M.

GEOB - SMEAR SLIDES DESCRIPTION

+ = present
 (+) = traces
 ++ = dominant

R/V	Leg				GeoB-Number				Observer				
S	O	2	5	1	B	2	1	8	4	0	-	1	Michael Strasser

Section No.	Smear Slide No.	Depth in section (cm)	Lithology	Texture			Minerals								Biogenic**						Rock		Comments					
				Sand	Silt	Clay	Accessory Minerals	Calcite	Clay	Dolomite	Inorganic calcite	Pyrite	Quartz	Volcanic glass	Clacar. Nannopl.	Foraminifera	Spicules	Diatoms	(Radiolaria)	Plant (organic)	Pumice	Lithic Fragments						
		6	silt with more broken foraminifera	10	60	30	+	+								+	+	+	+	+	+	+	+	+		mudstone		
		32	nanofossil ooze		30	70	(+)																			(+)		
		47	vitric ash	5	90	5	(+)																			+		
		141	clayey silt with sand				(+)	+																		(+)	mudstone	
		177	clayey silt with sand				(+)	+																		(+)	mudstone	
		237	nanofossil and few silt, less clay				+	+																		(+)	mudstone	
		295	nanofossil and few silt, less clay				+	+																		(+)	mudstone	
		442	silt nanofossil (sand)				+	+																		(+)	+dispersed ash	

SO251- ROV Station list

Station Number ROV PHOCA	Dive No. of ROV PHOCA	GeoB Station Nr.	Date (UTC)	Time Start (UTC)	At Bottom (UTC)	Off Bottom (UTC)	Time End (surface) (UTC)	Location	Depth (m)	ROV Bottom Time (h)
Hafentest	67	n.a.	17.10.2016	Harbour Test Yokohama, Japan						
33ROV01	68	GeoB21828	19.10.2016	01:29	03:03	08:11	09:28	MV 2, Nankai	2000	05:08
44ROV02	69	GeoB21838	21.10.2016	00:39	01:50	08:22	09:32	MV 3, Nankai	1980	06:32
48ROV03	70	GeoB21841	22.10.2016	02:34	04:51	07:45	08:48	MV 4, Nankai	1960	02:54
57ROV04	71	GeoB21850	26.10.2016	02:30	03:33	09:43	11:03	MV 4, Nankai	2070	06:10
60ROV05	72	GeoB21853	27.10.2016	09:37	10:43	12:22	13:44	MV 3, Nankai	1980	01:39
62ROV06	73	GeoB218555	27./28.10. 2016	23:45	00:57	07:37	09:00	MV 4, Nankai	2070	06:40
70 ROV07	74	GeoB21863	30./31.10. 2016	23:37	00:42	06:33	07:35	MV 4, Nankai	1990	05:51
Total: 7 scientific dives										34:54:00

GeoB21828							
Date	Time (UTC)	SHIP_Lon	SHIP_Lat	Water_Depth	SUB1_Lon	SUB1_Lat	Observations/Comments
10/19/2016	01:29:30	136.9215088	33.6758995	1993.5			IN THE WATER
10/19/2016	03:03:16	136.9215546	33.6761665	1992.1	136.9209205	33.6757422	AT THE BOTTOM
10/19/2016	03:13:53	136.9216003	33.6762085	1992.00	136.9215947	33.6764688	bacterial mats?
10/19/2016	03:23:43	136.9216919	33.6761436	1992.2	136.921695	33.6764512	skeleton
10/19/2016	03:30:14	136.9216766	33.6761589	1992.00	136.9219302	33.6749102	Fish
10/19/2016	03:30:15	136.9216766	33.6761589	1992.00	136.9219302	33.6749102	Fish
10/19/2016	03:30:33	136.9216766	33.6761589	1991.6	136.9217337	33.6760955	Clamshells
10/19/2016	03:31:01	136.9216766	33.6761551	1991.6	136.9218797	33.6751497	Fish
10/19/2016	03:31:10	136.9216766	33.6761589	1991.6	136.9218797	33.6751497	shrimp
10/19/2016	03:36:20	136.9215698	33.6761665	1991.3	136.922051	33.6753417	Backteria Mat
10/19/2016	03:44:12	136.9215698	33.6761398	1994.3	136.92158	33.6764315	Fish
10/19/2016	03:44:12	136.9215698	33.6761398	1994.3	136.92158	33.6764315	Fish
10/19/2016	03:45:16	136.9215698	33.676136	1990.9	136.9219215	33.6760088	Debris
10/19/2016	03:45:41	136.9215698	33.6761398	1993.2	136.9216975	33.676289	Backteria Mat
10/19/2016	03:55:53	136.9217072	33.6761475	1991.3	136.9218035	33.6763388	Course to W
10/19/2016	03:56:22	136.9217072	33.6761436	1991.9	136.9223473	33.6755253	netz?
10/19/2016	03:57:59	136.9217072	33.6761398	1991.6	136.9218585	33.6761817	Backteria Mat
10/19/2016	03:58:48	136.9217072	33.6761436	1992.7	136.9220662	33.6756867	Clamshells
10/19/2016	04:01:31	136.9217072	33.6761513	1991.5	136.9215133	33.6787052	Clamshells
10/19/2016	04:04:45	136.9216919	33.6761475	1990.5	136.9210895	33.6756942	Fish
10/19/2016	04:10:48	136.9217072	33.6761932	1992.5	136.9213322	33.6760437	Backteria Mat
10/19/2016	04:10:52	136.9217072	33.6761894	1992.5	136.9213322	33.6760437	Clamshells
10/19/2016	04:13:22	136.9217072	33.676178	1991.8	136.9207548	33.675566	Backteria Mat
10/19/2016	04:14:07	136.9217072	33.6761665	1991.9	136.9213937	33.6761675	Striations on seafloor
10/19/2016	04:14:24	136.9217072	33.6761627	1992.4	136.920859	33.6756463	HD ON
10/19/2016	04:16:25	136.9216919	33.6761322	1992.3	136.9204878	33.6754492	clams, maybe alive
10/19/2016	04:18:55	136.9216614	33.6761398	1992.6	136.9209402	33.6755862	Backteria Mat
10/19/2016	04:33:00	136.9215393	33.6761055	1991.6	136.9206835	33.674152	Clamshells
10/19/2016	04:33:05	136.9215393	33.6761017	1991.6	136.9206835	33.674152	HD OFF
10/19/2016	04:33:35	136.9215393	33.6760979	1992.2	136.9209623	33.6747972	crab
10/19/2016	04:33:45	136.921524	33.6760979	1992.3	136.9211283	33.675129	HD ON
10/19/2016	04:40:20	136.9214935	33.6761742	1992.2	136.9218775	33.6720503	small mound
10/19/2016	04:41:22	136.9214935	33.6761742	1992.00	136.9217052	33.6759475	sea star
10/19/2016	04:43:15	136.9214935	33.6761665	1992.5	136.921924	33.6757252	Fish
10/19/2016	04:47:05	136.9215088	33.6761665	1991.8	136.9221888	33.6747535	Backteria Mat
10/19/2016	04:48:46	136.9215088	33.676178	1991.3	136.9215695	33.6762798	mantra
10/19/2016	04:51:05	136.921524	33.6761971	1991.5	136.92158	33.6760092	small sediment mounds
10/19/2016	05:02:36	136.9214935	33.6761475	1992.9	136.9215993	33.6758925	shrimp
10/19/2016	05:05:20	136.9215546	33.6761703	1992.7	136.9221445	33.6747718	seastar
10/19/2016	05:17:49	136.9215546	33.6761856	1991.6	136.9219485	33.6760347	clast(large)
10/19/2016	05:20:15	136.9215851	33.676178	1991.6	136.92225	33.6756283	Photo
10/19/2016	05:20:18	136.9215851	33.676178	1991.6	136.92225	33.6756283	Photo
10/19/2016	05:35:52	136.9216766	33.6761703	1990.9	136.9217207	33.676424	Backteria Mat
10/19/2016	05:39:52	136.9216614	33.6761665	1992.1	136.9239358	33.674716	Clamshells
10/19/2016	05:45:19	136.9216766	33.6761513	1991.6	136.9270827	33.6762587	bamboo debris
10/19/2016	05:54:54	136.9215088	33.6761627	1992.9	136.9230507	33.6764897	GEAR DEPLOYED
10/19/2016	05:55:10	136.9215088	33.6761703	1992.3	136.9230507	33.6764897	T stick
10/19/2016	06:02:20	136.921524	33.6761513	1992.3	136.9225998	33.676477	Photo
10/19/2016	06:02:34	136.921524	33.6761513	1991.9	136.922739	33.67649	Photo
10/19/2016	06:16:39	136.9216919	33.6761856	1991.6	136.9233922	33.6764723	T stick out
10/19/2016	06:25:06	136.9217072	33.676136	1993.9	136.9219323	33.6758628	Backteria Mat
10/19/2016	06:25:07	136.9217072	33.676136	1993.9	136.9219323	33.6758628	Fish
10/19/2016	06:25:49	136.9217072	33.6761398	1992.8	136.9219323	33.6758628	HD ON
10/19/2016	06:28:21	136.9217224	33.6761475	1992.1	136.9217562	33.6763843	HD OFF
10/19/2016	06:31:58	136.9217072	33.676178	1991.5	136.9219882	33.6759447	HD ON
10/19/2016	06:34:14	136.9217224	33.676178	1991.2	136.9218863	33.6760633	HD OFF
10/19/2016	06:37:56	136.9217377	33.6761665	1992.2	136.9217967	33.6763485	stick out
10/19/2016	06:40:04	136.9217224	33.6761398	1993.1	136.921921	33.6759583	HD ON
10/19/2016	06:41:27	136.9217224	33.6761169	1992.3	136.921921	33.6759583	Photo
10/19/2016	06:41:28	136.9217072	33.6761169	1992.3	136.921921	33.6759583	Photo
10/19/2016	06:41:49	136.9217072	33.6761131	1993.8	136.9218628	33.6755707	HD OFF
10/19/2016	06:42:20	136.9217072	33.6761017	1992.4	136.9218628	33.6755707	Fish
10/19/2016	06:43:16	136.9216919	33.6761017	1992.9	136.9218628	33.6755707	Clamshells
10/19/2016	06:45:36	136.9216766	33.6761055	1993.1	136.9214948	33.6759507	Clamshells
10/19/2016	06:50:13	136.9216003	33.6761208	1991.6	136.920963	33.6754858	GEAR DEPLOYED
10/19/2016	07:01:54	136.9215698	33.676178	1991.3	136.921439	33.6768578	t stick out
10/19/2016	07:07:27	136.9215546	33.6761513	1991.5	136.921439	33.6768578	Photo
10/19/2016	07:08:09	136.9215393	33.6761551	1991.8	136.921439	33.6768578	Photo
10/19/2016	07:08:54	136.921524	33.6761627	1991.9	136.921439	33.6768578	Photo
10/19/2016	07:09:13	136.921524	33.6761627	1992.6	136.921439	33.6768578	Photo
10/19/2016	07:09:53	136.9214935	33.6761665	1992.3	136.921439	33.6768578	Clamshells
10/19/2016	07:10:32	136.9214935	33.6761665	1992.2	136.921439	33.6768578	Fish
10/19/2016	07:10:55	136.9214935	33.6761665	1992.5	136.921439	33.6768578	HD ON
10/19/2016	07:12:09	136.9214935	33.6761589	1992.1	136.921439	33.6768578	Photo
10/19/2016	07:12:09	136.9214935	33.6761589	1992.1	136.921439	33.6768578	Photo
10/19/2016	07:12:10	136.9214935	33.6761589	1992.1	136.921439	33.6768578	Photo
10/19/2016	07:12:16	136.9214935	33.6761551	1993.1	136.921439	33.6768578	HD OFF
10/19/2016	07:12:52	136.9214935	33.6761475	1992.6	136.921439	33.6768578	HD ON
10/19/2016	07:14:09	136.9214783	33.6761475	1993.3	136.921439	33.6768578	Photo
10/19/2016	07:14:24	136.9214783	33.6761475	1993.00	136.921439	33.6768578	Photo
10/19/2016	07:16:00	136.9214935	33.6761475	1992.3	136.921439	33.6768578	Photo
10/19/2016	07:17:25	136.9214935	33.676136	1992.4	136.921439	33.6768578	Photo
10/19/2016	07:17:38	136.9214935	33.6761322	1992.00	136.921439	33.6768578	HD ON
10/19/2016	07:18:25	136.9214935	33.6761398	1993.3	136.921439	33.6768578	HD OFF
10/19/2016	07:22:31	136.9214935	33.6761322	1993.3	136.921439	33.6768578	HD ON
10/19/2016	07:22:54	136.9214935	33.6761322	1993.4	136.921439	33.6768578	HD OFF
10/19/2016	07:26:01	136.921524	33.6761169	1992.00	136.921439	33.6768578	GEAR DEPLOYED
10/19/2016	07:38:41	136.9216614	33.6761017	1994.9	136.921439	33.6768578	t stick out
10/19/2016	07:42:54	136.9217224	33.6761246	1995.2	136.921439	33.6768578	Photo
10/19/2016	07:43:07	136.9217224	33.6761284	1995.8	136.921439	33.6768578	Photo
10/19/2016	07:44:37	136.9217072	33.6761398	1994.2	136.921439	33.6768578	Backteria Mat
10/19/2016	07:44:58	136.9217072	33.6761436	1993.9	136.921439	33.6768578	Photo
10/19/2016	07:57:16	136.9217072	33.6761246	1993.1	136.921439	33.6768578	GEAR DEPLOYED
10/19/2016	07:57:30	136.9217072	33.6761246	1994.2	136.921439	33.6768578	t stick in
10/19/2016	08:08:53	136.921524	33.6761971	1992.00	136.921439	33.6768578	t stick out
10/19/2016	08:11:10	136.9215393	33.6761742	1992.4	136.921439	33.6768578	OFF THE BOTTOM
10/19/2016	09:28:02	136.9216919	33.6757736	1993.3	136.921439	33.6768578	ON DECK

GeoB21838

Date	Time (UTC)	SHIP_Lon	SHIP_Lat	Water_Depth	SUB1_Lon	SUB1_Lat	Observations/Comments
10/21/2016	00:39:36	136.6699219	33.6346626	1947.1			IN THE WATER
10/21/2016	00:55:16	136.6699524	33.6347656	1948.7	136.6693777	33.6329077	test
10/21/2016	01:50:20	136.6701508	33.6346817	1945.8	136.6694817	33.6331768	AT THE BOTTOM
10/21/2016	01:57:15	136.6701202	33.6346817	1944.5	136.6694817	33.6331768	Fish
10/21/2016	01:59:11	136.6700897	33.6346931	1947.8	136.6694817	33.6331768	dead clam shells
10/21/2016	02:09:49	136.6699677	33.6346207	1945.8	136.6694817	33.6331768	Clamshells
10/21/2016	02:12:57	136.6699677	33.634613	1947	136.6694817	33.6331768	Shell Debris
10/21/2016	02:17:57	136.6702423	33.6346703	1945.2	136.6694817	33.6331768	Shell Debris
10/21/2016	02:24:04	136.6708679	33.6346779	1944.1	136.6694817	33.6331768	Shell Debris
10/21/2016	02:32:02	136.6710358	33.6346054	1944.1	136.6694817	33.6331768	Fish
10/21/2016	02:35:45	136.671051	33.634697	1943.3	136.6694817	33.6331768	Fish
10/21/2016	02:35:51	136.671051	33.6347008	1944.8	136.6694817	33.6331768	Fish
10/21/2016	02:37:11	136.6710205	33.6347427	1942.4	136.6694817	33.6331768	beer can
10/21/2016	02:37:21	136.6710205	33.6347504	1942.7	136.6694817	33.6331768	Shell Debris
10/21/2016	02:40:03	136.670929	33.6347694	1945.4	136.6694817	33.6331768	MeBoCORK B sighting
10/21/2016	02:40:12	136.670929	33.6347656	1945.9	136.6694817	33.6331768	HD ON
10/21/2016	02:40:35	136.670929	33.6347542	1945.2	136.6694817	33.6331768	Photo
10/21/2016	02:41:11	136.6709137	33.6347427	1942.4	136.6694817	33.6331768	Photo
10/21/2016	02:41:57	136.6708984	33.6347275	1945.1	136.6694817	33.6331768	HD OFF
10/21/2016	02:55:53	136.6710358	33.6345482	1944.2	136.6694817	33.6331768	HD ON
10/21/2016	03:11:31	136.6714783	33.6336899	1941.9	136.6694817	33.6331768	HD OFF
10/21/2016	03:11:52	136.6714783	33.6336899	1942.3	136.6694817	33.6331768	large clast
10/21/2016	03:13:06	136.671463	33.6336784	1942.3	136.6694817	33.6331768	more clasts
10/21/2016	03:13:42	136.6714478	33.6336823	1942.4	136.6694817	33.6331768	underway to PLUG1
10/21/2016	03:13:45	136.671463	33.6336823	1942.5	136.6694817	33.6331768	Fish
10/21/2016	03:17:22	136.671402	33.6337013	1942.8	136.6694817	33.6331768	Fish
10/21/2016	03:19:54	136.6714478	33.6336899	1942.2	136.6694817	33.6331768	Shell Debris
10/21/2016	04:05:30	136.6712952	33.6338081	1942.3	136.6694817	33.6331768	Fish
10/21/2016	04:06:44	136.6713257	33.6337852	1941.8	136.6694817	33.6331768	sea star
10/21/2016	04:28:18	136.6714935	33.6337242	1943.4	136.6694817	33.6331768	schimäre
10/21/2016	04:32:23	136.6714172	33.6337624	1942.3	136.6694817	33.6331768	Fish
10/21/2016	04:50:02	136.6712799	33.6337738	1941.8			Shell Debris
10/21/2016	04:51:27	136.6712952	33.6337738	1941.2			canister
10/21/2016	04:55:23	136.6713562	33.6337624	1942.4			Shell Debris
10/21/2016	04:56:29	136.671402	33.6337624	1942.9			Fish
10/21/2016	05:19:30	136.6713867	33.6337242	1942.4			coral on porch
10/21/2016	05:31:31	136.671402	33.6337318	1940.7			Fish
10/21/2016	06:10:52	136.6714478	33.6337967	1941.6			Photo
10/21/2016	06:26:39	136.6713562	33.6337395	1942			Photo
10/21/2016	06:47:00	136.671463	33.6337929	1942.6			Photo
10/21/2016	06:56:21	136.6713867	33.63377	1942			Sea cucumber
10/21/2016	07:27:21	136.6714325	33.6337585	1942.8			hummocky surface
10/21/2016	07:32:33	136.6713867	33.6338043	1941.7			Clamshells
10/21/2016	07:44:12	136.6713409	33.6338234	1943.1			Fish
10/21/2016	07:52:57	136.6713257	33.6338005	1941.3			cardboard box or canister
10/21/2016	07:58:39	136.6714172	33.6337318	1942.3			Fish
10/21/2016	07:59:24	136.6714172	33.6337128	1942.4			HD ON
10/21/2016	08:01:04	136.6714172	33.6336823	1941.8			HD OFF
10/21/2016	08:04:47	136.671402	33.6336899	1942.6			Fish
10/21/2016	08:08:22	136.6713867	33.6337204	1940.7			Fish
10/21/2016	08:11:18	136.6713867	33.6337585	1941			sea spider
10/21/2016	08:13:56	136.6713562	33.6338196	1941.7			metal box
10/21/2016	08:22:23	136.6714325	33.6337967	1941.4			OFF THE BOTTOM

GeoB21841

Date	Time (UTC)	SHIP_Lon	SHIP_Lat	Water_Depth	SUB1_Lon	SUB1_Lat	Observations/Comments
10/22/2016	02:26:40	136.6354218	33.6555252	1983.4			test
10/22/2016	02:34:16	136.6340637	33.6562767	1968.8			IN THE WATER
10/22/2016	04:51:11	136.6340637	33.6562729	1968.1	136.632671	33.6547292	AT THE BOTTOM
10/22/2016	05:01:07	136.6340637	33.6562424	1968.5	136.632671	33.6547292	Fish
10/22/2016	05:03:43	136.6340637	33.6562729	1968.3	136.632671	33.6547292	clasts
10/22/2016	05:05:59	136.6340485	33.6562653	1967.1	136.632671	33.6547292	rocks
10/22/2016	05:07:57	136.6340027	33.6562805	1969.8	136.632671	33.6547292	Asselspinne
10/22/2016	05:13:58	136.6339722	33.6563454	1966.7	136.632671	33.6547292	Fish
10/22/2016	05:18:24	136.6339722	33.6563721	1970.3	136.632671	33.6547292	HD ON
10/22/2016	05:20:30	136.6339264	33.6563454	1968.5	136.632671	33.6547292	Photo
10/22/2016	05:20:30	136.6339264	33.6563454	1968.5	136.632671	33.6547292	Photo
10/22/2016	05:20:37	136.6339417	33.6563416	1967.9	136.632671	33.6547292	Photo
10/22/2016	05:21:07	136.6339417	33.6563416	1969.2	136.632671	33.6547292	Photo
10/22/2016	05:21:21	136.6339569	33.6563454	1967.8	136.632671	33.6547292	Photo
10/22/2016	05:48:01	136.6340485	33.6562576	1968.7	136.6328857	33.6548493	Photo
10/22/2016	05:48:22	136.6340637	33.65625	1967.8	136.6328857	33.6548493	tintenfisch
10/22/2016	05:48:24	136.6340637	33.6562538	1967.8	136.6328857	33.6548493	Photo
10/22/2016	06:27:28	136.6339874	33.6563606	1968.4	136.6339427	33.6562203	HD OFF
10/22/2016	07:45:36	136.6339417	33.6563644	1970.5	136.6337823	33.6560907	OFF THE BOTTOM
10/22/2016	08:48:31	136.634079	33.6561241	1970.4			ON DECK

GeoB21850

Date	Time (UTC)	SHIP_Lon	SHIP_Lat	Water_Depth	SUB1_Lon	SUB1_Lat	Observations/Comments
10/26/2016	02:17:45	136.6343842	33.6557274	1968	0	0	test
10/26/2016	02:30:03	136.6347198	33.6563072	1976.5	0	0	IN THE WATER
10/26/2016	03:33:29	136.6346588	33.6563606	1977.8	136.6336553	33.655687	AT THE BOTTOM
10/26/2016	03:51:55	136.6346283	33.6562653	1973.7	136.634239	33.6560963	Photo
10/26/2016	03:52:09	136.6346283	33.6562614	1971.7	136.634239	33.6560963	Photo
10/26/2016	03:52:26	136.6346283	33.6562614	1972	136.6344007	33.6561307	Photo
10/26/2016	03:58:19	136.6346436	33.6562729	1972.8	136.6346472	33.6562095	HD ON
10/26/2016	04:03:12	136.6346741	33.6562805	1978.1	136.634598	33.6561988	HD OFF
10/26/2016	04:03:27	136.6346741	33.6562805	1977.7	136.634598	33.6561988	Photo
10/26/2016	04:07:01	136.6346436	33.6562653	1973.6	136.6346483	33.6562032	Photo
10/26/2016	05:37:49	136.63414	33.6563263	1972.8	136.6338235	33.6560177	Clamshells
10/26/2016	05:40:35	136.6341553	33.6563339	1972.8	136.6340215	33.6560403	HD ON
10/26/2016	06:10:43	136.6341553	33.6563683	1972.8	136.6338608	33.6559563	Photo
10/26/2016	06:10:52	136.6341553	33.6563721	1972.8	136.6338608	33.6559563	Photo
10/26/2016	06:28:08	136.6342621	33.6562157	1972.8	136.6337787	33.655958	Clamshells
10/26/2016	07:19:38	136.6342773	33.6563416	1972.8	136.6338315	33.6560083	HD OFF
10/26/2016	07:28:20	136.6342926	33.6562538	1972.8	136.6338552	33.6559857	Photo
10/26/2016	07:28:37	136.6342926	33.65625	1972.8	136.6338658	33.6559878	Photo
10/26/2016	08:03:26	136.6341705	33.6563683	1972.8	136.6336965	33.6559498	Fish
10/26/2016	08:25:23	136.6342468	33.6563377	1972.8	136.6335255	33.6565543	Clamshells
10/26/2016	08:36:16	136.6342316	33.6563187	1972.8	136.63333	33.6567658	Clamshells
10/26/2016	08:36:35	136.6342316	33.6563377	1972.8	136.63333	33.6567658	Sea Star
10/26/2016	08:43:40	136.6344452	33.6573181	1972.8	136.6369458	33.6613082	Corals
10/26/2016	08:54:13	136.6347351	33.6587296	1972.8	136.6334517	33.6586788	Sea Star
10/26/2016	08:54:13	136.6347351	33.6587296	1972.8	136.6334517	33.6586788	Sea Star
10/26/2016	08:54:49	136.6347656	33.6588211	1972.8	136.6334935	33.6586317	Fish
10/26/2016	08:58:27	136.6347351	33.6590004	1972.8	136.6295222	33.6582683	MeBo Borehole found
10/26/2016	08:59:58	136.6347351	33.6590271	1972.8	136.629508	33.6583222	TStick is on the left of the MeBo rod (visually)
10/26/2016	09:03:23	136.6347809	33.6590462	1972.8	136.633646	33.6589195	White patches
10/26/2016	09:07:34	136.6347504	33.6590233	1972.8	136.6336593	33.6589397	Photo of the TStick
10/26/2016	09:07:39	136.6347504	33.6590271	1972.8	136.6336593	33.6589397	HD ON
10/26/2016	09:07:49	136.6347504	33.6590233	1972.8	136.6336463	33.6589495	Photo
10/26/2016	09:16:20	136.6347809	33.6590385	1972.8	136.6336527	33.6589222	TStick retrieved and in the ROV
10/26/2016	09:26:05	136.6347961	33.6589279	1972.8	136.6336752	33.6589555	Starting the operation to retrieve the MeBo Plug 2
10/26/2016	09:35:28	136.6347961	33.6588402	1972.8	136.633683	33.6589517	MeBo Plug 2 is unplugged
10/26/2016	09:40:23	136.6347656	33.6588478	1972.8	136.6336773	33.6589613	Instrument retrieved from the borehole
10/26/2016	09:41:12	136.6347656	33.6588478	1972.8	136.6336418	33.6589652	MeBo Plug is in the drawer
10/26/2016	09:41:50	136.6347809	33.6588478	1972.8	136.6336307	33.6589545	HD OFF
10/26/2016	09:43:14	136.6347961	33.6588593	1972.8	136.6336208	33.6589037	OFF THE BOTTOM
10/26/2016	09:43:25	136.6347961	33.6588593	1972.8	136.6336208	33.6589037	ROV begins the ascent from the seafloor
10/26/2016	11:03:21	136.6347656	33.65905	2055.5	136.6335707	33.6584365	ON DECK

GeoB21853

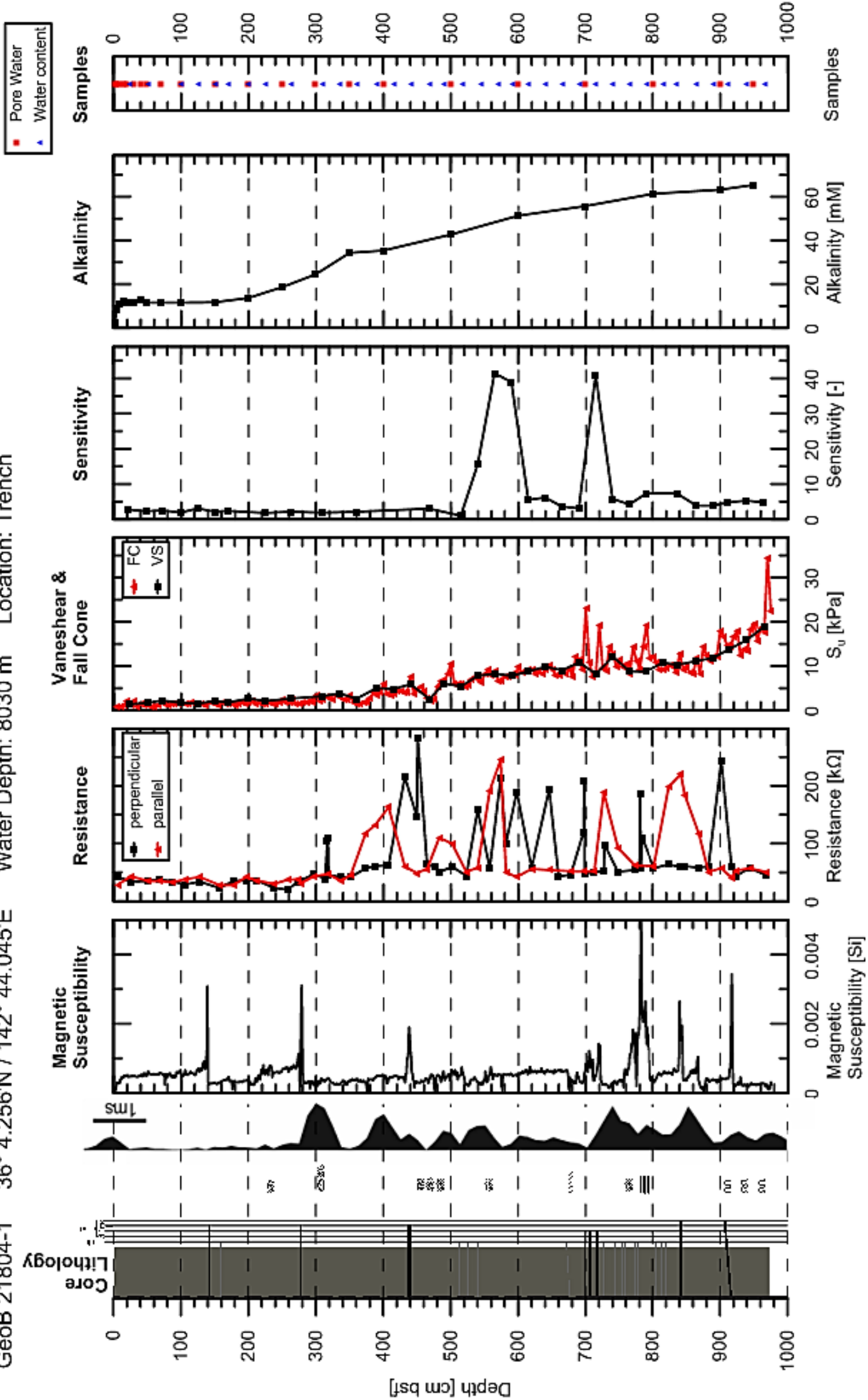
Date	Time (UTC)	SHIP_Lon	SHIP_Lat	Water_Depth	SUB1_Lon	SUB1_Lat	Observations/Comments
10/27/2016	08:16:14	136.8813629	33.6733475	2012.7			test
10/27/2016	09:37:13	136.6709442	33.6337662	1941.5			IN THE WATER
10/27/2016	10:43:51	136.6710205	33.6343651	1942.6	136.6713368	33.6339658	AT THE BOTTOM
10/27/2016	11:21:15	136.6710205	33.6343079	1941.5	136.6711647	33.6351022	clast
10/27/2016	11:26:00	136.6710205	33.6343002	1941.5	136.6709285	33.632219	hills and ridges, rough topography
10/27/2016	11:29:51	136.6710205	33.6343231	1941.5	136.6716532	33.6359435	eel
10/27/2016	11:42:58	136.6710052	33.6342926	1941.5	136.6715247	33.6366245	Sighting CORK-B
10/27/2016	11:44:23	136.6709747	33.6342812	1941.5	136.6710755	33.6335773	Recovery CORK-B
10/27/2016	11:44:23	136.6709747	33.6342812	1941.5	136.6714668	33.6368288	Photo
10/27/2016	11:44:23	136.6709747	33.6342812	1941.5	136.6714668	33.6368288	Photo
10/27/2016	11:44:58	136.6709747	33.6342735	1941.5	136.6714668	33.6368288	Photo
10/27/2016	11:46:17	136.6710052	33.6342735	1941.5	136.6714668	33.6368288	HD ON
10/27/2016	11:50:54	136.67099	33.6343002	1941.5	136.6715052	33.6368017	HD OFF
10/27/2016	11:51:18	136.6709747	33.634304	1941.5	136.6714998	33.6367798	Photo
10/27/2016	11:51:38	136.6709747	33.6343117	1941.5	136.6714625	33.6367727	Photo
10/27/2016	11:53:52	136.6709747	33.6343384	1941.5	136.6714862	33.6366812	Fish
10/27/2016	11:55:19	136.6709595	33.6343498	1941.5	136.671411	33.6368855	MeBoPLUG 1 sighting
10/27/2016	12:02:11	136.6709442	33.6343117	1941.5	136.671411	33.6368855	Photo
10/27/2016	12:02:30	136.6709595	33.6343117	1941.5	136.671411	33.6368855	HD ON
10/27/2016	12:02:51	136.6709595	33.6343155	1941.5	136.671411	33.6368855	Photo
10/27/2016	12:02:53	136.6709595	33.6343155	1941.5	136.671411	33.6368855	Photo
10/27/2016	12:12:19	136.6709442	33.634285	1941.5	136.671411	33.6368855	Photo
10/27/2016	12:22:46	136.6710205	33.6343498	1941.5	136.6714508	33.6370517	OFF THE BOTTOM
10/27/2016	13:44:33	136.6710815	33.6342926	1941.5			ON DECK

GeoB21853

Date	Time (UTC)	SHIP_Lon	SHIP_Lat	Water_Depth	SUB1_Lon	SUB1_Lat	Observations/Comments
10/27/2016	23:40:17	136.6343231	33.6568069	1974.3			test
10/27/2016	23:45:15	136.6343384	33.6567802	1976.3			IN THE WATER
10/28/2016	00:57:35	136.634491	33.6568031	1976.4	136.6339952	33.6561108	AT THE BOTTOM
10/28/2016	01:43:40	136.6342773	33.6568108	1976.4	136.6339798	33.6565907	Photo
10/28/2016	01:43:40	136.6342773	33.6568108	1976.4	136.6339798	33.6565907	Photo
10/28/2016	01:43:40	136.6342773	33.6568108	1976.4	136.6339505	33.656596	Photo
10/28/2016	01:43:40	136.6342773	33.6568108	1976.4	136.6339132	33.6565537	HD ON
10/28/2016	01:43:40	136.6342773	33.6568108	1976.4	136.6338897	33.6565533	Photo
10/28/2016	01:43:40	136.6342773	33.6568108	1976.4	136.6338997	33.656571	HD OFF
10/28/2016	05:11:18	136.6342468	33.6591301	1976.4	136.6332778	33.6584467	sighting MeBo rod
10/28/2016	05:12:51	136.6341553	33.659111	1976.4	136.6332778	33.6584467	Fish
10/28/2016	05:45:52	136.6342316	33.6591873	1976.4	136.6335882	33.6589425	MTL sighting
10/28/2016	05:46:20	136.6342316	33.6591873	1976.4	136.6335882	33.6589425	Photo
10/28/2016	06:02:27	136.6342468	33.6591187	1976.4	136.6335785	33.6589597	Fish
10/28/2016	07:37:28	136.6341705	33.6591682	1976.4	136.6336107	33.6589252	OFF THE BOTTOM
10/28/2016	09:00:38	136.6381836	33.6557007	1976.4	136.63574	33.6571463	ON DECK

Leg 251A Japan Trench

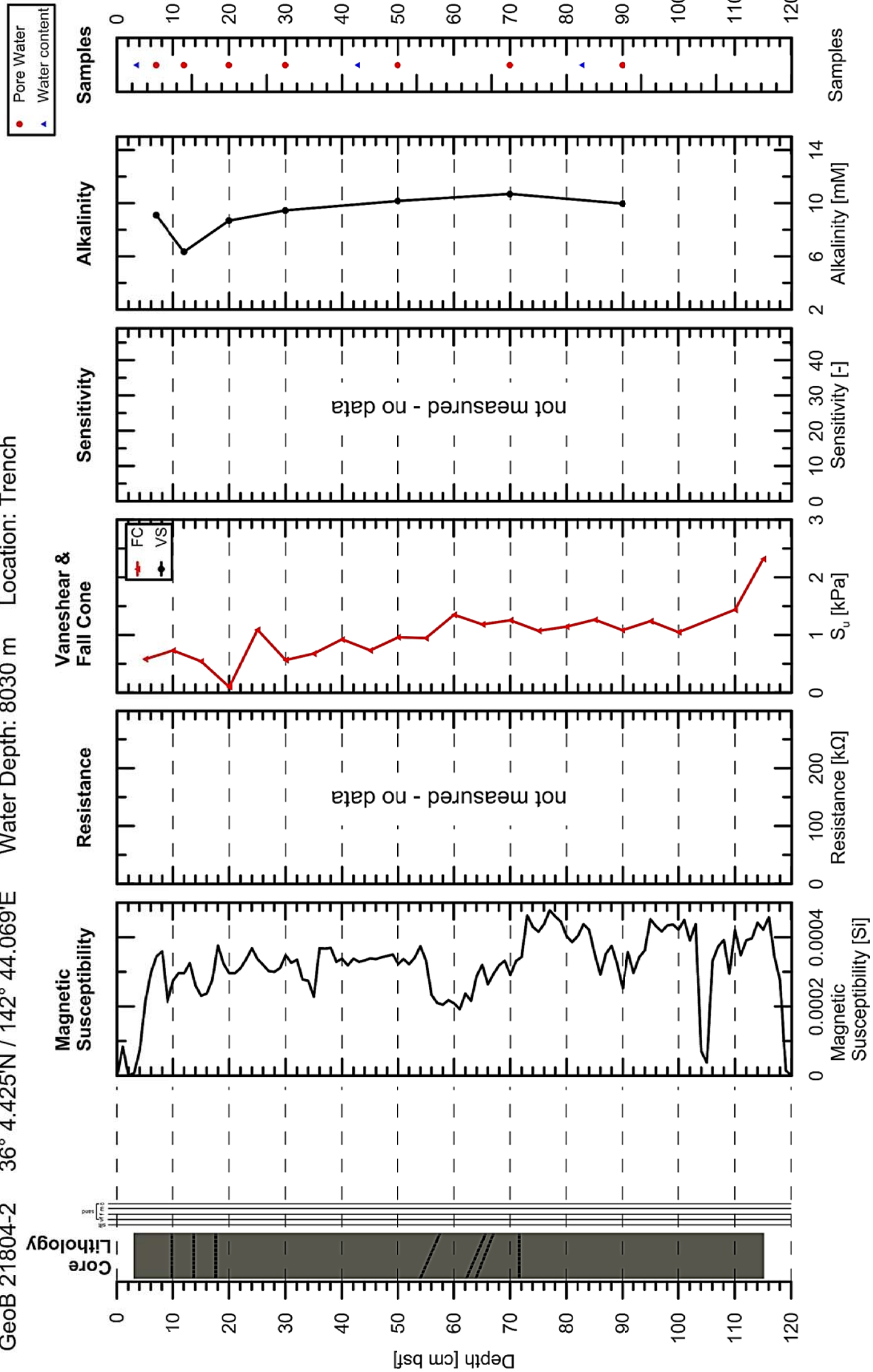
GeoB 21804-1 36° 4.256'N / 142° 44.045'E Water Depth: 8030 m Location: Trench



Leg 251A Japan Trench

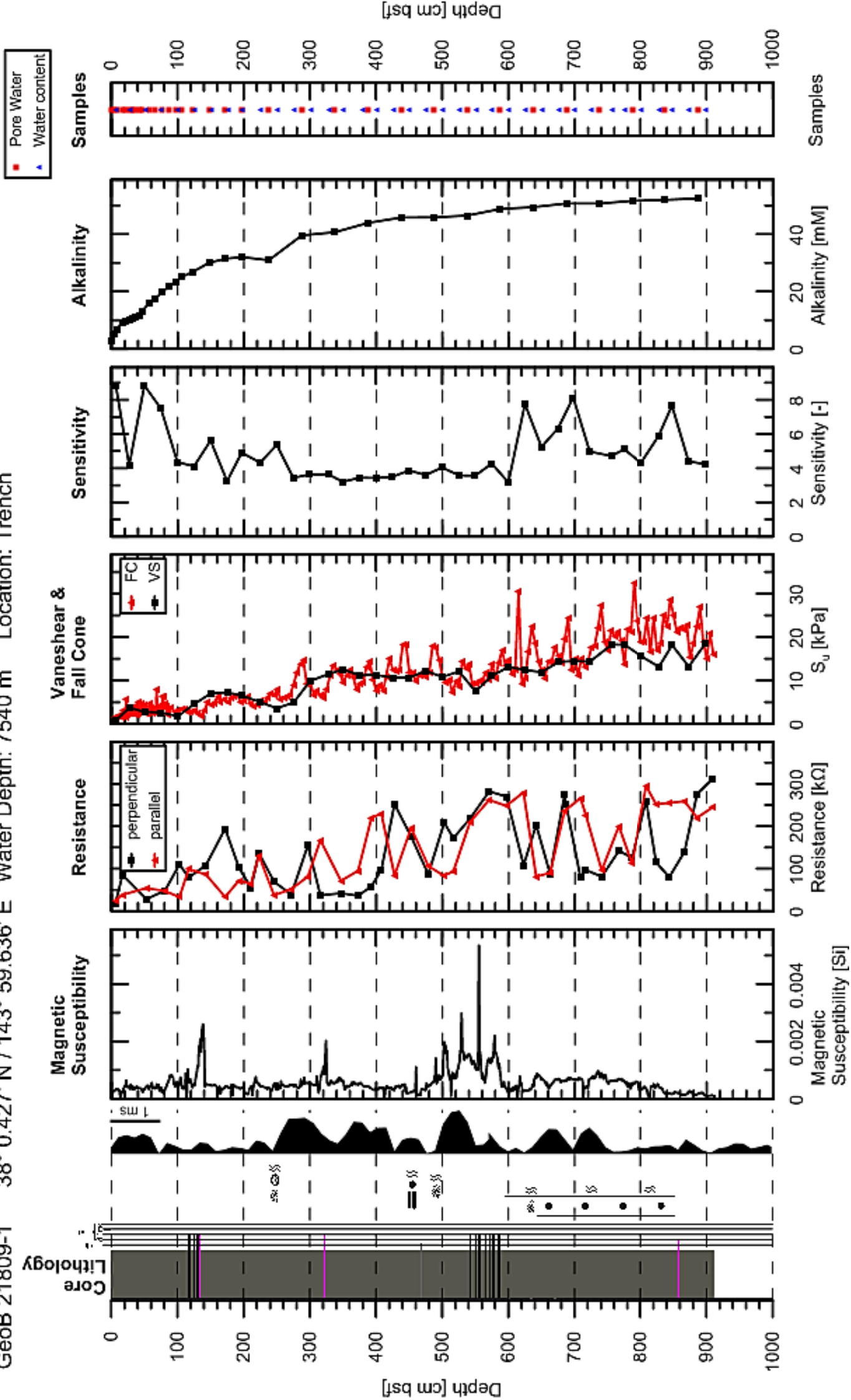
GeoB 21804-2 36° 4.425'N / 142° 44.069'E

Water Depth: 8030 m Location: Trench



Leg 251A Japan Trench

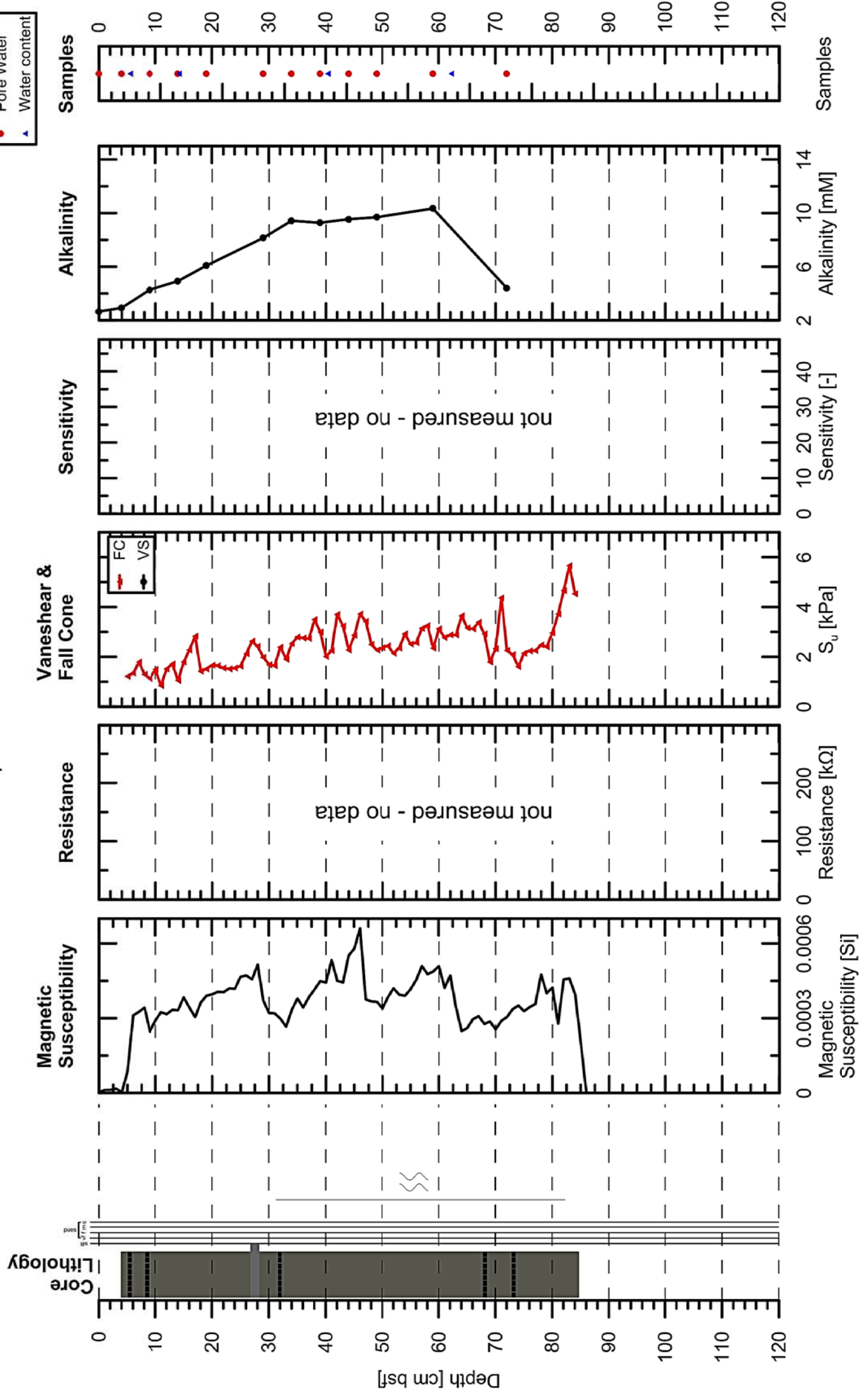
GeoB 21809-1 38° 0.427' N / 143° 59.636' E Water Depth: 7540 m Location: Trench



Leg 251A Japan Trench

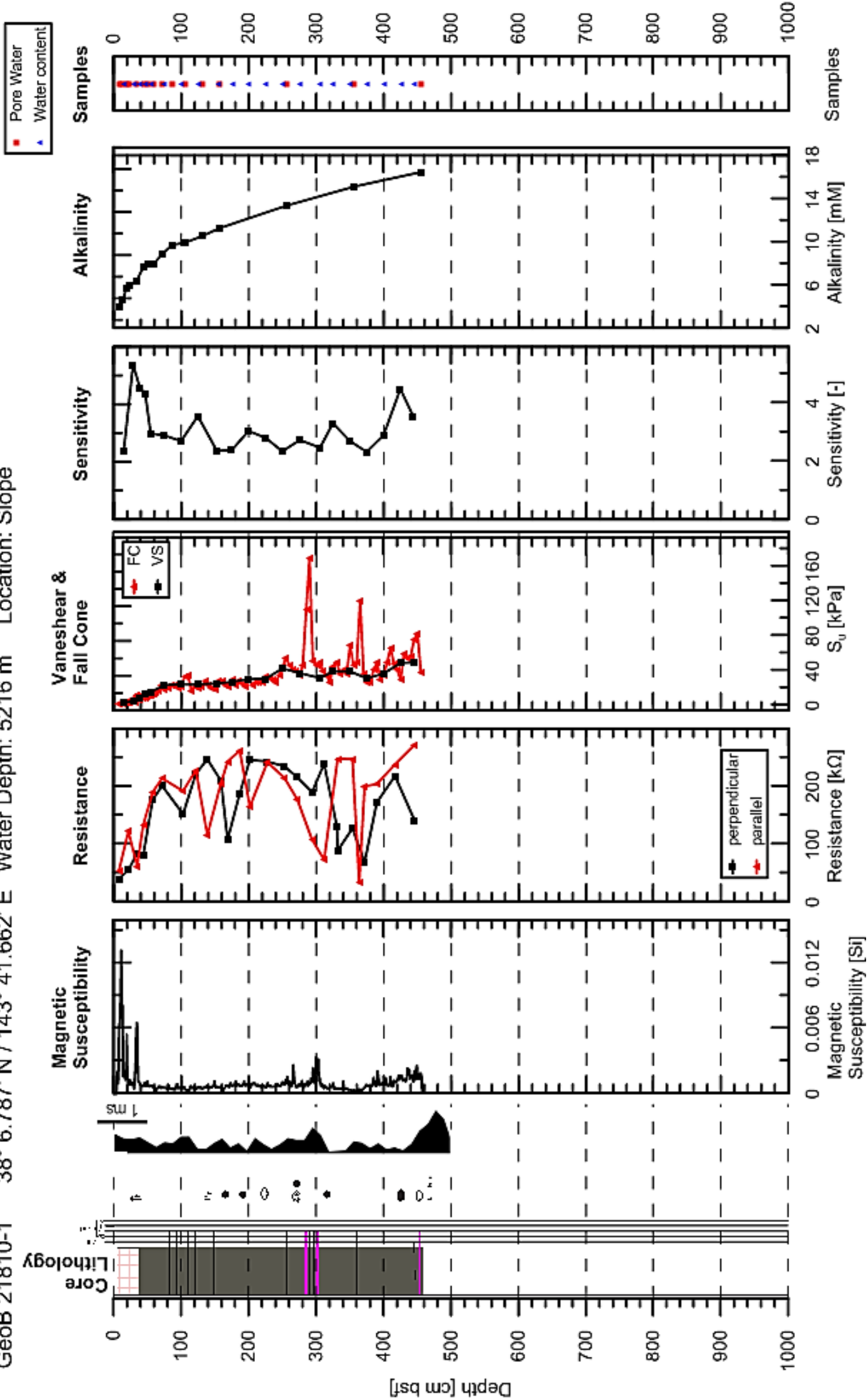
GeoB 21809-2 38° 0.427'N / 143° 59.636'E

Water Depth: 7540 m Location: Trench



Leg 251A Japan Trench

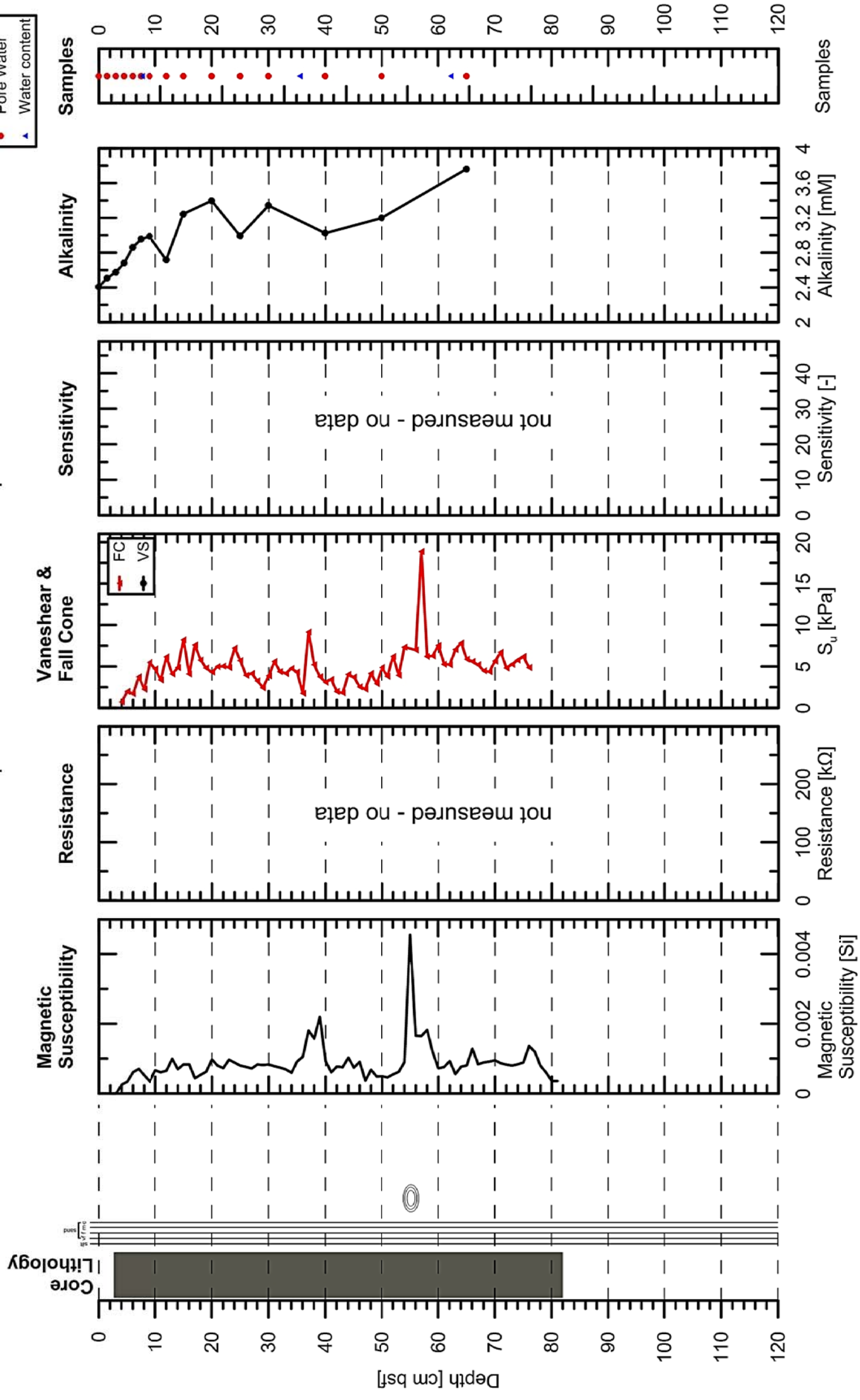
GeoB 21810-1 38° 6.787' N / 143° 41.662' E Water Depth: 5216 m Location: Slope



Leg 251A Japan Trench

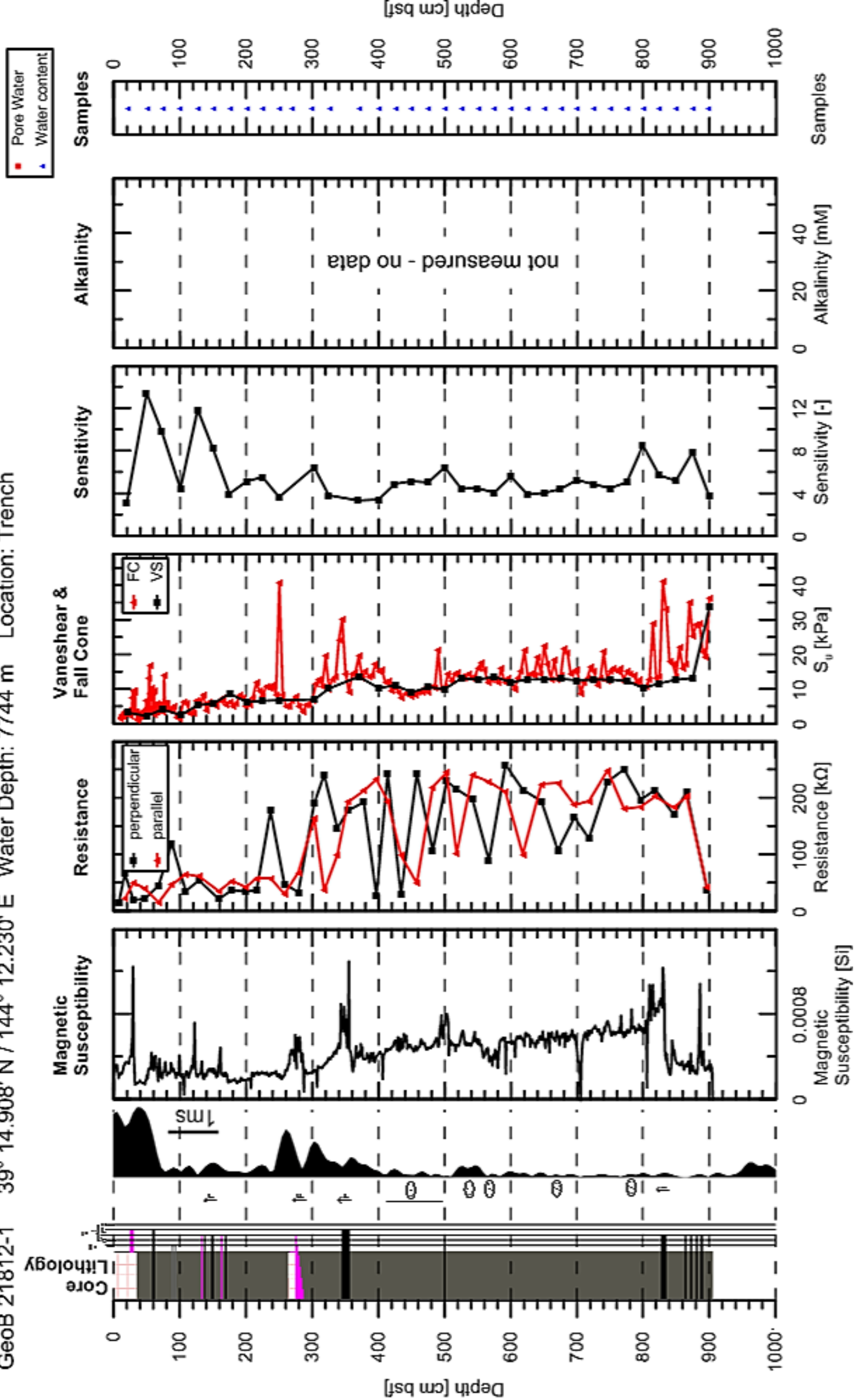
GeoB 21810-2 38° 6.787'N / 143° 41.662'E

Water Depth: 5216 m Location: Slope



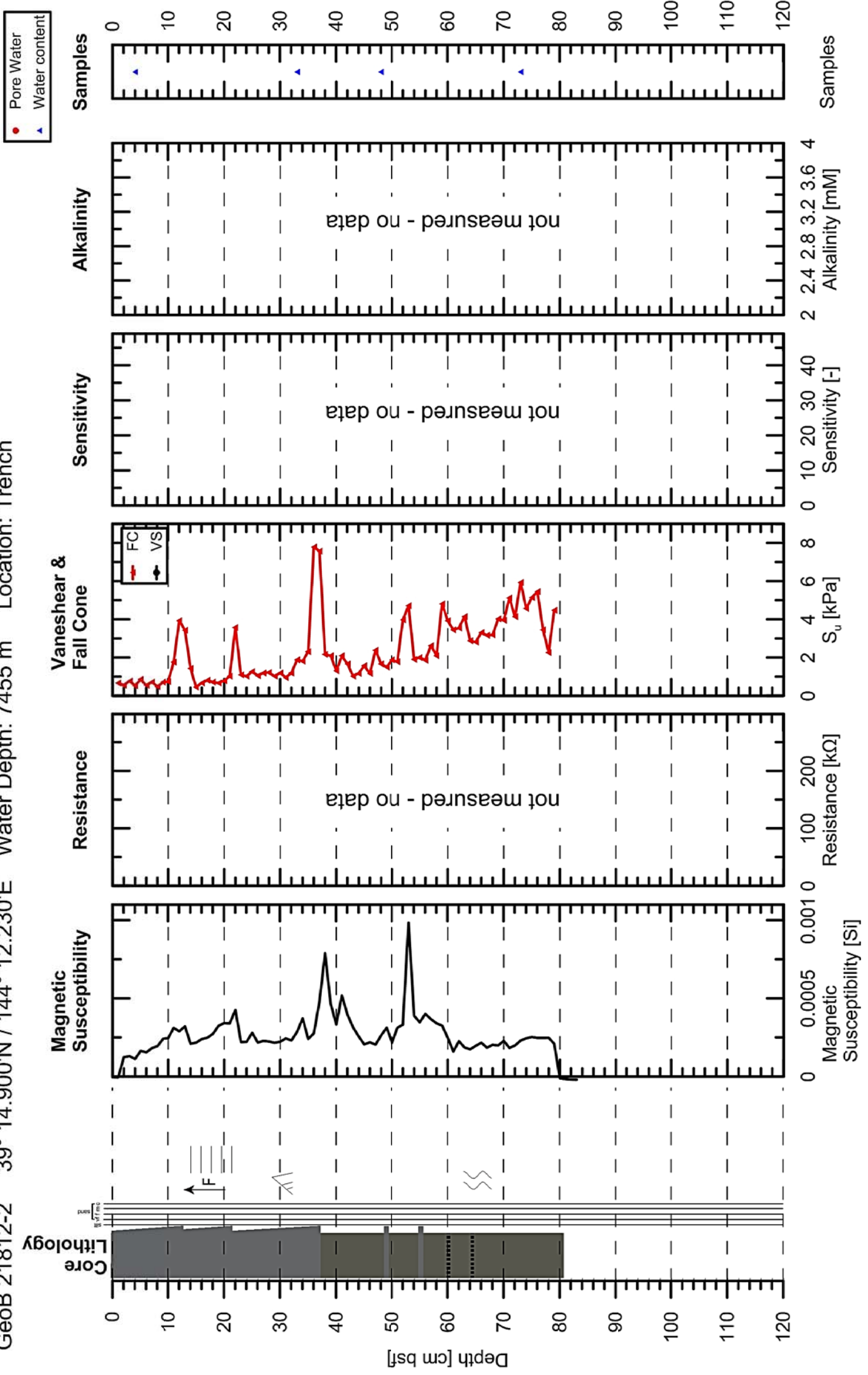
Leg 251A Japan Trench

GeoB 21812-1 39° 14.908' N / 144° 12.230' E Water Depth: 7744 m Location: Trench



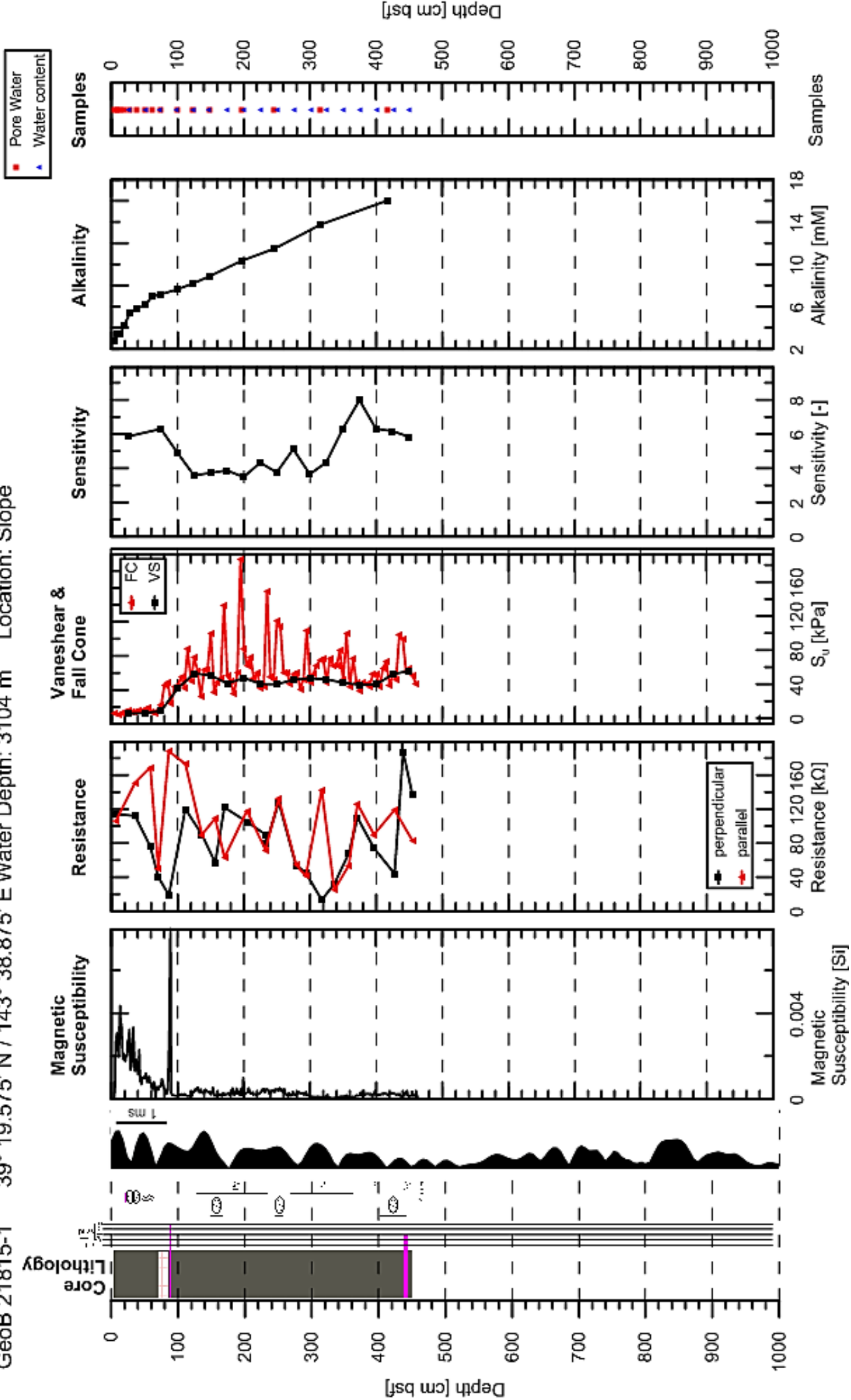
Leg 251A Japan Trench

GeoB 21812-2 39° 14.900'N / 144° 12.230'E Water Depth: 7455 m Location: Trench



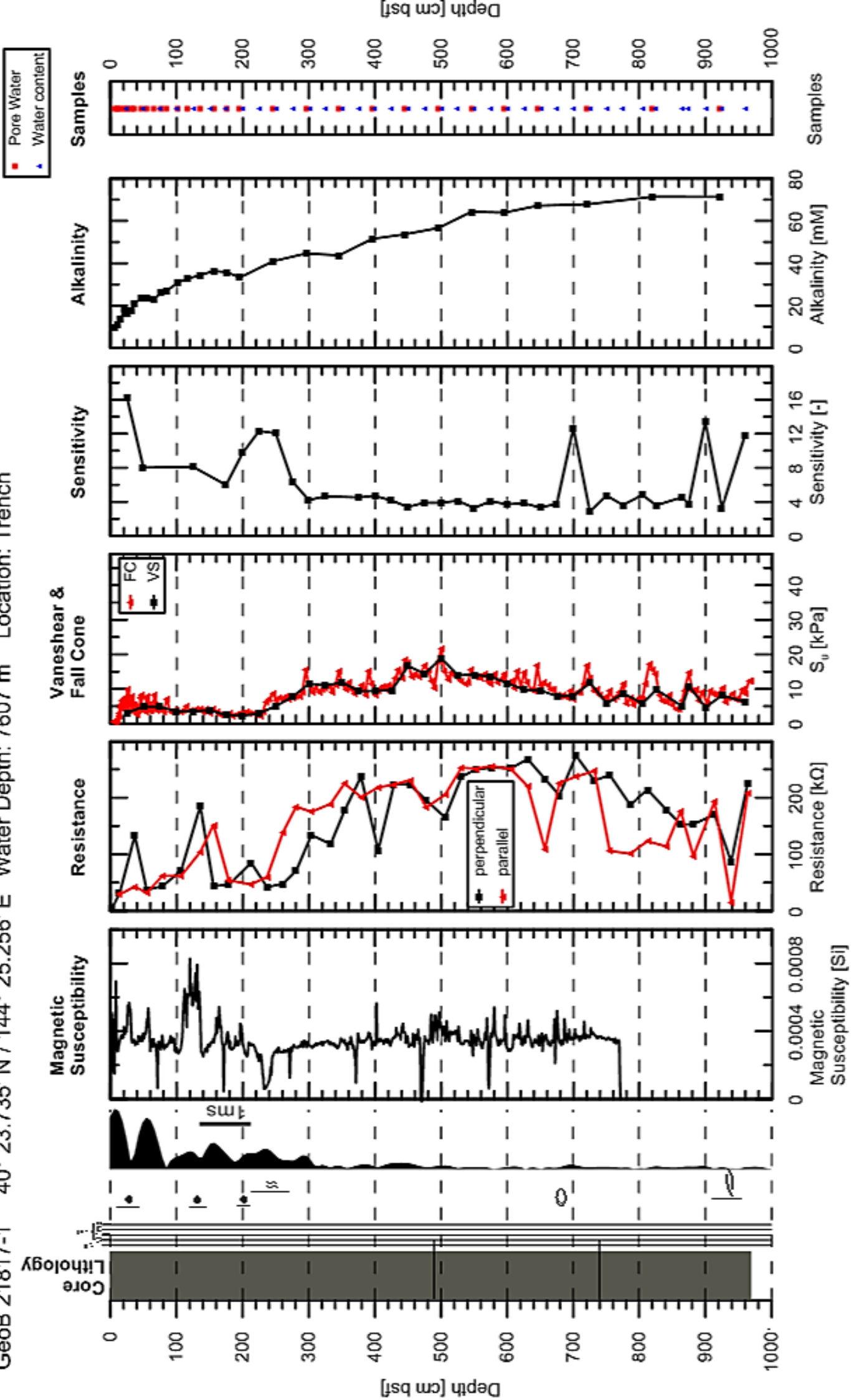
Leg 251A Japan Trench

GeoB 21815-1 39° 19.575' N / 143° 38.875' E Water Depth: 3104 m Location: Slope



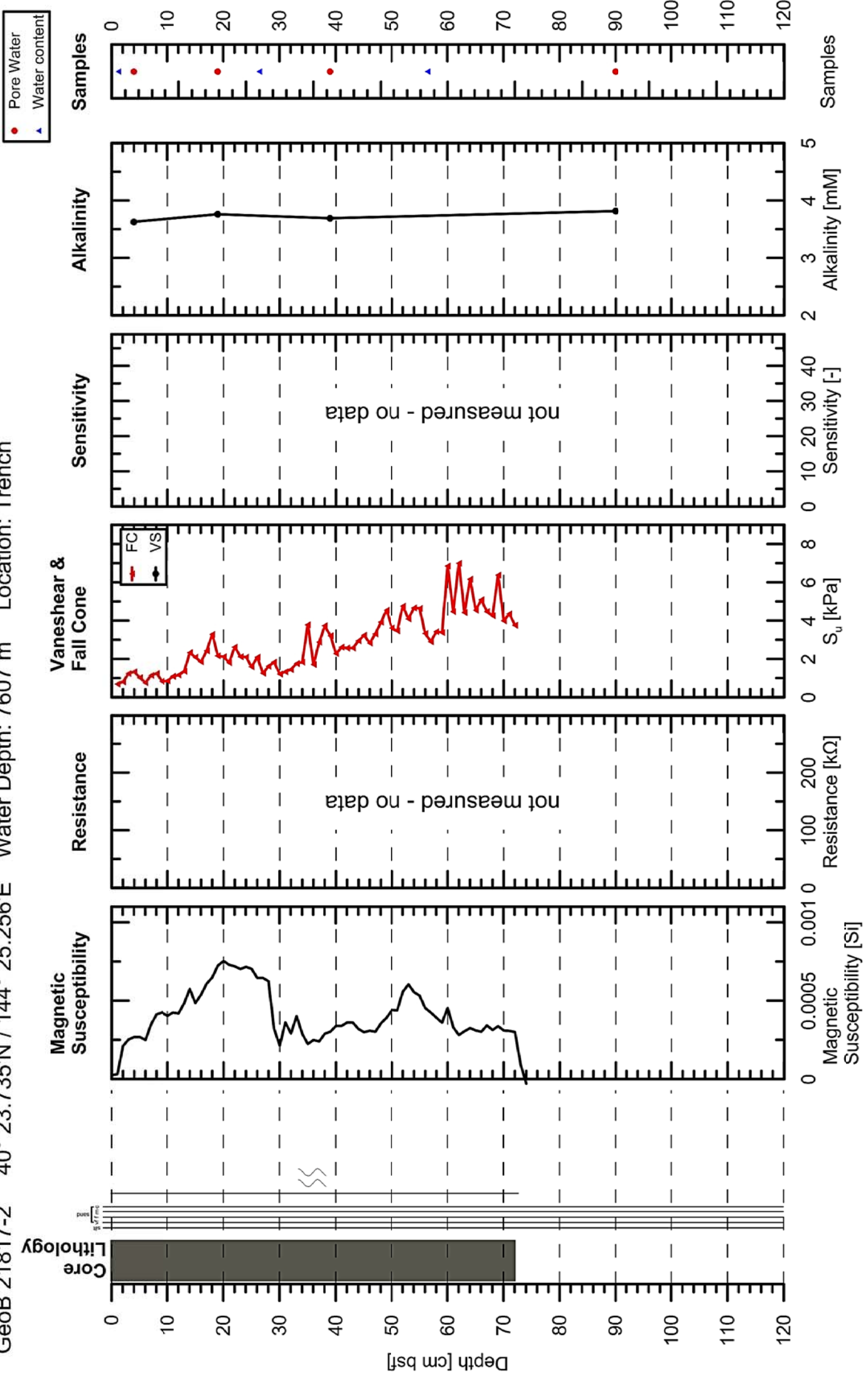
Leg 251A Japan Trench

GeoB 21817-1 40° 23.735' N / 144° 25.256' E Water Depth: 7607 m Location: Trench



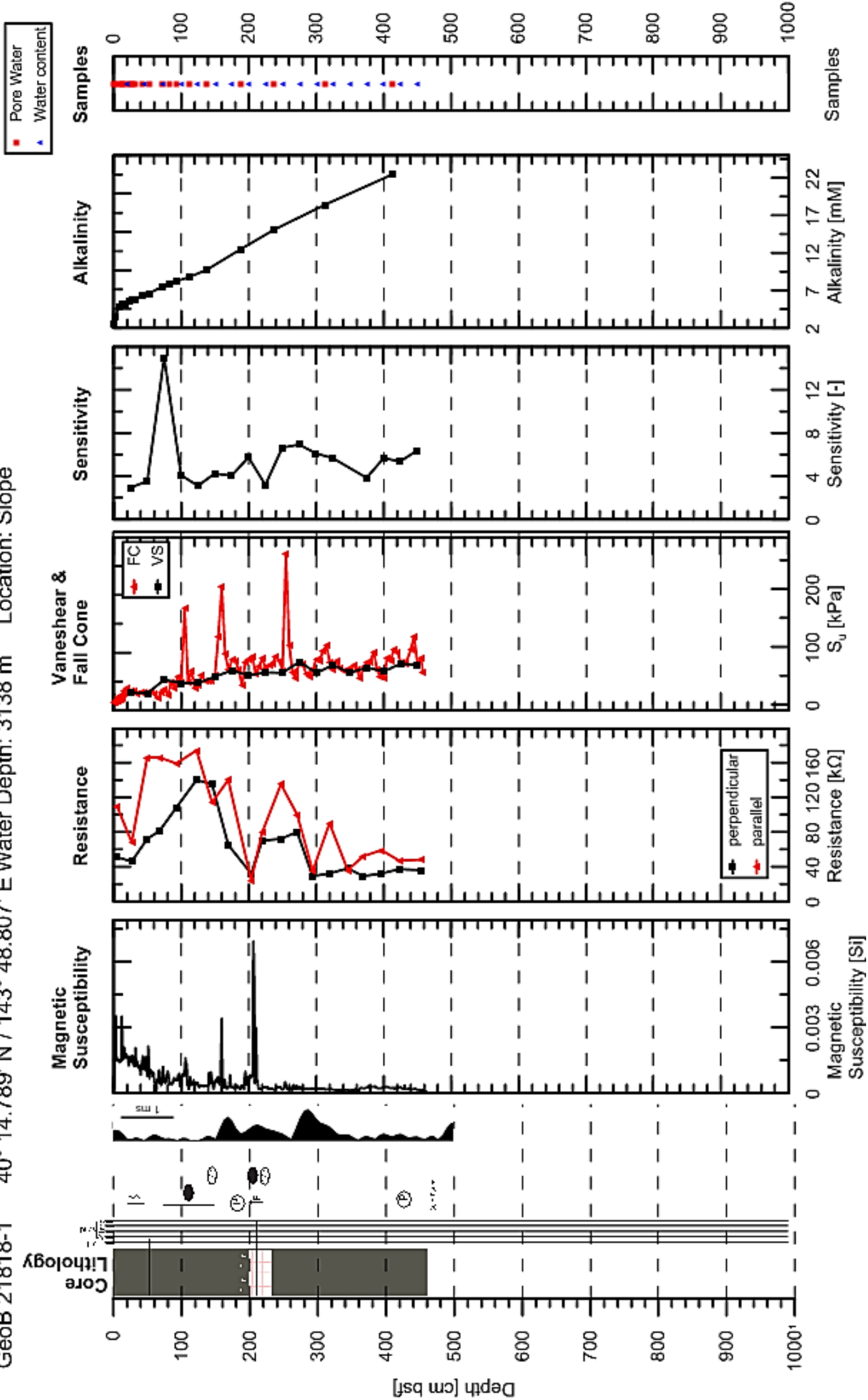
Leg 251A Japan Trench

GeoB 21817-2 40° 23.735'N / 144° 25.256'E Water Depth: 7607 m Location: Trench



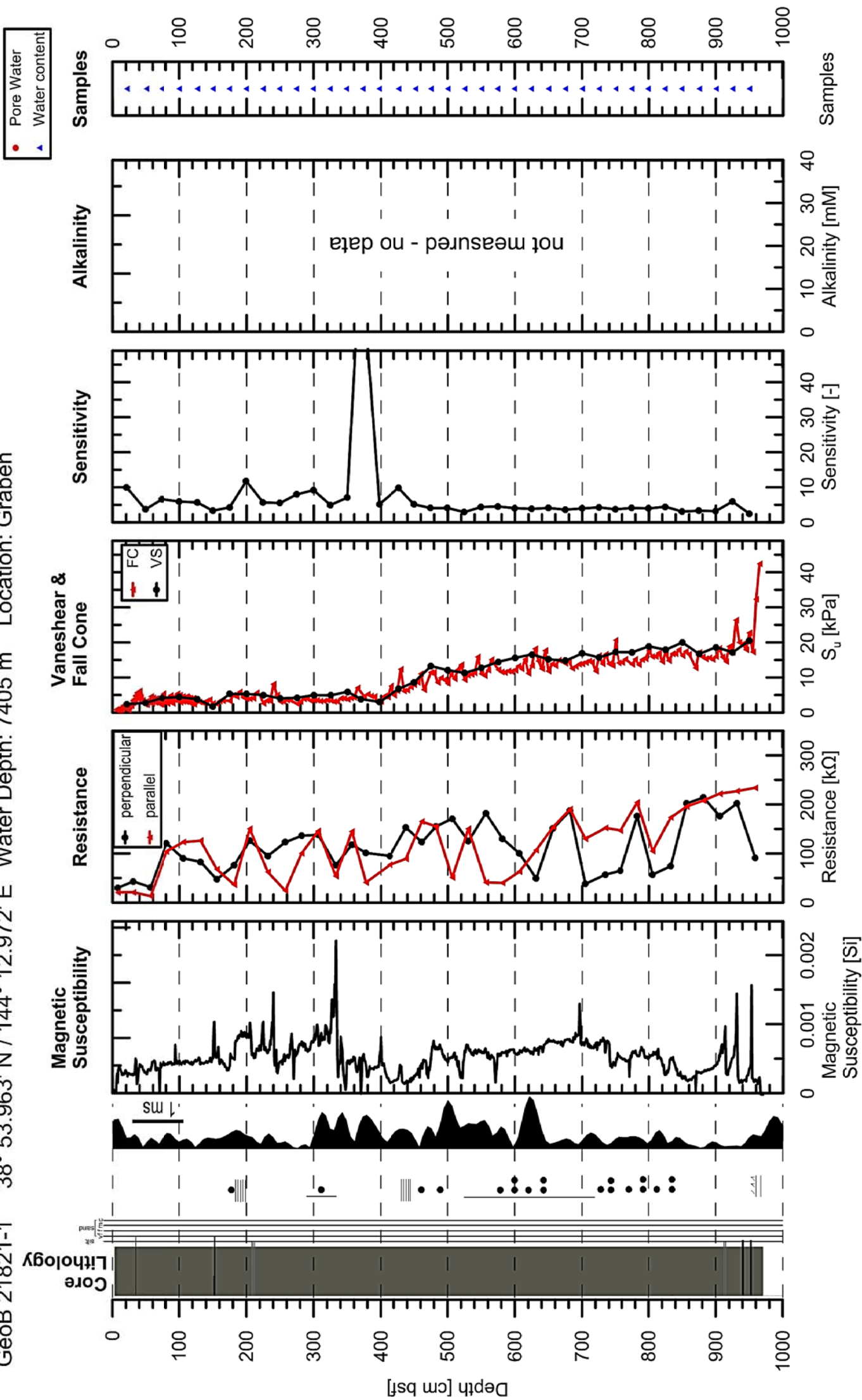
Leg 251A Japan Trench

GeoB 21818-1 40° 14.789' N / 143° 48.807' E Water Depth: 3138 m Location: Slope



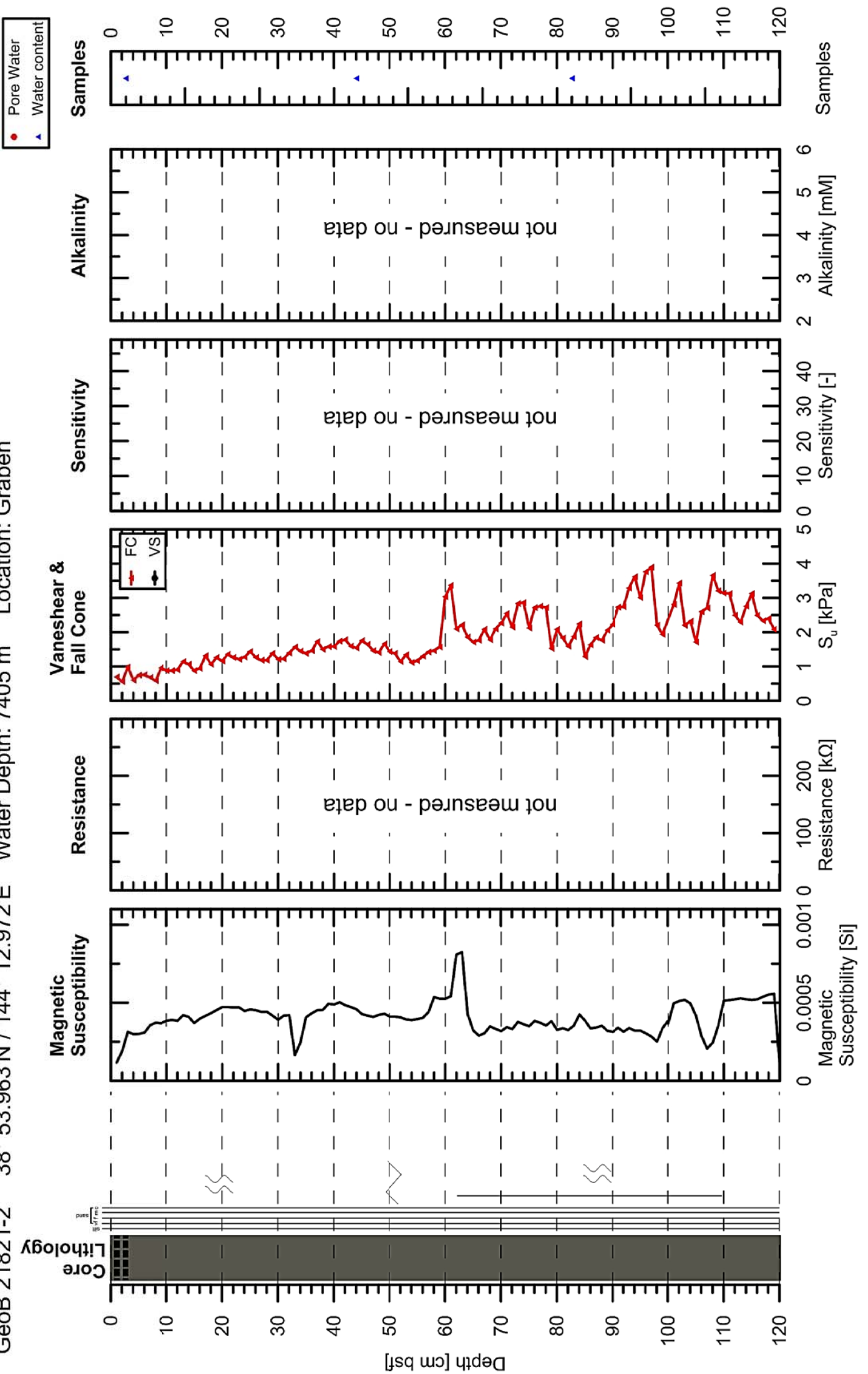
Leg 251A Japan Trench

GeoB 21821-1 38° 53.963' N / 144° 12.972' E Water Depth: 7405 m Location: Graben



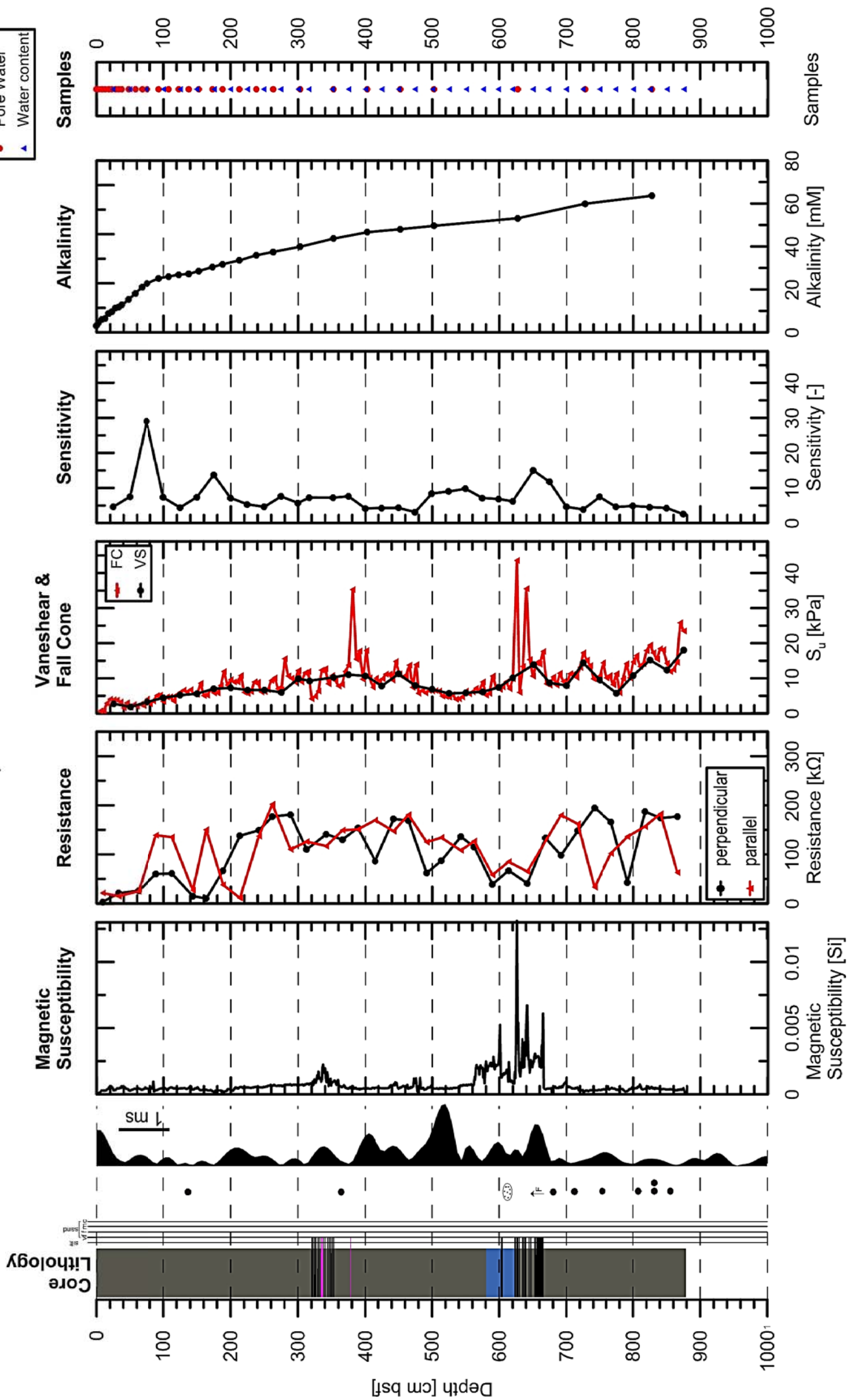
Leg 251A Japan Trench

GeoB 21821-2 38° 53.963'N / 144° 12.972'E Water Depth: 7405 m Location: Graben



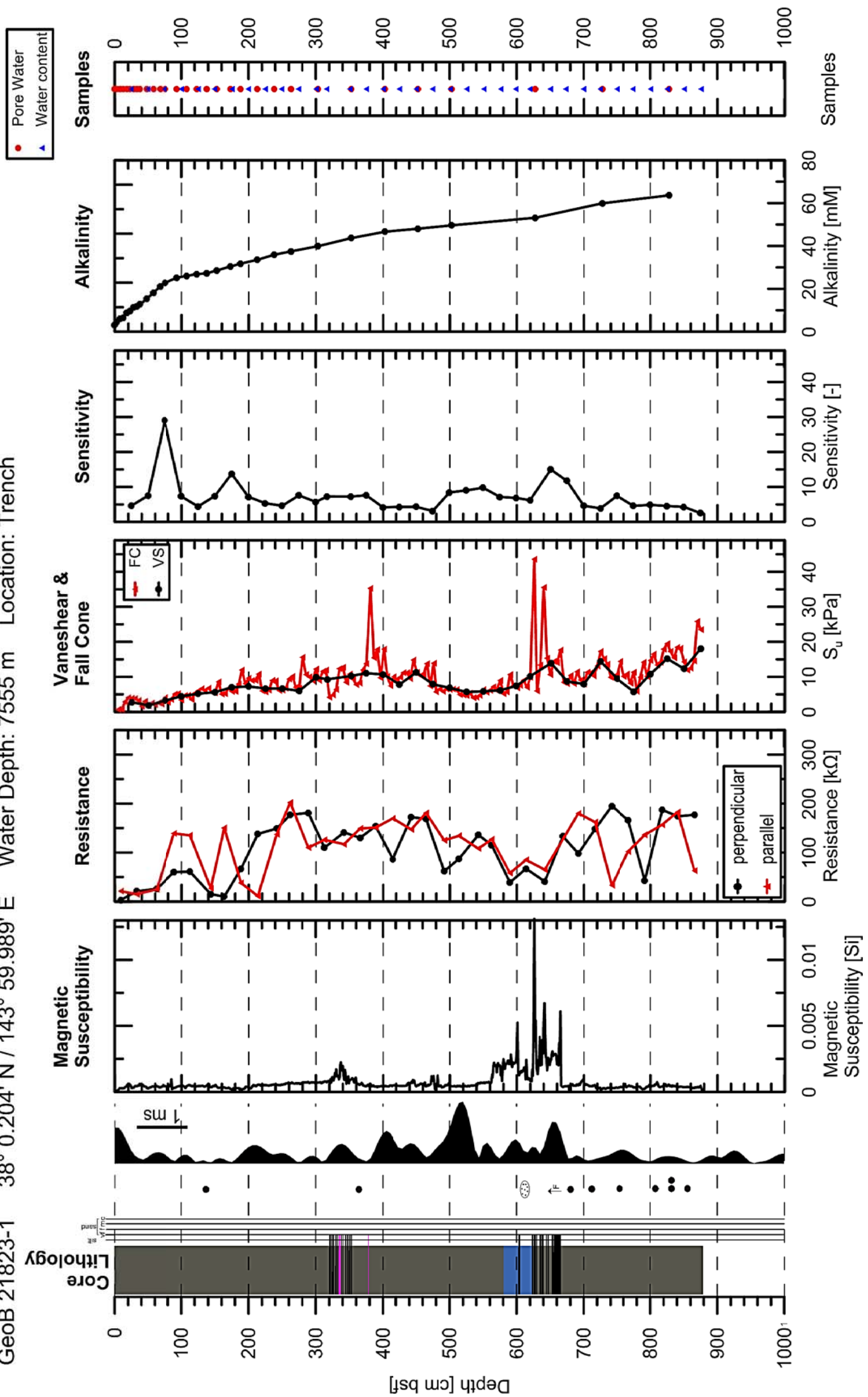
Leg 251A Japan Trench

GeoB 21823-1 38° 0.204' N / 143° 59.989' E Water Depth: 7555 m Location: Trench



Leg 251A Japan Trench

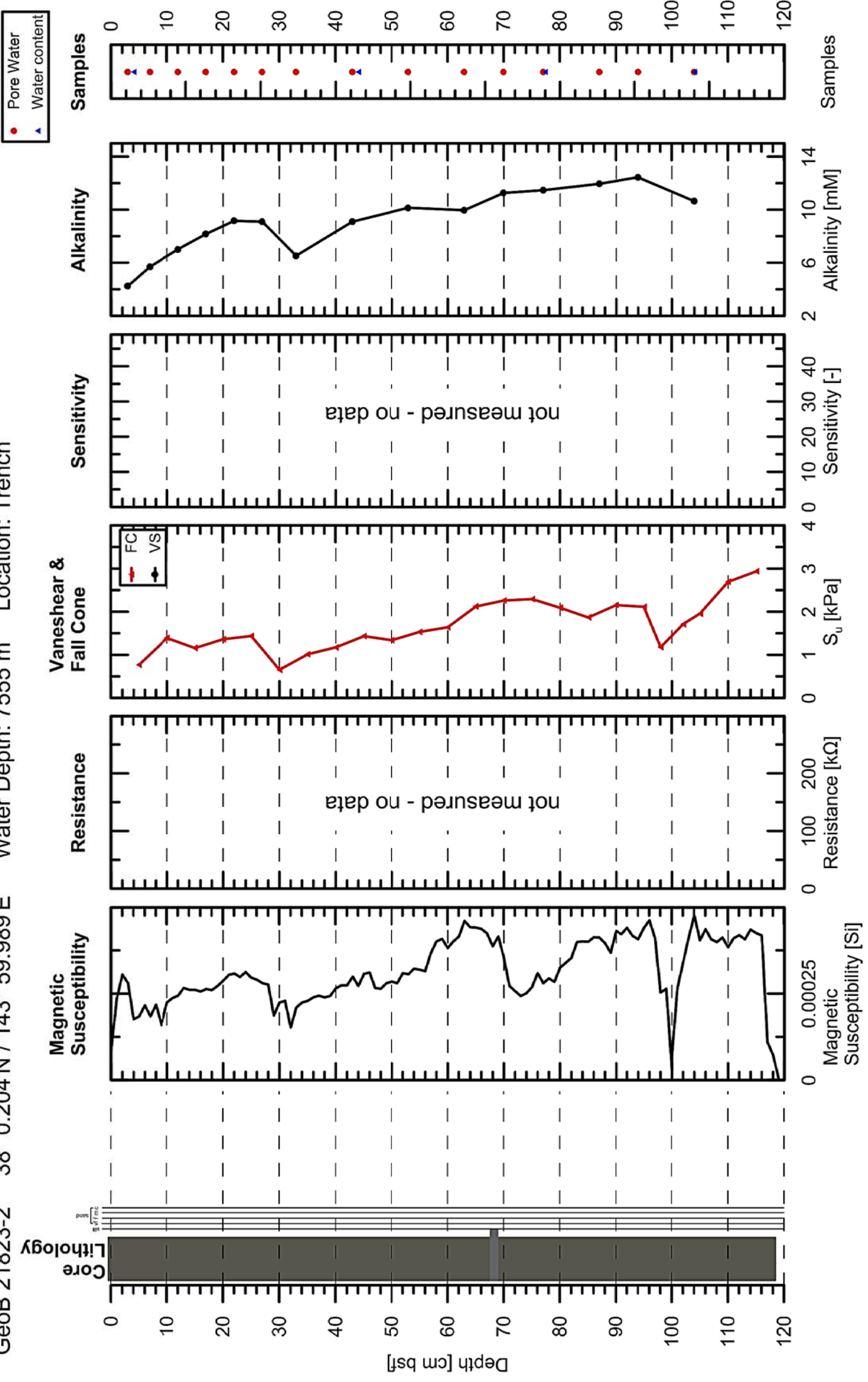
GeoB 21823-1 38° 0.204' N / 143° 59.989' E Water Depth: 7555 m Location: Trench



Leg 251A Japan Trench

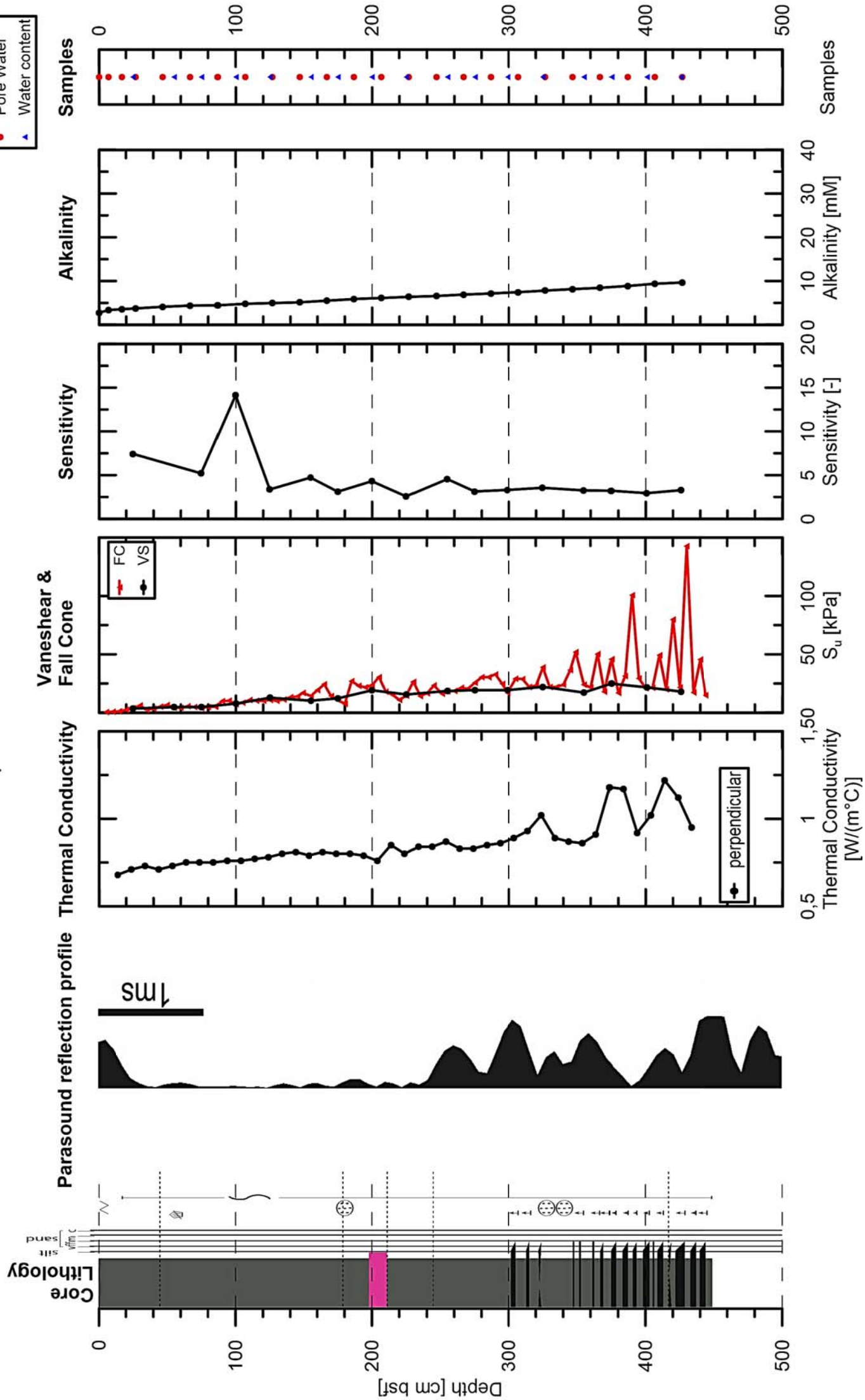
GeoB 21823-2 38° 0.204'N / 143° 59.989'E

Water Depth: 7555 m Location: Trench



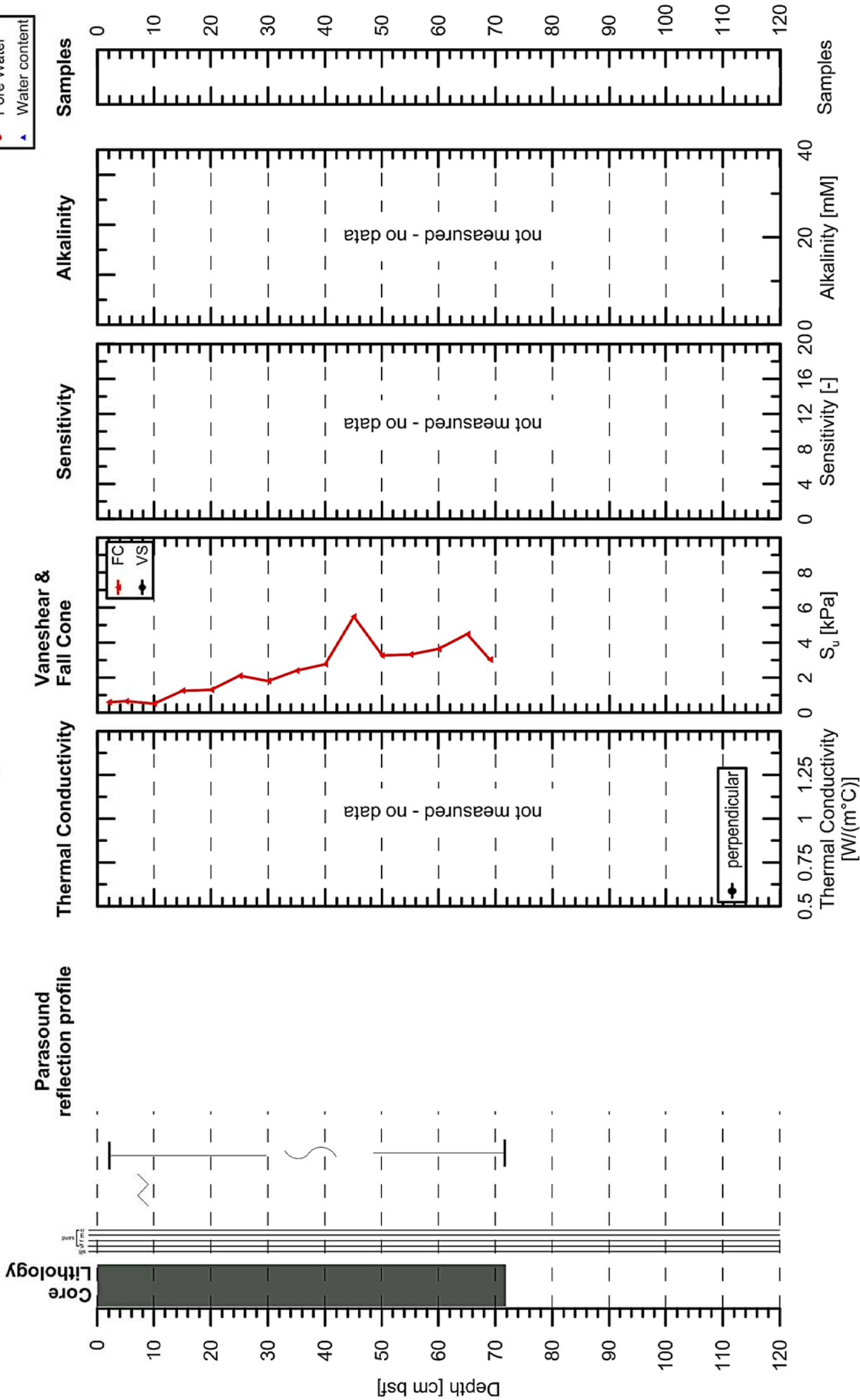
Leg 251B Kumano Basin

GeoB 21829-1 33° 40.159' N 136° 47.802' E Water Depth: 2031 m Location: NNE



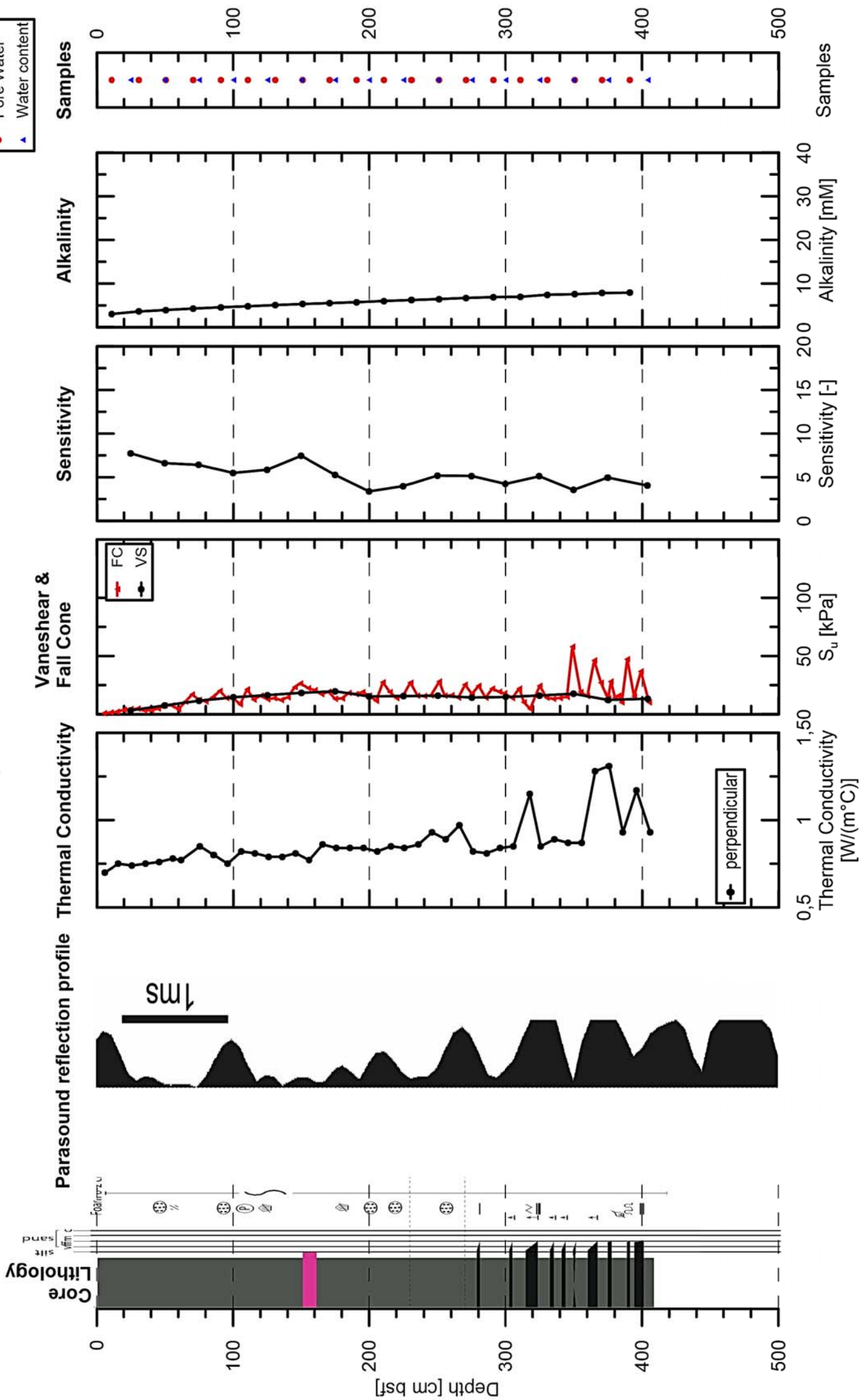
Leg 251B Kumano Basin

GeoB 21829-2 33° 40.159' N / 136° 47.802' E Water Depth: 2031 m Location: NNE



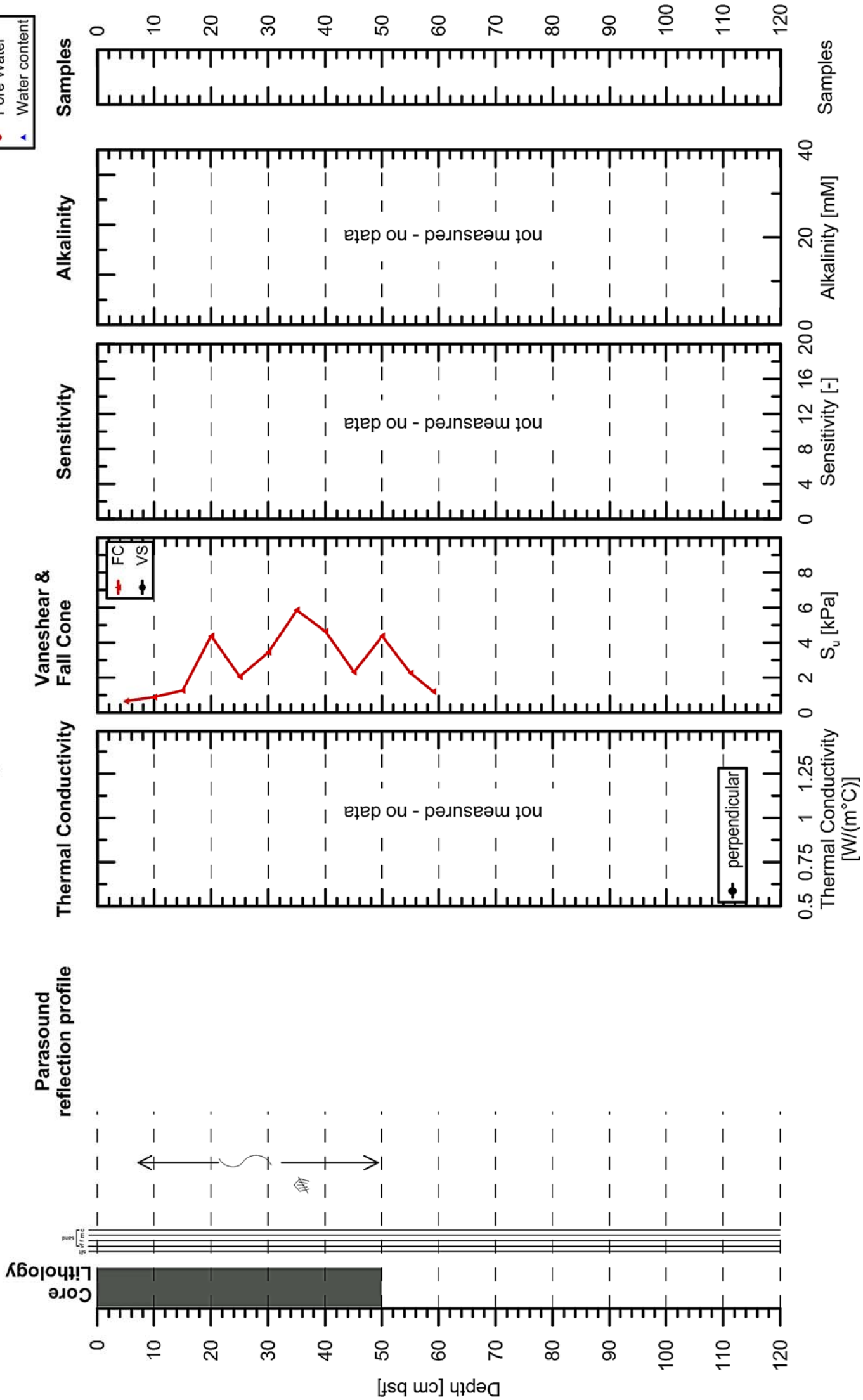
Leg 251B Kumano Basin

GeoB 21831-1 33° 32.915' N 136° 49.892' E Water Depth: 2039 m Location: SSE



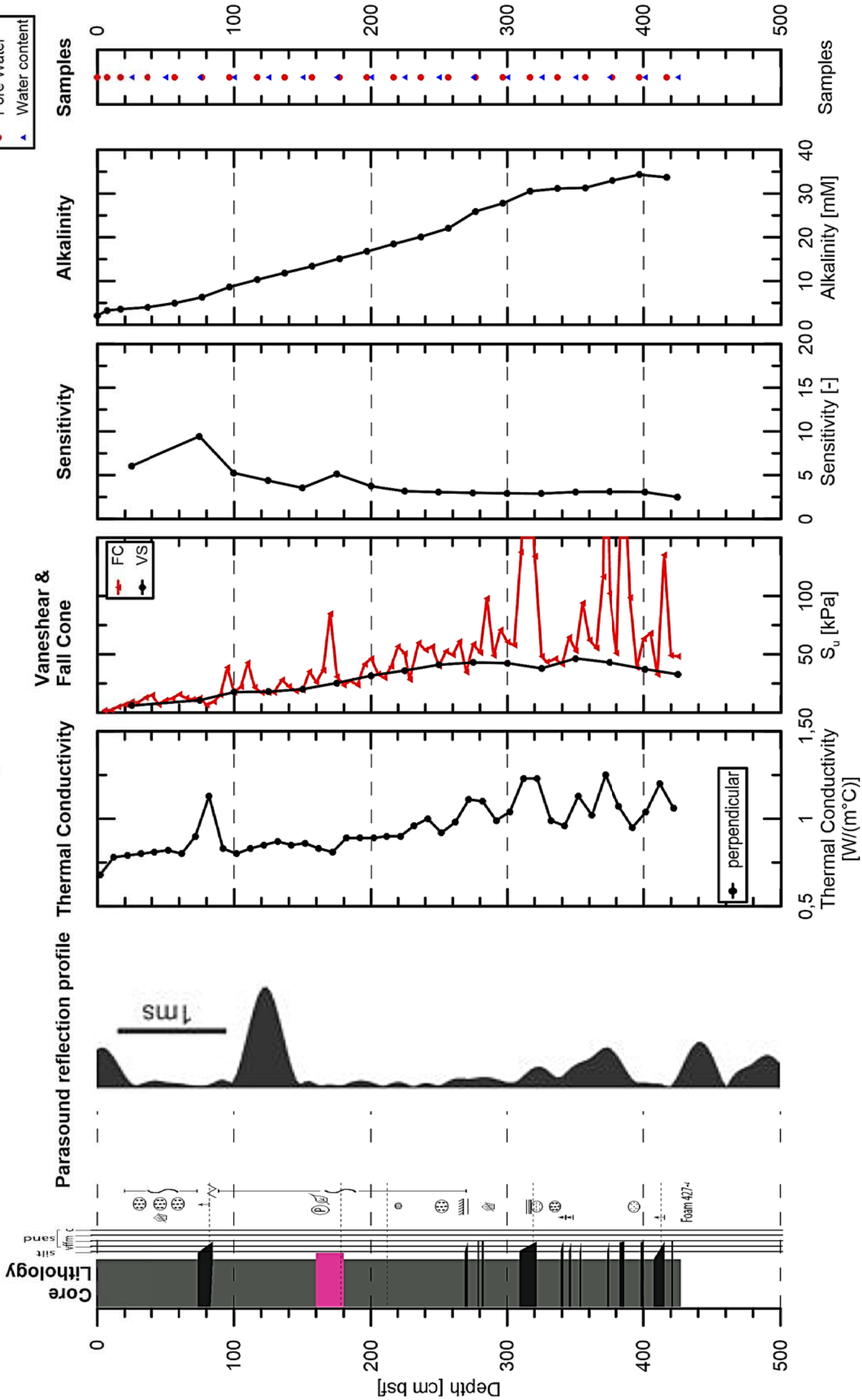
Leg 251B Kumano Basin

GeoB 21831-2 33° 32.915' N / 136° 49.892' E Water Depth: 2039 m Location: SSE



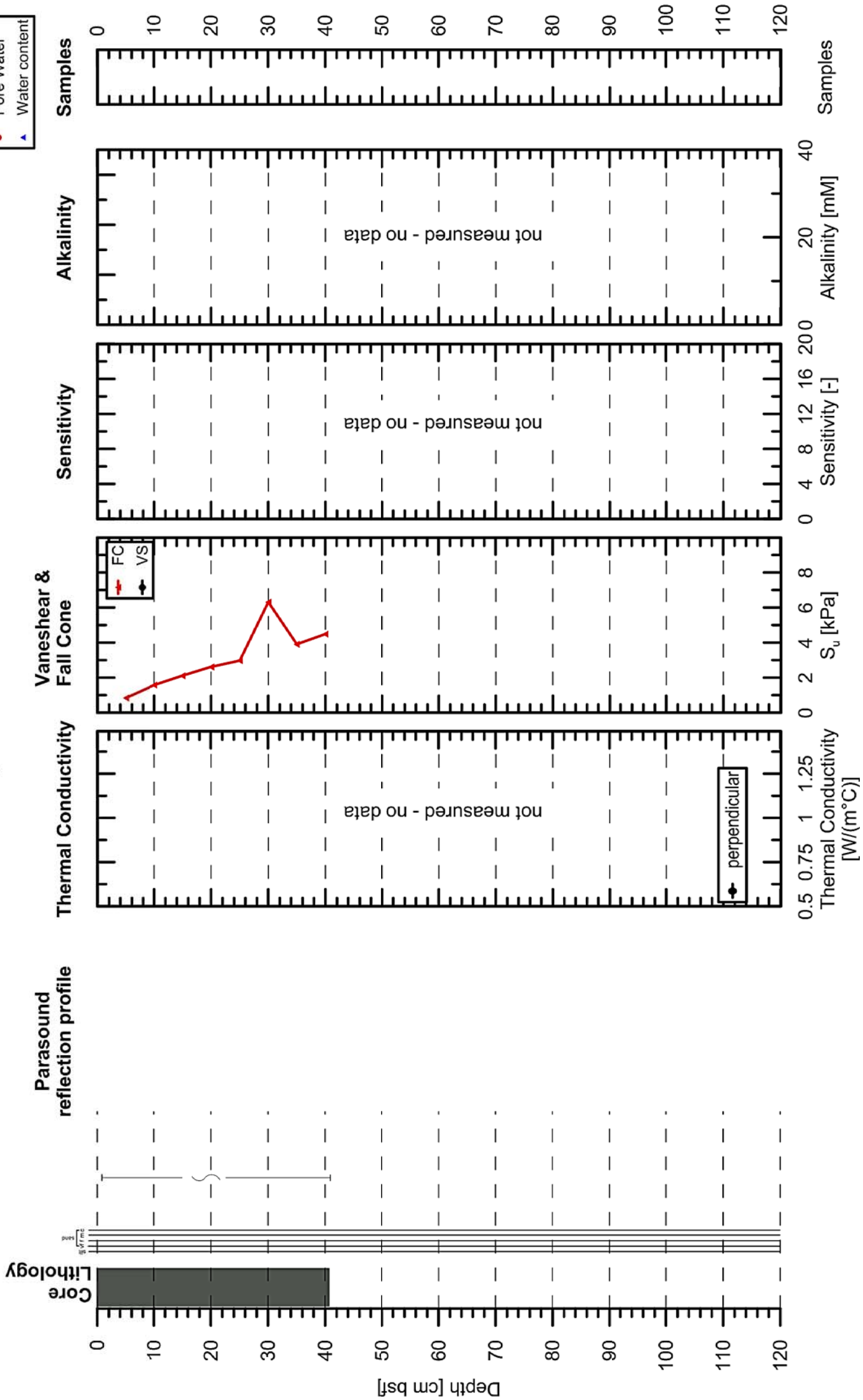
Leg 251B Kumano Basin

GeoB 21833-1 33° 27.746' N 136° 32.614' E Water Depth: 2054 m Location: South-Central



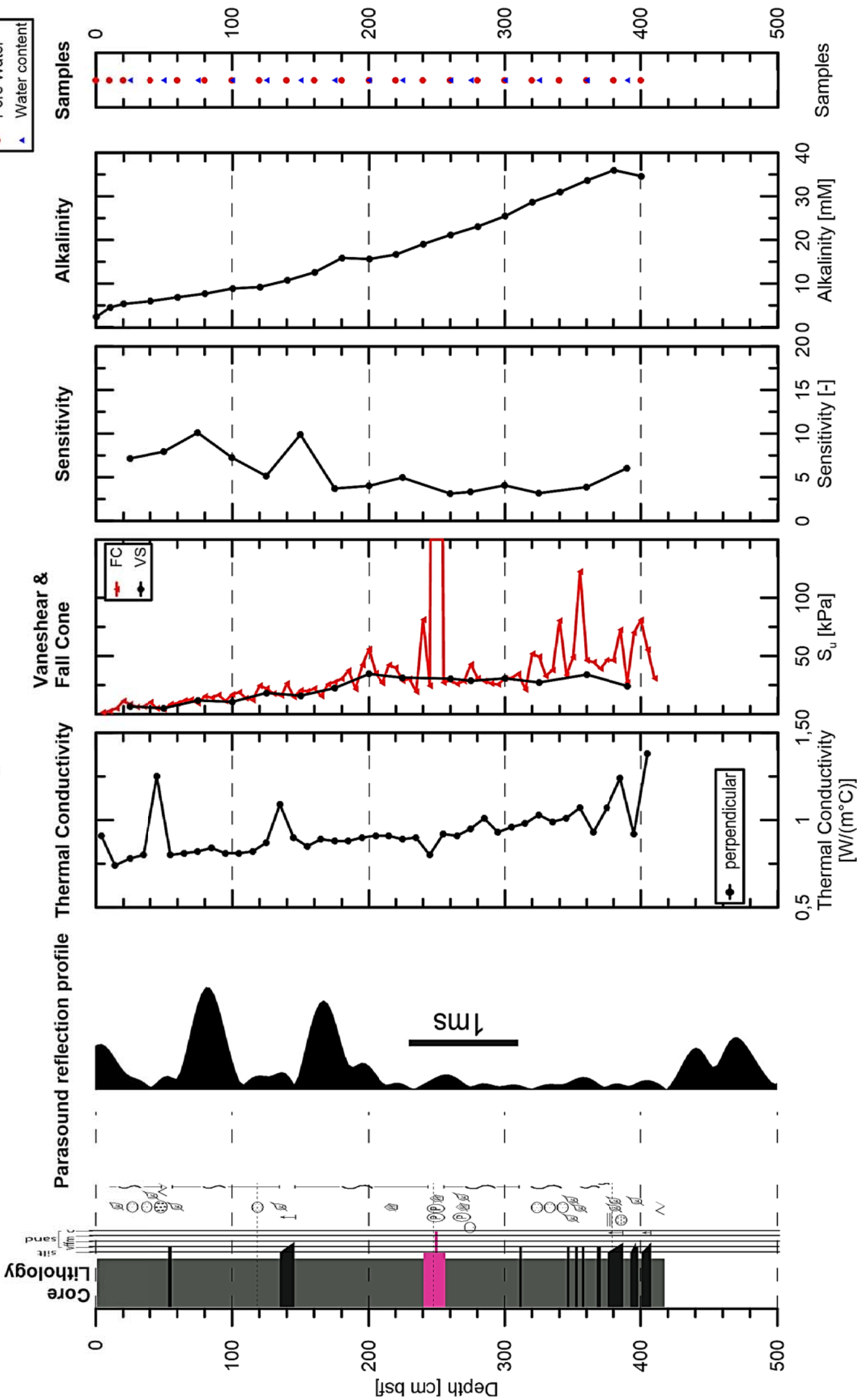
Leg 251B Kumano Basin

GeoB 21833-2 33° 27.746' N / 136° 32.614' E Water Depth: 2054 m Location: south-central



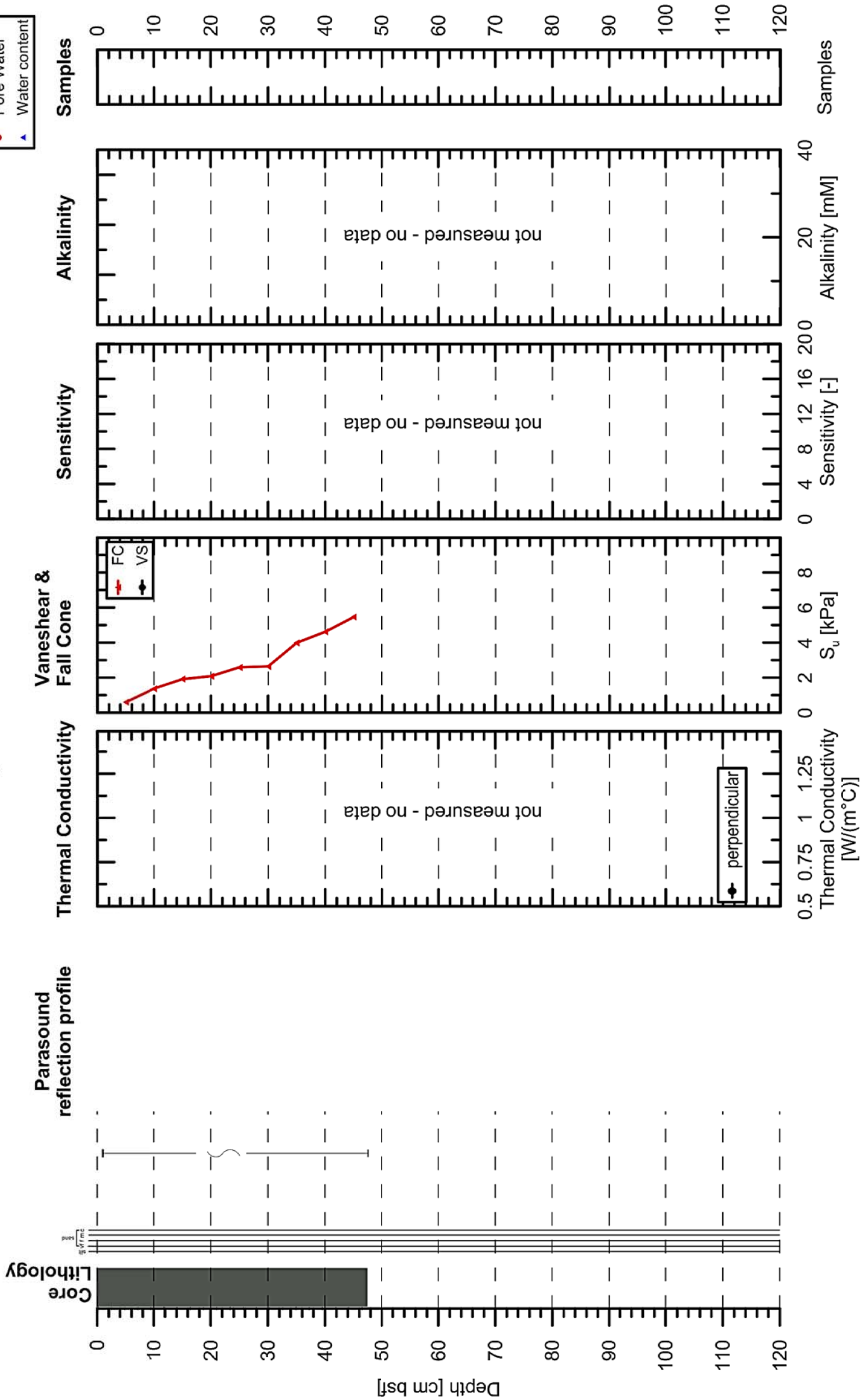
Leg 251B Kumano Basin

GeoB 21834-1 33° 35.732' N 136° 27.409' E Water Depth: 2041 m Location: North-Central



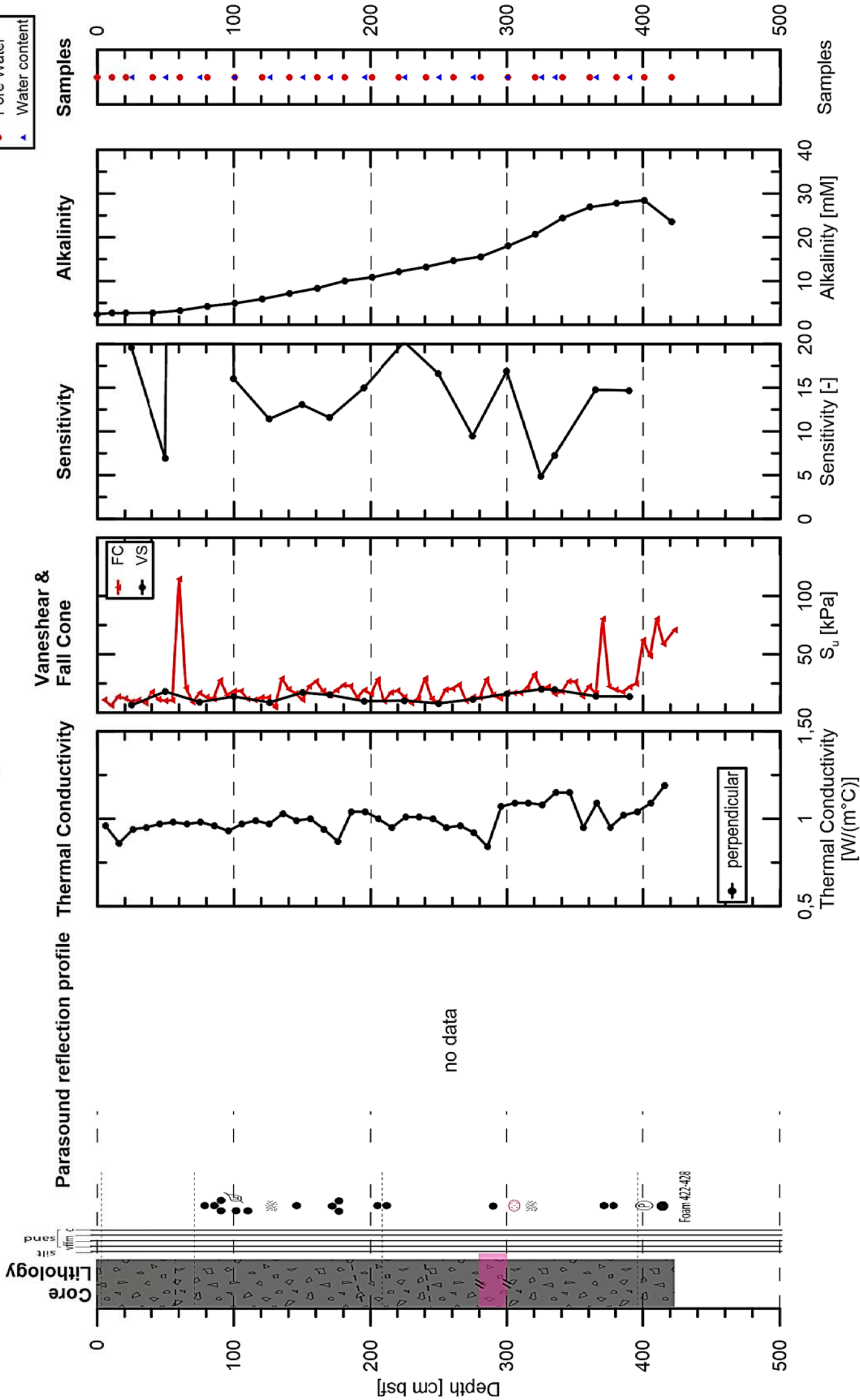
Leg 251B Kumano Basin

GeoB 21834-2 33° 35.732' N / 136° 27.409' E Water Depth: 2041 m Location: north-central



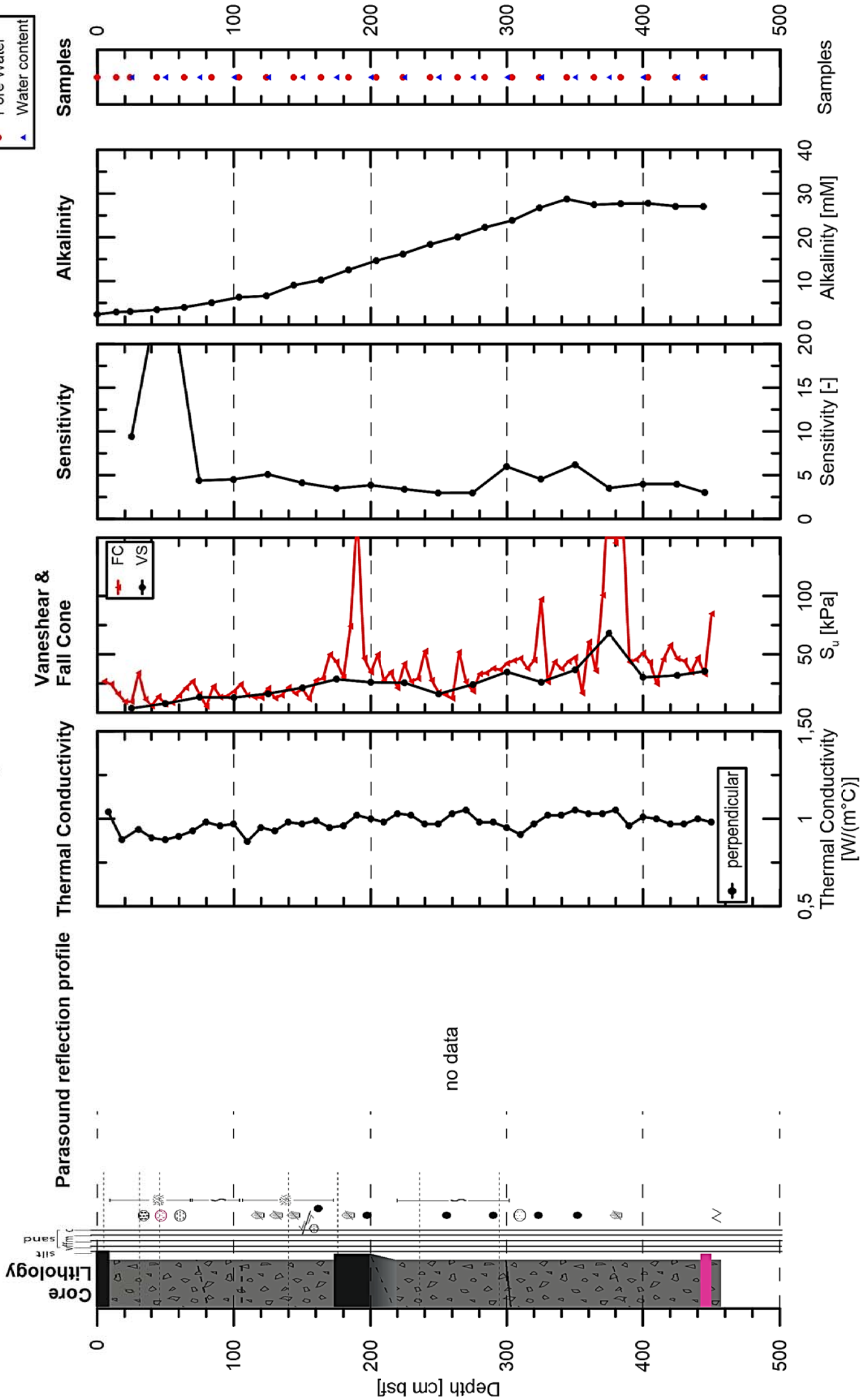
Leg 251B Kumano Basin

GeoB 21836-1 33° 15.131' N 136° 35.820' E Water Depth: 1919 m Location: SSW



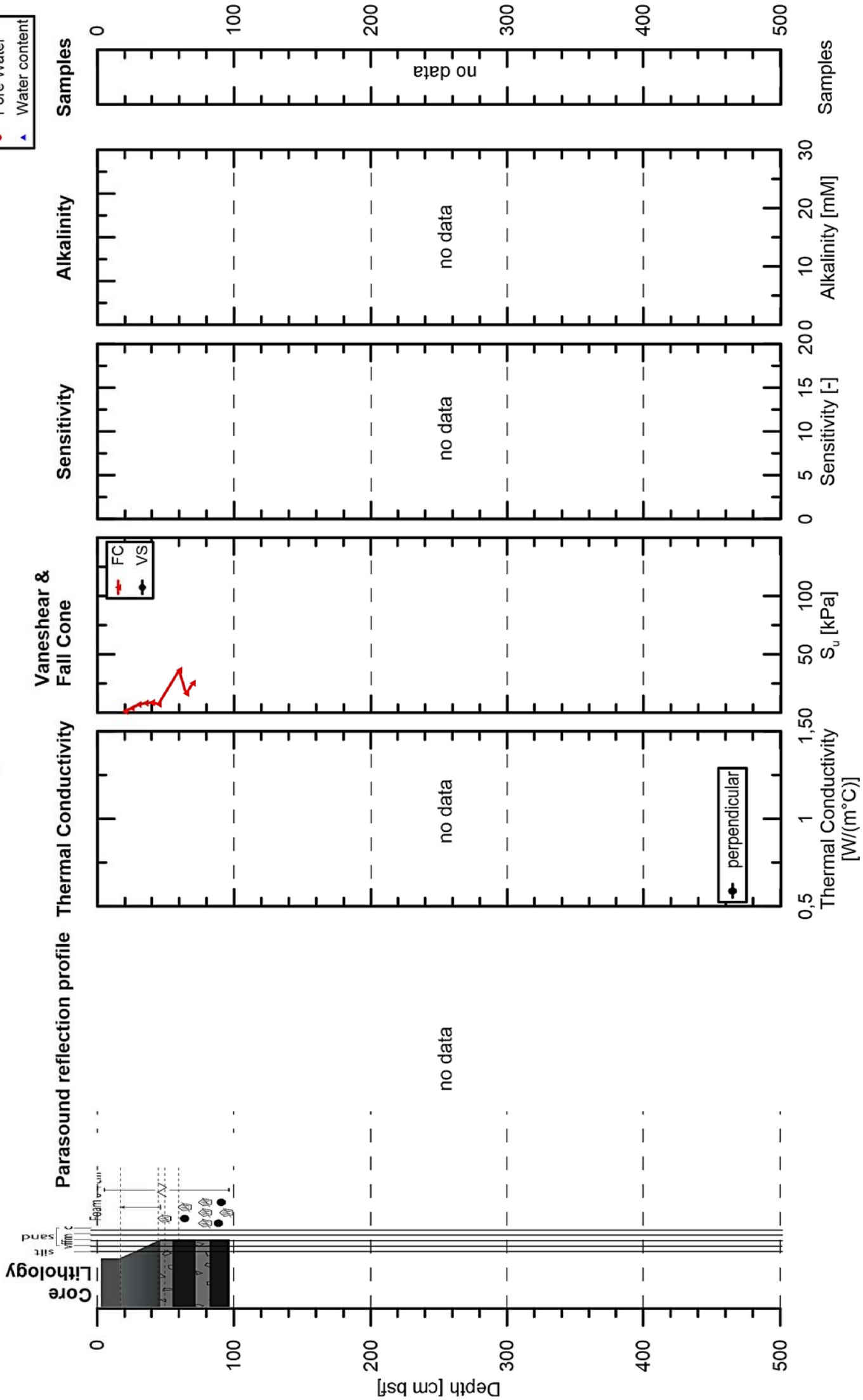
Leg 251B Kumano Basin

GeoB 21840-1 33° 15.148' N 136° 34.743' E Water Depth: 1823 m Location: SSW



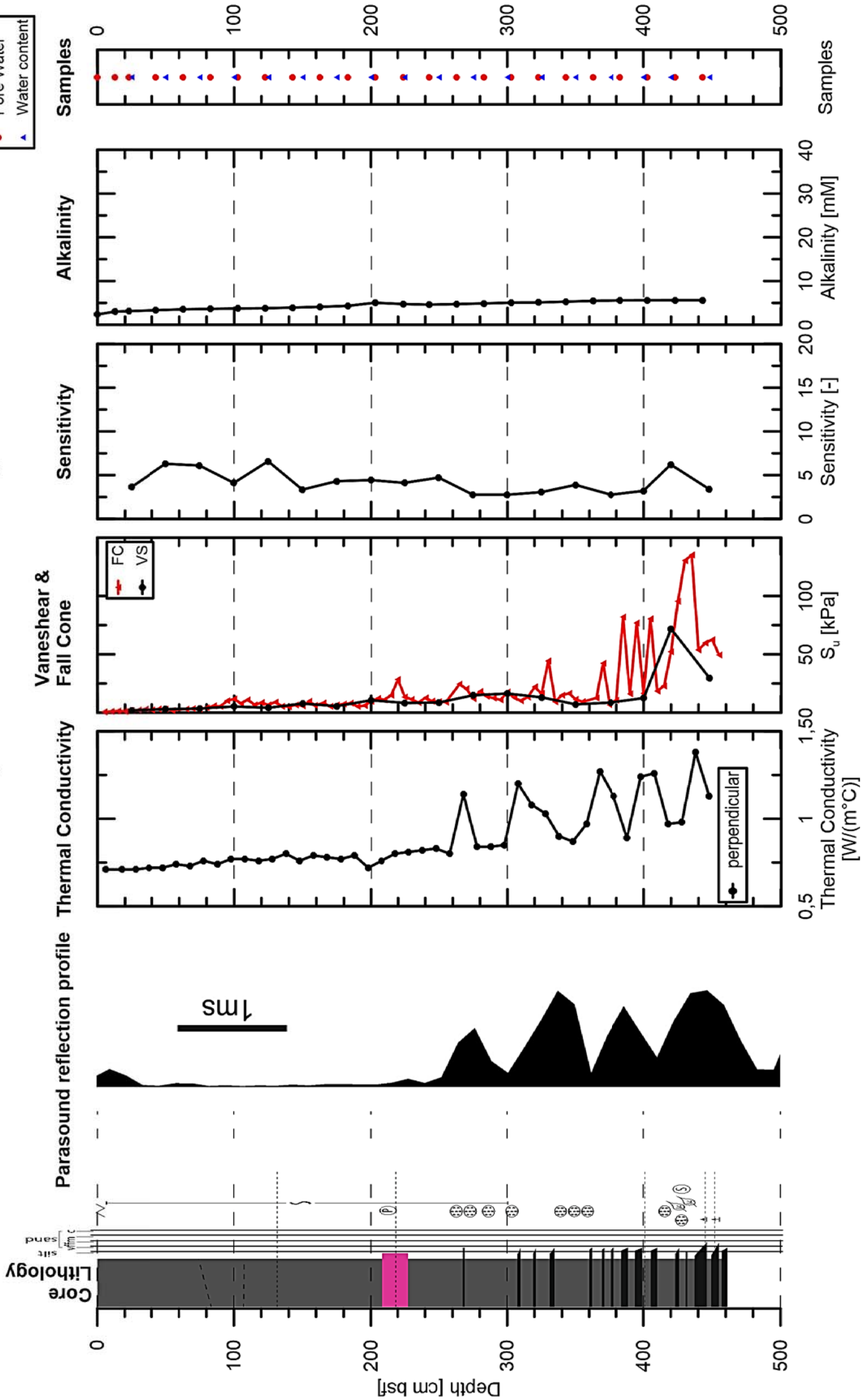
Leg 251B Kumano Basin

GeoB 21842-1 33° 42.854' N 137° 05.226' E Water Depth: 1830 m Location: MV#1



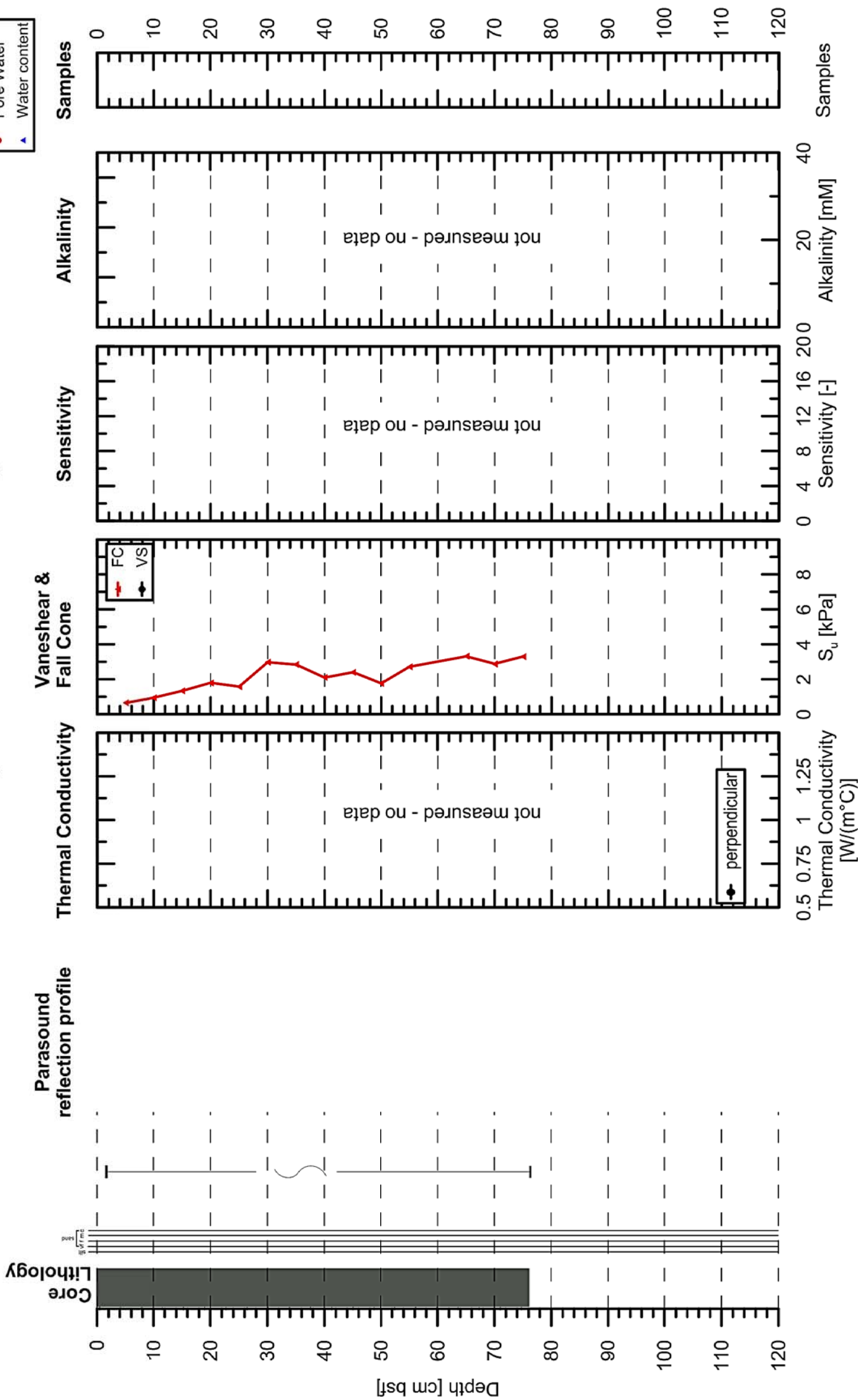
Leg 251B Kumano Basin

GeoB 21843-1 33° 41.620' N 137° 00.739' E Water Depth: 1987 m Location: background MV#1



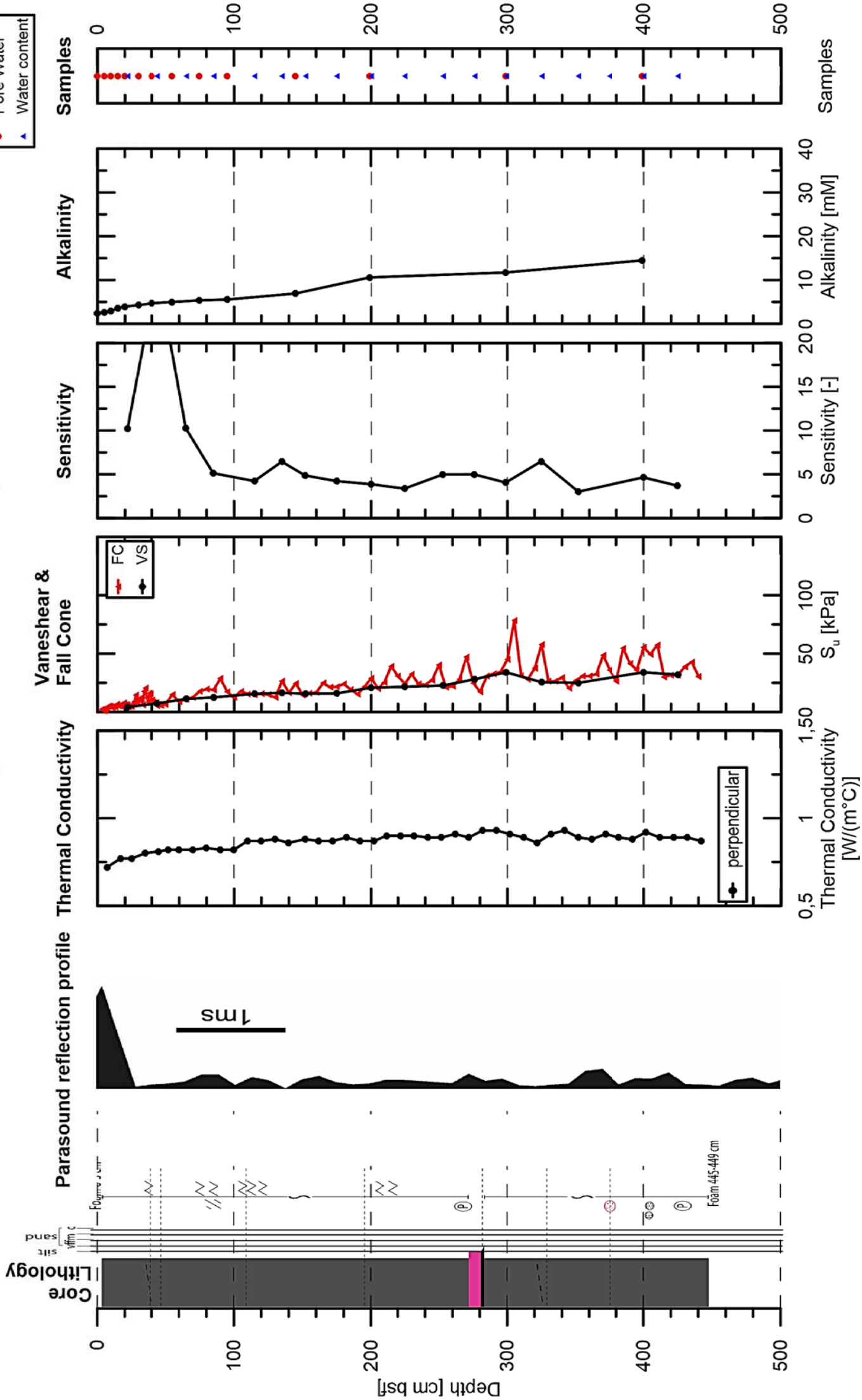
Leg 251B Kumano Basin

GeoB 21843-2 33° 41.620' N / 137° 00.739' E Water Depth: 1987 m Location: background MV#1



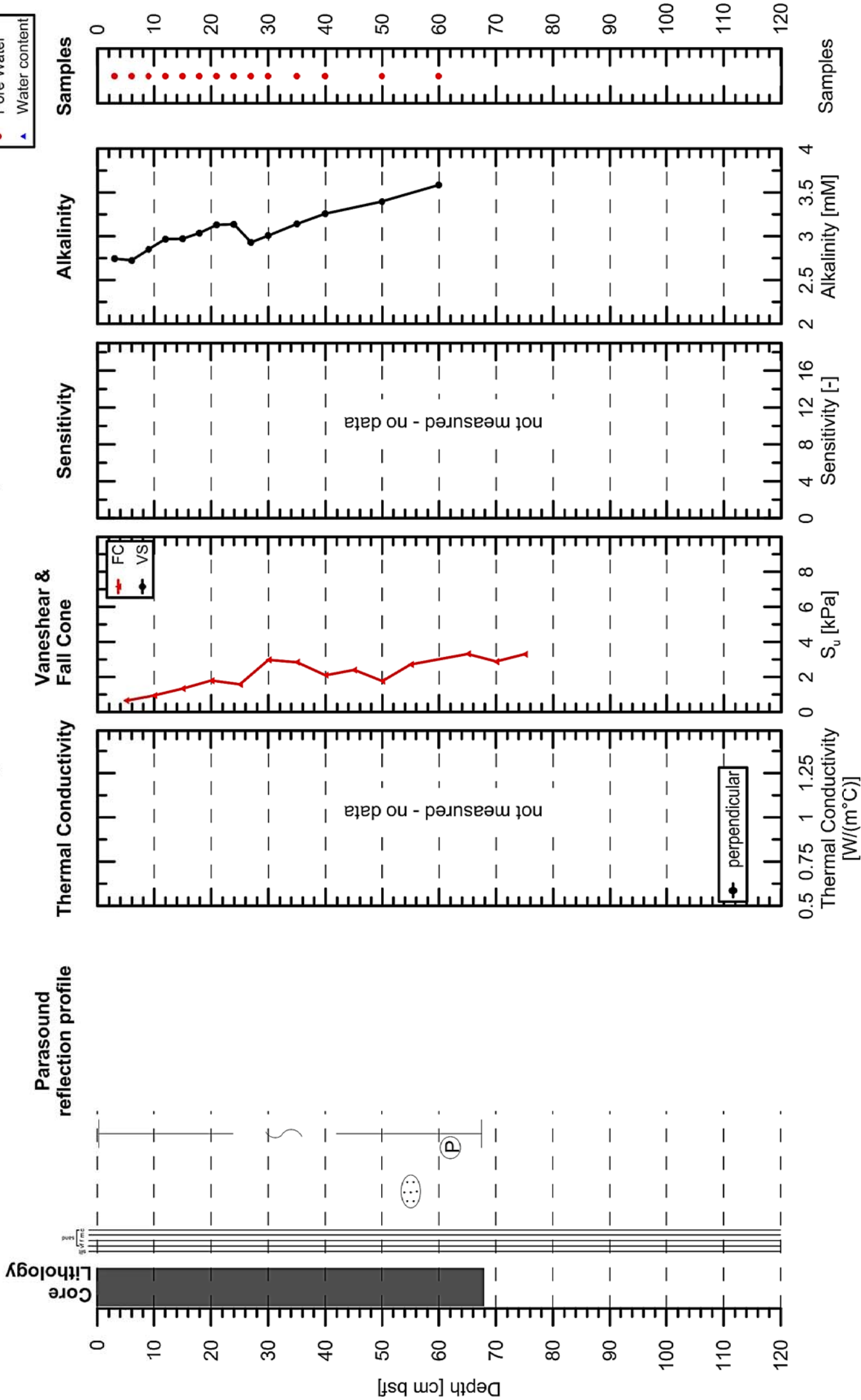
Leg 251B Kumano Basin

GeoB 21845-1 33° 12.489' N 136° 44.349' E Water Depth: 2860 m Location: Slope



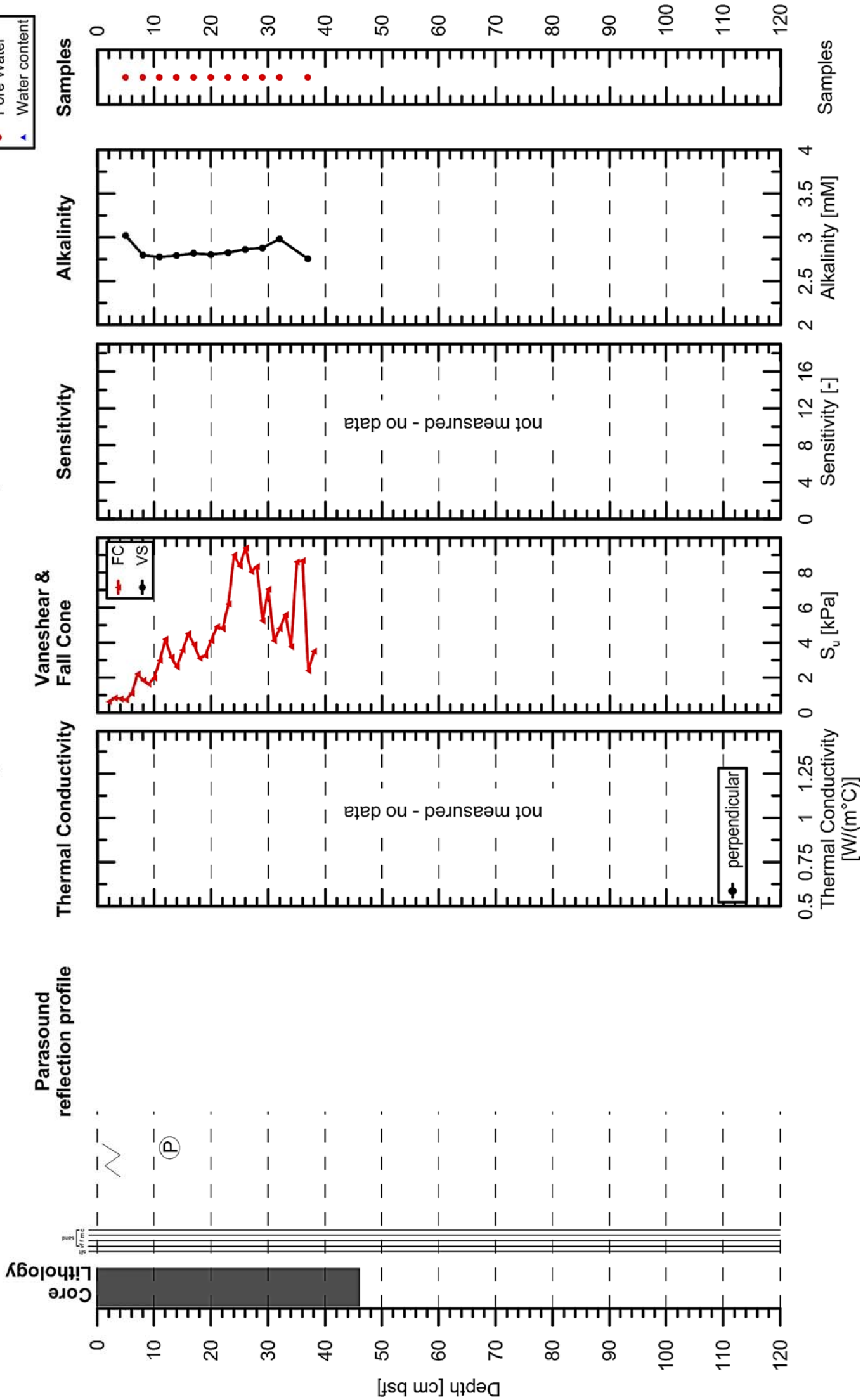
Leg 251B Kumano Basin

GeoB 21845-4 33° 12.454' N / 136° 44.357' E Water Depth: 2860 m Location: Slope



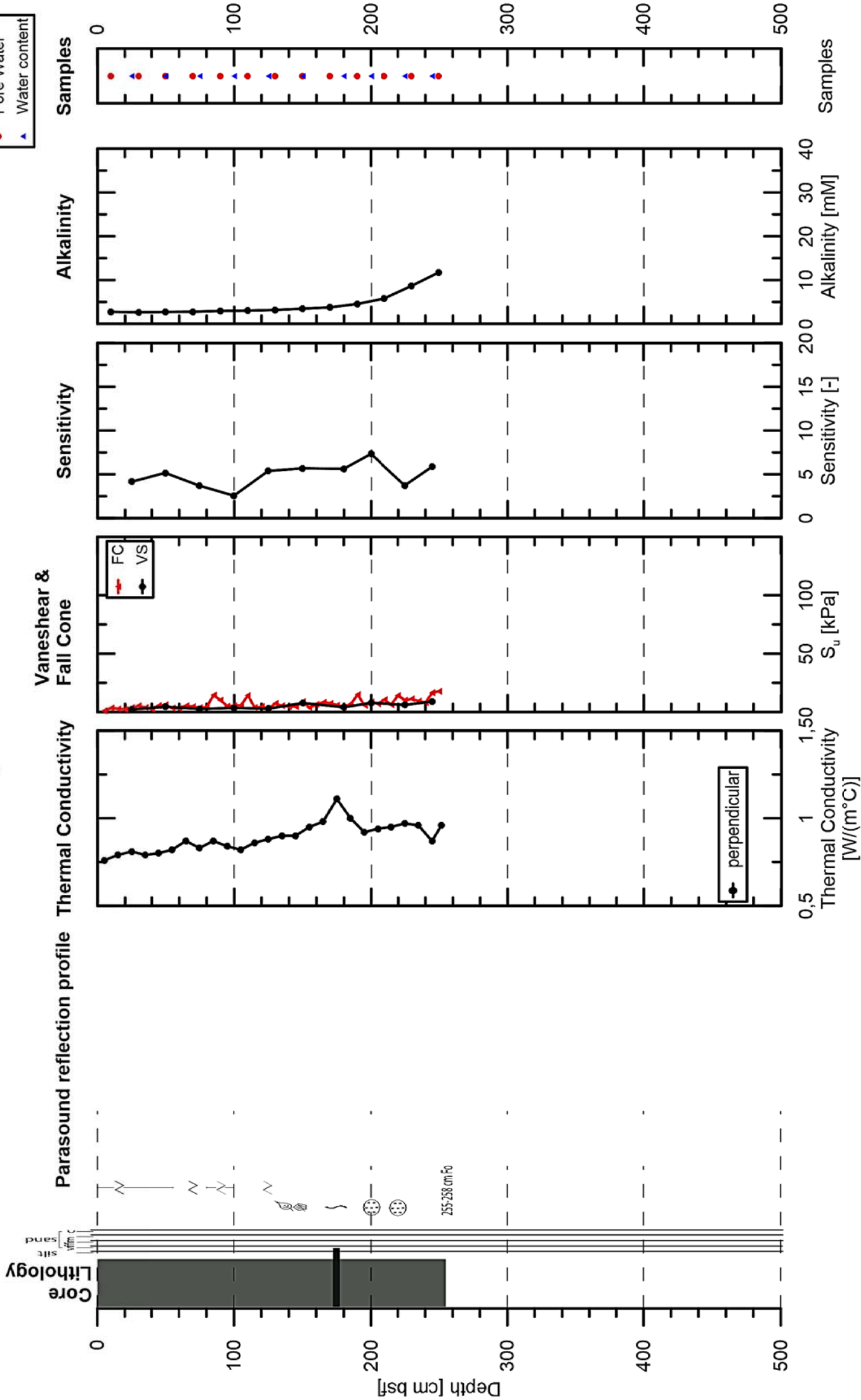
Leg 251B Kumano Basin

GeoB 21846-2 33° 09.760' N / 136° 38.710' E Water Depth: 2882 m Location: Slope



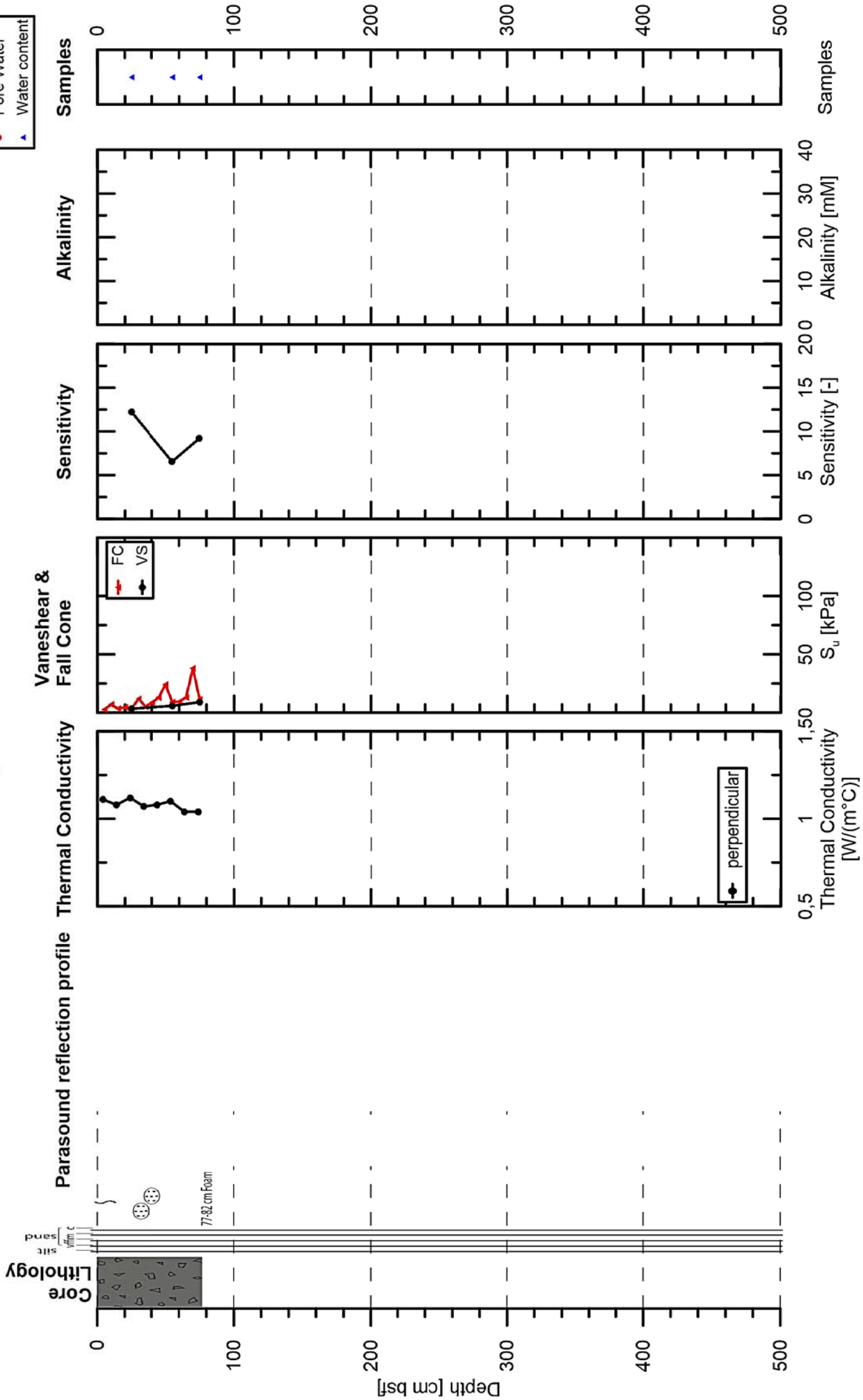
Leg 251B Kumano Basin

GeoB 21858-2 33° 49.298' N 136° 01.442' E Water Depth: 1920 m Location: NNE



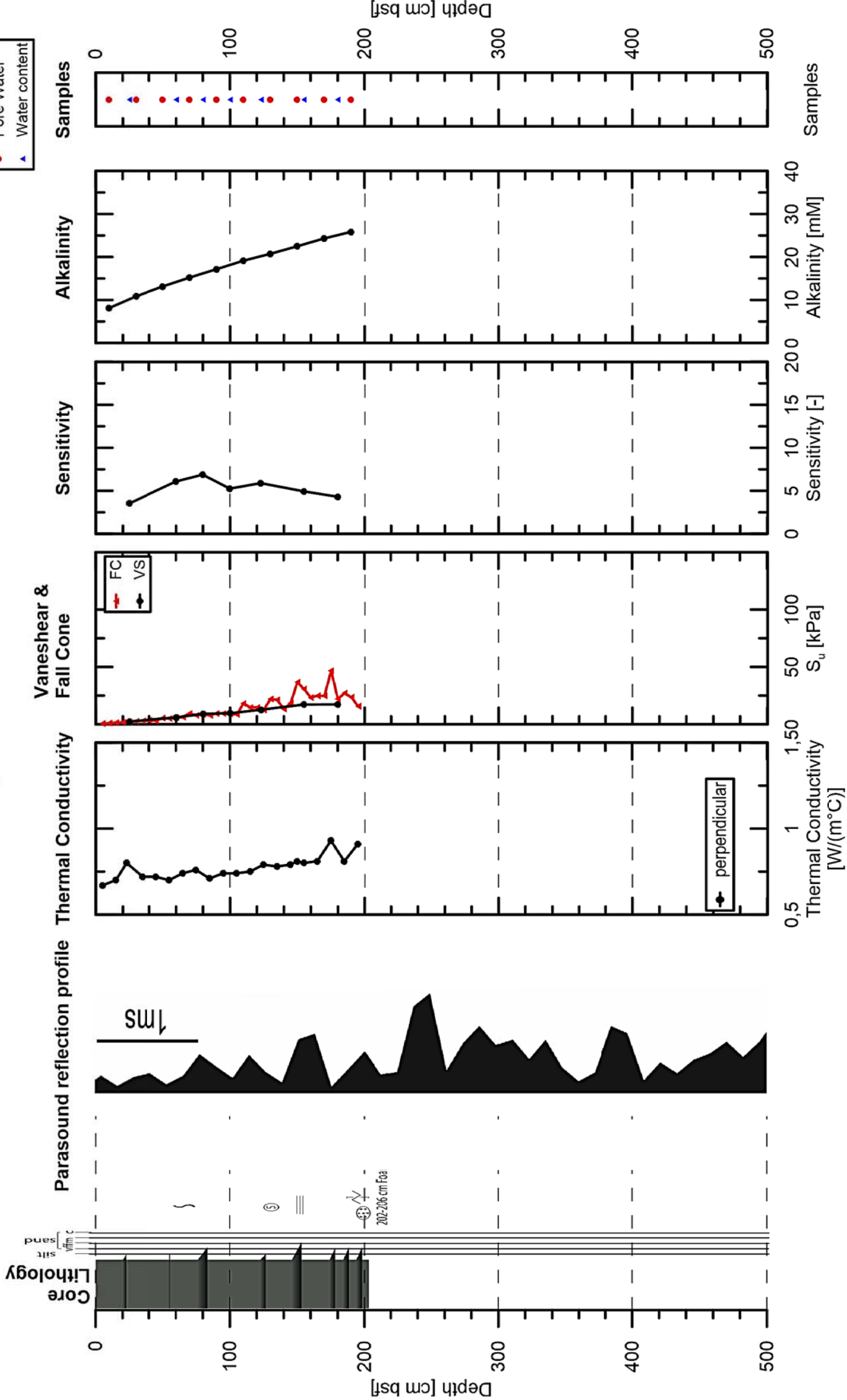
Leg 251B Kumano Basin

GeoB 21860-2 33° 40.675' N 136° 55.129' E Water Depth: 2003 m Location: NNE



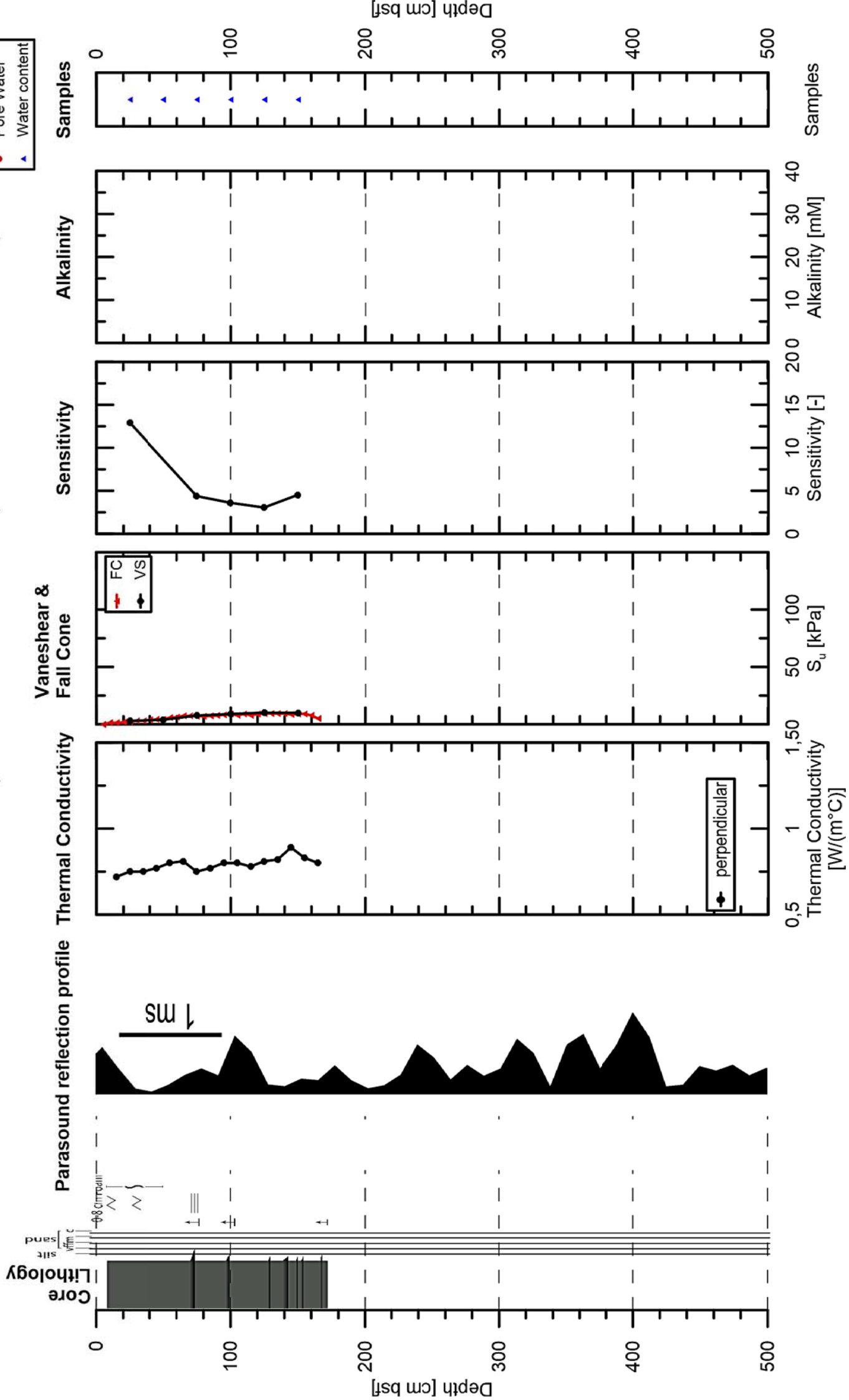
Leg 251B Kumano Basin

GeoB 21861-2 33° 47.382' N 137° 16.097' E Water Depth: 2162 m Location: isolated basin



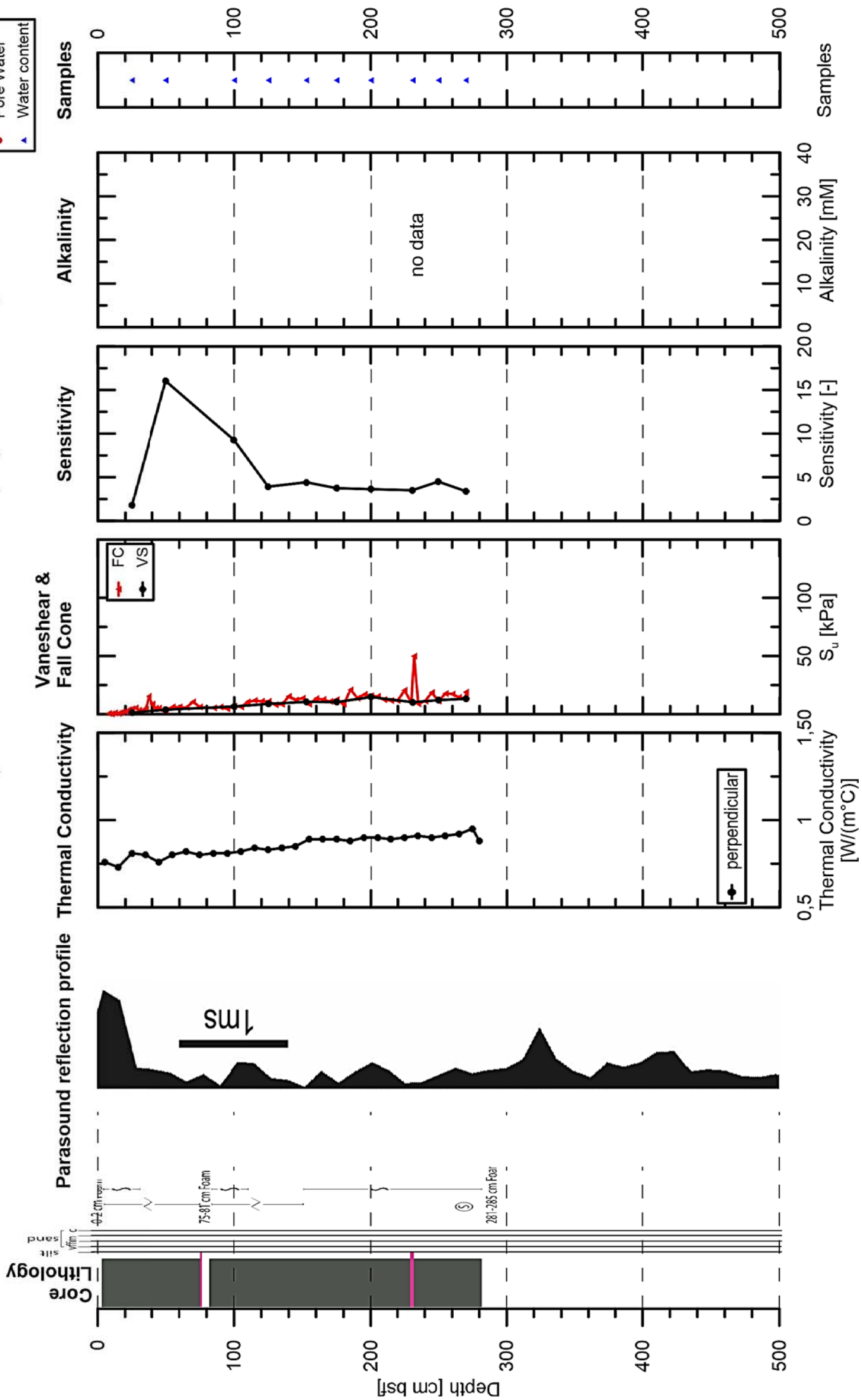
Leg 251B Kumano Basin

GeoB 21864-2 33° 46.599' N 137° 29.057' E Water Depth: 2036 m Location: N (Holocene turbidite record)



Leg 251B Kumano Basin

GeoB 21866-2 33° 09.752' N 137° 38.805' E Water Depth:2890 m Location: Slope (GeoB 21846-1)



From report No. 289 onwards this series is published under the new title:

Berichte aus dem MARUM und dem Fachbereich Geowissenschaften der Universität Bremen

A complete list of all publications of this series from no. 1 to 292 (1986 – 2012) was printed at last in issue no. 292.

- No. 289 – Mohtadi, M. and cruise participants (2012).** Report and preliminary results of RV SONNE Cruise SO 223T. TransGeoBioC. Pusan – Suva, 09.09.2012 – 08.10.2012. 47 pages.
- No. 290 – Hebbeln, D., Wienberg, C. and cruise participants (2012).** Report and preliminary results of R/V Maria S. Merian cruise MSM20-4. WACOM – West-Atlantic Cold-water Corals Ecosystems: The West Side Story. Bridgetown – Freeport, 14 March – 7 April 2012. 120 pages.
- No. 291 – Sahling, H. and cruise participants (2012).** R/V Heincke Cruise Report HE-387. Gas emissions at the Svalbard continental margin. Longyearbyen – Bremerhaven, 20 August – 16 September 2012. 170 pages.
- No. 292 – Pichler, T., Häusler, S. and Tsuonis, G. (2013).** Abstracts of the 3rd International Workshop "Research in Shallow Marine and Fresh Water Systems". 134 pages.
- No. 293 – Kucera, M. and cruise participants (2013).** Cruise report of RV Sonne Cruise SO-226-3. Dip-FIP - The extent and structure of cryptic diversity in morphospecies of planktonic Foraminifera of the Indopacific Warm Pool. Wellington – Kaohsiung, 04.03.2013 – 28.03.2013. 39 pages.
- No. 294 – Wienberg, C. and cruise participants (2013).** Report and preliminary results of R/V Poseidon cruise P451-2. Practical training cruise onboard R/V Poseidon - From cruise organisation to marine geological sampling: Shipboard training for PhD students on R/V Poseidon in the Gulf of Cádiz, Spain. Portimao – Lisbon, 24 April – 1 May 2013. 65 pages.
- No. 295 – Mohtadi, M. and cruise participants (2013).** Report and preliminary results of R/V SONNE cruise SO-228, Kaohsiung-Townsville, 04.05.2013-23.06.2013, EISPAC-WESTWIND-SIODP. 107 pages.
- No. 296 – Zonneveld, K. and cruise participants (2013).** Report and preliminary results of R/V POSEIDON cruise POS448. CAPRICCIO – Calabrian and Adriatic Past River Input and Carbon Conversion In the Eastern Mediterranean. Messina – Messina, 6 – 23 March 2013. 47 pages.
- No. 297 – Kopf, A. and cruise participants (2013).** Report and preliminary results of R/V SONNE cruise SO222. MEMO: MeBo drilling and in situ Long-term Monitoring in the Nankai Trough accretionary complex, Japan. Leg A: Hong Kong, PR China, 09.06.2012 – Nagoya, Japan, 30.06.2012. Leg B: Nagoya, Japan, 04.07.2012 – Pusan, Korea, 18.07.2012. 121 pages.
- No. 298 – Fischer, G. and cruise participants (2013).** Report and preliminary results of R/V POSEIDON cruise POS445. Las Palmas – Las Palmas, 19.01.2013 – 01.02.2013. 30 pages.
- No. 299 – Hanebuth, T.J.J. and cruise participants (2013).** CORIBAR – Ice dynamics and meltwater deposits: coring in the Kveithola Trough, NW Barents Sea. Cruise MSM30. 16.07. – 15.08.2013, Tromsø (Norway) – Tromsø (Norway). 74 pages.
- No. 300 – Bohrmann, G. and cruise participants (2014).** Report and Preliminary Results of R/V POSEIDON Cruise P462, Izmir – Izmir, 28 October – 21 November, 2013. Gas Hydrate Dynamics of Mud Volcanoes in the Submarine Anaximander Mountains (Eastern Mediterranean). 51 pages.
- No. 301 – Wefer, G. and cruise participants (2014).** Report and preliminary results of R/V SONNE Cruise SO219A, Tohoku-Oki Earthquake – Japan Trench, Yokohama – Yokohama, 08.03.2012 – 06.04.2012. 83 pages.
- No. 302 – Meinecke, G. (2014).** HROV: Entwicklung und Bau eines hybriden Unterwasserfahrzeugs – Schlussbericht. 10 pages.
- No. 303 – Meinecke, G. (2014).** Inverse hydroakustische USBL-Navigation mit integrierter Kommunikation – Schlussbericht. 10 pages.
- No. 304 – Fischer, G. and cruise participants (2014).** Report and preliminary results of R/V POSEIDON cruise POS464, Las Palmas (Canary Islands) – Las Palmas (Canary Islands), 03.02.2014 – 18.02.2014. 29 pages.
- No. 305 – Heuer, V.B. and cruise participants (2014).** Report and preliminary results of R/V POSEIDON cruise POS450, DARCSEAS II – Deep seafloor Archaea in the Western Mediterranean Sea: Carbon Cycle, Life Strategies, and Role in Sedimentary Ecosystems, Barcelona (Spain) – Malaga (Spain), April 2 – 13, 2013. 42 pages.
- No. 306 – Bohrmann, G. and cruise participants (2015).** Report and preliminary results of R/V METEOR cruise M112, Dynamic of Mud Volcanoes and Seeps in the Calabrian Accretionary Prism, Ionian Sea, Catania (Italy) – Catania (Italy), November 6 – December 15, 2014. 217 pages.
- No. 307 – Fischer, G. and cruise participants (2015).** Report and preliminary results of R/V POSEIDON cruise POS481, Las Palmas (Canary Islands) – Las Palmas (Canary Islands), 15.02.2015 – 03.03.2015. 33 pages.
- No. 308 – Wefer, G. and Freudenthal, T. (2016).** MeBo200 – Entwicklung und Bau eines ferngesteuerten Bohrgerätes für Kernbohrungen am Meeresboden bis 200 m Bohrteufe, Schlussbericht. 9 pages.
- No. 309 – Sahling, H. and cruise participants (2016).** R/V POSEIDON cruise POS498, Recovery of Observatories at Athina Mud Volcano, Izmir (Turkey) – Catania (Italy), 18 April – 1 May, 2016. 63 pages.
- No. 310 – Fischer, G. and cruise participants (2016).** Report and preliminary results of R/V POSEIDON cruise POS495, Las Palmas (Canary Islands) – Las Palmas (Canary Islands), 18.02.2016 – 02.03.2016. 29 pages.
- No. 311 – Bohrmann, G. and cruise participants (2016).** Report and preliminary results of R/V POSEIDON cruise POS499, Calabrian Mud Volcanoes, Catania (Italy) – Catania (Italy), 04 May – 22 May, 2016. 76 pages.
- No. 312 – Kopf, A., Fleischmann, T. and cruise participants (2016).** Report and preliminary results of R/V POSEIDON cruise POS500, LISA, Ligurian Slope AUV mapping, gravity coring and seismic reflection, Catania (Italy) – Malaga (Spain), 25.05.2016 – 09.06.2016. 58 pages.
- No. 313 – Stegmann, S. and cruise participants (2017).** Report and preliminary results of R/V POSEIDON cruise POS472, NORGEotech, Geotechnical in situ investigation of slope stability in Norway, Trondheim (Norway) – Tromsø (Norway), 27.07.2014 – 12.08.2014. 103 pages.
- No. 314 – Bohrmann, G. and cruise participants (2017).** R/V MARIA S. MERIAN Cruise Report MSM57, Gas Hydrate Dynamics at the Continental Margin of Svalbard, Reykjavik – Longyearbyen – Reykjavik, 29 July – 07 September 2016. 204 pages.
- No. 315 – Sahling, H. and cruise participants (2017).** R/V METEOR Cruise Report M114, Natural hydrocarbon seepage in the southern Gulf of Mexico, Kingston – Kingston, 12 February – 28 March 2015. 214 pages.
- No. 316 – Mohtadi, M. and cruise participants (2017).** R/V SONNE Cruise Report SO256, TACTEAC, Temperature And Circulation History of The East Australian Current, Auckland (New Zealand) – Darwin (Australia), 17 April – 09 May 2017. 70 pages.
- No. 317 – Bohrmann, G. and cruise participants (2017).** R/V METEOR Cruise Report M134, Emissions of Free Gas from Cross-Shelf Troughs of South Georgia: Distribution, Quantification, and Sources for Methane Ebullition Sites in Sub-Antarctic Waters, Port Stanley (Falkland Islands) – Punta Arenas (Chile), 16 January – 18 February 2017. 220 pages.
- No. 318 – Strasse, M., Kopf, A. and cruise participants (2017).** Report and preliminary results of R/V SONNE cruise SO251, Extreme events Archived in the Geological Record of Japan's Subduction margins (EAGER-Japan), Leg A SO251-1, Yokohama - Yokohama, 04.10.2016 – 15.10.2016, Leg B SO251-2, Yokohama - Yokohama, 18.10.2016 – 02.11.2016. 217 pages.